

From the Institute of Systems Neuroscience
at Heinrich Heine University Düsseldorf

Effective connectivity of task-evoked and resting-state brain networks: Relationships to aging and behavior

Dissertation

to obtain the academic title of Doctor of Philosophy (Ph.D.) in Medical Sciences from
the Faculty of Medicine at Heinrich Heine University Düsseldorf

submitted by

Shufei Zhang

(2025)

As an inaugural dissertation printed by permission of the Faculty of Medicine at
Heinrich Heine University Düsseldorf

signed:

Dean: Prof. Dr. Nikolaj Klöcker

Examiner/s: PD Dr. Oleksandr Popovych, Prof. Dr. Esther Florin

*To my parents and sister:
Your steadfast support has been my foundation.
I will always be grateful.*

Parts of this work have been published:

Zhang, S., Jung, K., Langner, R., Florin, E., Eickhoff, S. B., & Popovych, O. V. (2024). Impact of data processing varieties on DCM estimates of effective connectivity from task-fMRI. *Human Brain Mapping*, 45(8), e26751. <https://doi.org/10.1002/hbm.26751>

Zhang, S., Jung, K., Langner, R., Florin, E., Eickhoff, S. B., & Popovych, O. V. (2025). Predicting response speed and age from task-evoked effective connectivity. *Network Neuroscience*, 9(2), 591-614. https://doi.org/10.1162/netn_a_00447

Zhang, S., Zheng, W., Li, Z., & Wu, H. (2025). Network Specificity in Predicting Childhood Trauma Characteristics Using Effective Connectivity. *Alpha Psychiatry*, 26(3), 43988. <https://doi.org/10.31083/AP43988>

Zusammenfassung

Die Erforschung neuronaler Grundlagen menschlichen Verhaltens ist ein Kernziel der Neurobiologie. Traditionelle Methoden wie funktionelle Konnektivität (FC) basierend auf Pearson-Korrelationen in fMRT-Daten werden häufig zur Vorhersage individueller Verhaltensunterschiede genutzt, erfassen jedoch keine dynamischen kausalen Interaktionen. Effektive Konnektivität (EC) quantifiziert dagegen gerichtete, biologisch plausible Wechselwirkungen und ermöglicht tiefere Einblicke in Gehirn-Verhaltens-Beziehungen. EC-Studien stehen jedoch vor Herausforderungen wie methodischer Variabilität, unerforschem prädiktiven Nutzen zustandsspezifischer Konnektivität und klinischer Anwendbarkeit.

Diese Arbeit adressiert diese Herausforderungen. Zunächst untersucht sie, wie Datenverarbeitungsmethoden (GLM in blockbasiertem vs. ereignisbezogenem Design) und Aktivierungskontraste die EC-Schätzung während einer Reiz-Reaktions-Kompatibilitätsaufgabe (SRC) beeinflussen. Ergebnisse zeigen deutliche Variationen in EC-Stärke und -Zuverlässigkeit über Parameterkonstellationen hinweg, mit einem Kompromiss zwischen Sensitivität und Stabilität. Die Parameterwahl muss an Forschungsziele geknüpft werden. Basierend darauf vergleicht diese Arbeit den Nutzen intrinsischer und aufgabenmodulierter Komponenten aufgabeninduzierter EC zur Vorhersage von Alter und Reaktionszeit (RT) in der SRC-Aufgabe. Beide EC-Modalitäten zeigen spezifische verhaltensbezogene Merkmale: Aufgabenmodulierte EC korreliert stärker mit RT, intrinsische EC sagt Alter besser vorher. Entscheidend ist die GLM-Wahl: Nur ereignisbezogene Designs liefern statistisch signifikante Vorhersagen für beide EC-Modalitäten. Abschließend wird Ruhezustands-EC hinzugezogen, um deren Vorhersagekraft für den Schweregrad von Kindheitstraumata über großflächige Netzwerke zu untersuchen. Das Default-Mode-Netzwerk erwies sich als robustester Prädiktor, was dessen klinische Relevanz als möglicher Indikator für traumabedingte Krankheitszustände unterstreicht.

Zusammenfassend stellt diese Arbeit EC als vielversprechendes Maß zur Modellierung von Gehirn-Verhaltens-Beziehungen dar. Durch Evaluierung methodischer Variabilität und netzwerkübergreifender Prädiktionsanalysen verbindet sie grundlagenorientierte Neurobiologie mit verhaltensbezogenen Anwendungen.

Summary

Understanding the neural basis of human behavior is a central goal of neuroimaging. Traditional neuroimaging measures such as functional connectivity (FC), derived from *Pearson* correlations in functional magnetic resonance imaging (fMRI) data, have been widely utilized to predict individual variability in behaviors. However, FC fails to capture the dynamic causal interactions between regions. In contrast, effective connectivity (EC) quantifies directed and biologically plausible interactions between brain regions, offering deeper mechanistic insights into the brain-behavior relationship. Despite its promise, EC research has faced challenges involving methodological variability, underexplored predictive utilities of brain state-specific connectivity, and clinical translation.

This thesis addresses these challenges by first evaluating how data processing choices, such as general linear model (GLM) designs (block-based vs. event-related) and activation contrasts, impact task-evoked EC estimates during a stimulus-response compatibility (SRC) task. The results revealed evident variations in EC strength and certainty across parameter selections, showing a trade-off between sensitivity and stability. The results highlight the need to select parameters aligning with specific research objectives. Building on these methodological insights, the thesis compared the predictive utilities of intrinsic and task-modulated components of task-evoked EC for age and reaction time (RT) during the SRC task. The results demonstrated that both EC modalities captured unique behavioral variance: task-modulated EC shows stronger associations with RT, while intrinsic EC exhibits higher predictive power for age. Notably, the prediction pattern is significantly impacted by the types of GLM designs, showing that only event-related designs yield statistically significant predictive power for both EC modalities. Finally, the thesis extends to resting-state EC, examining the predictive power for childhood maltreatment severity across large-scale networks. The results identify the default mode network as the most robust predictor, highlighting its clinical relevance as a potential biomarker for trauma-related disorders.

In summary, the thesis positions the EC as a promising measure for modeling brain-behavior relationships. By addressing methodological variability in EC estimation and examining its predictive power across networks, this work bridges the gap between methodological neuroimaging research and behavioral applications.

List of abbreviations

Anti	incompatible condition
BOLD	blood-oxygen-level dependent
CM	childhood maltreatment
CTQ	Childhood Trauma Questionnaire
DCM	dynamic causal modeling
DMN	default mode network
EC	effective connectivity
FC	functional connectivity
fMRI	functional magnetic resonance imaging
GLM	general linear model
GSR	global signal regression
Pro	compatible condition
rDCM	regression DCM
RT	reaction time
SRC	stimulus-response compatibility

Table of contents

1. Introduction	1
1.1 Brain Functional Networks and Behaviors	3
1.1.1 Task-Evoked Networks: The Stimulus-Response Compatibility Task	4
1.1.2 Large-Scale Resting-State Networks	4
1.2 Effective Connectivity (EC): From Theory to Methodology	5
1.2.1 Dynamic Causal Modeling (DCM): Theory and Applications	5
1.2.2 Regression DCM: Advancements and Applications	6
1.3 Methodological Challenges in EC Estimation	7
1.3.1 Impact of Data-Processing Variability on EC Estimates	7
1.4 Predictive Modeling of Brain-Behavior Relationships	8
1.4.1 Individual Differences in Task-Evoked EC: Behavioral Relevance	9
1.4.2 Resting-State EC as a Biomarker for Childhood Maltreatment	10
1.5 Ethics Protocols	11
1.6 Aims of Thesis	11
1.6.1 Impact of Data Processing Parameters on EC	11
1.6.2 Dissecting Brain State-Specific EC for Behavioral Prediction	12
1.6.3 Identifying Network Biomarkers of Childhood Trauma via Resting-State EC	12
2. Study 1: Impact of data processing varieties on DCM estimates of effective connectivity from task-fMRI	14
3. Study 2: Predicting response speed and age from task-evoked effective connectivity	15
4. Study 3: Network Specificity in Predicting Childhood Trauma Characteristics Using Effective Connectivity	16
5. Discussion	17
5.1 Data Processing Effects on Task-Evoked EC	17
5.2 Behavioral Prediction: Brain State-Specific EC	19
5.3 Default Mode Network as a Trauma Biomarker in Resting-State EC	21
5.4 Limitations and Future Directions	22
5.5 Conclusion	24
6. References	26

1. Introduction

Understanding how brain networks relate to human behavior requires methods beyond correlational measures, such as functional connectivity (FC). FC quantifies synchronized brain activities between regions, which has been pivotal in linking brain connectivity to behaviors (Biswal et al., 2010). However, it fails to capture dynamic causal interactions (Friston, 2011; Friston et al., 2003), limiting insights into how brain networks dynamically influence behaviors. The limitation can be addressed by effective connectivity (EC), which models directed causal interactions and provides mechanistically deeper insights into the brain-behavior relationship (Friston, 2011). Several generative embedding approaches have been developed to estimate brain EC, such as the dynamic Bayesian networks (Rajapakse & Zhou, 2007), Granger causality mapping (Roebroeck et al., 2005), and structural equation modeling (Büchel & Friston, 1997). Among these approaches, dynamic causal modeling (DCM) offers a biologically meaningful framework for inferring brain EC (Friston et al., 2003). DCM mathematically models brain intrinsic EC at baseline (matrix A) and task-modulated EC induced by external stimuli (matrix B) (Marreiros et al., 2008; Zeidman, Jafarian, Corbin, et al., 2019), which enables studies of both brain state-specific connectivity components. Currently, DCM has been implemented to bridge brain connectivity with individual behavioral and clinical outcomes (Kahan & Foltynie, 2013; Kahan et al., 2019; Volz et al., 2015), demonstrating its potential to uncover brain-behavior relationships.

Despite its promise, three significant challenges are hindering EC research, including methodological variability, behavioral prediction, and clinical translation. First, the methodological variability in data processing parameters substantially introduces inconsistency in fMRI results (Botvinik-Nezer et al., 2020; Carp, 2012). While the influence of analytical variability has been widely discussed in FC studies (Cole et al., 2010; Power et al., 2017; Smith et al., 2013), EC research has received limited attention. Although a recent study has investigated the effect of the global signal on resting-state EC estimates, reporting a minor impact (Almgren et al., 2020), the broader issue of analytical flexibility in EC research, particularly regarding task-evoked EC, has been largely neglected. Addressing this gap systematically is critical to ensuring reliable and robust estimations of EC parameters.

Second, while previous FC studies have demonstrated superior performance of task-evoked FC over resting-state FC in predicting individual fluid intelligence (Greene et al., 2018) and general cognitive ability (W. Zhao et al., 2023), and reading skills (Jiang et al., 2020), the contradictory evidence persists (Kraljević et al., 2024). This inconsistency raises a critical question of whether the connectivity of different states differentially contributes to explaining individual variability in behaviors and phenotypic traits. Here, DCM offers a unique opportunity to address this issue by mathematically isolating the brain's intrinsic and task-modulated components of task-evoked EC (Zeidman, Jafarian, Corbin, et al., 2019). This approach enables direct comparisons of how each brain state-specific connectivity profile independently contributes to predicting individual differences in behavior and traits.

Third, resting-state fMRI is widely used in clinical research to map the brain's intrinsic functional architecture, owing to its simplicity and applicability in vulnerable populations (O'Connor & Zeffiro, 2019). This approach has been proven particularly valuable for studying how childhood maltreatment (CM), encompassing physical, sexual, and emotional abuse, as well as neglect (Gilbert et al., 2009), influences the brain's intrinsic connectivity. CM experiences may increase the risk of developing mood disorders, substance abuse, and suicidal behaviors (Fuller-Thomson et al., 2016; Green et al., 2010; Merrick et al., 2017). Previous literature (Gerin et al., 2023; Goetschius et al., 2020; Marusak et al., 2015) has linked these outcomes to resting-state FC alterations involving the default mode network (DMN) and the salience network. However, such work overlooks interregional dynamic influence inside brain networks, which can be mechanistically complemented by EC (Friston, 2011). While EC has been utilized to identify biomarkers of CM-related psychiatric disorders (Kessler et al., 2020), existing studies are limited by small, hypothesis-driven node selections or computational constraints of DCM (Frässle et al., 2017). Additionally, accumulating evidence has suggested that CM is associated with alterations in the complex and distributed brain networks (Teicher & Samson, 2016). The absence of comprehensive EC analyses hinders the understanding of how trauma impacts brain network dynamics and insights into trauma-related biomarkers.

The overarching aim of this thesis is to characterize the EC of task-evoked and resting-state brain networks and evaluate its relationship to aging and behavior. This work

advances EC from methodology to behaviors by integrating methodological, behavioral, and clinical perspectives through three interconnected studies. The first study focuses on methodological variability, systematically quantifying the impact of data-processing parameters on task-evoked EC estimates, focusing on the stimulus-response compatibility (SRC) (Fitts & Deininger, 1954) network. It provides a solid methodological foundation for reliable and robust EC analyses for behavioral predictions and clinical applications. Building on the methodological foundation, the second study examines brain state-specific predictions in behavior. It compares predictive utilities of brain state-specific EC components (intrinsic vs. task-modulated) for individual differences in age and reaction time (RT) during the SRC task. This study aims to determine whether state-specific EC differentially predicts behaviors, enhancing understanding of the unique predictive roles of different brain states. The third study extends EC research to clinical translation by identifying network-specific biomarkers of childhood trauma using resting-state EC, which seeks to identify interpretable and robust networks of trauma-related disorders. Based on the foundations and insights from the first and second studies, this exploration examines the clinical application of resting-state EC, providing insights into diagnosing and treating trauma-related disorders. By systematically addressing methodological variability, brain state-specific effects, and clinical biomarkers, this work bridges neuroimaging research with individual behaviors and trauma-related outcomes.

The following introduction begins with an overview of brain functional networks derived from task-evoked and resting-state fMRI paradigms. Next, it provides a detailed discussion of EC, focusing on the models employed in task-evoked and resting-state fMRI research, namely DCM for task-evoked EC and regression DCM (rDCM) for resting-state EC. Then, it discusses the challenges of data processing variability on EC estimates and explores the potential of EC for linking brain network dynamics with individual behaviors and clinical outcomes.

1.1 Brain Functional Networks and Behaviors

A key approach to studying human brain organization is to divide brain regions into spatially distinct but functionally connected networks, facilitating the exchange of information among these regions (van den Heuvel & Hulshoff Pol, 2010). In the context of resting-state fMRI, functional networks are typically identified using FC, defined by

temporal correlations in blood-oxygen-level-dependent (BOLD) signal fluctuations during rest, which reflects the brain's intrinsic functional architecture (Biswal et al., 1995; Biswal et al., 2010; Menon & Uddin, 2010). In contrast, task-evoked functional networks are commonly defined by synchronized activation patterns in response to specific stimuli (Dosenbach et al., 2008). Over the past decades, these two paradigms have elucidated diverse networks, such as the triple-network model (default mode, central executive, and salience networks), which underpin behaviors and pathophysiological dysfunctions (Menon, 2011). This section generally discusses two types of brain functional networks, exemplified by an SRC task (Fitts & Deininger, 1954) and large-scale resting-state networks (Schaefer et al., 2018; Yeo et al., 2011).

1.1.1 Task-Evoked Networks: The Stimulus-Response Compatibility Task

The SRC task is a psychological experiment paradigm designed to study cognitive action control during conflict processing (Fitts & Deininger, 1954). This task involves two conditions: compatible and incompatible. In the compatible condition, participants respond to the stimulus on the same side; in the incompatible condition, they respond to the stimulus on the opposite side (Langner et al., 2015). Psychologically, the incompatible condition leads to slower RTs and a lower accuracy rate, reflecting the incompatibility effect during the conflict processing (Eimer, 1995; Fitts & Deininger, 1954), which is influenced by age-related differences (Korsch et al., 2014; Langner et al., 2015; Proctor et al., 2005). Neurally, this incompatibility activates a front-parietal-insular network, which includes regions such as the anterior insula (AI), intraparietal sulcus (IPS), dorsolateral prefrontal cortex (DLPFC), dorsal premotor cortex, pre-supplementary motor area, mid-cingulate cortex, and temporoparietal junction (Cieslik et al., 2010; Langner et al., 2015). This activation pattern underscores the task's utility in investigating age-related changes in conflict processing and their neural correlates, which enables the study of relationships between the SRC network and individual variability in behaviors and aging.

1.1.2 Large-Scale Resting-State Networks

Large-scale resting-state networks are typically identified using data-driven approaches that analyze brain spontaneous activity patterns without specific hypotheses. For instance, Yeo et al. (2011) clustered resting-state FC to parcellate the entire cortex into 7 or 17 networks, identifying systems such as the visual network, somatosensory network,

dorsal attention network, ventral attention network, limbic network, fronto-parietal network, and DMN. Schaefer et al. (2018) expanded on this work by integrating the gradient and similarity approaches to provide higher-resolution parcellation schemes ranging from 100 to 1,000 parcels, thereby allowing for a more detailed understanding of network organization at a finer spatial scale. This atlas (Schaefer et al., 2018; Yeo et al., 2011) is crucial for capturing the brain's functional organization, as it allows for a comprehensive examination of network connectivity, particularly in linking network abnormalities to neurological and psychiatric disorders (Bruin et al., 2023).

1.2 Effective Connectivity (EC): From Theory to Methodology

Understanding how brain network dynamics shape human cognition and behaviors remains a challenge in neuroscience. Traditional approaches, such as FC, have provided valuable insights by identifying correlations between regions, but they overlook causal interdependence (Friston, 2011). To address this limitation, EC, quantified by DCM, modeled directed influences between regions (Friston et al., 2003), which offers a more mechanistic insight into how brain network dynamics drive behaviors (Friston, 2011; Friston et al., 2003). This approach enables researchers to investigate the directionality of neural communication and link network dynamics to cognitive and behavioral processes. This section discusses the concepts and methodologies of EC utilized in the thesis.

1.2.1 Dynamic Causal Modeling (DCM): Theory and Applications

DCM, introduced by Friston, has provided an efficient framework for investigating task-evoked EC (Friston et al., 2003). By modeling neural dynamics influenced by external stimuli and internal neural processes, it has been widely utilized in tasks such as working memory, resolving response conflicts, and aging-related studies (Boudrias et al., 2012; Cieslik et al., 2011; Jung et al., 2018; Kahan et al., 2019; Loehrer et al., 2016; Morken et al., 2017; Volz et al., 2015), underscoring its applicability in investigating the neural mechanisms behind specific cognitive processes.

Mathematically, DCM separates neural dynamics into brain intrinsic (endogenous) activity and task-modulated (exogenous) interactions (Friston et al., 2003):

$$\frac{dz}{dt} = \left(A + \sum_k B^{(k)} u_k(t) \right) z + Cu(t)$$

In this model, z represents neural states of regions of interest (ROI) across time points. Matrix A encodes brain intrinsic connectivity, reflecting baseline directional connectivity between brain regions in the absence of external influences. Matrix B represents task-modulated connectivity, quantifying how experimental conditions (indexed by k) modulate network interactions. The term $u_k(t)$ specifies the timing of condition k , with each k representing a distinct experimental condition. Finally, matrix C describes the influence of all external experimental inputs (i.e., stimuli or task-related manipulations) on the neural dynamics of the considered ROIs.

This framework of DCM explains how brain regions interact and respond to task-evoked stimuli. However, the neural states z cannot be directly observed in fMRI data. To link neural dynamics to the observable BOLD signals, DCM employs the observation equation:

$$y(t) = h(z(t)) + \epsilon(t)$$

Here, $y(t)$ denotes the observed BOLD signal at time t , while $h(\cdot)$ represents the hemodynamic response function that maps neural activity to the BOLD signal, and $\epsilon(t)$ accounts for noise in the observed data. The model estimates the coupling parameters of the connectivity matrices by optimizing them to ensure that the simulated BOLD signals closely align with the variance observed in the empirical BOLD signals.

1.2.2 Regression DCM: Advancements and Applications

Traditional DCM typically limits the analysis to fewer than 10 network nodes as the number of connections increases rapidly with network size, leading to a substantial computational burden (Frässle et al., 2017; Seghier & Friston, 2013). As a recent variant of DCM, regression DCM (rDCM) addresses the computational challenge inherent in the conventional DCM approach (Frässle et al., 2017). By reformulating the DCM model in the frequency domain and employing Bayesian linear regression for model inversion (Frässle et al., 2017), rDCM enables the estimation of EC in large-scale networks, making it well adapted for resting-state fMRI (Frässle, Harrison, et al., 2021).

In the original linear DCM model (Friston et al., 2003), neural dynamics are modeled in the time domain and described by the following equation:

$$\frac{dx}{dt} = Ax + Cu.$$

In this equation, x represents the neuronal states, matrix A encodes the endogenous connectivity, and C denotes the external inputs u to neural activity.

The rDCM reformulates this model in the frequency domain:

$$i\omega\hat{x} = A\hat{x} + C\hat{u}$$

Here, terms \hat{x} and \hat{u} represent frequency-based representations of neural activity and external inputs, respectively. By transforming the model into the domain of frequency, rDCM captures EC in large-scale networks with greater computational efficiency (Frässle, Harrison, et al., 2021). Although initially designed for task data (Frässle et al., 2017), rDCM has been extended to resting-state fMRI (Frässle, Harrison, et al., 2021), allowing for the quantification of intrinsic EC without external stimuli. This extension underscores the flexibility and adaptability of rDCM, making it a valuable tool for large-scale resting-state EC analyses.

1.3 Methodological Challenges in EC Estimation

Evaluating the impact of data processing variability on neuroimaging outcomes is critical for the validity and reproducibility of fMRI research (Botvinik-Nezer et al., 2020; Lindquist et al., 2019). While established pipelines exist for analyzing fMRI data, there is still no consensus on data processing parameters across pipelines, which considerably introduces variations in results (Botvinik-Nezer et al., 2020). Many methodological studies have been conducted on FC (Cole et al., 2010; Power et al., 2014; Smith et al., 2013), yet the impact of data processing choices on task-evoked EC remains underexplored. This section discusses several parameters of interest that may influence task-evoked EC estimations.

1.3.1 Impact of Data-Processing Variability on EC Estimates

Global signal regression (GSR) is a crucial preprocessing step for removing psychological noise (Power et al., 2017). However, its application remains controversial (Fox et al., 2009; Murphy & Fox, 2017; Power et al., 2017). While GSR improves the sensitivity to detect significant connectivity measures (Varikuti et al., 2017), this may also distort brain activations and connectivity measures in networks (Anderson et al., 2011; Murphy et al., 2009). Recent work (Almgren et al., 2020) suggests GSR showed a minor influence on resting-state EC estimates, while its impact on task-evoked EC remains unclear.

The general linear model (GLM) design is an essential step in modeling brain BOLD signals in response to task stimuli, utilizing the hemodynamic response function (Buxton et al., 2004). The block-based design groups similar events into blocks, optimizing the hemodynamic responses of the involved brain regions under the same experimental conditions (Logothetis, 2008). In contrast, the event-related design treats discrete events individually, analyzing brain responses to each event in isolation (Huettel, 2012). These designs may differentially affect task-evoked activation and FC (Friston et al., 1999; Liu et al., 2001) and DCM's model selections (Daunizeau et al., 2011). However, a direct comparison of task-evoked EC between these two designs has not been evaluated.

Significance thresholding is a critical step in fMRI analyses, substantially contributing to the variability of fMRI results (Botvinik-Nezer et al., 2020). Methodological variability in thresholding approaches (e.g., voxel-wise vs. cluster-corrected) may introduce uncertainty in generating task-evoked ROIs to estimate EC. For example, a stricter method may reduce false-positive voxels but risk excluding meaningful signals. However, the impact of thresholding variability on task-evoked EC estimates remains unexplored.

The activation contrasts isolate brain activation in response to specific task conditions, and its selection directly shapes task-evoked EC (Zeidman, Jafarian, Corbin, et al., 2019). Contrasts define the neural processes modeled in DCM, emphasizing distinct cognitive components. For instance, the incompatible contrast (Anti) isolates conflict-related processes, while the combined contrast (Anti+Pro) captures a general engagement during the SRC task. Varied contrasts define how experimental conditions impact EC estimates, highlighting distinct cognitive components (Zeidman, Jafarian, Corbin, et al., 2019). However, the selection of contrasts and its impact on task-evoked EC remains unclear.

In sum, the thesis aims to evaluate how analytical flexibility impacts EC reproducibility and provides evidence-based guidelines for robust network inference in task-fMRI.

1.4 Predictive Modeling of Brain-Behavior Relationships

A key goal of neuroimaging is to link individual brain dynamics to cognition, behaviors, or even clinical outcomes (Biswal et al., 2010; Huth et al., 2016). To achieve this goal,

machine learning approaches such as connectome-based predictive modeling have been applied to FC (Shen et al., 2017; Zhang et al., 2022; K. Zhao et al., 2023). These approaches have advanced our understanding of brain-behavior relationships by detecting stable connectivity fingerprints, which are predictive of individual differences in both healthy and clinical populations (Zhang et al., 2022; K. Zhao et al., 2023). However, while FC can capture undirected interdependencies between brain regions, its correlational calculation limits insights into dynamic causal interactions (Friston, 2011). This gap can be addressed by EC, which quantifies directed neural influences between regions (Friston, 2011; Friston et al., 2003) and has emerged as a promising framework for exploring brain-behavior relationships (Kahan & Foltynie, 2013; Zeidman, Jafarian, Corbin, et al., 2019). Nevertheless, two critical questions remain: (1) Do brain state-specific components of task-evoked EC (brain intrinsic vs. task-modulated) differentially predict individual behaviors and phenotypic traits? (2) Can large-scale resting-state EC analyses identify network-specific biomarkers for clinical outcomes? This section discusses these two questions below.

1.4.1 Individual Differences in Task-Evoked EC: Behavioral Relevance

Previous FC literature has suggested that task-evoked states may promote better prediction of individual traits and general cognitive abilities as compared to states during resting (Greene et al., 2018; Jiang et al., 2020; W. Zhao et al., 2023). This difference may be related to distinct characteristics between the two brain states (Greene et al., 2018). Compared to the unconstrained resting state (Buckner et al., 2013), where multiple brain states were jointly expressed (Leonardi et al., 2014), task-evoked states may have lower variability and amplify individual differences through task-related manipulation (Elton & Gao, 2015; Finn et al., 2017; Geerligs et al., 2015; Greene et al., 2018). However, a recent study (Kraljević et al., 2024) has suggested that this improvement may not be universal, raising a question about how specific brain states contribute to predicting individual behaviors and traits.

To address this question, DCM (Friston et al., 2003) may provide a suitable framework for analyzing state-specific (intrinsic and task-modulated) EC in task-evoked fMRI data. Intrinsic EC refers to the brain's inherent connectivity at baseline, while task-modulated EC reflects context-dependent connectivity driven by specific stimuli (Zeidman, Jafarian, Corbin, et al., 2019). While two types of EC have demonstrated notable

prediction accuracy in predicting individual phenotypes and task performance (Beck et al., 2021; Diersch et al., 2021), the lack of a direct comparison between the brain's intrinsic and task-modulated EC prevents determining whether state-specific neural dynamics uniquely contribute to behavioral predictions. Isolating brain intrinsic and task-modulated EC of task-evoked EC and examining their predictive performance may help clarify whether do intrinsic and task-modulated EC differentially predict individual behaviors and phenotypical traits?

1.4.2 Resting-State EC as a Biomarker for Childhood Maltreatment

Childhood maltreatment (CM), characterized by abuse modalities (physical, sexual, emotional) and neglect, is recognized as a critical psychological stressor (Gilbert et al., 2009). Individuals with a CM history exhibit a higher risk for psychiatric disorders like mood disorders and suicidal behaviors (Fuller-Thomson et al., 2016; Green et al., 2010; Merrick et al., 2017). To investigate the neurobiological effects of CM experiences, resting-state fMRI has become a powerful tool due to its simplicity in data acquisition, capacity to map multiple neural systems, and applicability to vulnerable populations (O'Connor & Zeffiro, 2019). Previous resting-state fMRI studies have identified aberrant FC in the salience network and DMN in individuals exposed to CM experiences, suggesting an association with mental disorders and socio-affective functioning (Gerin et al., 2023; Goetschius et al., 2020; Marusak et al., 2015). However, the correlational calculation of FC cannot reveal causal interaction information within networks, which can be addressed by EC (Friston, 2011). For example, a previous study (Kessler et al., 2020) explored EC to demonstrate that CM disrupted the inhibitory ability of the medial prefrontal cortex to the amygdala, suggesting that EC may have the potential to identify biomarkers in psychiatric disorders. Although EC can be used to reveal causal mechanisms, most EC studies have constrained network nodes within a limited number of nodes due to the computational demands of DCM (Frässle et al., 2018; Frässle et al., 2017). This approach may conflict with evidence that CM is associated with changes in complex and distributed large-scale networks (Teicher & Samson, 2016). The lack of large-scale network EC analyses may prohibit a comprehensive insight into large-scale networks and their predictive specificity with childhood trauma experiences.

1.5 Ethics Protocols

The study protocols for Studies 1 and 2 were approved by the ethics committee of the University Duisburg-Essen, Germany (reference number: 11-4678). Data usage from the 1000BRAINS project was additionally approved by the ethics committee of the University of Düsseldorf, Germany (reference number: 5193). The study protocol for Study 3 was approved by the ethics committee of the Affiliated Brain Hospital, Guangzhou Medical University, China (approval number: 2013 (074)). All studies were conducted in accordance with the Declaration of Helsinki.

1.6 Aims of Thesis

The thesis advances the study of EC by addressing gaps in methodology and prediction specificity between brain states and networks and formulating three research questions for the thesis. First, despite the wide range of applications of DCM, the lack of consensus on data processing pipelines and the impact on EC estimates remains poorly understood. I investigate how data processing parameters influence task-evoked EC estimates within the task-evoked SRC network. Second, given that distinct brain states (intrinsic vs. task-evoked states) may capture unique attributes relevant to behavioral and phenotypic prediction, I directly compare the predictive performance of intrinsic and task-modulated EC derived from task-evoked DCM in explaining individual differences in age and RT during the SRC task. Third, the computational constraints of traditional DCM limited large-scale resting-state EC estimation and thereby precluded insights into network-specific biomarkers of clinical outcomes such as childhood trauma exposure. I address this by utilizing the rDCM to infer whole-brain and network-specific resting-state EC and compare its ability to predict childhood trauma exposure across large-scale cortical networks.

1.6.1 Study 1: Impact of Data Processing Parameters on EC

The research first systematically evaluated how data-processing parameters affect task-evoked EC estimates of DCM within the SRC network derived from the 1,000BRAINS project (Caspers et al., 2014). Aligning with previous literature (Cieslik et al., 2010; Langner et al., 2015), nine network nodes were defined based on incompatibility-related activations (incompatible > compatible conditions): the anterior mid-cingulate cortex (aMCC), and bilateral IPS, DLPFC, AI, and premotor cortex (PMC). As

aforementioned, we then specifically investigated four data-processing parameters: (1) regression of global signals (with vs. without GSR), (2) GLM designs (event-related vs. block-based), (3) activation contrasts (Anti vs. Anti+Pro), and (4) significance thresholding (cluster-corrected vs. voxel-wise thresholds). Through comprehensive comparisons of EC strength variations (Zeidman, Jafarian, Seghier, et al., 2019) and parameter certainty (Zeidman, Kazan, et al., 2019) between conditions of each parameter, our findings demonstrated that methodological variability significantly modulates EC characteristics within an SRC network, providing methodological recommendations for further EC analyses. By addressing these gaps through a systematic approach, this thesis aims to provide a comprehensive empirical framework for understanding the impact of analytical choices on EC and its utility in predicting individual differences.

1.6.2 Study 2: Dissecting Brain State-Specific EC for Behavioral Prediction

Building on methodological perspectives, this study examines whether brain state-specific connectivity differentially predicts individual behaviors. The research further evaluated whether intrinsic and task-modulated EC better predict individual characteristics, focusing on individual age and RT during an SRC task. Using task-evoked DCM, we distinguished intrinsic EC (represented by matrix A) and task-modulated EC (represented by matrix B) to assess their predictive capabilities. The analysis explored how variations in GLM designs, cross-validation schemes, predictive models, and the application of Bayesian model reduction influenced the comparative performance of these EC components. Results reveal that intrinsic and task-modulated EC capture distinct aspects of age and RT, with GLM design choices significantly impacting their predictive performance. These findings remained robustly consistent across different cross-validation schemes and predictive models and were less affected by the inclusion of the Bayesian model reduction. The study highlights the significance of methodological considerations in understanding the relationship between the brain's intrinsic and task-modulated connectivity patterns and individual characteristics.

1.6.3 Study 3: Identifying Network Biomarkers of Childhood Trauma via Resting-State EC

This study shifts its focus to resting-state EC and networks, assessing the prediction

accuracy of whole-brain and network-specific EC in predicting individual characteristics, particularly CM scores. Resting-state fMRI data were acquired for 8 minutes. The Schaefer atlas (100 parcels) (Schaefer et al., 2018; Yeo et al., 2011) is utilized to reconstruct large-scale networks. Using rDCM within the Schaefer atlas framework, whole-brain and network-specific resting-state EC is estimated, and its predictive capabilities are evaluated. The research also examined how variations of feature selection thresholds and predictive models impacted the comparative performance of each prediction case. The results revealed that resting-state EC within the DMN consistently demonstrated significant predictive power in CM scores, indicating a critically important role of the DMN in CM.

Study 1: Impact of data processing varieties on DCM estimates of effective connectivity from task-fMRI

Shufei Zhang^{1,2}, Kyesam Jung^{1,2}, Robert Langner^{1,2}, Esther Florin³, Simon B. Eickhoff^{1,2}, Oleksandr V. Popovych^{1,2}

¹Institute of Neuroscience and Medicine, Brain and Behaviour (INM-7), Research Centre Jülich, Germany

²Institute for Systems Neuroscience, Medical Faculty, Heinrich-Heine University Düsseldorf, Germany

³Institute of Clinical Neuroscience and Medical Psychology, Medical Faculty, Heinrich-Heine University Düsseldorf, Germany

*Corresponding author: o.popovych@fz-juelich.de

Published in Human Brain Mapping, 2024;45:e26751.

<https://doi.org/10.1002/hbm.26751>



Own contributions

Writing the manuscript, preparing figures, performing data analyses, and contributing to the interpretation of results.

RESEARCH ARTICLE

WILEY

Impact of data processing varieties on DCM estimates of effective connectivity from task-fMRI

Shufei Zhang^{1,2} | Kyesam Jung^{1,2} | Robert Langner^{1,2} | Esther Florin³  | Simon B. Eickhoff^{1,2} | Oleksandr V. Popovich^{1,2} 

¹Institute of Neuroscience and Medicine, Brain and Behaviour (INM-7), Research Centre Jülich, Jülich, Germany

²Institute for Systems Neuroscience, Medical Faculty, Heinrich-Heine University Düsseldorf, Düsseldorf, Germany

³Institute of Clinical Neuroscience and Medical Psychology, Medical Faculty, Heinrich-Heine University Düsseldorf, Düsseldorf, Germany

Correspondence

Oleksandr V. Popovich, Institute of Neuroscience and Medicine, Brain and Behaviour (INM-7), Research Centre Jülich, Jülich, Germany.
Email: o.popovich@fz-juelich.de

Funding information

Horizon 2020 Framework Programme, Grant/Award Numbers: 826421, 945539; DFG, Grant for open access publication, Grant/Award Number: 491111487

Abstract

Effective connectivity (EC) refers to directional or causal influences between interacting neuronal populations or brain regions and can be estimated from functional magnetic resonance imaging (fMRI) data via dynamic causal modeling (DCM). In contrast to functional connectivity, the impact of data processing varieties on DCM estimates of task-evoked EC has hardly ever been addressed. We therefore investigated how task-evoked EC is affected by choices made for data processing. In particular, we considered the impact of global signal regression (GSR), block/event-related design of the general linear model (GLM) used for the first-level task-evoked fMRI analysis, type of activation contrast, and significance thresholding approach. Using DCM, we estimated individual and group-averaged task-evoked EC within a brain network related to spatial conflict processing for all the parameters considered and compared the differences in task-evoked EC between any two data processing conditions via between-group parametric empirical Bayes (PEB) analysis and Bayesian data comparison (BDC). We observed strongly varying patterns of the group-averaged EC depending on the data processing choices. In particular, task-evoked EC and parameter certainty were strongly impacted by GLM design and type of activation contrast as revealed by PEB and BDC, respectively, whereas they were little affected by GSR and the type of significance thresholding. The event-related GLM design appears to be more sensitive to task-evoked modulations of EC, but provides model parameters with lower certainty than the block-based design, while the latter is more sensitive to the type of activation contrast than is the event-related design. Our results demonstrate that applying different reasonable data processing choices can substantially alter task-evoked EC as estimated by DCM. Such choices should be made with care and, whenever possible, varied across parallel analyses to evaluate their impact and identify potential convergence for robust outcomes.

KEYWORDS

analytical flexibility, global signal regression, MRI data processing, stimulus–response compatibility, task-evoked effective connectivity

This is an open access article under the terms of the [Creative Commons Attribution](https://creativecommons.org/licenses/by/4.0/) License, which permits use, distribution and reproduction in any medium, provided the original work is properly cited.

© 2024 The Author(s). *Human Brain Mapping* published by Wiley Periodicals LLC.

1 | INTRODUCTION

One of the main approaches to studying the human brain consists in representing it as a collection of complex networks involving sets of brain areas engaged in different functions and continuously sharing information within and between the networks (van den Heuvel & Hulshoff Pol, 2010). In the framework of functional connectivity (FC), brain areas showing high temporal co-activations are defined as functional networks during tasks or resting state (Menon, 2011). Both task-evoked and resting-state FC of functional magnetic resonance imaging (fMRI) have shown high similarities to each other as reported by several papers (Beheshtian et al., 2021; Cole et al., 2014; Cole et al., 2016; Heckner et al., 2021), see also a recent review (Bernstein-Eliav & Tavor, 2024). Withal, the current FC studies frequently focused on the resting state (Greene et al., 2018), which has widely been used to investigate brain organization (Eickhoff et al., 2018; Yeo et al., 2011) and brain-behavior relationships (Biswal et al., 2010; Shen et al., 2017). However, the lack of external reference time points (e.g., stimulus onsets) and the absence of control over mental processes (Cole et al., 2016) as well as the typical FC calculation approach (Pearson correlation) limit the application of resting-state FC to dynamic interactions evoked by contextual modulation.

Task-evoked effective connectivity (EC) is supposed to estimate the directional or causal information flow among network nodes modulated by task demands (Friston et al., 2003). For this purpose, the dynamic causal modeling (DCM) approach was developed and is firmly established in neuroimaging research (Frässle et al., 2017; Frässle et al., 2018; Friston et al., 2014). Task-evoked EC estimated by DCM was shown to reflect the interregional directional information flows (Friston, 2011; Friston et al., 2003; Menon, 2011; Menon & Uddin, 2010) and has been linked to human cognitive and executive performance in tasks such as finger tapping, working memory, response conflict resolution, reading, and so forth (Boudrias et al., 2012; Cieslik et al., 2011; Jung et al., 2018; Kahan et al., 2019; Loehrer et al., 2016; Morken et al., 2017; Volz et al., 2015).

Despite the success and relevance of DCM-based estimates of EC, the impact of variations in data processing parameters on DCM outcomes has not consistently been addressed. For task-evoked brain activity, it has been demonstrated that the present analytical flexibility in the field can have substantial effects on the reported results and, thus, on the reproducibility of neuroimaging findings (Botvinik-Nezer et al., 2020; Carp, 2012). Similarly, the influence of data processing varieties has also been a topic of intense discussion in studies on FC (Cole et al., 2010; Power et al., 2014; Power et al., 2017; Smith et al., 2013). However, issues and challenges of analytical flexibility in estimating task-evoked EC have rather been neglected so far and call for further investigation. Here we therefore focus on four important aspects of data processing in a typical DCM analysis.

The preprocessing of fMRI data concentrates on the cleaning of the acquired data from noise, which is essential for an appropriate extraction of the signals (Churchill et al., 2015). Typically, the cleaning includes several steps such as slice-timing correction (Parker & Razlighi, 2019; Sladky et al., 2011), motion correction (Friston

et al., 1996; Yan et al., 2013), nuisance regression (Liu et al., 2017; Power et al., 2017), temporal filtering (Davey et al., 2013), and spatial smoothing (Friston et al., 2000). Of these, global signal regression (GSR) has received much attention as a nuisance variable with a substantial impact on estimates of FC (Murphy & Fox, 2017) and will therefore be examined for its influence on task-evoked EC in this study. In particular, GSR has been thought to remove physiological noise (Power et al., 2017) and help to detect significant FC (Fox et al., 2009; Varikuti et al., 2017). However, the application of GSR is controversial and may potentially distort activation and connectivity measures in the network-specific ways (Anderson et al., 2011; Glasser et al., 2018; Murphy et al., 2009; Saad et al., 2012). Furthermore, the impact of GSR on resting-state FC was often assumed to be major (Murphy & Fox, 2017), while GSR was recently shown to have only a minor influence on resting-state EC estimations (Almgren et al., 2020). As its impact on task-evoked EC has remained unclear, we investigated it in the present study.

Another important methodological issue pertains to the question of which design of the general linear model (GLM) is optimal for subsequently analyzing task-evoked EC. According to presentations and types of task stimuli, block- and event-related designs have been used to model brain blood-oxygen-level-dependent (BOLD) signals to task events by convoluting the temporal function of their occurrence with the hemodynamic response function (HRF) (Buxton et al., 2004). The block-based design aggregates multiple (similar) events into blocks to maximize hemodynamic responses of engaged brain regions during the same experimental conditions (Logothetis, 2008). The event-related design models discrete events separately from each other and analyzes brain responses to individual events independently (Huetzel, 2012). The choice of GLM design has not only been shown to impact task-evoked activation and FC (Friston et al., 1999; Liu et al., 2001), but also the model selection in DCM (Daunizeau et al., 2011). However, the immediate impact of GLM design type (block- vs. event-related) on task-evoked EC has not been explored yet, which is why we addressed it in this study.

Besides the type of design, there are at least two more factors in the analysis of task-fMRI data that may influence EC estimates derived from DCM: significance thresholding of voxels at the level of individual subjects and the choice of activation contrast of interest. The selection of significance thresholding methods at the group level impacted the data-analytical stability of fMRI results (Botvinik-Nezer et al., 2020; Roels et al., 2015). However, the significance thresholding at the individual level and its impact on task-evoked EC have not appropriately been discussed yet. The activation contrast indicates the brain activation driven by a specific task condition and reflects the context-dependent task-evoked EC (Zeidman, Jafarian, Corbin, et al., 2019). Previous studies have already demonstrated that DCM estimated different task-evoked modulatory EC (M-EC) with selected network nodes if various contrasts were specified as modulatory inputs (Kuhnke et al., 2021; Ma et al., 2014). However, it is still unknown how M-EC is statistically changed when different contrasts are considered for time series extraction and used to define the modulatory inputs in DCM analyses.

Based on these considerations, our study aimed to investigate the impact of GSR, GLM design, significance thresholding, and activation contrasts on task-evoked EC. The main objective was to illustrate how important choices made during data processing can influence the results of the task-evoked fMRI analysis and DCM estimations of the task-based EC on an example of the stimulus–response compatibility (SRC) task (Fitts & Deininger, 1954). The workflow included several steps: (1) preprocessing task-evoked images and reconstructing the SRC network nodes with different conditions of data processing (GSR and GLM designs); (2) extracting the respective BOLD time series from the SRC network nodes for individual subjects under different conditions with respect to GSR, GLM design, significance thresholding, and activation contrasts; (3) calculating the individual and group-averaged task-evoked EC patterns for each data processing condition; and (4) evaluating between-group differences in task-evoked EC as well as relative differences in EC parameter certainty between any two conditions of the data processing (with vs. without GSR, event-related vs. block-based designs, corrected vs. uncorrected thresholding, and whole task vs. incompatible contrasts). We show that different data processing choices result in substantially different task-evoked EC at the group level, especially for the factors of GLM design and activation contrast. The obtained results could be of relevance for evaluating analytical flexibility in task-evoked EC estimations.

2 | METHODS

2.1 | Participants and fMRI data

Our study included an initial sample of 271 subjects (148 males, 123 females, 18–85 years old, mean age: 52.3 ± 16.6 years) recruited from the subject pool of the 1000BRAINS project (Caspers et al., 2014), which was conducted at the Research Centre Jülich. Before MRI data collection, the written informed consent of each subject was acquired. The study protocol was approved by the health care ethics committee of the University Duisburg-Essen (reference number: 11-4678). The study was approved by the local ethics committee and performed in accordance with the declaration of Helsinki.

Details about fMRI data included in the 1000BRAINS project can be found elsewhere (Caspers et al., 2014). In the present study, only selected structural MRI (sMRI) and task-based fMRI (t-fMRI) data were used for analyses. Both sMRI and fMRI datasets were acquired on a 3-T Siemens scanner (Tim-TRIO, Siemens Medical System, Erlangen, Germany). The sMRI scans were obtained using an anatomical 3D T1w MPRAGE sequence with the following parameters: repetition time (TR) = 2.0 s, echo time (TE) = 3.03 ms, flip angle = 9° , 176 sagittal slices, field of view = $256 \times 256 \text{ mm}^2$, voxel resolution = $1 \times 1 \times 1 \text{ mm}^3$. The t-fMRI dataset was scanned by gradient-echo echo-planar imaging sequence with the following parameters: TR = 2.03 s, TE = 30 ms, flip angle = 80° , field of view = 200 mm, 33 axial slices (ascending), slice thickness = 3.3 mm, inter-slice gap = 0.66 mm, voxel resolution = $3.1 \times 3.1 \times 3.3 \text{ mm}^3$, acquisition time = 27 min, and 10 s.

2.2 | Experimental protocol

The present study followed the standard spatial SRC paradigm (Fitts & Deininger, 1954). In particular, participants were required to respond to lateralized visual stimuli by pressing an ipsilateral or contralateral button as correctly and fast as possible (Figure 1). The whole experiment had 24 blocks and consisted of incompatible (Anti) and compatible (Pro) conditions. The Anti-condition required participants to react to the lateralized stimulus by pressing the opposite button, while the Pro-condition required participants to press the ipsilateral button. Before one block started, a 2-s instruction was presented to indicate the condition (incompatible or compatible) of the following block. Each block contained 13 to 16 trials, in which filled circles (see Figure 1) were presented for 0.2 s either on the left or right side of the screen with an equal probability (50%) to be on either side. The time intervals between event onsets were uniformly jittered from 2 to 4.5 s. The rest periods between blocks were randomly jittered by a uniform distribution ranging from 15 to 19 s. Either experimental condition was covered in 12 blocks, which were presented in a pseudo-randomized order with a stochastic paradigm.

2.3 | Preprocessing

The sMRI and fMRI images were preprocessed using functions from FSL (Jenkinson et al., 2012), ANTs (Tustison et al., 2014), Workbench (Glasser et al., 2013), and AFNI (Cox, 1996) software packages.

The sMRI preprocessing included the following steps: (1) reorientation and cropping (functions *fslreorient2std* and *robustfov*) (Glasser et al., 2013), (2) AC-PC alignment (*flirt*) (Glasser et al., 2013), (3) brain extraction (*antsBrainExtraction*) (Esteban et al., 2019; Tustison et al., 2010), (4) tissue segmentation of gray matter (GM), cerebrospinal fluid (CSF), and white matter (WM) (*fast*) (Zhang et al., 2001), and (6) nonlinear spatial normalization (*antsRegistration*) (Avants et al., 2008).

The fMRI module included the following steps: (1) removal of four dummy volumes (*fslroi*); (2) two-pass head-motion correction, which

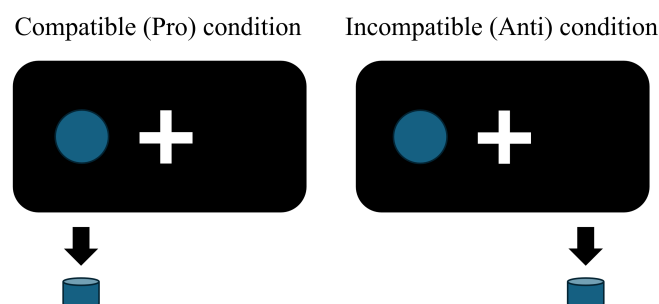


FIGURE 1 Schematic illustration of the spatial stimulus–response compatibility (SRC) task. A lateral stimulus on the screen (blue circle) called for a button press either on the ipsilateral or contralateral side, which is referred to as compatible (Pro) or incompatible (Anti) experimental condition, respectively.

initially realigned all time points to the first volume, and subsequently to the averaged realigned volumes (*mcflirt*) (Jenkinson et al., 2002); (3) intensity normalization (scaled to 10,000; *fslmaths*); (4) co-registration between the averaged functional volume and structural images (*antsRegistration*) (Avants et al., 2008); (5) functional normalization using the structural normalization matrix (*antsApplyTransForms*); (6) spatial smoothing with an 8-mm full-width at half-maximum Gaussian kernel (*wb_command*) (Glasser et al., 2013); (7) regression of 27 nuisance regressors comprising 24 motion parameters (Friston et al., 1996) as well as the global signal of the whole brain, WM, and CSF (*fsl_glm*), and 8) high-pass temporal filtering (cut-off at 128 s, *fslmaths*) (<https://fsl.fmrib.ox.ac.uk/fsl/fslwiki/>). To study the impact of GSR, we applied an alternative pipeline without GSR in step 7 and regressed out only the other 26 regressors.

Our pipeline of data preprocessing mainly included specific functions of FSL, AFNI, and ANTs software, and selected functions were recommended by previous literature (Carp, 2012) as well as tested on the used dataset for high-quality data processing. Our choice of structural and functional preprocessing modules was based on recommendations of HCP and fMRIPrep pipelines (Esteban et al., 2019; Glasser et al., 2013), and applied a FEAT-based statistical approach of FSL for extracting activation contrasts (Woolrich et al., 2004).

After a quality check of all preprocessing steps, 5 subjects were excluded because of bad quality in the spatial normalization, and 266 subjects were included in the subsequent analyses.

2.4 | First-level fMRI statistics

To model brain activation in response to task conditions as reflected by the dynamics of BOLD signals, we considered both event-related and block-based designs of the GLM (Woolrich et al., 2004) (*FSL/film_gls*). Our experimental protocol was designed in a way such that the BOLD signal could be modeled at the level of individual trials or blocks, and the experimental conditions of interest were modeled in the GLM in three different ways (1) event-related model using all trials (All-Trials), (2) event-related model using only “successful” trials (i.e., trials with correct responses; S-Trials), or (3) blocked design (Blocks). Thus, both All-Trials and S-Trials cases represent event-related designs, but the S-Trials design excluded the error trials, where subjects gave incorrect responses to stimuli (i.e., wrong response lateralization) or responded too fast or too slowly (reaction time, $RT < 150$ ms or $RT > 1500$ ms) or did not respond at all. The trials were considered in the framework of a given activation contrast of the investigated compatible/incompatible experimental conditions, see below. The explanatory variables of the event-related GLM included the on-off step functions starting at the onset time of each trial with a fixed “on” duration of 0.2 s of the stimulus length (an example can be seen in Supplementary Figure S1). The block-based GLM, in turn, used the starting time and full length of each of the 24 experimental blocks as onset and duration times, respectively, of the step function of the explanatory variables. The event-related design had four regressors of interest comprising compatible and incompatible conditions with right- and left-sided stimulus

presentation, respectively, while the block-based design had only two regressors representing compatible and incompatible blocks of trials.

After task designs had been specified, the double-gamma HRF and their temporal derivatives were modeled to estimate whole-brain voxel-wise BOLD responses to the abovementioned task events (Woolrich et al., 2004). We also included temporal derivatives of the task regressors in the GLM design matrix to accommodate slight variations in the timing of the HRF across the brain and improve the fit of the data (Woolrich et al., 2004).

After model estimation, we computed four task contrasts: incompatible condition (Anti), compatible condition (Pro), incompatible versus compatible condition (Anti > Pro) (subtracted contrasts, Anti - Pro), and incompatible + compatible condition (Anti + Pro) (sum contrasts) in all GLMs (an example can be seen in supplementary Figure S1). The Anti - Pro contrast aims to detect brain regions that are more sensitive to the Anti-condition than to the Pro-condition, whereas the Anti + Pro contrast aims to detect brain regions responding to either experimental condition.

2.5 | Second-level fMRI statistics

To reconstruct the brain network activated during the SRC task at the group level, we calculated second-level fMRI statistics for our different experimental designs using the *FSL/randomize* tool. The SRC paradigm aims to elucidate brain activity related to solving response conflicts arising from spatial incompatibility, which is why the Anti-Pro contrast would be the most appropriate for network detection that was activated stronger at the spatial incompatibility condition, as compared to the other contrasts discussed. For reconstructing the incompatibility-related brain network, the following steps were performed during the second-level analysis of the fMRI data: (1) Contrast maps (Anti > Pro) of individual subjects were merged into 4D images for all subjects, and a one-sample permutation test (Winkler et al., 2014) was conducted 10,000 times for All-Trials, S-Trials, and Blocks designs separately. (2) Threshold-free cluster enhancement (TFCE) with family-wise error (FWE) correction (Smith & Nichols, 2009) was applied for dealing with the issue of multiple comparisons ($p_{TFCE+FWE} < 0.05$). This resulted in several clusters of brain voxels demonstrating significantly stronger responses during the Anti-condition than during the Pro-condition (significant positive differences between Anti and Pro conditions) across subjects. The second-level statistical maps are illustrated in Figure 2 for all three GLM designs with GSR; the cases without GSR are illustrated in Supplementary Figure S2.

2.6 | Task-evoked network and individual time series extraction

After the second-level fMRI statistics were completed, the local maxima of the group-level Anti-Pro contrast map were identified using the SPM 12 (v7219) package (<http://www.fil.ion.ucl.ac.uk/spm/>). Consistent with previous literature (Cieslik et al., 2010; Langner

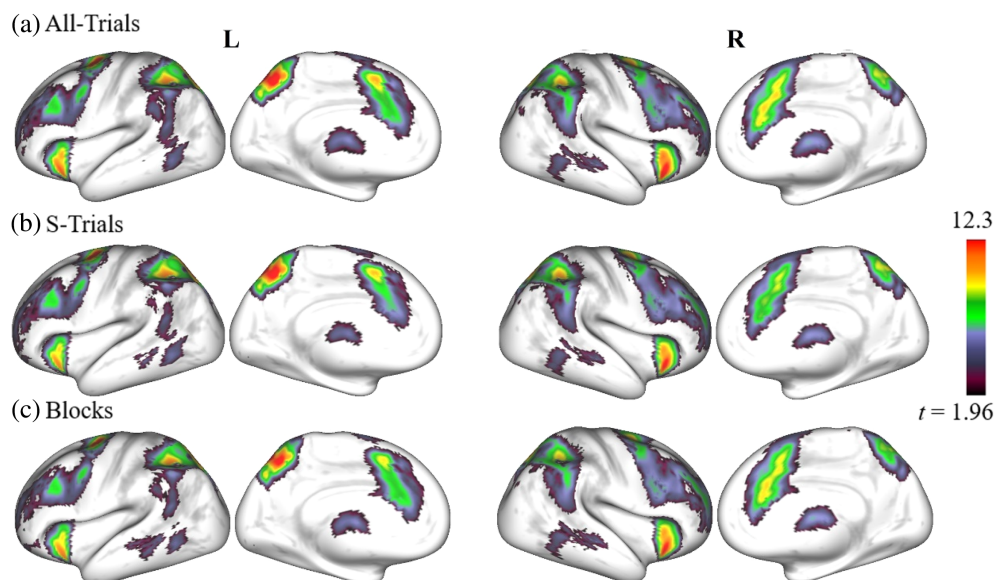


FIGURE 2 Results of the second-level functional magnetic resonance imaging (fMRI) analysis with different general linear model (GLM) designs: (a) All-Trials, (b) S-Trials, and (c) Blocks designs (see text for details). All maps illustrate the t -values (scaling is given in the color bar) of the t tests reflecting the statistically significant voxels across all subjects ($p_{\text{TFCE}+\text{FWE}} < 0.05$) of the contrast difference between incompatible and compatible experimental conditions (Anti > Pro contrast). For visualization, each thresholded statistical map was projected to fs_LR 32k surfaces (<https://www.humanconnectome.org/software/connectome-workbench>). Used notations: L/R, left/right hemisphere; All-/S-Trials, experimental designs with all/successful trials; Blocks, experimental designs modeled by blocks; TFCE, threshold-free cluster enhancement; FWE, family-wise error.

TABLE 1 MNI peak coordinates (x, y, z) of the local maxima of t -values based on the second-level fMRI statistics of the Anti-Pro contrast with global signal regression.

Peak	All-Trials				S-Trials				Blocks			
	x	y	z	t	x	y	z	t	x	y	z	t
LDLPFC	-40	22	28	7.2	-44	22	30	7.0	-40	22	28	6.9
RDLPCF	36	30	28	6.7	36	30	28	6.7	36	26	24	5.9
LPMC	-24	-8	48	16.3	-24	-8	48	16.6	-24	-8	48	15.2
RPMC	24	-8	48	11.1	24	-8	48	11.4	24	-6	48	10.3
LIPS	-34	-46	38	11.1	-34	-46	38	11.0	-34	-46	38	10.9
RIPS	36	-44	40	10.7	36	-44	40	11.1	36	-44	40	10.2
LAI	-30	18	-10	12.1	-30	18	-10	11.0	-32	18	-10	11.6
RAI	30	20	-4	13.5	30	20	-4	13.0	30	20	-6	12.6
AMCC	-2	8	46	10.4	-4	6	46	10.0	0	8	48	9.7

Note: Used notations: All-/S-Trials, experimental designs with all trials or only successful trials; Blocks, experimental designs modeled by blocks. Bold values are statistically significant.

Abbreviations: AI, anterior insula; AMCC, anterior midcingulate cortex; DLPFC, dorsolateral prefrontal cortex; IPS, intraparietal sulcus; L/R, left/right; PMC, premotor cortex.

et al., 2015), we detected 9 regions of the task-evoked brain network as major constituents: anterior midcingulate cortex (AMCC), bilateral intraparietal sulcus (IPS), premotor cortex (PMC), dorsolateral prefrontal cortex (DLPFC), and anterior insula (AI). These brain regions were selected to reconstruct the SRC network for the Anti-Pro contrast. The Montreal Neurological Institute (MNI) peak coordinates of the second-level statistical maps and the corresponding t -values are given in Table 1 for all three GLM designs after GSR. Examples of the spheres (10-mm radius) encircled around the corresponding peaks and

representing the SRC network nodes (regions of interest [ROI]) are illustrated in Figure 3a.

MNI peak coordinates without GSR can be seen in Supplementary Table S1.

After SRC networks were reconstructed for the considered conditions of GLM designs and GSR, we focused on the extraction of BOLD signals of the network nodes reflecting the task-evoked activity of individual subjects. The steps performed for time series extraction were the following:

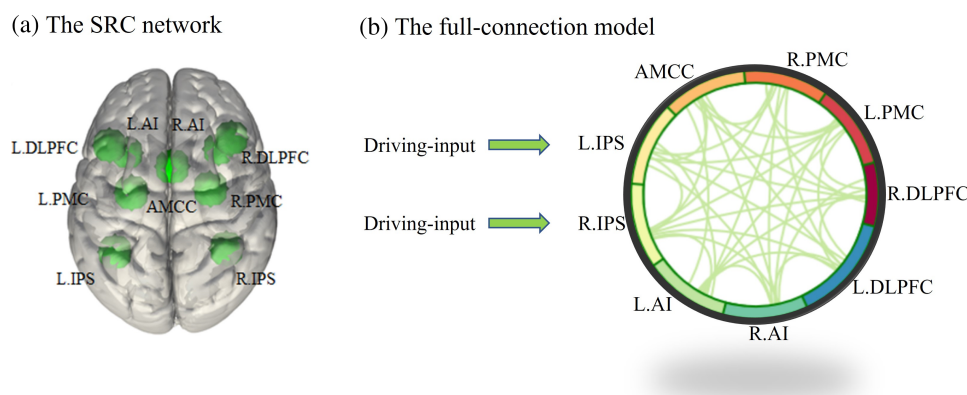


FIGURE 3 Illustration of the stimulus-response compatibility (SRC) network. (a) An example SRC network with nine nodes for the event-related general linear model design, where the peak coordinates from Table 1 are encircled by spheres of a 10-mm radius. (b) The corresponding full-connection model used in dynamic causal modeling (DCM), see text for the node abbreviations. LIPS and RIPS are the driving-input nodes receiving external (visual) stimuli of the task, while all connections inside the SRC network are bidirectional. Used notations: L/R, left/right; DLPFC, dorsolateral prefrontal cortex; PMC, premotor cortex; IPS, intraparietal sulcus; AI, anterior insula; AMCC, anterior midcingulate cortex.

1. The group-level SRC network nodes (group-level node ROIs: spheres of 10 mm radius centered at the peak coordinates from Table 1, see Figure 3a) were overlaid with thresholded contrast maps of individual subjects.
2. The local maxima and the corresponding voxel coordinates of the individual contrasts were searched for in the intersection between the group-level node ROIs and individual thresholded maps.
3. For each network node, the detected coordinates of the individual local maxima were selected as centers of individual spheres with a 4-mm radius, and these spheres were then considered as network nodes for individual subjects (subject-level node ROIs).
4. Within every subject-level node ROI, only voxels masked according to the individual thresholded contrast maps (see step 1) were considered, while the other voxels under the threshold were excluded. Then, the first eigenvariate was extracted from the BOLD signals of the masked significant voxels for every individual network ROI by using FSL/*fslmeants* and considered as time series of individual network nodes.

In step 1, we did not use the fixed network ROIs as observed at the group level but overlaid them with the thresholded contrast maps of individual subjects to ensure that the voxels used to summarize individual signals represented the task effects rather than irrelevant noise processes. If there was no overlap between individual thresholded contrast maps and the group-level network ROIs, the respective subject was excluded from further analyses, as an empty intersection would lead to incomplete network reconstruction and BOLD extraction for individual subjects. As expected, the selected kind of significance thresholding of individual contrast maps strongly influenced the amount of overlap between individual activation clusters and group-level SRC network nodes, with stricter thresholding reducing the sample size available for subsequent DCM analyses. Here, we applied two thresholding approaches to the considered contrasts for individual subjects with different levels of strictness: voxel-

wise thresholding with uncorrected $p < .05$ and cluster-wise corrected $p < .05$ approaches, which we subsequently refer to as uncorrected and corrected thresholding, respectively. For the latter approach, cluster-level inference was used to define contiguous voxels of individual thresholded maps by using FSL/*cluster*.

For the extraction of individual BOLD signals, four contrasts were considered in this study as candidates for voxel masking: Anti, Pro, Anti + Pro, and Anti - Pro. Since the current study was focused on task-evoked EC within the brain network showing incompatibility effects, we discarded the Pro contrast. Although we observed strong group-based incompatibility effects as reflected by high t -values of the second-level statistics of the Anti-Pro contrast (Table 1 and Figure 2), individual Anti - Pro contrast maps did not display such a clear and pronounced activation (an example can be seen in Supplementary Figure S1). We found that individual Anti - Pro contrasts yielded rather sparse and weak activation maps after significance thresholding such that many subjects did not qualify for further analyses as their individual thresholded Anti - Pro contrast maps failed to overlap with the group-level SRC network nodes. Aimed at the consideration of relatively large samples, we then discarded the Anti - Pro contrast from further analysis. Hence, we applied the thresholding schemes mentioned above to individual Anti and Anti + Pro contrast maps for time series extraction for individual subjects (see Supplementary Figure S1). Therefore, four kinds of thresholded contrast maps were considered for individual time series extraction in this study: corrected Anti, corrected Anti + Pro, uncorrected Anti, and uncorrected Anti + Pro. Summary information on the participant samples that were included in subsequent analyses, after subject exclusions discussed above, can be found in Table 2 for the different contrasts and GLM designs with GSR (see Supplementary Table S2 for conditions without GSR).

The considered conditions of the data processing can be summarized as follows: (1) two GSR conditions, where the whole-brain global signal was either regressed out or not (i.e., with or without GSR);

TABLE 2 Sample sizes for different conditions of the data processing with GSR.

	All-Trials		S-Trials		Blocks	
	Corrected	Uncorrected	Corrected	Uncorrected	Corrected	Uncorrected
Anti	149/148	210/208	136/136	207/203	160/158	213/205
Anti + Pro	164/164	215/212	149/148	206/201	173/171	216/210

Note: The two subject numbers given in each table cell correspond to the subject samples qualified for BOLD signal extraction for SRC network nodes of individual subjects/explained variance (EV) criterion of DCM, see Sec. 2.6/Sec. 2.7 for details. Used notations: GSR, global signal regression; All-/S-Trials, experimental designs with all/successful trials; Blocks, experimental designs modeled by blocks; Anti, incompatible contrast; Anti + Pro, incompatible + compatible contrast.

(2) three GLM designs (i.e., All-Trials, S-Trials, and Blocks); (3) two individual first-level brain activation contrasts of Anti and Anti + Pro used for BOLD signal extraction for SRC network nodes of individual subjects; and (4) two thresholding approaches for the individual contrasts based on either voxel-level uncorrected $p_{\text{uncorr}} < 0.05$ or on cluster-wise corrected $p_{\text{corr}} < 0.05$ thresholding. These conditions resulted in $2 \times 3 \times 2 \times 2 = 24$ cases of data processing investigated in this study.

2.7 | Dynamic causal modeling

The present study evaluated task-evoked EC within the SRC network via a two-level DCM analysis (Zeidman, Jafarian, Seghier, et al., 2019) as implemented in SPM 12 (<https://www.fil.ion.ucl.ac.uk/spm/>). The DCM approach consists of approximating the neural mass dynamics z (t) by the following system of differential equations:

$$\frac{dz}{dt} = \left(A + \sum_k B^{(k)} u_k(t) \right) z + C u(t)$$

where the matrices A and $B^{(k)}$ stand for parameters of intrinsic and task-modulated connectivity, respectively, and $u_k(t)$ encodes the timing of the experimental condition k . Matrix C represents the influence of all external experimental inputs (stimulation) $u(t)$ on the neural dynamics of the considered ROIs.

At the first level, the DCM approach (Friston et al., 2003) was used to estimate the network-based EC between the nodes of the SRC networks using the individual BOLD time series of the corresponding ROIs of individual subjects. The standard DCM analysis involves several parameters (Friston et al., 2003): (1) driving input that models external (e.g., visual) input to the network and forces the activity of the network nodes, and the input matrix C that defines the immediate influence of the driving input on the selected network nodes; (2) intrinsic connectivity (matrix A) that denotes task-independent baseline connections among the nodes; and (3) modulatory connectivity (matrix B_j) induced by the experimental (task-dependent) condition decoded by variable u_j in the above equation and the respective cognitive processes. We also note that the u -variables were not mean-centered in the model, which allows us to interpret the A matrix as an intrinsic connectivity matrix, whereas all modulatory effects on EC due to experimental conditions

are summarized in matrix B , as mentioned above (Zeidman, Jafarian, Seghier, et al., 2019).

One may observe that GLM designs (event-related or block-based) influence the activation contrast estimation and also the formulation of driving and modulatory inputs in the DCM model specification. For a consistent formulation of the driving and modulatory task-dependent inputs to DCM, we followed the same formulation style throughout the GLM design, time series extraction for individual subjects, and DCM analysis (Supplementary Figure S3). For example, if the condition of the event-related design and Anti contrast were considered for fMRI analysis and BOLD signal extraction, the driving and modulatory stimuli of DCM would also be event-related, and the task-evoked M-EC would be driven by Anti trials only.

For investigating the impact of data processing parameters on task-evoked EC within the SRC network, a full-connection model was considered to be a good candidate (Tuominen et al., 2023). In the SRC network considered here, the IPS nodes were considered to act as hubs of sensorimotor integration during visually guided actions (Anderson et al., 2014), and the bilateral IPS nodes were thus selected as the driving-input nodes receiving external (visual) input (Figure 3b). To compare the impact of the data processing conditions introduced above on the task-evoked EC, we considered 24 DCM cases for every combination of data processing conditions mentioned above.

During the first-level DCM analysis, where EC was estimated for individual subjects, we also evaluated the quality of the modeling and calculated the fraction of variance of empirical BOLD signals that can be explained by the variance of the simulated BOLD signals generated by the optimized models (i.e., for optimized connectivity matrices aimed at the best fit between empirical and simulated BOLD signals). In line with the literature (Zeidman, Jafarian, Corbin, et al., 2019), we applied a 10% threshold of the explained variance as a criterion for our subjects to qualify for DCM analysis. As a result, up to nine subjects had to be excluded from further analysis from those participants already qualified for BOLD extraction from the SRC network nodes of individual subjects, with the exact number depending on the selected data processing condition (see Table 2 and Supplementary Table S2).

For the second-level DCM analysis, a parametric empirical Bayes (PEB) framework (Zeidman, Jafarian, Seghier, et al., 2019) was used to estimate the DCM parameters for group-level EC. The PEB model can decompose the subject-wise variability of EC into group effects and additive random effects (Friston et al., 2016). We adopted a two-step

PEB scheme involving single-group and between-group analyses (Zeidman, Jafarian, Seghier, et al., 2019). In the first step, we used the single-group PEB analysis to investigate the group-mean EC (commonalities) for each processing condition. In the second step, we applied the between-group PEB analysis to analyze the differences of EC at the group level between the considered data processing conditions (i.e., the EC differences resulted from the application of any two different data processing conditions to the considered subject cohort). For both single- and between-group PEB analyses, a 95% posterior probability (PP > 95%) threshold was taken as a strong evidence threshold rather than a statistical *p*-value (Zeidman, Jafarian, Seghier, et al., 2019).

In parallel to PEB analyses, we also compared the relative difference in EC parameter certainty between any two processing conditions using Bayesian data comparison (BDC) as implemented in SPM12 v7771 (Zeidman, Kazan, Todd, et al., 2019). In contrast to Bayesian model selection, BDC allows for a systematic comparison between different datasets, such as those obtained from different data processing approaches as in this study. BDC analysis helps to make statistical inferences about the parameter certainty (reduction in uncertainty) of coupling parameters estimated for a given data set based on the relative entropy (Zeidman, Kazan, Todd, et al., 2019). A difference in the entropy between two data sets in the range between 1.1 and 3 nats (natural units of information) and between 3 and 5 nats can be considered as “positive evidence” and “strong evidence,” respectively, that the estimated parameters are more certain for one data set than for the other. A difference greater than 5 nats is indicative of “very strong evidence” (Tuominen et al., 2023; Zeidman, Kazan, Todd, et al., 2019). Based on this approach, we performed BDC analyses between two considered conditions with common subjects and extracted the relative differences in parameter certainty between them.

In our study, we focused on the impact of data processing conditions on the task-evoked M-EC (matrix B) within the SRC network. Based on the single-group PEB analysis, we observed the group-mean task-evoked M-EC for all conditions and identified varied EC patterns corresponding to different selections of data processing parameters. A systematic comparison was then performed directly between data processing conditions via between-group PEB analysis.

3 | RESULTS

In this study, we investigated the task-evoked M-EC (matrix B) depending on the condition of the data processing parameters (see Section 2). We considered 24 data processing conditions involving two GSR conditions, three GLM designs, two activation contrasts, and two significance thresholding methods. We investigated the impact of these conditions on the SRC network localization, analysis sample size, DCM model fits, task-evoked M-EC of matrix B, and its certainty as we illustrate below. Briefly, we observed that (1) variation of the data processing parameters resulted in varied group-mean EC patterns; (2) the GLM designs and activation contrasts largely influence

EC strength and parameter certainty; and (3) GSR and significance thresholding have a rather little impact on EC.

3.1 | Task-evoked network localization

Based on the second-level fMRI analysis, the brain activation maps were obtained at the group level (Figure 2 and Supplementary Figure S2), and the peak coordinates of the SRC network nodes were determined (Table 1 and Supplementary Table S1). The data processing conditions of GLM design (All-Trials, S-Trials, and Blocks) and GSR (with/without) are relevant at this stage, and the remaining conditions of the activation contrast and significance thresholding will be applicable later at the time series extraction for the network nodes of individual subjects. When applying GSR, the results of the second-level fMRI analysis were very similar across the three GLM designs with very high volumetric overlap as indicated by a large Dice coefficient *D* (Taha & Hanbury, 2015) (Supplementary Table S3). In particular, the overlap in the brain activation between the All-Trials and Blocks cases was comparable with the overlap between All-Trials and S-Trials, with *D* = 0.94, respectively. We did, however, detect small differences in peak coordinates between GLM design types for the L.DLPFC, R.DLPFC, R.PMC, L.AI, R.AI, and AMCC nodes (between the All-/S-Trials and Blocks) and the L.DLPFC and AMCC nodes (between All-Trials and S-Trials). The factor GSR (i.e., with/without GSR) also showed a weak influence on the peak coordinates of the SRC network nodes: variations were observed in the R.PMC and R.AI nodes in Blocks, R.PMC, L.AI, and AMCC nodes in All-Trials, and L.DLPFC, L.AI, and AMCC nodes in S-Trials (compare Table 1 and Supplementary Table S1).

3.2 | Analysis samples

Next, we examined the effects of processing conditions on the sample size of subjects available for subsequent DCM analysis. Different subject samples were qualified for individual time series extraction under different conditions of data processing. The type of significance thresholding (see Section 2) was found to be most relevant at this stage, as compared to the other three processing parameters considered. The sizes of the qualified subject samples are listed in Table 2 (left-side numbers in the table cells), where the large impact of the significance thresholding can be seen. In many cases, the cluster-corrected thresholding entailed excluding 50 more subjects than the uncorrected thresholding, which corresponded to more than 25% of the relative sample reduction. The choice of contrast (i.e., Anti vs. Anti + Pro) only slightly influenced the sample size in the range of 15 subjects. The factor of GLM design also weakly influenced the sample size of the qualified (or excluded) subjects, although the relative difference here reached up to 15% when comparing Blocks and S-Trials designs (Table 2). The Blocks design entailed the largest sample qualified for time series extraction and subsequent DCM analyses, whereas the S-Trials design led to the smallest sample eligible for

further analyses. We replicated the above findings for the case without GSR (Supplementary Table S2).

3.3 | DCM model fits

The goodness-of-fit of DCM can be evaluated by the fraction of variance of empirical BOLD signals that can be explained by the variance of the simulated BOLD signals generated by the model. Therefore, we calculated the fractions of the explained variance for all subjects qualified for BOLD signal extraction. We found that the DCM-simulated BOLD signals can on average account for about 25% of the empirical variance (Supplementary Table S4). Only a few subjects (0–8) fell below 10% (Table 2). Varying the GSR condition (for other fixed conditions) also weakly affected the sample size with the differences in the range of nine subjects (Supplementary Table S2). Here, the differences between conditions were found to be statistically insignificant after multiple-comparison corrections, and the modeling performed well for all conditions and most subjects.

3.4 | Group-mean EC estimation

We estimated the averaged task-evoked EC for considered data processing conditions (24 conditions) at the group level using the single-group PEB analysis. We found that selecting one or another setup of the data processing influenced the results of DCM calculations and led to different group-mean task-evoked EC values. We first illustrate this by counting the numbers of evident edges ($PP > 95\%$, see Section 2) of task-evoked EC without counting self-connections (Table 3). The edge number ($PP > 95\%$) of the task-evoked M-EC (matrix B) was discovered to be varied depending on the selected approach of data processing. For example, the number of evident edges within the SRC network (in matrix B) may range from 42 (S-Trials, uncorrected Anti + Pro) to 13 (Blocks, corrected Anti), which corresponds to a variation of the fraction of edges of the task-evoked M-EC of the SRC network from 58% to 18%, respectively (Table 3 and Figure 4).

The choice of GLM design resulted in very different task-evoked EC patterns, where the task-evoked M-EC of the Blocks-design is much sparser than those of All-Trials and S-Trials designs (Figure 4 and Supplementary Figure S4). The uncorrected significance

thresholding led to a denser task-evoked EC compared with the corrected condition for the Anti activation contrast. The Anti + Pro contrast resulted in more evident edges of the task-evoked EC than the Anti contrast did, except for the uncorrected All-Trials-condition. Without GSR application, small differences in task-evoked EC were observed as compared to the case when GSR was applied (Figure 4, Table 3, Supplementary Figure S4, and Supplementary Table S5). Nevertheless, we corroborated the above conclusions also for the case without GSR.

3.5 | Between-group differences in task-evoked EC

To evaluate the differences in the task-evoked M-EC (matrix B) between varied conditions of a given data processing parameter (i.e., All-Trials vs. Blocks; with-GSR vs. without-GSR; corrected vs. uncorrected thresholding; Anti + Pro vs. Anti contrast), a between-group PEB analysis (see Section 2) was applied. We found that the considered data processing conditions of the GLM design and activation contrast led to strongly different task-evoked EC values (Figures 5 and 6, and Supplementary Figures S5 and S6), while EC was little affected by GSR application and thresholding approach (Supplementary Figures S7 and S8). Moreover, some M-EC edges were discovered to be consistently present when combining group-mean PEB and between-group PEB analyses (Supplementary Figure S9). For example, four edges were observed to be stable between conditions of All-Trials and Block GLM designs, while 10 EC edges were found to be stable between conditions of Anti + Pro and Anti contrasts.

3.6 | Differences between block- and event-related GLM designs

We observed strongly different patterns of the task-evoked M-EC (matrix B) between event-related (All-Trials and S-Trials) and block-based GLM (Figure 5 for All-Trials vs. Blocks, Supplementary Figure S5 for S-Trials vs. Blocks). All-Trials design showed stronger positive modulation of the connections from the network nodes (LIPS and RIPS) receiving external (visual) driving inputs to the rest of the network. At the same time, these driving-input nodes received

TABLE 3 Numbers of the group-level evident edges showing a high posterior probability of task-evoked M-EC (matrix B) within the SRC network.

	All-Trials		S-Trials		Blocks	
	Corrected	Uncorrected	Corrected	Uncorrected	Corrected	Uncorrected
Anti	31	36	35	39	13	15
Anti + Pro	38	39	37	42	33	32

Note: All task-evoked EC exceeded the 95% posterior probability threshold (excluding self-connections) and was calculated by the single-group PEB analysis for the considered conditions of the data processing with GSR (see Section 2 for details and notations). Used notations: SRC, stimulus-response compatibility; All-/S-Trials, experimental designs with all/successful trials; Blocks, experimental designs modeled by blocks.

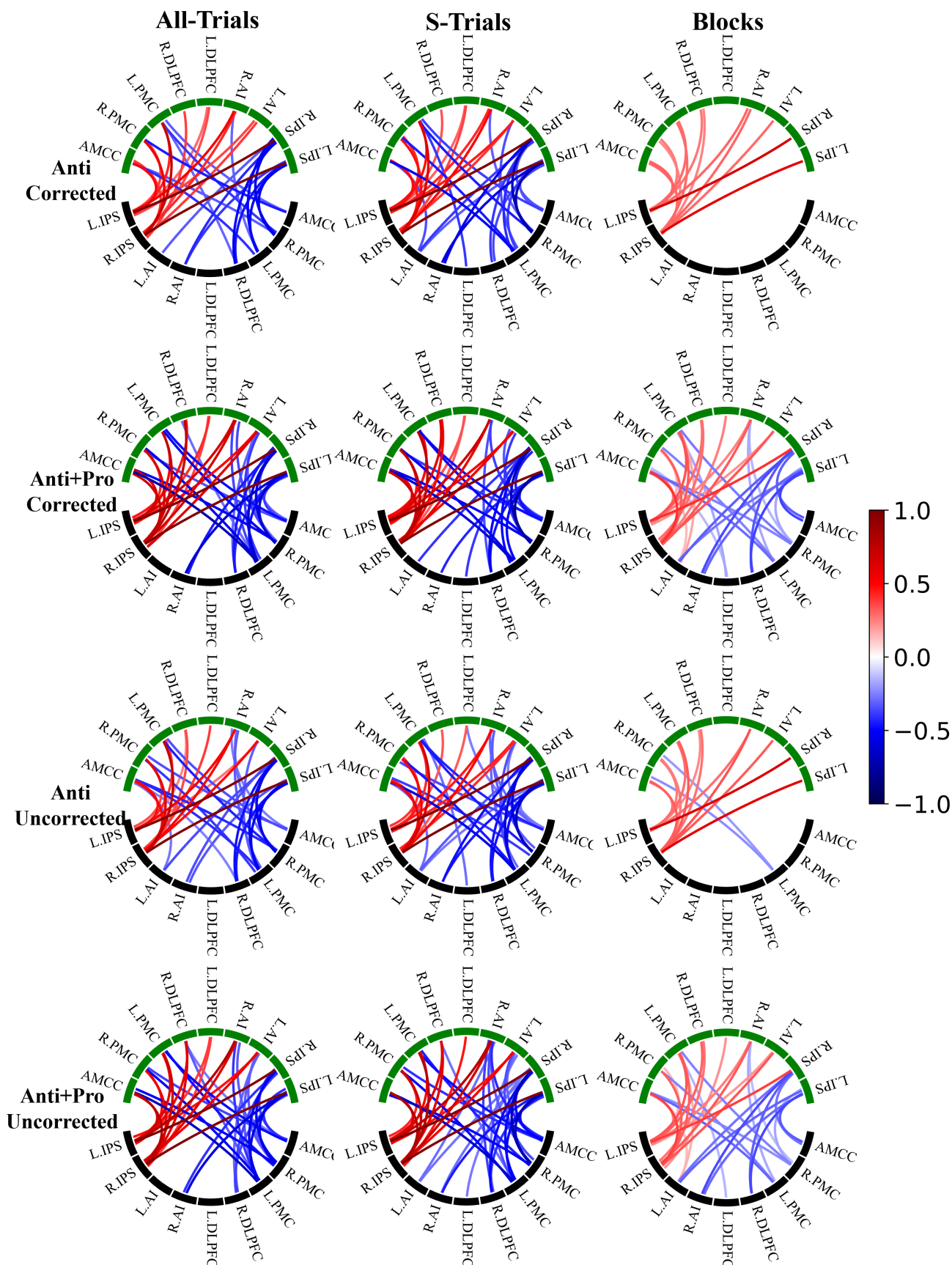


FIGURE 4 Legend on next page.

stronger negative modulation of EC from the other network nodes for the All-Trials design than for the Blocks design (Figure 5). The mentioned effects hold for both contrasts considered (Anti and Anti + Pro) and significance thresholding (corrected/uncorrected) conditions. However, the matrices of the differences (All-Trials vs. Blocks) of the task-evoked EC are sparser for the Anti contrast than for the Anti + Pro contrast, which indicates that more edges were strongly affected for the latter contrast by changing the GLM design between event-related and block-based ones. The Anti + Pro contrast may thus be considered as being more sensitive to the type of GLM design than is the Anti contrast (Figure 5). Analogously, by comparing the

corrected and uncorrected thresholding used for individual BOLD extraction we found that the former (corrected) case appeared to be somewhat less sensitive to the selection of the GLM design (Figure 5).

Similar conclusions can be drawn from the comparison between S-Trials and Blocks GLM designs, as illustrated in Supplementary Figure S5. Indeed, S-Trials and Blocks designs resulted in strongly different task-evoked M-EC, where the Anti + Pro contrast is more sensitive to the variation of the GLM design than is the Anti contrast. Likewise, the uncorrected thresholding might be more sensitive to the GLM design for the Anti contrast, which is, however, not apparent for the Anti + Pro case (Supplementary Figure S5). Finally, we found no

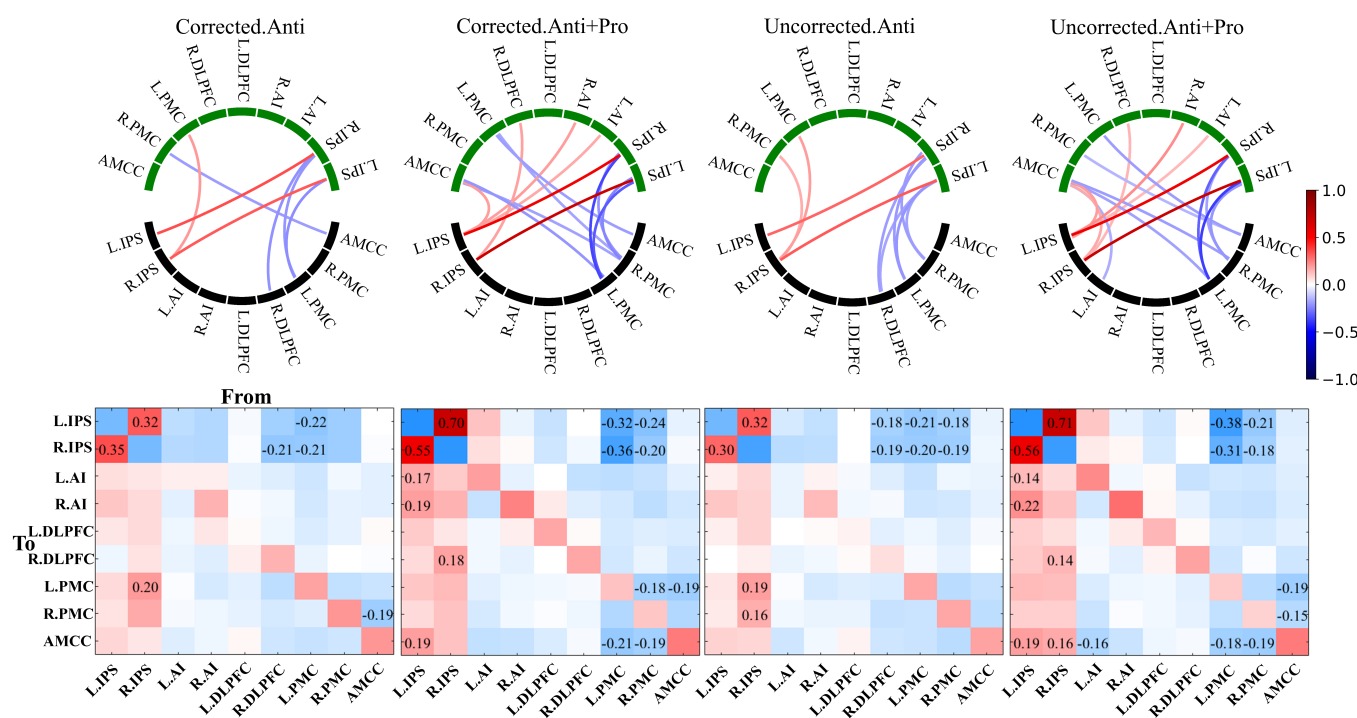


FIGURE 5 Comparison of task-evoked modulation of effective connectivity (M-EC) (matrix B) between the considered general linear model (GLM) designs (All-Trials vs. Blocks). The results of PEB analyses at the group level are illustrated for the differences of B matrices, where the latter of Block designs was subtracted from that of All-Trials designs (All-Trials–Blocks). The other considered conditions of the data processing (contrast and thresholding) are indicated in the titles of the plots. In the circular network plots (upper row), the evident EC edges (PP > 95%) of the difference All-Trials–Blocks are depicted. The lower (black) and the upper (green) network nodes correspond to the sources (“from”) and destinations (“to”) of the illustrated directed connectivity, respectively (see Section 2 for the nodes’ abbreviations). The values of the M-EC are reflected by color as indicated in the color bar. In the matrix plots (lower row), EC values are also depicted by color, and the values above PP > 95% threshold are indicated by numbers in the corresponding cells. The network nodes indicated in the horizontal and vertical axes correspond to the sources (“from”) and destinations (“to”) of the directed connectivity, respectively. Used notations: All-/S-Trials, experimental designs with all/successful trials; Blocks, experimental designs modeled by blocks; Anti, incompatible contrast; Anti + Pro, incompatible + compatible contrast; L/R, left/right; DLPFC, dorsolateral prefrontal cortex; PMC, premotor cortex; IPS, intraparietal sulcus; AI, anterior insula; AMCC, anterior midcingulate cortex.

FIGURE 4 Group-mean task-evoked M-EC (matrix B) for the considered conditions of the data processing indicated on the top and left sides of the circular plots with global signal regression (GSR) (see Section 2 for details and notations). The lower (black) and the upper (green) network nodes correspond to the sources (“from”) and destinations (“to”) of the illustrated directed connectivity, respectively. The values of the connectivity differences are reflected by color as indicated in the color bar. Only the M-EC (PP > 95%) was displayed by connections in the circular maps. Used notations: All-/S-Trials, experimental designs with all/successful trials; Blocks, experimental designs modeled by blocks; Anti, incompatible contrast; Anti + Pro, incompatible + compatible contrast; L/R, left/right; DLPFC, dorsolateral prefrontal cortex; PMC, premotor cortex; IPS, intraparietal sulcus; AI, anterior insula; AMCC, anterior midcingulate cortex.

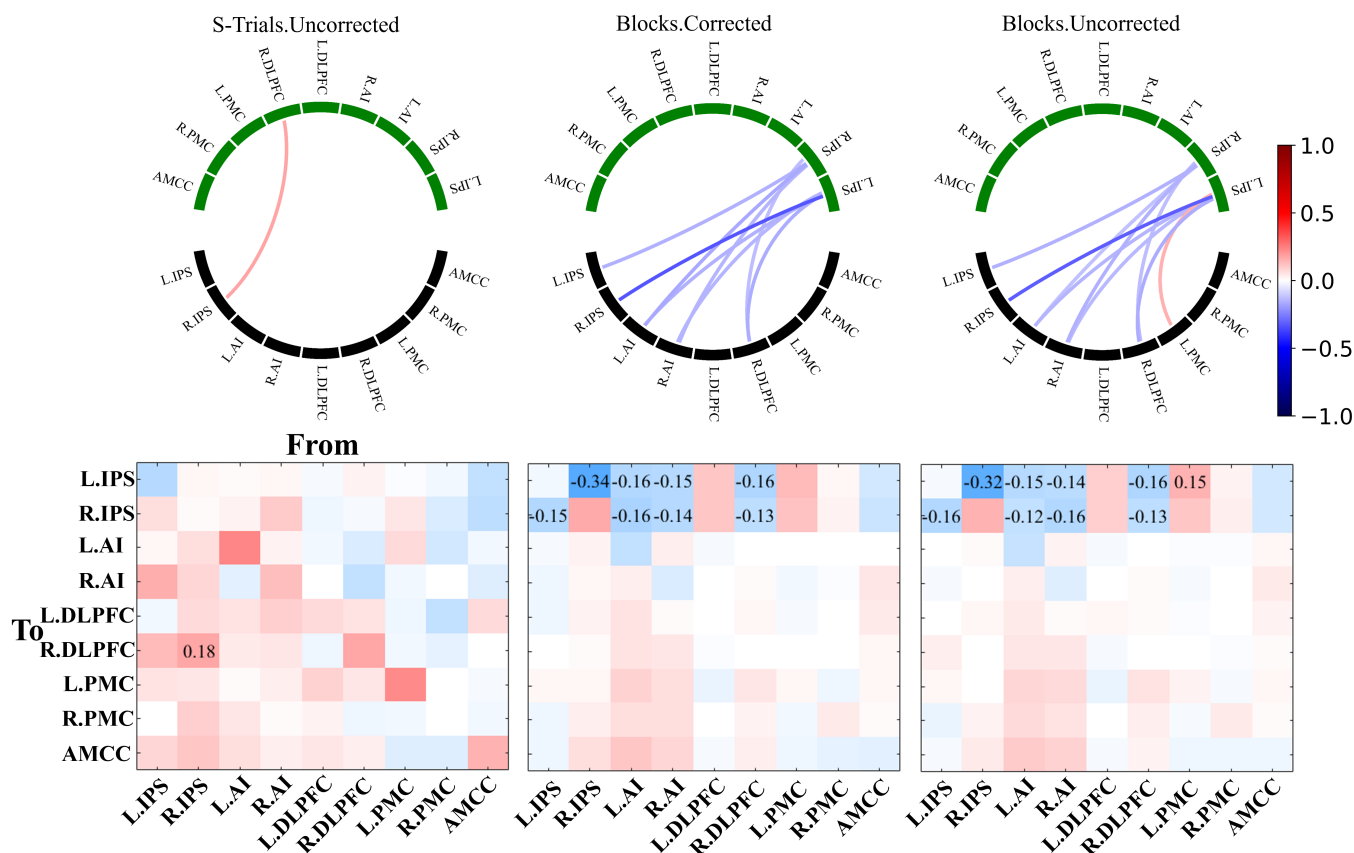


FIGURE 6 Comparison of task-evoked M-EC (matrix B) between the considered contrasts Anti + Pro and Anti. The results of parametric empirical Bayes (PEB) analyses at the group level are illustrated for the differences of B matrices, where the latter of the Anti contrast was subtracted from that of Anti + Pro-contrast (Anti + Pro – Anti). The other considered conditions of the data processing (GLM design and thresholding) are indicated in the titles of the plots. In the circular network plots (upper row), the evident EC edges (PP > 95%) of the difference Anti + Pro – Anti are depicted. The lower (black) and the upper (green) network nodes correspond to the sources (“from”) and destinations (“to”) of the illustrated directed connectivity, respectively. The values of the modulatory connectivity are reflected by color as indicated in the color bar. In the matrix plots (lower row), EC values are also depicted by color, and the values above PP > 95% threshold are indicated by numbers in the corresponding cells. The network nodes indicated in the horizontal and vertical axes correspond to the sources (“from”) and destinations (“to”) of the directed connectivity, respectively. Used notations: All-/S-Trials, experimental designs with all/successful trials; Blocks, experimental designs modeled by blocks; Anti, incompatible contrast; Anti + Pro, incompatible + compatible contrast; L/R, left/right; DLPFC, dorsolateral prefrontal cortex; PMC, premotor cortex; IPS, intraparietal sulcus; AI, anterior insula; AMCC, anterior midcingulate cortex.

strong differences in group-level task-evoked EC between All-Trials and S-Trials GLM designs (Supplementary Figure S6). This is in contrast to the differences observed in the group-mean EC (Figure 4), where the All-Trials and S-Trials GLM designs exhibited different connectivity within the SRC network. However, a detailed statistical analysis using the between-group PEB analysis did not confirm the differential impact of these conditions on task-evoked EC.

3.7 | Impact of the task-evoked activation contrasts

We observed strong effects of the considered contrasts (Anti and Anti + Pro) on task-evoked EC in the between-group PEB analysis (Figure 6). The main differences in EC for these contrasts were found in the edges coming from the rest of the network nodes to the driving-input nodes (L.IPS and R.IPS). This phenomenon seems to be most

pronounced for the Blocks design, whereas only one edge was affected for the S-Trials design, which comes from the R.IPS node to the “internal” node R.DLPFC (Figure 6, leftmost column). The Anti + Pro and Anti contrasts led to different modulations between driving-input nodes (L.IPS and R.IPS) and the rest of the network (Figure 6). The Blocks design appears to be more sensitive to the selection of one or another contrast, whereas the event-related design was less affected by the contrast. The task-evoked EC of the “internal” edges within the SRC network (i.e., excluding the input-driven nodes L.IPS and R.IPS) appeared to be not affected by the contrast variability for all other data processing conditions considered.

3.8 | Impact of GSR and significance thresholding

Different significance thresholding and GSR applications resulted in varied patterns of evident edges (PP > 95%) of group-mean task-

evoked EC as indicated by the single-group PEB analysis (Figure 4 and Supplementary Figure S4). However, there were no strong differences in the task-evoked EC when the between-group PEB analysis was performed for a more sophisticated comparison between the conditions of the significance thresholding and GSR (Supplementary Figures S7 and S8). We therefore conclude that the task-evoked EC can be stable with respect to variations of the significance thresholding at the extraction of individual BOLD signals and the application of GSR.

3.9 | Between-group differences in parameter certainty

The between-group BDC analyses demonstrated very strong evidence for differences in parameter certainty between conditions of GLM designs (Figure 7 and Supplementary Table S6) and between activation contrasts (Figure 7 and Supplementary Table S7). Block designs showed much higher parameter certainty than the event-related designs (differences from 58 to 67 nats), but there was practically no evidence for a difference in parameter certainty between All-Trials and S-Trials cases (<1.1 nats except for the corrected Anti + Pro contrast with 2.3 nats). The Anti contrast displayed higher parameter certainty (from 7 to 11 nats) than the Anti + Pro contrast. No evidence was obtained for the certainty differences between GSR conditions (Supplementary Table S8) and between significance thresholding conditions (Supplementary Table S9), except for some evidence for the corrected Anti + Pro contrast in the All-/S-Trials case between GSR conditions (difference of 2.3 and 2.6 nats).

4 | DISCUSSION

Our study examined the impact of several important data processing parameters on task-evoked M-EC within a brain network involved in solving spatial incompatibility-induced response conflicts. In total, we considered 24 data processing conditions resulting from the combination of four factors: GSR, GLM design, activation contrast, and significance thresholding. In this study, we used the full-connection model (i.e., with all connections between network nodes being equally admissible) to evaluate the EC estimates resulting from different data processing conditions, which ensured the same initial conditions for each DCM analysis (Tuominen et al., 2023). Furthermore, different data processing approaches investigated here can lead to altered time series even for the same subject, which might thus result in different optimal models for different cases. We therefore did not perform an exhaustive DCM model selection among potential SRC network topologies (by removal of specific connections) to infer a sparser model using Bayesian model reduction and selection approaches (Friston et al., 2016; Stephan et al., 2009). Instead, EC was calculated for the fully connected model of a network with nine nodes and then compared between different data processing conditions. Our study applied a two-level DCM analysis that involved single- and between-group PEB analyses as well as BDC. The single-group PEB analysis showed that task-evoked EC was sensitive to different choices of the considered data processing. The between-group PEB analysis indicated that varying the type of GLM design and activation contrast may lead to strongly different task-evoked EC and parameter certainty, whereas the connectivity and parameter certainty were little affected by GSR and significance thresholding.

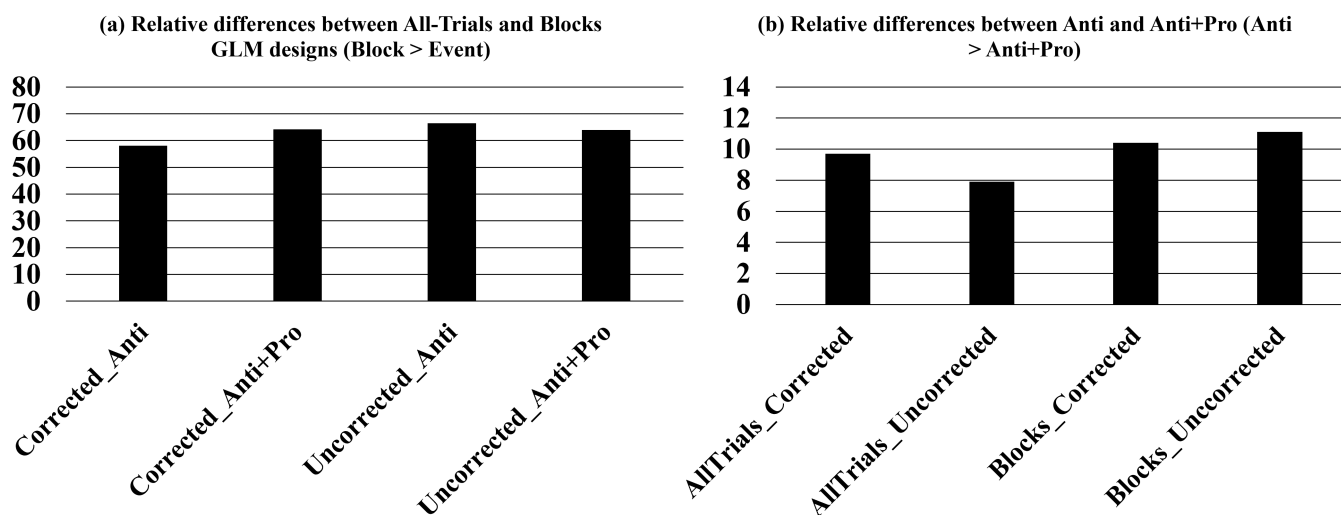


FIGURE 7 The parameter certainty of Bayesian data comparison (BDC) for two specific conditions. In panels (a) and (b), we present the BDC comparisons separately for (Block > All-Trials) and (Anti > Anti + Pro), respectively. The Supplementary materials provide additional comparisons for conditions such as S-Trials > Block and Anti > Anti + Pro of S-Trials (Supplementary Table S6 and S7). The bar represents the relative differences in parameter certainty (negative entropy) between the conditions. Notably, the Block design exhibits a significantly higher parameter certainty compared to the All-/S-Trials design. Similarly, the Anti contrast demonstrates a notably stronger parameter certainty in comparison to the Anti + Pro contrast.

4.1 | Impact of GLM design

The fMRI analyses displayed consistent task-evoked activation patterns (Figure 2 and Table 1) across considered GLM designs, while the two event-related designs showed slightly higher peaks of *t*-values. We note here that the employed event-related GLM resolved the stimulus laterality of the experimental setup (Supplementary Figure S1), which cannot be accomplished for the block-based design. We however confirmed that the event-related GLM without modeling the laterality condition resulted in practically the same results in the second-level analysis.

The single-group PEB analysis showed that event-related designs had a denser task-evoked M-EC than the block-based design (Figure 4 and Table 3), which is consistently manifested in the interactive connections between driving-input nodes and the “internal” nodes of the network. These connections may indicate that the experimental visual inputs could effectively exert influences on “internal” nodes (Friston et al., 2003). Although the event-related GLM designs showed more strongly evident (with $PP > 95\%$) modulatory connections than the block-based design, the minimal number of evident EC edges in the latter case can still reach 18% (compared to 58% for the event-related case) of the network capacity with 13 connections in the task-evoked modulatory component of EC (matrix B) from 72 possible edges without self-connections (Table 3). This may suggest that both types of GLM design can evoke M-EC within the SRC network driven by task stimuli, although EC is more responsive to the task-induced modulations for the event-related GLM.

The between-group PEB analysis further showed that strongly altered task-evoked EC was associated with variations of GLM design. Here, the event-related designs in most cases showed stronger positive and negative connections than did the block-based design at the group level and thus stronger responses to the experiment (Figure 5). The strongly different edges mostly were the interactive connections between the driving-input and “internal” nodes. This result agrees with other findings from the literature that experimental manipulations can perturb the brain's neural activities and EC parameters (Friston et al., 2003; Kahan & Foltynie, 2013). In contrast to our study, previous research (Daunizeau et al., 2011) attempted to find an optimized GLM design for a better model selection in DCM using the Laplace-Chernoff risk, that is, a measure of model selection error rates. In this case, within-subject experimental sessions were conducted with a block (consecutive identical trials) and an event-related (randomized trials) design, and block-based and event-related Laplace-Chernoff risks were compared. Although the experimental sessions included different trial-presenting paradigms, and task-evoked EC values were not compared with each other, the reported findings suggest that the type of GLM design can impact the DCM analyses, at least for the model selection (Daunizeau et al., 2011). The GLM design was also found to impact functional localizations in task-evoked activation studies (Bühler et al., 2008; Tie et al., 2009), when the two GLM design types were compared directly. In particular, the event-related design was found to lead to stronger activation and functional localization in putative language areas (Tie et al., 2009), while the block-based design exhibited more activation

in nonspecific areas (Bühler et al., 2008). The difference may have been caused by different shapes of the hemodynamic responses, when different GLM models were convolved with the HRF (Mechelli, Henson, et al., 2003; Mechelli, Price, et al., 2003). Here, the variance of the BOLD signal was better explained by GLM models of event-related design, where the predicted hemodynamic responses reached the peak earlier but returned to baseline later (Mechelli, Henson, et al., 2003).

Our study analyzed data collected during an SRC task using a mixed block/event experimental protocol (Fitts & Deininger, 1954; Petersen & Dubis, 2012), which presents stimuli in a stochastic manner within blocks of trials with the same task set (i.e., respond with ipsilateral or contralateral button presses, respectively). On the one hand, this protocol is fair to compare both block-based and event-related GLMs. On the other hand, it reduced the anticipation effects and was able to extract transient activities in event-related designs (Dosenbach et al., 2006). As mentioned above, the event-related design went along with stronger positive and negative connections from the driving-input nodes to “internal” nodes and backward, respectively, than what the block-based design did. When examining the averaged absolute intensity of task-evoked M-EC ($PP > 95\%$) for each condition (Supplementary Table S10), both All-Trials and S-Trials designs showed higher connectivity intensity than Blocks designs. The driving-input connections may reflect the change rate of neural responses induced by the task stimuli presented (Kahan & Foltynie, 2013; Zeidman, Jafarian, Corbin, et al., 2019; Zeidman, Jafarian, Seghier, et al., 2019). The stronger positive and negative connections involving driving-input nodes may suggest a higher responsivity of EC to task modulations in the event-related designs than in the block-based design. The EC sensitivity to the task-induced modulations can be enhanced/reduced by other parameters of the data processing (see Table 3 and Figure 4). For example, EC for the block-based design appeared to be more responsive to the task-evoked modulations for the Anti + Pro contrast than for the Anti contrast.

While small numerical differences in M-EC values were observed at the group level between All-Trials and S-Trials designs (Table 3 and Figure 4), no strong difference was detected by the two-group PEB comparisons (Supplementary Figure S6). Comparing these GLM designs aimed at revealing a possible impact of including error trials in the analyses of task-evoked fMRI data and EC. Usually, incorrect trials are regressed out or excluded from consideration before analysis (Ma et al., 2014; Zeidman, Jafarian, Corbin, et al., 2019), because incorrect trials are supposed to bring additional noise to the task-driven data and may thus negatively affect the results. The small difference in EC between the All-Trials and S-Trials designs observed in our study might be due to the low rate of error trials of about 3% (Supplementary Figure S10) and the strict threshold for EC parameters ($PP > 95\%$).

Consistent with our findings from connectivity strength comparisons, the BDC analyses also suggested very strong differences ($nats > 5$) between event-related and block-based designs, but no difference between the different cases of event-related designs (All-Trials vs. S-Trials). The parameter certainty of BDC reflects the confidence that we can place into estimated connections from a given model and is

thought to be positively correlated to the signal-to-noise ratio (Zeidman, Kazan, Todd, et al., 2019). The stronger parameter certainty in the block-based design may thus indicate a greater stability of EC estimates than obtained with event-related designs. We also verified that the event-related design resulted in broader posterior distributions of the M-EC parameters, which, together with lower certainty, may indicate an enhanced variability of the parameters and noise in the event-related modeling approach. Nevertheless, it is interesting to observe that the event-related GLM and DCM designs led to a larger number of strongly evident (with $PP > 95\%$) M-EC parameters and stronger connectivity intensity than did the block-based design (Figure 4). In our DCM model specification, block-based designs included a longer time period of a constant experimental condition, which may reduce the effect of data variability and noise and may thus contribute to higher confidence about parameter estimates. On the other hand, fewer evident connections and smaller total modulated connectivity for the block-based GLM design may also indicate a reduced sensitivity of this condition to the task-evoked modulation of neuronal dynamics and connectivity as compared to the event-related designs.

Furthermore, different GLM designs may better reflect different cognitive substrates, where the event-related and block-based designs can be more sensitive to transient and sustained brain activity, respectively (Petersen & Dubis, 2012; Visscher et al., 2003). The mentioned differences are, however, hardly reflected in the results of the neuroimaging analyses performed before DCM. For example, the brain activation maps strongly overlap for different processing conditions as reflected by large Dice coefficients and small differences in a few peak activation coordinates and their t -values (Table 1, and Supplementary Tables S1 and S3). The task-evoked brain activity extracted for individual subjects and used in DCM also exhibited a high similarity across different processing conditions. For example, the correlation between the BOLD signal time series of the event-related and block-based designs is larger than 0.9 (Supplementary Figure S11). The DCM was fitted equally well to these BOLD signals such that we cannot report any significant difference in the variance of the empirical data explained by DCM (Supplementary Table S4). Nevertheless, we found noticeably different task-evoked EC estimates for different data processing conditions, in particular, between event-related and block-based GLM and DCM designs, which makes the reported results intriguing. This may indicate an enhanced sensitivity of the DCM approach, which seems to have picked up rather subtle differences in the empirical brain activation data and DCM design (event-related and block-based) and translated them to substantial EC differences.

The sensitivity of the DCM approach to the choice of design (event-related vs. block-based) was confirmed by a brief examination of the M-EC obtained for the same BOLD time series extracted for individual subjects in the block-based GLM case for the uncorrected Anti + Pro contrast (Supplementary Figure S12). We again observed very different connectivity patterns for the event-related and block-based DCM designs, which resemble the connectivity patterns illustrated in Supplementary Figure S4 for the group-mean M-EC and their differences in Figure 5. The same applies to the differences in parameter certainty as calculated by BDC (compare Figure 7a to

Supplementary Figure S12d), although the input data in the latter case was the same, where we used the same BOLD time series but different DCM designs.

Jointly considering our findings regarding connectivity strength and parameter certainty, it is rather difficult to firmly conclude what type of design may (generally) be better for DCM analysis if both designs are equally reasonable to choose depending on the posed neuroscientific questions of the study. However, we systematically illustrated how different EC results can be for different GLM and DCM designs, highlighting the need for a sound rationale behind this impactful choice for any DCM analysis.

4.2 | Impact of activation contrasts

The PEB analyses showed strong differences in task-evoked EC between the Anti and Anti + Pro contrasts. The BDC analyses also revealed stronger parameter certainty (from 7.0 to 11.1 nats) for the Anti contrast relative to the Anti + Pro contrast (Supplementary Table S7). The Anti contrast reflects brain activation in response to incompatible trials, while the Anti + Pro contrast reflects brain responses to both incompatible and compatible trials. Psychologically, both Anti and Anti + Pro contrasts reflect a range of SRC task-related processes that comprise stimulus identification, attentional orientation, response selection including inhibition of the inadequate response tendency elicited in incompatible trials, and response execution (Cieslik et al., 2010). In contrast to the Anti + Pro sum contrast, the Anti contrast is more specifically focused on incompatibility-related processes (Munoz & Everling, 2004; Nee et al., 2007; Reuter-Lorenz & Park, 2010). M-EC is context-dependent, and the selection of contrast in the DCM model can reflect the dynamics corresponding to specific cognitive or executive processes (Kuhnke et al., 2021). In our case, Anti + Pro and Anti contrasts showed different M-EC patterns in group-mean EC (Figure 4 and supplementary Figure S4). We further found that the Anti + Pro condition featured a stronger (positive and negative) modulatory connectivity between the driving-input and “internal” nodes than did the Anti condition (Figure 6). Here, the sensitivity of EC to the contrast selection was additionally influenced by the type of GLM design, where the block-based condition appeared to be more sensitive to the difference between Anti and Anti + Pro contrasts. The Anti + Pro contrast, in turn, featured an enhanced sensitivity of task-evoked EC to the type of GLM design, especially when comparing event-related and block-based designs (see Figures 4 and 5). The difference in parameter certainty might be related to differences in signal variability between the two contrasts. As discussed above, the Anti + Pro contrast was assumed to reflect the averaged level of cognitive demands across all experimental conditions including compatible and incompatible cases (Figure 1), whereas considering the Anti contrast only was supposed to reflect states of higher cognitive demand arising from the need to solve incompatibility-induced response conflicts. We may suspect that the inclusion of the Pro contrast may lead to overall stronger data variability and, thereby, lower certainty of the connectivity parameters.

4.3 | GSR effects

We observed only small effects on the task-evoked brain activation and group-level EC induced by the application of GSR (Supplementary Figures S2 and S4). Accordingly, between-group PEB comparisons found no strong differences in EC between the cases with/without GSR (Supplementary Figure S8). The global signal is supposed to capture physiological and motion-related noise (Liu et al., 2017; Power et al., 2017) and the removal of the global signal is known to strongly influence resting-state FC (Anderson et al., 2011; Fox et al., 2009; Murphy et al., 2009; Varikuti et al., 2017). However, regarding EC, a recent study (Almgren et al., 2020) reported only minor differences in within-network EC estimates during the resting state before and after GSR. Our findings also agree with earlier studies in which the resting-state FC retained its significant coupling (Chang et al., 2009; Weissenbacher et al., 2009), and task-evoked FC between functionally related areas was not substantially affected (Mascali et al., 2021) when GSR was applied. We also consistently observed a minor difference in parameter certainty (from -2.6 to 1.6 nats) between the conditions with and without GSR (Supplementary Table S8). However, the effect of the global signal may be influenced by other factors such as intensity normalization and spatial normalization methods. For instance, some studies found that signal intensity normalization and GSR may share a similar effect on fMRI data (Liu et al., 2017; Smith, 2004). Although they are two distinct preprocessing steps, the intensity normalization scales the signal to a common value that may potentially remove global signals as GSR is assumed to do. In the present study, we scaled images to a common value of 10,000, which may influence the effect of GSR. It might be interesting to see if other data processing steps, for example, linear and nonlinear spatial normalization can influence the impact of GSR on EC. Nevertheless, we observed a similarly weak impact of GSR in line with the results of (Almgren et al., 2020; Mascali et al., 2021), who used different data processing pipelines. However, the effect of the global signal in task-evoked fMRI still needs more specific and deeper investigation.

4.4 | Thresholding effects

The significance thresholding of the activation contrast maps influenced both the extraction of the individual regional BOLD signals and subject qualification for such a signal extraction. It was thus suspected to be an important parameter also for the estimation of task-evoked EC. Indeed, the choice of corrected versus uncorrected thresholding strongly influenced the size of the sample available for subsequent DCM analyses (see Table 2). Moreover, the density of the modulatory components (matrix B) of task-evoked EC was altered depending on the thresholding, especially for the Anti contrast, where the uncorrected thresholding led to more evident EC edges (Table 3 and Figure 4). Although sufficient sample sizes are important for the robustness and statistical power of neuroimaging analyses (Button et al., 2013), the proper sample size is not commonly determined (Guo et al., 2014). At some point, it has been suggested that for reaching sufficient statistical power, a sample size of 24 subjects would be

required for fMRI activation studies (Desmond & Glover, 2002), while a sample size of at least 20 subjects was suggested for DCM studies (Thirion et al., 2007). However, these numbers depend on the effect size of interest, which in turn may be influenced by many factors including tasks, acquisition parameters, and participants (Goulden et al., 2012). From the side of reproducibility, the typical sample size ($n = 100$) may reach a modest degree of replicability for task fMRI studies (Turner et al., 2018), although the sample size for high reproducibility varied across different tasks (Bossier et al., 2020).

The impact of sample size on EC estimation was not investigated in our study, and we included samples of ~ 150 to 220 subjects, mainly depending on the thresholding approach. The variation of $\sim 25\%$ of subjects was found to have little impact on task-evoked EC according to the between-group PEB analysis. The first reason for this insensitivity may be the high probability threshold ($PP > 95\%$) of our PEB analysis. We observed numerically different densities of group-mean EC in conditions of corrected versus uncorrected contrasts, but the difference was not large enough for direct comparisons via PEB analysis to become strong (see Supplementary Figure S7). A second reason may be related to the thresholding itself. During the SRC network reconstructions for individual subjects, the cluster-corrected (vs. uncorrected) thresholding resulted in fewer significant voxels, leading to empty network nodes when overlapping individual maps with the ROIs obtained from the second-level analysis and, thereby, to subject disqualification for BOLD extraction. Different thresholding may not affect the voxels in the vicinity of peak coordinates, and the BOLD signals extracted for the subject samples qualified for both corrected and uncorrected thresholding hardly differed from each other (Supplementary Figure S4). This may be another reason why the sophisticated between-group PEB analysis did not find any strong differences in M-EC between these two conditions (Supplementary Figure S7).

The results from BDC also showed a very minor difference ranging from -0.2 to 1.1 nats in parameter certainty between corrected and uncorrected thresholding approaches (Supplementary Table S9). This was observed despite different sample sizes resulting from the two thresholding approaches. Our findings thus indicate that the choice of significance thresholding influenced the sample size but did not much impact task-evoked EC.

4.5 | Limitations

Some limitations should be considered. First of all, the trade-off of using multiple software applications, such as FSL, ANTs, AFNI, and Workbench, instead of using a single software solution, such as SPM, might be considered. While this approach can increase functionality and flexibility and make it easier to be conducted in computational clusters, it may also increase complexity and potentially impact comparisons to a literature that used SPM throughout. To address this question, we used the spatially preprocessed images as described in the Methods and then applied the SPM-based pipeline for the entire analysis of the task-evoked fMRI data and EC calculation by DCM (see also Arias et al., 2021; Hofmann & Straube, 2019; Park

et al., 2018), which combined non-SPM pipelines for data processing, but estimated EC using the SPM functions. The application of the SPM pipeline largely confirmed our main conclusions with respect to the differences between event-related and block-based GLM and DCM designs with some quantitative distinctions (see Supplementary Figure S13, Supplementary Tables S11 and S12, and the pertinent discussion in the supplementary material).

The second possible limitation can be that the present study was initiated from the end-user perspective and focused on EC changes when different data processing decisions were made. This may impact interpretations of results because our study was not designed to ask a statistically well-formed question or a specific hypothesis testing, but focused on exploratory investigations. Third, the generality of our findings may be limited to the specific task paradigm and sample characteristics considered here, which may be evaluated in further studies.

5 | CONCLUSION

This study investigated the impact of four important data processing choices on the results of task-evoked fMRI analyses and EC estimations via DCM in the framework of the SRC task. Our results showed that the type of GLM design (event-related or block-based) and type of activation contrast strongly affect task-dependent EC estimation. In contrast, the other two processing factors examined here, GSR application and significance thresholding, appear to have only a weak influence on within-network task-evoked EC estimation. The event-related design may confer a higher responsivity of EC to task stimuli, while the block-based design featured a higher sensitivity of EC to the type of activation contrast. Our findings showcase the differential impact that various data processing choices may have on the estimation of task-evoked EC, highlighting the importance of thoroughly considering and further assessing these choices to help build better models that allow for valid neuroscientific interpretations.

ACKNOWLEDGMENTS

The authors gratefully acknowledge the computing time granted through the Jülich-Aachen Research Alliance (JARA) on the super-computer JURECA (Jülich Supercomputing Centre, 2021) at Forschungszentrum Jülich. Open Access funding enabled and organized by Projekt DEAL.

FUNDING INFORMATION

This work was supported by the Portfolio Theme Supercomputing and Modeling for the Human Brain by the Helmholtz Association, and the European Union's Horizon 2020 Research and Innovation Programme under Grant Agreements 945539 (HBP SGA3, DOI: 10.3030/945539) and 826421 (VirtualBrainCloud, DOI: 10.3030/826421). Open access publication was funded by the Deutsche Forschungsgemeinschaft (DFG, German Research Foundation)—491111487. The funders had no role in the study design, data collection, analysis, decision to publish, or preparation of the manuscript.

CONFLICT OF INTEREST STATEMENT

The authors declare no conflict of interest.

DATA AVAILABILITY STATEMENT

The raw data of the 1000BRAINS project used in this study are not immediately available for public sharing because the authors do not have permission to share data. The codes are available in the (<https://github.com/CogPsycho2023/DCMs1>).

ORCID

Esther Florin  <https://orcid.org/0000-0001-8276-2508>

Oleksandr V. Popovich  <https://orcid.org/0000-0001-9994-1764>

REFERENCES

- Almgren, H., Van de Steen, F., Razi, A., Friston, K., & Marinazzo, D. (2020). The effect of global signal regression on DCM estimates of noise and effective connectivity from resting state fMRI. *NeuroImage*, 208, 116435. <https://doi.org/10.1016/j.neuroimage.2019.116435>
- Anderson, B. A., Laurent, P. A., & Yantis, S. (2014). Value-driven attentional priority signals in human basal ganglia and visual cortex. *Brain Research*, 1587, 88–96. <https://doi.org/10.1016/j.brainres.2014.08.062>
- Anderson, J. S., Druzgal, T. J., Lopez-Larson, M., Jeong, E.-K., Desai, K., & Yurgelun-Todd, D. (2011). Network anticorrelations, global regression, and phase-shifted soft tissue correction. *Human Brain Mapping*, 32(6), 919–934. <https://doi.org/10.1002/hbm.21079>
- Arias, A. J., Ma, L., Bjork, J. M., Hammond, C. J., Zhou, Y., Snyder, A., & Moeller, F. G. (2021). Altered effective connectivity of the reward network during an incentive-processing task in adults with alcohol use disorder. *Alcoholism: Clinical and Experimental Research*, 45(8), 1563–1577. <https://doi.org/10.1111/acer.14650>
- Avants, B. B., Epstein, C. L., Grossman, M., & Gee, J. C. (2008). Symmetric diffeomorphic image registration with cross-correlation: Evaluating automated labeling of elderly and neurodegenerative brain. *Medical Image Analysis*, 12(1), 26–41. <https://doi.org/10.1016/j.media.2007.06.004>
- Beheshtian, E., Jalilianhasanpour, R., Modir Shanechi, A., Sethi, V., Wang, G., Lindquist, M. A., Caffo, B. S., Agarwal, S., Pillai, J. J., Gujar, S. K., & Sair, H. I. (2021). Identification of the somatomotor network from language task-based fMRI compared with resting-state fMRI in patients with brain lesions. *Radiology*, 301(1), 178–184. <https://doi.org/10.1148/radiol.2021204594>
- Bernstein-Eliav, M., & Tavor, I. (2024). The prediction of brain activity from connectivity: Advances and applications. *The Neuroscientist*, 30(3), 367–377. <https://doi.org/10.1177/10738584221130974>
- Biswal, B. B., Mennes, M., Zuo, X.-N., Gohel, S., Kelly, C., Smith Steve, M., Colcombe, S., Dagonowski, A.-M., Ernst, M., Fair, D., Hampson, M., Hoptman, M. J., Hyde, J. S., Kiviniemi, V. J., Kötter, R., Li, S.-J., ... Milham, M. P. (2010). Toward discovery science of human brain function. *Proceedings of the National Academy of Sciences*, 107(10), 4734–4739. <https://doi.org/10.1073/pnas.0911855107>
- Bossier, H., Roels, S. P., Seurinck, R., Banaschewski, T., Barker, G. J., Bokde, A. L. W., Quinlan, E. B., Desrivieres, S., Flor, H., Gridis, A., Garavan, H., Gowland, R., Heinz, A., Ittermann, B., Martinot, J.-L., Artiges, E., Nees, F., Papadopoulos Orfanos, D., Poustka, L., ... Moerkerke, B. (2020). The empirical replicability of task-based fMRI as a function of sample size. *NeuroImage*, 212, 116601. <https://doi.org/10.1016/j.neuroimage.2020.116601>
- Botvinik-Nezer, R., Holzmeister, F., Camerer, C. F., Dreber, A., Huber, J., Johannesson, M., Kirchler, M., Iwanir, R., Mumford, J. A., Adcock, R. A., Avesani, P., Baczowski, B. M., Bajracharya, A., Bakst, L., Ball, S., Ball, M., Bault, N., Beaton, D., Beitner, J., ... Schonberg, T. (2020).

- Variability in the analysis of a single neuroimaging dataset by many teams. *Nature*, 582(7810), 84–88. <https://doi.org/10.1038/s41586-020-2314-9>
- Boudrias, M.-H., Gonçalves, C. S., Penny, W. D., Park, C.-h., Rossiter, H. E., Tallelli, P., & Ward, N. S. (2012). Age-related changes in causal interactions between cortical motor regions during hand grip. *NeuroImage*, 59(4), 3398–3405. <https://doi.org/10.1016/j.neuroimage.2011.11.025>
- Bühler, M., Vollstädt-Klein, S., Klemen, J., & Smolka, M. N. (2008). Does erotic stimulus presentation design affect brain activation patterns? Event-related vs. blocked fMRI designs. *Behavioral and Brain Functions*, 4(1), 30. <https://doi.org/10.1186/1744-9081-4-30>
- Button, K. S., Ioannidis, J. P. A., Mokrysz, C., Nosek, B. A., Flint, J., Robinson, E. S. J., & Munafò, M. R. (2013). Power failure: Why small sample size undermines the reliability of neuroscience. *Nature Reviews Neuroscience*, 14(5), 365–376. <https://doi.org/10.1038/nrn3475>
- Buxton, R. B., Uludağ, K., Dubowitz, D. J., & Liu, T. T. (2004). Modeling the hemodynamic response to brain activation. *NeuroImage*, 23, S220–S233. <https://doi.org/10.1016/j.neuroimage.2004.07.013>
- Carp, J. (2012). On the plurality of (methodological) worlds: Estimating the analytic flexibility of fMRI experiments. *Frontiers in Neuroscience*, 6, 33928–33940. <https://doi.org/10.3389/fnins.2012.00149>
- Caspers, S., Moebus, S., Lux, S., Pundt, N., Schütz, H., Mühleisen, T. W., Gras, V., Eickhoff, S. B., Romanzetti, S., Stöcker, T., Stirnberg, R., Kirlangic, M. E., Minnerop, M., Pieperhoff, P., Mödder, U., Das, S., Evans, A. C., Jöckel, K.-H., Erbel, R., ... Amunts, K. (2014). Studying variability in human brain aging in a population-based German cohort—Rationale and design of 1000BRAINS. *Frontiers in Aging Neuroscience*, 6, 149–162. <https://doi.org/10.3389/fnagi.2014.00149>
- Chang, C., Cunningham, J. P., & Glover, G. H. (2009). Influence of heart rate on the BOLD signal: The cardiac response function. *NeuroImage*, 44(3), 857–869. <https://doi.org/10.1016/j.neuroimage.2008.09.029>
- Churchill, N. W., Spring, R., Afshin-Pour, B., Dong, F., & Strother, S. C. (2015). An automated, adaptive framework for optimizing preprocessing pipelines in task-based functional MRI. *PLoS One*, 10(7), e0131520. <https://doi.org/10.1371/journal.pone.0131520>
- Cieslik, E. C., Zilles, K., Grefkes, C., & Eickhoff, S. B. (2011). Dynamic interactions in the fronto-parietal network during a manual stimulus-response compatibility task. *NeuroImage*, 58(3), 860–869. <https://doi.org/10.1016/j.neuroimage.2011.05.089>
- Cieslik, E. C., Zilles, K., Kurth, F., & Eickhoff, S. B. (2010). Dissociating bottom-up and top-down processes in a manual stimulus-response compatibility task. *Journal of Neurophysiology*, 104(3), 1472–1483. <https://doi.org/10.1152/jn.00261.2010>
- Cole, D., Smith, S., & Beckmann, C. (2010). Advances and pitfalls in the analysis and interpretation of resting-state FMRI data. *Frontiers in Systems Neuroscience*, 4, 1459–1473. <https://doi.org/10.3389/fnsys.2010.00008>
- Cole, M. W., Ito, T., Bassett, D. S., & Schultz, D. H. (2016). Activity flow over resting-state networks shapes cognitive task activations. *Nature Neuroscience*, 19(12), 1718–1726. <https://doi.org/10.1038/nn.4406>
- Cole, M. W., Bassett, D. S., Power, J. D., Braver, T. S., & Petersen, S. E. (2014). Intrinsic and task-evoked network architectures of the human brain. *Neuron*, 83(1), 238–251. <https://doi.org/10.1016/j.neuron.2014.05.014>
- Cox, R. W. (1996). AFNI: Software for analysis and visualization of functional magnetic resonance neuroimages. *Computers and Biomedical Research*, 29(3), 162–173. <https://doi.org/10.1006/cbmr.1996.0014>
- Daunizeau, J., Preuschoff, K., Friston, K., & Stephan, K. (2011). Optimizing experimental design for comparing models of brain function. *PLoS Computational Biology*, 7(11), e1002280. <https://doi.org/10.1371/journal.pcbi.1002280>
- Davey, C. E., Grayden, D. B., Egan, G. F., & Johnston, L. A. (2013). Filtering induces correlation in fMRI resting state data. *NeuroImage*, 64, 728–740. <https://doi.org/10.1016/j.neuroimage.2012.08.022>
- Desmond, J. E., & Glover, G. H. (2002). Estimating sample size in functional MRI (fMRI) neuroimaging studies: Statistical power analyses. *Journal of Neuroscience Methods*, 118(2), 115–128. [https://doi.org/10.1016/S0165-0270\(02\)00121-8](https://doi.org/10.1016/S0165-0270(02)00121-8)
- Dosenbach, N. U. F., Visscher, K. M., Palmer, E. D., Miezin, F. M., Wenger, K. K., Kang, H. C., Burgund, E. D., Grimes, A. L., Schlaggar, B. L., & Petersen, S. E. (2006). A core system for the implementation of task sets. *Neuron*, 50(5), 799–812. <https://doi.org/10.1016/j.neuron.2006.04.031>
- Eickhoff, S. B., Yeo, B. T. T., & Genov, S. (2018). Imaging-based parcellations of the human brain. *Nature Reviews Neuroscience*, 19(11), 672–686. <https://doi.org/10.1038/s41583-018-0071-7>
- Esteban, O., Markiewicz, C. J., Blair, R. W., Moodie, C. A., Isik, A. I., Erramuzpe, A., Kent, J. D., Goncalves, M., DuPre, E., Snyder, M., Oya, H., Ghosh, S. S., Wright, J., Durnez, J., Poldrack, R. A., & Gorgolewski, K. J. (2019). fMRIPrep: A robust preprocessing pipeline for functional MRI. *Nature Methods*, 16(1), 111–116. <https://doi.org/10.1038/s41592-018-0235-4>
- Fitts, P. M., & Deininger, R. L. (1954). S-R compatibility: Correspondence among paired elements within stimulus and response codes. *Journal of Experimental Psychology*, 48(6), 483–492. <https://doi.org/10.1037/h0054967>
- Fox, M. D., Zhang, D., Snyder, A. Z., & Raichle, M. E. (2009). The global signal and observed anticorrelated resting state brain networks. *Journal of Neurophysiology*, 101(6), 3270–3283. <https://doi.org/10.1152/jn.90777.2008>
- Frässle, S., Lomakina, E. I., Kasper, L., Manjaly, Z. M., Leff, A., Pruessmann, K. P., Buhmann, J. M., & Stephan, K. E. (2018). A generative model of whole-brain effective connectivity. *NeuroImage*, 179, 505–529. <https://doi.org/10.1016/j.neuroimage.2018.05.058>
- Frässle, S., Lomakina, E. I., Razi, A., Friston, K. J., Buhmann, J. M., & Stephan, K. E. (2017). Regression DCM for fMRI. *NeuroImage*, 155, 406–421. <https://doi.org/10.1016/j.neuroimage.2017.02.090>
- Friston, K. J. (2011). Functional and effective connectivity: A review. *Brain Connectivity*, 1(1), 13–36. <https://doi.org/10.1089/brain.2011.0008>
- Friston, K. J., Harrison, L., & Penny, W. (2003). Dynamic causal modelling. *NeuroImage*, 19(4), 1273–1302. [https://doi.org/10.1016/S1053-8119\(03\)00202-7](https://doi.org/10.1016/S1053-8119(03)00202-7)
- Friston, K. J., Josephs, O., Zarahn, E., Holmes, A. P., Rouquette, S., & Poline, J. B. (2000). To smooth or not to smooth?: Bias and efficiency in fMRI time-series analysis. *NeuroImage*, 12(2), 196–208. <https://doi.org/10.1006/nimg.2000.0609>
- Friston, K. J., Kahan, J., Biswal, B., & Razi, A. (2014). A DCM for resting state fMRI. *NeuroImage*, 94, 396–407. <https://doi.org/10.1016/j.neuroimage.2013.12.009>
- Friston, K. J., Litvak, V., Oswal, A., Razi, A., Stephan, K. E., van Wijk, B. C. M., Ziegler, G., & Zeidman, P. (2016). Bayesian model reduction and empirical Bayes for group (DCM) studies. *NeuroImage*, 128, 413–431. <https://doi.org/10.1016/j.neuroimage.2015.11.015>
- Friston, K. J., Williams, S., Howard, R., Frackowiak, R. S. J., & Turner, R. (1996). Movement-related effects in fMRI time-series. *Magnetic Resonance in Medicine*, 35(3), 346–355. <https://doi.org/10.1002/mrm.1910350312>
- Friston, K. J., Zarahn, E., Josephs, O., Henson, R. N. A., & Dale, A. M. (1999). Stochastic designs in event-related fMRI. *NeuroImage*, 10(5), 607–619. <https://doi.org/10.1006/nimg.1999.0498>
- Glasser, M. F., Coalson, T. S., Bijsterbosch, J. D., Harrison, S. J., Harms, M. P., Anticevic, A., Van Essen, D. C., & Smith, S. M. (2018). Using temporal ICA to selectively remove global noise while preserving global signal in functional MRI data. *NeuroImage*, 181, 692–717. <https://doi.org/10.1016/j.neuroimage.2018.04.076>
- Glasser, M. F., Sotiropoulos, S. N., Wilson, J. A., Coalson, T. S., Fischl, B., Andersson, J. L., Xu, J., Jbabdi, S., Webster, M., Polimeni, J. R., Van Essen, D. C., & Jenkinson, M. (2013). The minimal preprocessing pipelines for the Human Connectome Project. *NeuroImage*, 80, 105–124. <https://doi.org/10.1016/j.neuroimage.2013.04.127>

- Goulden, N., Elliott, R., Suckling, J., Williams, S. R., Deakin, J. F. W., & McKie, S. (2012). Sample size estimation for comparing parameters using dynamic causal modeling. *Brain Connectivity*, 2(2), 80–90. <https://doi.org/10.1089/brain.2011.0057>
- Greene, A. S., Gao, S., Scheinost, D., & Constable, R. T. (2018). Task-induced brain state manipulation improves prediction of individual traits. *Nature Communications*, 9(1), 2807. <https://doi.org/10.1038/s41467-018-04920-3>
- Guo, Q., Thabane, L., Hall, G., McKinnon, M., Goeree, R., & Pullenayegum, E. (2014). A systematic review of the reporting of sample size calculations and corresponding data components in observational functional magnetic resonance imaging studies. *NeuroImage*, 86, 172–181. <https://doi.org/10.1016/j.neuroimage.2013.08.012>
- Heckner, M. K., Cieslik, E. C., Küppers, V., Fox, P. T., Eickhoff, S. B., & Langner, R. (2021). Delineating visual, auditory and motor regions in the human brain with functional neuroimaging: A BrainMap-based meta-analytic synthesis. *Scientific Reports*, 11(1), 9942. <https://doi.org/10.1038/s41598-021-88773-9>
- Hofmann, D., & Straube, T. (2019). Resting-state fMRI effective connectivity between the bed nucleus of the stria terminalis and amygdala nuclei. *Human Brain Mapping*, 40(9), 2723–2735. <https://doi.org/10.1002/hbm.24555>
- Huettel, S. A. (2012). Event-related fMRI in cognition. *NeuroImage*, 62(2), 1152–1156. <https://doi.org/10.1016/j.neuroimage.2011.08.113>
- Jenkinson, M., Bannister, P., Brady, M., & Smith, S. (2002). Improved optimization for the robust and accurate linear registration and motion correction of brain images. *NeuroImage*, 17(2), 825–841. <https://doi.org/10.1006/nimg.2002.1132>
- Jenkinson, M., Beckmann, C. F., Behrens, T. E. J., Woolrich, M. W., & Smith, S. M. (2012). Fsl. *NeuroImage*, 62(2), 782–790. <https://doi.org/10.1016/j.neuroimage.2011.09.015>
- Jülich Supercomputing Centre. (2021). JURECA: Data centric and booster modules implementing the modular supercomputing architecture at Jülich Supercomputing Centre. *Journal of Large-Scale Research Facilities*, 7, 182–190. <https://doi.org/10.17815/jlsrf-7-182>
- Jung, K., Friston, K. J., Pae, C., Choi, H. H., Tak, S., Choi, Y. K., Park, B., Park, C.-A., Cheong, C., & Park, H.-J. (2018). Effective connectivity during working memory and resting states: A DCM study. *NeuroImage*, 169, 485–495. <https://doi.org/10.1016/j.neuroimage.2017.12.067>
- Kahan, J., & Foltynie, T. (2013). Understanding DCM: Ten simple rules for the clinician. *NeuroImage*, 83, 542–549. <https://doi.org/10.1016/j.neuroimage.2013.07.008>
- Kahan, J., Mancini, L., Flandin, G., White, M., Papadaki, A., Thornton, J., Yousry, T., Zrinzo, L., Hariz, M., Limousin, P., Friston, K., & Foltynie, T. (2019). Deep brain stimulation has state-dependent effects on motor connectivity in Parkinson's disease. *Brain*, 142(8), 2417–2431. <https://doi.org/10.1093/brain/awz164>
- Kuhnke, P., Kiefer, M., & Hartwigsen, G. (2021). Task-dependent functional and effective connectivity during conceptual processing. *Cerebral Cortex*, 31(7), 3475–3493. <https://doi.org/10.1093/cercor/bhab026>
- Langner, R., Cieslik, E. C., Behrwind, S. D., Roski, C., Caspers, S., Amunts, K., & Eickhoff, S. B. (2015). Aging and response conflict solution: Behavioural and functional connectivity changes. *Brain Structure and Function*, 220(3), 1739–1757. <https://doi.org/10.1007/s00429-014-0758-0>
- Liu, T. T., Frank, L. R., Wong, E. C., & Buxton, R. B. (2001). Detection power, estimation efficiency, and predictability in event-related fMRI. *NeuroImage*, 13(4), 759–773. <https://doi.org/10.1006/nimg.2000.0728>
- Liu, T. T., Nalci, A., & Falahpour, M. (2017). The global signal in fMRI: Nuisance or information? *NeuroImage*, 150, 213–229. <https://doi.org/10.1016/j.neuroimage.2017.02.036>
- Loehrer, P. A., Nettersheim, F. S., Jung, F., Weber, I., Huber, C., Dembek, T. A., Pelzer, E. A., Fink, G. R., Tittgemeyer, M., & Timmermann, L. (2016). Ageing changes effective connectivity of motor networks during bimanual finger coordination. *NeuroImage*, 143, 325–342. <https://doi.org/10.1016/j.neuroimage.2016.09.014>
- Logothetis, N. K. (2008). What we can do and what we cannot do with fMRI. *Nature*, 453(7197), 869–878. <https://doi.org/10.1038/nature06976>
- Ma, L., Steinberg, J. L., Cunningham, K. A., Lane, S. D., Kramer, L. A., Narayana, P. A., Kosten, T. R., Bechara, A., & Moeller, F. G. (2014). Inhibitory behavioral control: A stochastic dynamic causal modeling study using network discovery analysis. *Brain Connectivity*, 5(3), 177–186. <https://doi.org/10.1089/brain.2014.0275>
- Mascali, D., Moraschi, M., DiNuzzo, M., Tommasin, S., Fratini, M., Gili, T., Wise, R. G., Mangia, S., Macaluso, E., & Giove, F. (2021). Evaluation of denoising strategies for task-based functional connectivity: Equalizing residual motion artifacts between rest and cognitively demanding tasks. *Human Brain Mapping*, 42(6), 1805–1828. <https://doi.org/10.1002/hbm.25332>
- Mechelli, A., Henson, R. N. A., Price, C. J., & Friston, K. J. (2003). Comparing event-related and epoch analysis in blocked design fMRI. *NeuroImage*, 18(3), 806–810. [https://doi.org/10.1016/S1053-8119\(02\)00027-7](https://doi.org/10.1016/S1053-8119(02)00027-7)
- Mechelli, A., Price, C. J., Henson, R. N. A., & Friston, K. J. (2003). Estimating efficiency a priori: A comparison of blocked and randomized designs. *NeuroImage*, 18(3), 798–805. [https://doi.org/10.1016/S1053-8119\(02\)00040-X](https://doi.org/10.1016/S1053-8119(02)00040-X)
- Menon, V. (2011). Large-scale brain networks and psychopathology: A unifying triple network model. *Trends in Cognitive Sciences*, 15(10), 483–506. <https://doi.org/10.1016/j.tics.2011.08.003>
- Menon, V., & Uddin, L. Q. (2010). Saliency, switching, attention and control: A network model of insula function. *Brain Structure and Function*, 214(5), 655–667. <https://doi.org/10.1007/s00429-010-0262-0>
- Morken, F., Helland, T., Hugdahl, K., & Specht, K. (2017). Reading in dyslexia across literacy development: A longitudinal study of effective connectivity. *NeuroImage*, 144, 92–100. <https://doi.org/10.1016/j.neuroimage.2016.09.060>
- Munoz, D. P., & Everling, S. (2004). Look away: The anti-saccade task and the voluntary control of eye movement. *Nature Reviews Neuroscience*, 5(3), 218–228. <https://doi.org/10.1038/nrn1345>
- Murphy, K., Birn, R. M., Handwerker, D. A., Jones, T. B., & Bandettini, P. A. (2009). The impact of global signal regression on resting state correlations: Are anti-correlated networks introduced? *NeuroImage*, 44(3), 893–905. <https://doi.org/10.1016/j.neuroimage.2008.09.036>
- Murphy, K., & Fox, M. D. (2017). Towards a consensus regarding global signal regression for resting state functional connectivity MRI. *NeuroImage*, 154, 169–173. <https://doi.org/10.1016/j.neuroimage.2016.11.052>
- Nee, D. E., Wager, T. D., & Jonides, J. (2007). Interference resolution: Insights from a meta-analysis of neuroimaging tasks. *Cognitive, Affective, & Behavioral Neuroscience*, 7(1), 1–17. <https://doi.org/10.3758/CABN.7.1.1>
- Park, H.-J., Friston, K. J., Pae, C., Park, B., & Razi, A. (2018). Dynamic effective connectivity in resting state fMRI. *NeuroImage*, 180, 594–608. <https://doi.org/10.1016/j.neuroimage.2017.11.033>
- Parker, D. B., & Razlighi, Q. R. (2019). The benefit of slice timing correction in common fMRI preprocessing pipelines. *Frontiers in Neuroscience*, 13, 465275–465296. <https://doi.org/10.3389/fnins.2019.00821>
- Petersen, S. E., & Dubis, J. W. (2012). The mixed block/event-related design. *NeuroImage*, 62(2), 1177–1184. <https://doi.org/10.1016/j.neuroimage.2011.09.084>
- Power, J. D., Mitra, A., Laumann, T. O., Snyder, A. Z., Schlaggar, B. L., & Petersen, S. E. (2014). Methods to detect, characterize, and remove motion artifact in resting state fMRI. *NeuroImage*, 84, 320–341. <https://doi.org/10.1016/j.neuroimage.2013.08.048>
- Power, J. D., Plitt, M., Laumann, T. O., & Martin, A. (2017). Sources and implications of whole-brain fMRI signals in humans. *NeuroImage*, 146, 609–625. <https://doi.org/10.1016/j.neuroimage.2016.09.038>
- Reuter-Lorenz, P. A., & Park, D. C. (2010). Human neuroscience and the aging mind: A new look at old problems. *The Journals of Gerontology: Series B*, 65B(4), 405–415. <https://doi.org/10.1093/geronb/gbq035>

- Roels, S. P., Bossier, H., Loeys, T., & Moerkerke, B. (2015). Data-analytical stability of cluster-wise and peak-wise inference in fMRI data analysis. *Journal of Neuroscience Methods*, 240, 37–47. <https://doi.org/10.1016/j.jneumeth.2014.10.024>
- Saad, Z. S., Gotts, S. J., Murphy, K., Chen, G., Jo, H. J., Martin, A., & Cox, R. W. (2012). Trouble at rest: How correlation patterns and group differences become distorted after global signal regression. *Brain Connectivity*, 2(1), 25–32. <https://doi.org/10.1089/brain.2012.0080>
- Shen, X., Finn, E. S., Scheinost, D., Rosenberg, M. D., Chun, M. M., Papademetris, X., & Constable, R. T. (2017). Using connectome-based predictive modeling to predict individual behavior from brain connectivity. *Nature Protocols*, 12(3), 506–518. <https://doi.org/10.1038/nprot.2016.178>
- Sladky, R., Friston, K. J., Tröstl, J., Cunnington, R., Moser, E., & Windischberger, C. (2011). Slice-timing effects and their correction in functional MRI. *NeuroImage*, 58(2), 588–594. <https://doi.org/10.1016/j.neuroimage.2011.06.078>
- Smith, S. M. (2004). Overview of fMRI analysis. *The British Journal of Radiology*, 77(suppl_2), S167–S175. <https://doi.org/10.1259/bjr/33553595>
- Smith, S. M., & Nichols, T. E. (2009). Threshold-free cluster enhancement: Addressing problems of smoothing, threshold dependence and localisation in cluster inference. *NeuroImage*, 44(1), 83–98. <https://doi.org/10.1016/j.neuroimage.2008.03.061>
- Smith, S. M., Vidaurre, D., Beckmann, C. F., Glasser, M. F., Jenkinson, M., Miller, K. L., Nichols, T. E., Robinson, E. C., Gholamreza, S.-K., Woolrich, M. W., Barch, D. M., Ugurbil, K., & Van Essen, D. C. (2013). Functional connectomics from resting-state fMRI. *Trends in Cognitive Sciences*, 17(12), 666–682. <https://doi.org/10.1016/j.tics.2013.09.016>
- Stephan, K. E., Penny, W. D., Daunizeau, J., Moran, R. J., & Friston, K. J. (2009). Bayesian model selection for group studies. *NeuroImage*, 46(4), 1004–1017.
- Taha, A. A., & Hanbury, A. (2015). Metrics for evaluating 3D medical image segmentation: Analysis, selection, and tool. *BMC Medical Imaging*, 15(1), 29. <https://doi.org/10.1186/s12880-015-0068-x>
- Thirion, B., Pinel, P., Mériaux, S., Roche, A., Dehaene, S., & Poline, J.-B. (2007). Analysis of a large fMRI cohort: Statistical and methodological issues for group analyses. *NeuroImage*, 35(1), 105–120. <https://doi.org/10.1016/j.neuroimage.2006.11.054>
- Tie, Y., Suarez, R. O., Whalen, S., Radmanesh, A., Norton, I. H., & Golby, A. J. (2009). Comparison of blocked and event-related fMRI designs for pre-surgical language mapping. *NeuroImage*, 47, T107–T115. <https://doi.org/10.1016/j.neuroimage.2008.11.020>
- Tuominen, J., Specht, K., Vaisvilaitė, L., & Zeidman, P. (2023). An information-theoretic analysis of resting-state versus task fMRI. *Network Neuroscience*, 1–18, 769–786. https://doi.org/10.1162/netn_a_00302
- Turner, B. O., Paul, E. J., Miller, M. B., & Barbey, A. K. (2018). Small sample sizes reduce the replicability of task-based fMRI studies. *Communications Biology*, 1(1), 62. <https://doi.org/10.1038/s42003-018-0073-z>
- Tustison, N. J., Avants, B. B., Cook, P. A., Zheng, Y., Egan, A., Yushkevich, P. A., & Gee, J. C. (2010). N4ITK: Improved N3 bias correction. *IEEE Transactions on Medical Imaging*, 29(6), 1310–1320. <https://doi.org/10.1109/TMI.2010.2046908>
- Tustison, N. J., Cook, P. A., Klein, A., Song, G., Das, S. R., Duda, J. T., Kandel, B. M., van Strien, N., Stone, J. R., Gee, J. C., & Avants, B. B. (2014). Large-scale evaluation of ANTs and FreeSurfer cortical thickness measurements. *NeuroImage*, 99, 166–179. <https://doi.org/10.1016/j.neuroimage.2014.05.044>
- van den Heuvel, M. P., & Hulshoff Pol, H. E. (2010). Exploring the brain network: A review on resting-state fMRI functional connectivity. *European Neuropsychopharmacology*, 20(8), 519–534. <https://doi.org/10.1016/j.euroneuro.2010.03.008>
- Varikuti, D. P., Hoffstaedter, F., Genon, S., Schwender, H., Reid, A. T., & Eickhoff, S. B. (2017). Resting-state test-retest reliability of a priori defined canonical networks over different preprocessing steps. *Brain Structure and Function*, 222(3), 1447–1468. <https://doi.org/10.1007/s00429-016-1286-x>
- Visscher, K. M., Miezin, F. M., Kelly, J. E., Buckner, R. L., Donaldson, D. I., McAvoy, M. P., Bhalodia, V. M., & Petersen, S. E. (2003). Mixed block/event-related designs separate transient and sustained activity in fMRI. *NeuroImage*, 19(4), 1694–1708. [https://doi.org/10.1016/S1053-8119\(03\)00178-2](https://doi.org/10.1016/S1053-8119(03)00178-2)
- Volz, L. J., Eickhoff, S. B., Pool, E.-M., Fink, G. R., & Grefkes, C. (2015). Differential modulation of motor network connectivity during movements of the upper and lower limbs. *NeuroImage*, 119, 44–53. <https://doi.org/10.1016/j.neuroimage.2015.05.101>
- Weissenbacher, A., Kasess, C., Gerstl, F., Lanzenberger, R., Moser, E., & Windischberger, C. (2009). Correlations and anticorrelations in resting-state functional connectivity MRI: A quantitative comparison of preprocessing strategies. *NeuroImage*, 47(4), 1408–1416. <https://doi.org/10.1016/j.neuroimage.2009.05.005>
- Winkler, A. M., Ridgway, G. R., Webster, M. A., Smith, S. M., & Nichols, T. E. (2014). Permutation inference for the general linear model. *NeuroImage*, 92, 381–397. <https://doi.org/10.1016/j.neuroimage.2014.01.060>
- Woolrich, M. W., Behrens, T. E. J., & Smith, S. M. (2004). Constrained linear basis sets for HRF modelling using variational Bayes. *NeuroImage*, 21(4), 1748–1761. <https://doi.org/10.1016/j.neuroimage.2003.12.024>
- Yan, C.-G., Craddock, R. C., He, Y., & Milham, M. (2013). Addressing head motion dependencies for small-world topologies in functional connectomics. *Frontiers in Human Neuroscience*, 7, 910–928. <https://doi.org/10.3389/fnhum.2013.00910>
- Yeo, B. T., Krienen, F. M., Sepulcre, J., Sabuncu, M. R., Lashkari, D., Hollinshead, M., Roffman, J. L., Smoller, J. W., Zöllei, L., Polimeni, J. R., Fischl, B., Liu, H., & Buckner, R. L. (2011). The organization of the human cerebral cortex estimated by intrinsic functional connectivity. *Journal of Neurophysiology*, 106(3), 1125–1165. <https://doi.org/10.1152/jn.00338.2011>
- Zeidman, P., Jafarian, A., Corbin, N., Seghier, M. L., Razi, A., Price, C. J., & Friston, K. J. (2019). A guide to group effective connectivity analysis, part 1: First level analysis with DCM for fMRI. *NeuroImage*, 200, 174–190. <https://doi.org/10.1016/j.neuroimage.2019.06.031>
- Zeidman, P., Jafarian, A., Seghier, M. L., Litvak, V., Cagnan, H., Price, C. J., & Friston, K. J. (2019). A guide to group effective connectivity analysis, part 2: Second level analysis with PEB. *NeuroImage*, 200, 12–25. <https://doi.org/10.1016/j.neuroimage.2019.06.032>
- Zeidman, P., Kazan, S. M., Todd, N., Weiskopf, N., Friston, K. J., & Callaghan, M. F. (2019). Optimizing data for modeling neuronal responses. *Frontiers in Neuroscience*, 12, 411195–411210. <https://doi.org/10.3389/fnins.2018.00986>
- Zhang, Y., Brady, M., & Smith, S. (2001). Segmentation of brain MR images through a hidden Markov random field model and the expectation-maximization algorithm. *IEEE Transactions on Medical Imaging*, 20(1), 45–57.

SUPPORTING INFORMATION

Additional supporting information can be found online in the Supporting Information section at the end of this article.

How to cite this article: Zhang, S., Jung, K., Langner, R., Florin, E., Eickhoff, S. B., & Popovych, O. V. (2024). Impact of data processing varieties on DCM estimates of effective connectivity from task-fMRI. *Human Brain Mapping*, 45(8), e26751. <https://doi.org/10.1002/hbm.26751>

Supplementary materials
for the manuscript entitled
Impact of data processing varieties on DCM estimates of effective connectivity from task-
fMRI
by
Shufei Zhang^{1,2}, Kyesam Jung^{1,2}, Robert Langner^{1,2}, Esther Florin³, Simon B. Eickhoff^{1,2},
Oleksandr V. Popovych^{1,2}

¹Institute of Neuroscience and Medicine, Brain and Behaviour (INM-7), Research Centre
Jülich, Germany

²Institute for Systems Neuroscience, Medical Faculty, Heinrich-Heine University Düsseldorf,
Germany

³Institute of Clinical Neuroscience and Medical Psychology, Medical Faculty, Heinrich-Heine
University Düsseldorf, Germany

*Corresponding author: o.popovych@fz-juelich.de

Supplementary Figures

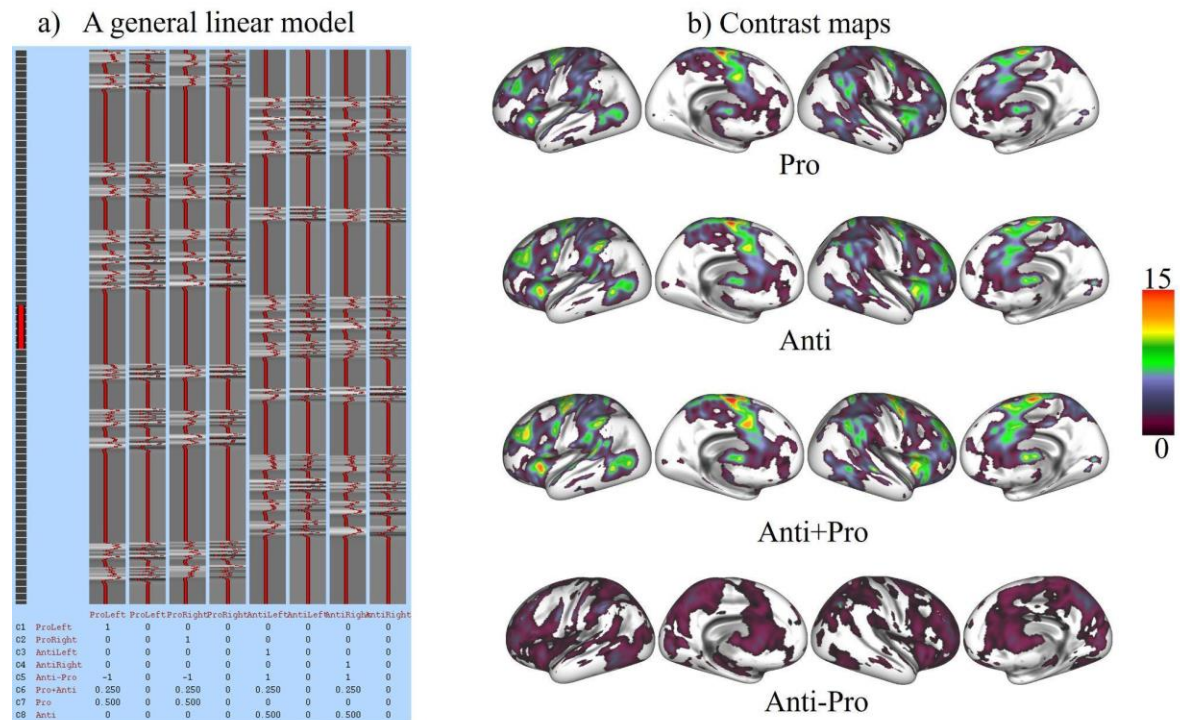


Fig. 1. The case for FSL general linear model (GLM) and contrast maps from the event-related design. A double gamma hemodynamic response function (odd columns) and temporal derivatives (even columns) are presented in the (a). Four contrast maps are shown in (b). The Pro or Anti contrast maps indicated the activated regions under congruent or incongruent conditions. The Anti+Pro contrast map indicated the group-mean activated regions under both conditions. The Anti > Pro contrast map indicated the activated regions associated with the incompatibility effect.

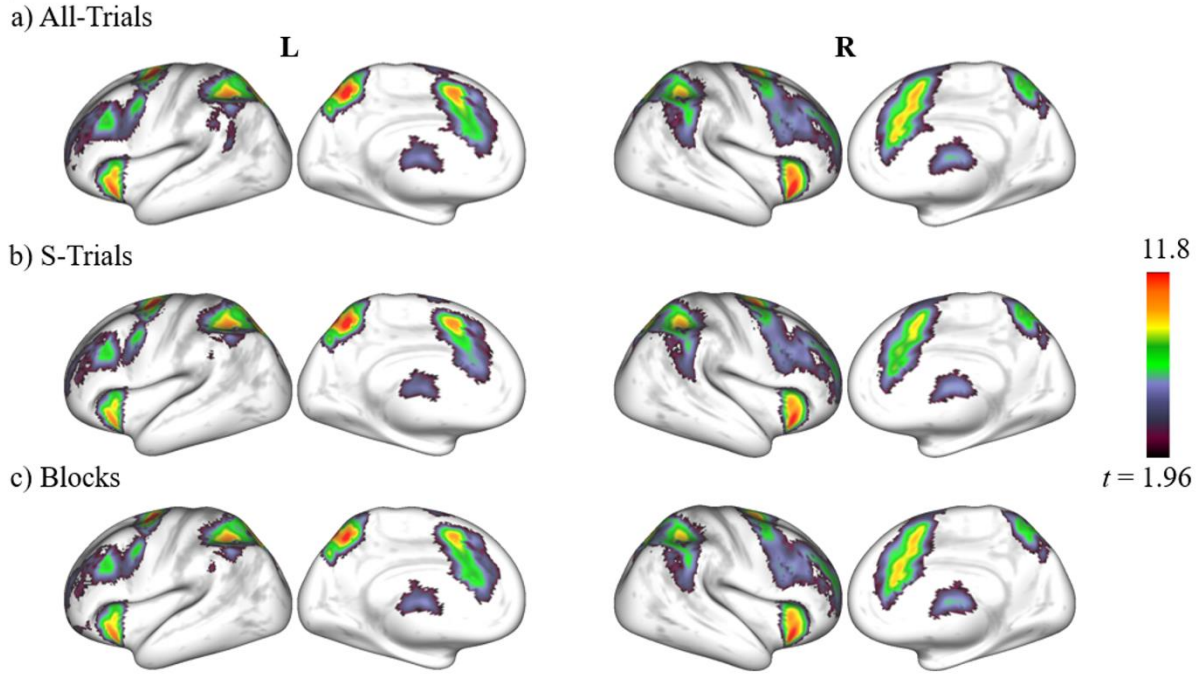


Fig. 2. Results of the second-level fMRI analysis for different GLM designs by considering (a) All-Trials, (b) S-Trials, and (c) Blocks designs without GSR. All maps illustrate the t -values (scaling of the color bar) of the t -tests reflecting the statistically significant voxels across all subjects ($p_{\text{TFCE+FWE}} < 0.05$, corrected by threshold-free cluster enhancement (TFCE) and family-wise error (FWE) rate methods) of the contrast difference between incongruent and congruent experimental conditions (Anti-Pro contrast). For better visualization, each thresholded statistical map was projected to fs_LR 32k surfaces.

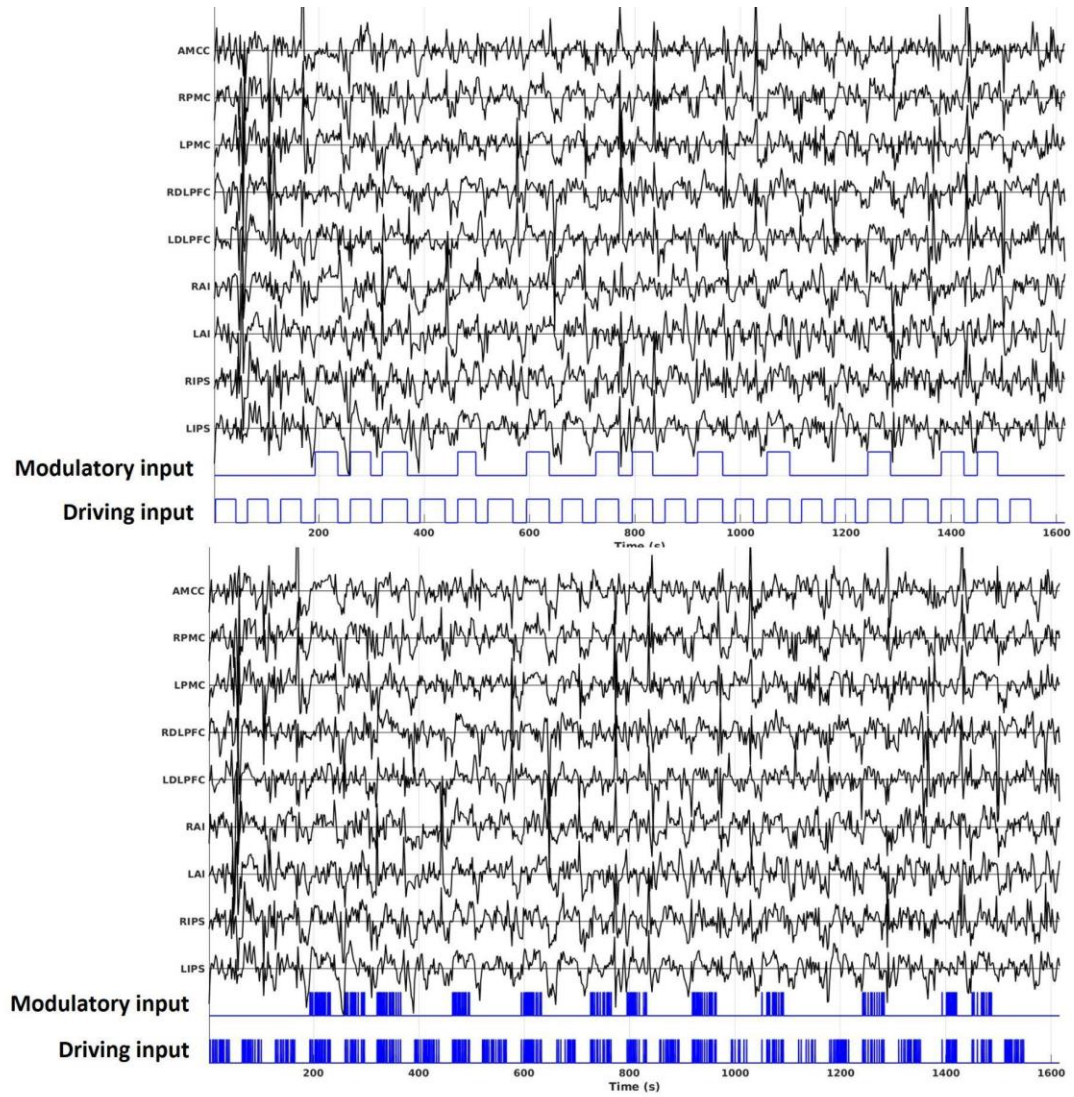
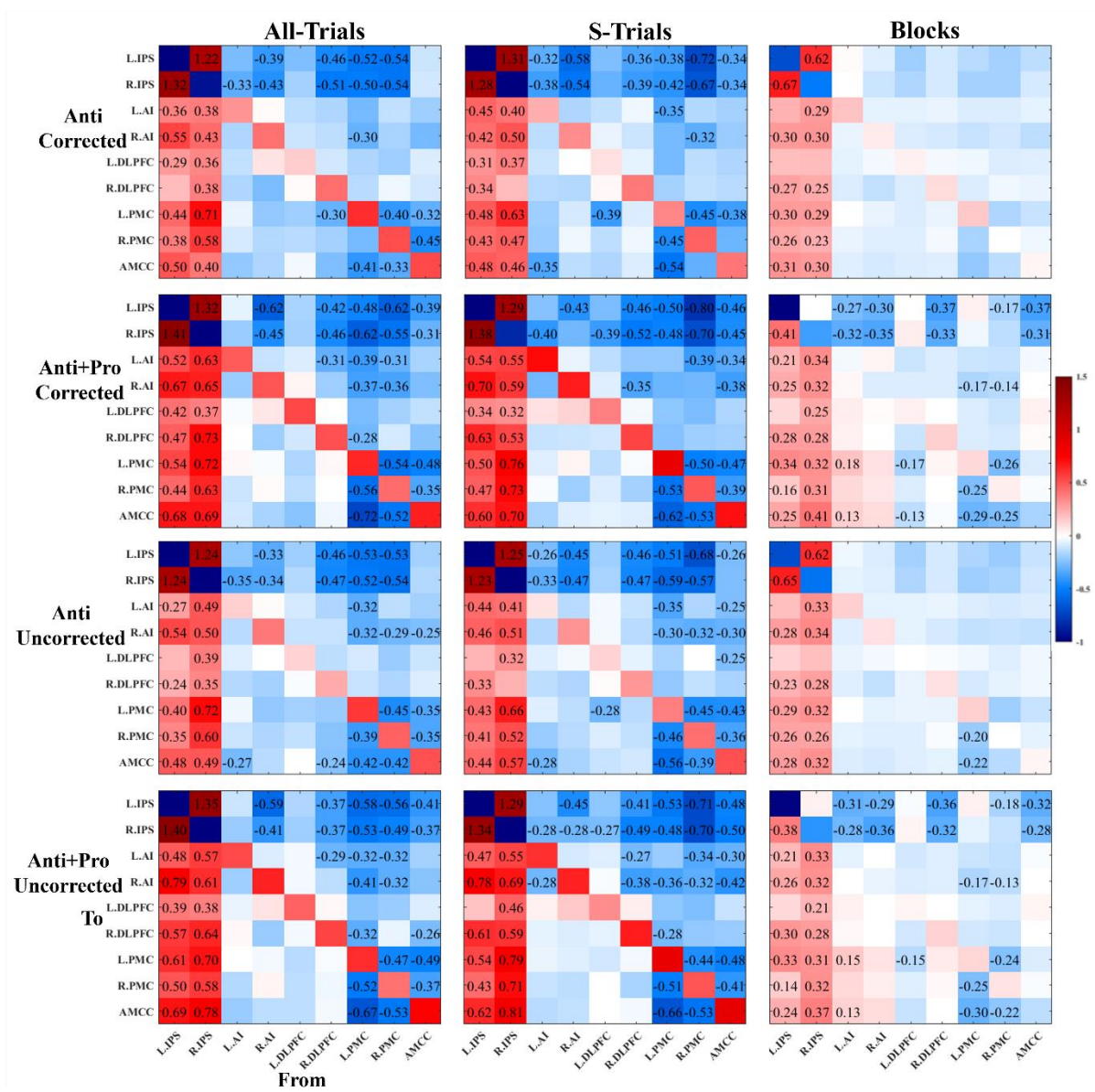


Fig. 3. The example of DCM model specifications from the block design (upper one) and event-related design (lower one) with the Anti-contrast. The first 9 rows illustrate the empirical BOLD signals of 9 nodes involved in the SRC network, while the last two rows indicate the modulatory input (also for the contrast) and driving input (i.e., visual stimuli).



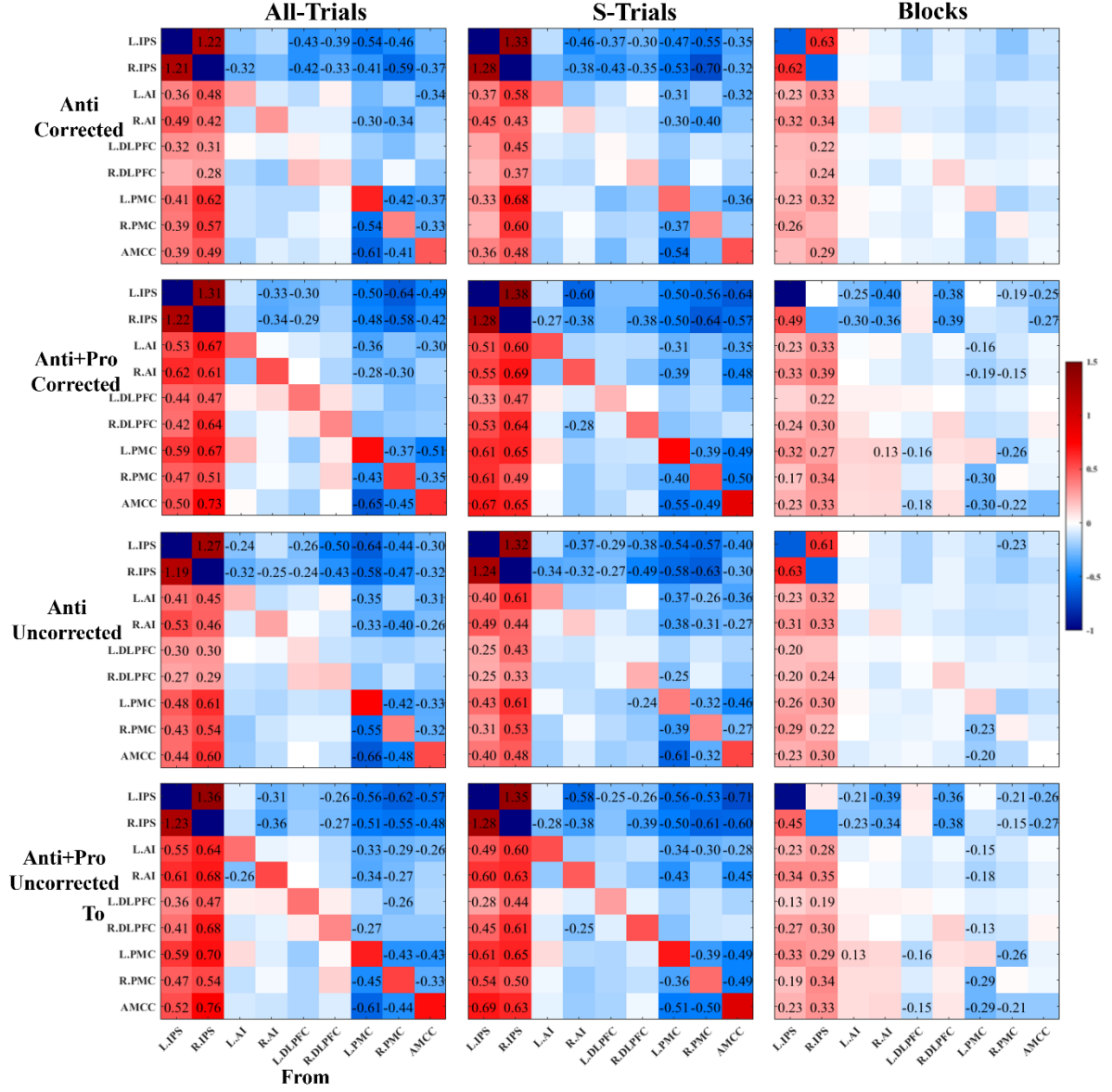


Fig. 4. Group-mean modulatory EC (B matrices) for each considered condition of the data processing indicated on the top and left sides of the plots with GSR (upper one) without GSR (lower one). The color encodes the strength of EC ranging from blue (negative EC) to red (positive EC), where the EC edges above the 95% posterior probability threshold are labeled by the black numbers. The connectivity is directed from the network nodes indicated on the horizontal axes to the network nodes indicated on the vertical axes. See Methods for details and notations.

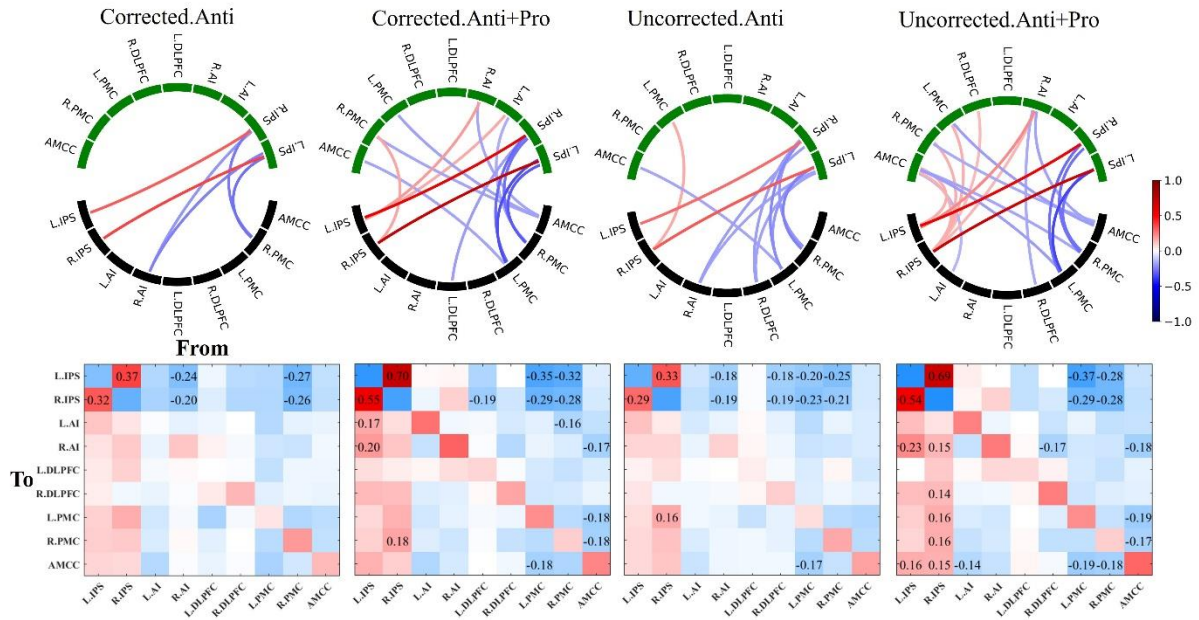


Fig. 5. Comparison of the task-evoked EC (matrix B) between the considered GLM designs (S-Trials vs. Blocks) using between-group PEB analyses. The other considered conditions of the data processing (contrast and thresholding) are indicated in the titles of the plots. In the circular network plots (upper row), the EC edges (exceeding the threshold of PP > 95%) at the group level of the difference S-Trials - Blocks are depicted. The black and green network nodes correspond to the sources ("from") and destinations ("to") of the illustrated directed connectivity, respectively. In the matrix plots (lower row), EC differences are also depicted by color, and numbers in the corresponding cells indicate values. The network nodes shown in the horizontal and vertical axes correspond to the sources ("from") and destinations ("to") of the directed connectivity, respectively. See Methods of the nodes' abbreviations.

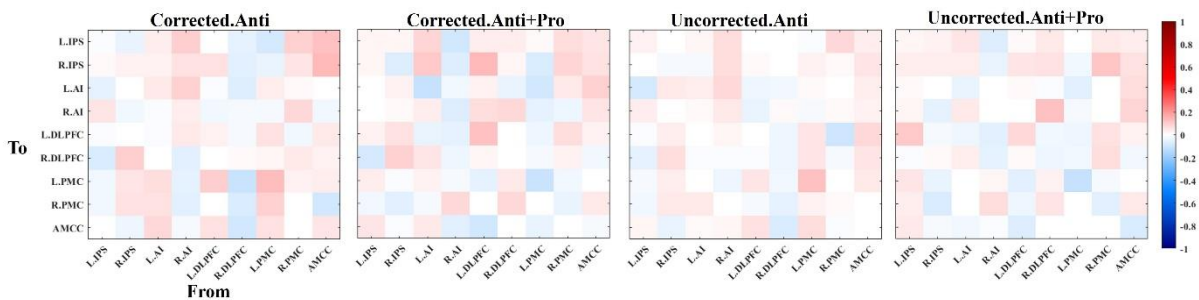


Fig. 6. Comparison of the task-evoked EC (matrix B) between the considered GLM designs (All-Trials vs. S-Trials) using between-group PEB analyses. The other considered conditions of the data processing (contrasts and thresholding) are indicated in the titles of the plots. The values of the connectivity differences are reflected by color as shown in the color bar, but no modulatory EC is above the 95% posterior probability threshold. See Methods of the nodes' abbreviations.

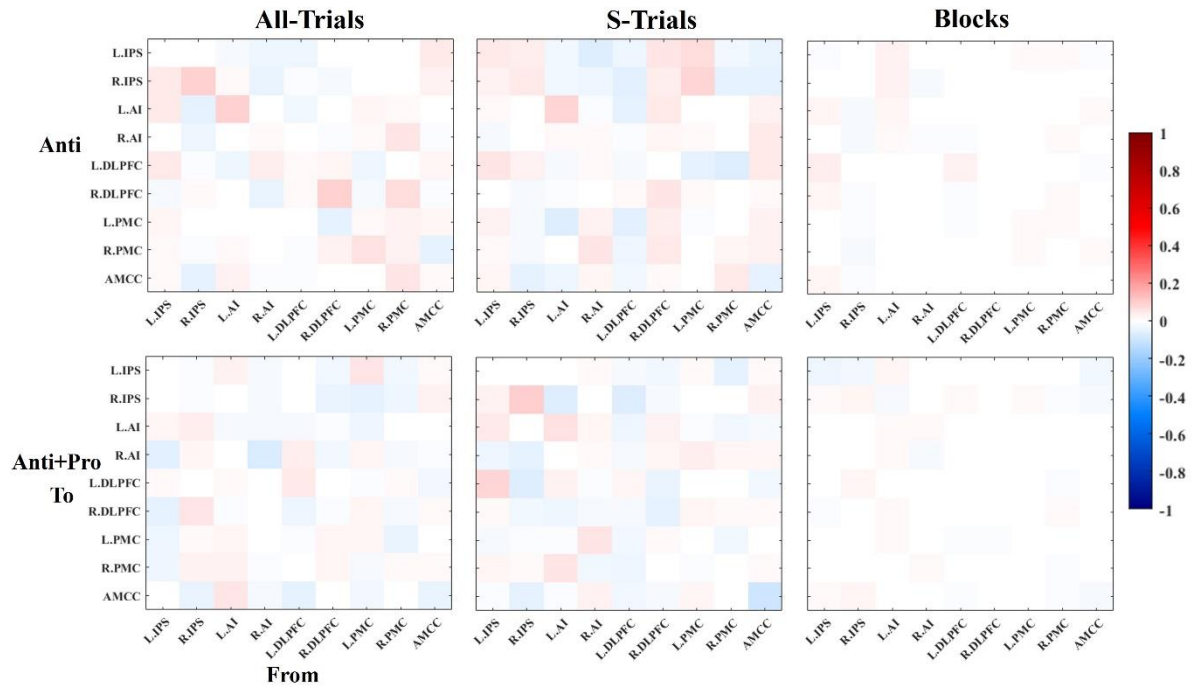


Fig. 7. Comparison of the task-evoked EC (matrix B) between the thresholding conditions (Corrected vs. Uncorrected) using between-group PEB analyses. The other considered conditions of the data processing (contrasts and GLM designs) are indicated in the titles of the plots. The values of the connectivity differences are reflected by color as shown in the color bar, but no modulatory EC is above the 95% posterior probability threshold. See Methods of the nodes' abbreviations.

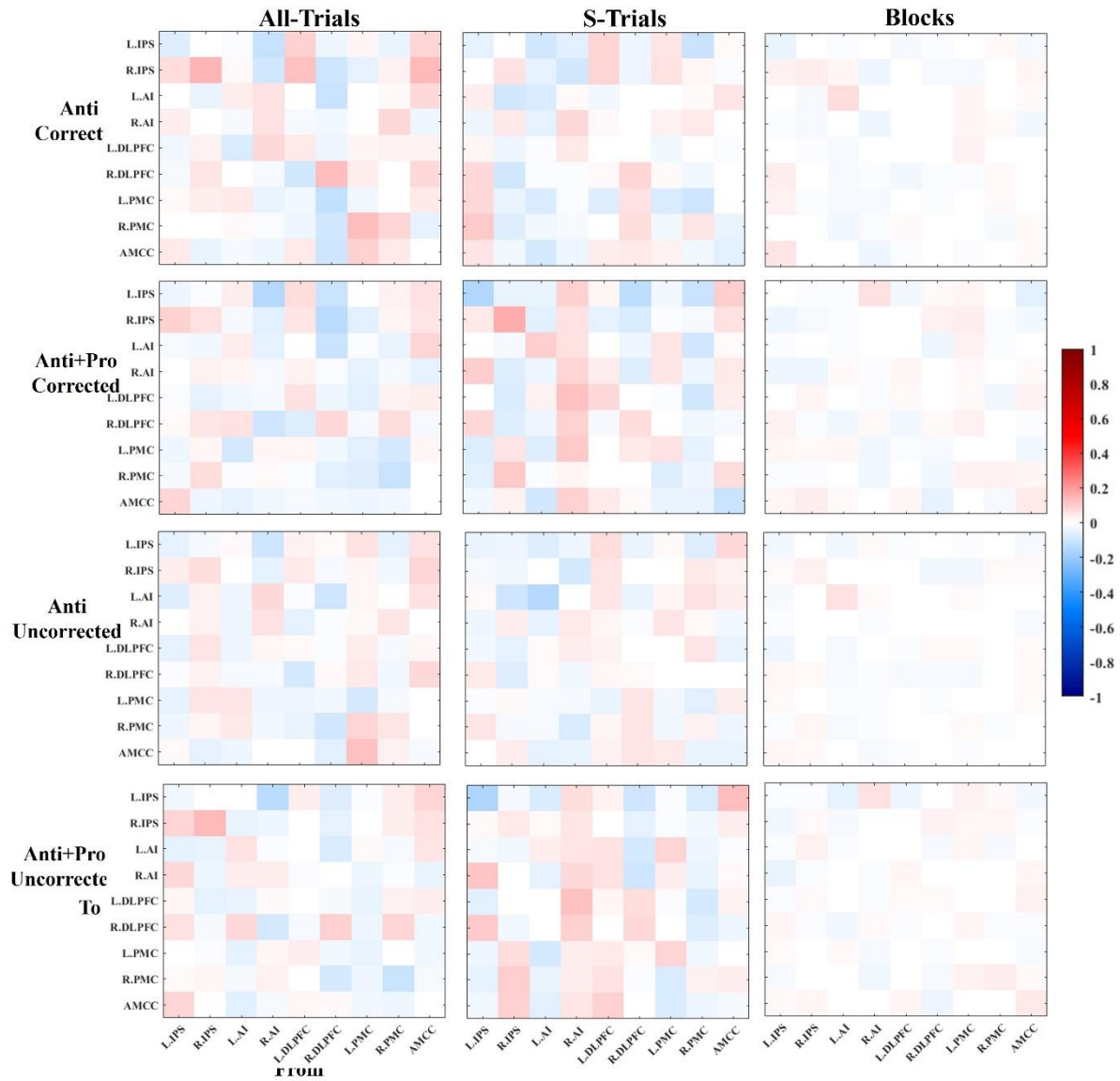


Fig. 8. Comparison of the task-evoked EC (matrix B) between the GSR conditions (With GSR vs. Without GSR). The results of PEB analyses at the group level are illustrated for the differences of B-matrices where the subtraction between conditions with and without GSR is performed: With GSR - Without GSR. The other considered conditions of the data processing (GLM designs, thresholding, and contrasts) are indicated in the titles of the plots. The values of the connectivity differences are reflected by color as indicated in the color bar, but no modulatory EC is above the threshold of 95% posterior probability. See Methods of the nodes' abbreviations.

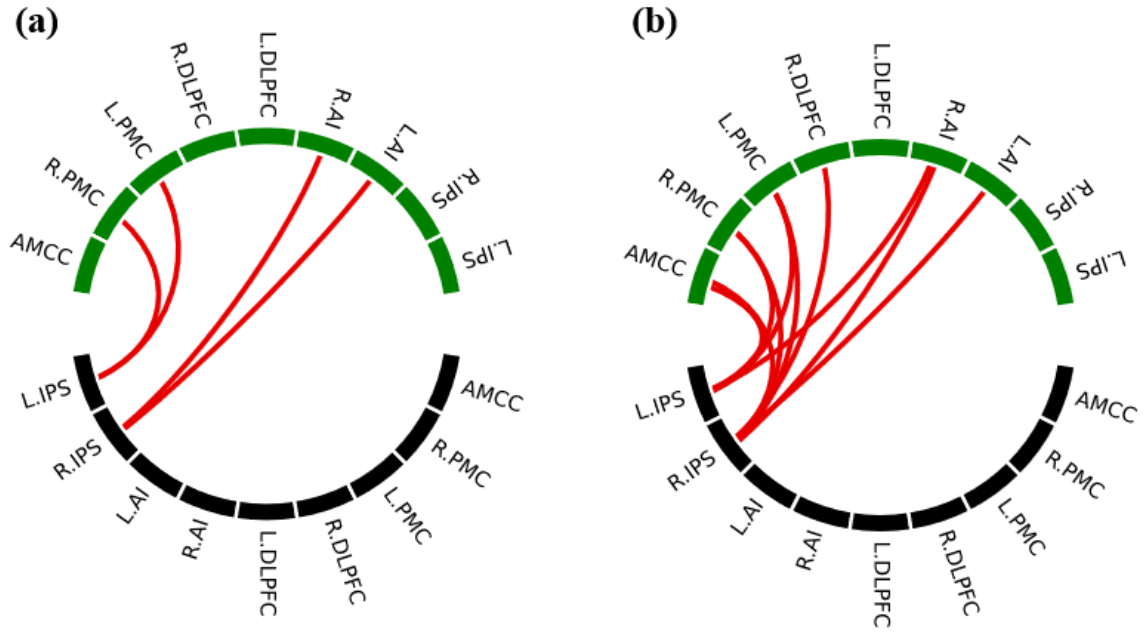


Fig. 9. The stable effective connectivity (EC) edges between group-mean and between-group PEB analyses for cases of (a) All-Trials > Black and (b) Anti+Pro > Anti. The calculation steps included: (1) For simplification, we extracted common EC edges (posterior probability/PP > 95%) from group-mean PEB analyses including the conditions of significance thresholding, All-Trials/Block GLM designs, and activation contrasts. This step offered EC edges that were stable across the conditions above. (2) After common group-mean EC edges (PP > 95%) were specified, we summed up EC edges showing strong evidence between-group PEB differences from all All-Trials > Block and all Anti+Pro > Anti between-group PEB analyses, respectively. (3) The stable EC edges of All-Trials > Block (Fig. 10a) were calculated by removing summed EC edges of All-Trials > Block from the common group-mean EC edges, and the stable EC edges of Anti+Pro > Anti (Fig. 10b) were calculated by removing summed EC edges of Anti+Pro > Anti from the common group-mean EC edges.

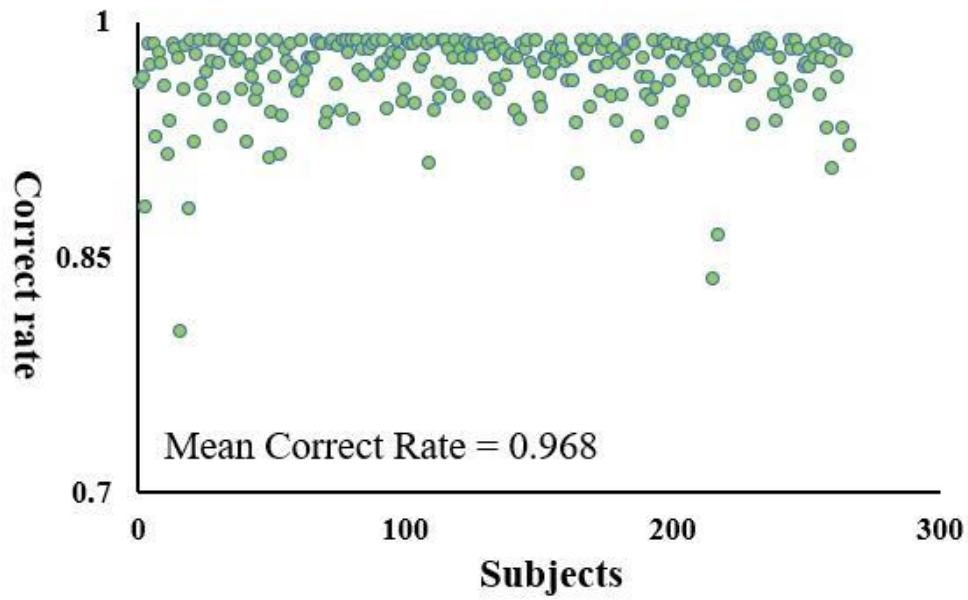


Fig. 10. The correct rate distribution across subjects ($n = 266$). The green dots indicate subjects, and the mean correct rate is 0.968. The individual correct rate was calculated by $1 - ((\text{erroneous trials} + \text{non-response trials}) / \text{all trials})$.

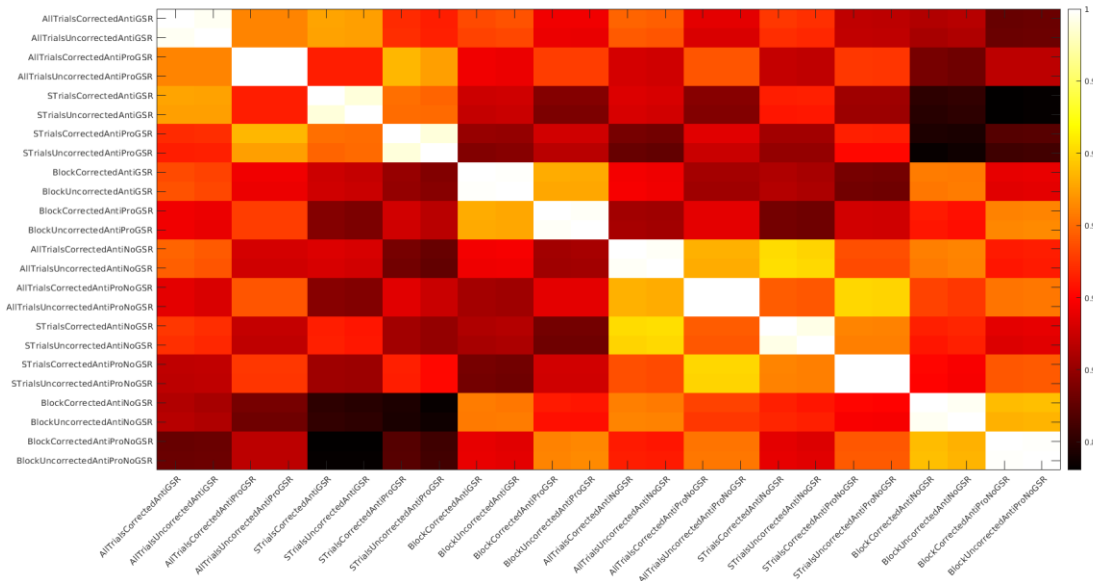


Fig. 11. Cross correlations (*Pearson*) between BOLD time series for any combined pair of considered data-processing conditions indicated on the axes. The time series were extracted for subject-level node ROIs for individual subjects from the same cohort of 90 subjects common (intersection) across all conditions. Node-wise cross-condition correlations were calculated for

individual subjects and then averaged across nodes and subjects into one correlation value depicted in color.

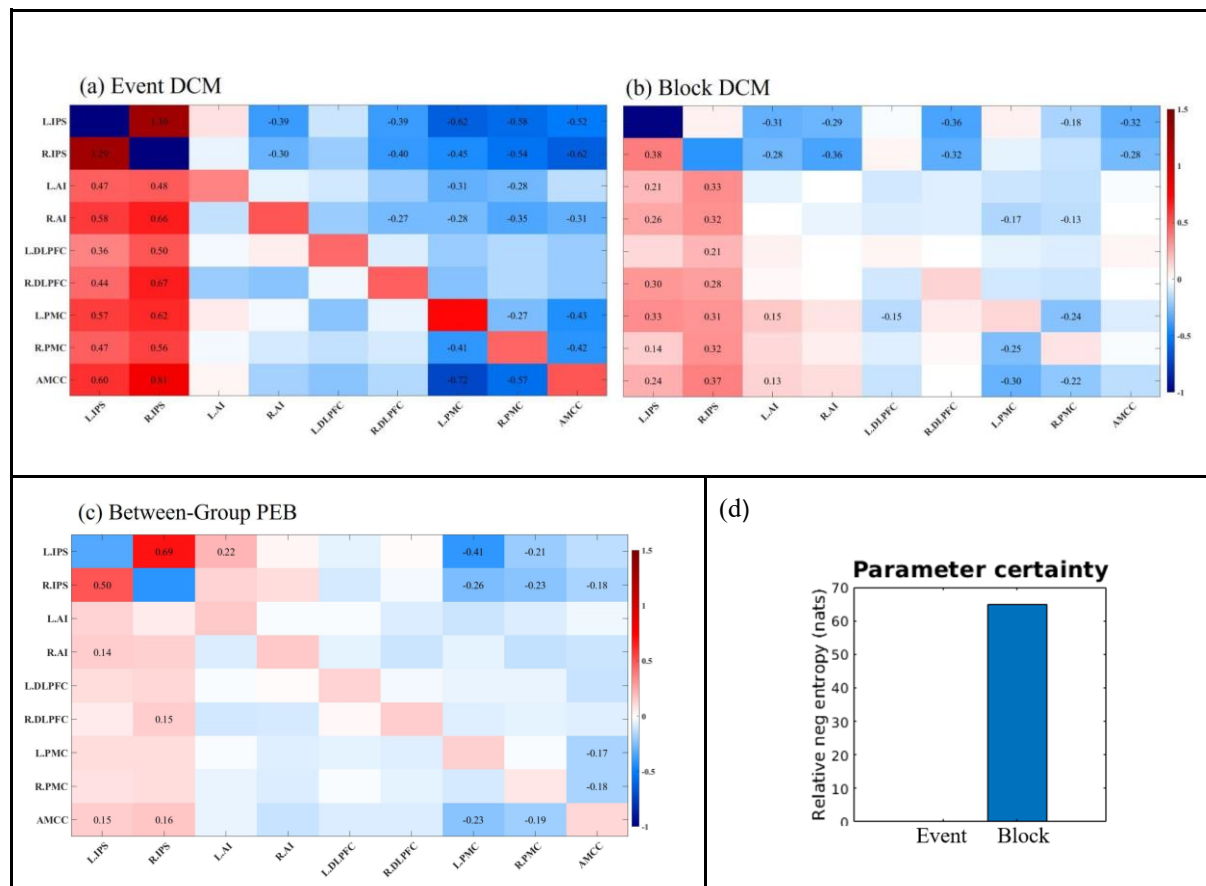
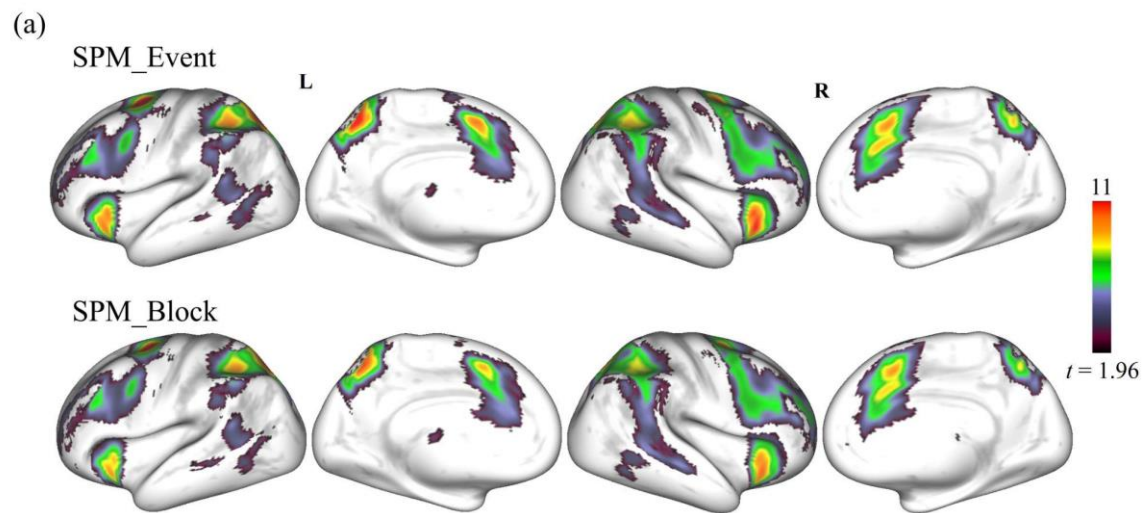


Fig. 12. Results of DCM calculations of the task-modulated EC (M-EC, matrix B) and its analysis for the case when the same BOLD signals extracted for the case of the block-based GLM of the uncorrected Anti+Pro contrast were supplied for modeling by the event-related and block-based DCM. (a) and (b) Connectivity patterns of the group-mean M-EC for event-related and block-based DCM designs as indicated in the titles of the plots. (c) and (d) The EC difference and parameter certainty between event-related and block-based designs. The strongly evident EC parameters ($PP > 95\%$) are indicated by numbers in the matrix cells.



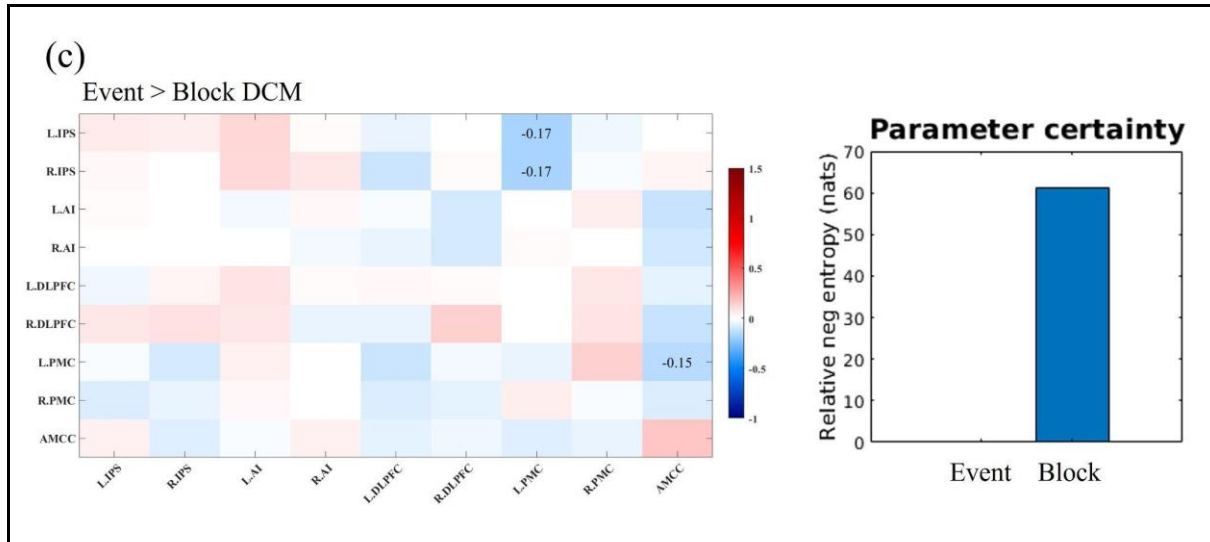


Fig. 13 Results of second-level fMRI statistics and sequential DCM analyses of the task-modulated EC (M-EC, matrix B) between event-related and block-based uncorrected Anti+Pro cases using the processing of SPM. (a) Results of the second-level fMRI analysis with different general linear model (GLM) designs, and were corrected by $p_{TFCE} < 0.05$. (b) Connectivity patterns of the group-mean M-EC for event-related and block-based DCM designs as indicated in the titles of the plots. (c) The EC difference and parameter certainty between event-related and block-based designs. The strongly evident EC parameters (PP > 95%) are indicated by numbers in the matrix cells.

Supplementary Methods

SPM-based pipeline

Here we verified whether and how the reported results and derived conclusions can be influenced if different pipelines for the processing and analysis of task-evoked fMRI data would be used. We therefore repeated the investigation workflow and conducted the data processing by SPM pipeline, and then compared the results of the task-fMRI data processing and analyses as well as DCM-calculated task-evoked EC for event-related (AllTrials) and block-based designs of the general linear model (GLM) and DCM for the uncorrected Anti+Pro contrast. The SPM processing used spatially normalized and smoothed functional images obtained as described in the Methods, where all data processing and analysis of the task-fMRI

data and DCM calculations were solely performed by SPM and included the following steps:

1. High-pass temporal filtering (128 s) was performed, and 27 regressors were convolved with hemodynamic response function during the first-level fMRI analysis by event-related and block-based GLM. Activation contrasts of Pro, Anti, Anti+Pro, and Anti-Pro were estimated.
2. A group-based activation as given by the Anti-Pro contrast was calculated and corrected by $p < 0.05$ with a family-wise error (FWE) rate (Supplementary Fig. S13a). The group-level peak coordinates (local maxima) were generated as SRC network nodes (Supplementary Table S11).
3. Individual peak coordinates generation and BOLD time series extraction were realized by the SPM volume-of-interest function that searched for the global maximal peak inside the spheres (radius = 10 mm) centered at the group-level peak coordinates, dilated the found individual peak of each regions of interest (ROI) into a sphere with a radius = 4 mm, employed the Anti+Pro contrast ($p < 0.05$ uncorrected) to remove insignificant voxels, and extracted the first eigenvariate as time series for DCM estimation.
4. Individual DCM estimation, calculation and checking of the explained variance (EV), evaluation of the group-mean EC by PEB, between-group PEB analysis, and Bayesian-data comparison (BDC) were the same as performed in the main text (see Methods).

Because of different data processing of the task-evoked fMRI, we observed some quantitative differences in results for the above SPM pipeline.

1. For the second-level fMRI analysis, we observed similar activation patterns between our analysis from the main text and the SPM pipeline (compare Fig. 2 and Supplementary Fig. S13a). For the later pipeline the Dice coefficient between the

activation maps of the event-related and block-based GLM is 0.94 as before (Supplementary Table S3), and the mean absolute difference between peak coordinates is 0.3 mm vs. 0.7 mm as before (Supplementary Tables S1 and S11). There are small differences of peak coordinates between the pipelines of 1.6 mm and 2.1 mm for the AllTrials and Block cases, respectively. The SPM pipeline in average led to somewhat smaller t-values of the activation peaks of 10.0 vs. 11.0 for the AllTrials and 9.3 vs. 10.4 for Blocks, which might be indicative for statistical quality of the modeled second-level activation maps (Supplementary Tables S1 and S11).

2. The same number of subjects (216) were qualified for the signal extraction and DCM analysis for the event-related case, while only 173 subjects (vs. 212) were approved by the SPM pipeline for the block-based design. We also observed differences in the modeling quality of DCM, where the pipeline from the main text offered a higher explained variance (EV) of DCM than the SPM pipeline of 24.6% vs. 19.1% and 22.9% vs. 17.9% for the AllTrials and Block cases, respectively (Supplementary Tables S4 and S12).
3. Based on the group-mean PEB analysis, we observed fewer strongly evident M-EC edges passing the threshold of the posterior probability (PP) > 95% for the SPM pipeline of 25 vs. 39 (-36%) for AllTrials and 28 vs. 32 (-13%) for Blocks (Table 3 and Supplementary Fig. S13b). At the same time, the average absolute connectivity intensity was also reduced for the SPM pipeline for 0.33 vs. 0.56 (-41%) for AllTrials and 0.23 vs. 0.26 (-12%) for Blocks (Supplementary Table S10 and Fig. S13b). Nevertheless, also for the SPM pipeline we still observed large differences in the group-mean connectivity patterns between event-related and block-based GLM and DCM designs (Supplementary Fig. S13b) as well as a larger connectivity intensity for the former design, but no pronounced difference in the number of strongly evident M-EC

edges.

4. The between-group PEB analysis still found differences in M-EC (All-Trials > Block), but only in 3 EC connections as compared to 14 edges reported for the pipeline used in the main text (Fig. 5 and Supplementary Fig. S13c).
5. The BDC analysis consistently demonstrated higher parameter certainty (Block > AllTrials GLM designs) also for the SPM pipeline (61 nats, Supplementary Fig. S13c) comparable to our results presented in the main text (64 nats, Fig. 7).

In summary, application of the SPM pipeline largely confirmed our main conclusions, where we can still observe that event-related and block-based GLM designs showed differences in EC patterns in spite of the fact that the quality of the processed and analyzed data was affected. We in particular observed lower statistics of the second-level analysis, a smaller subset of participants qualified for the DCM analysis, a smaller fraction of the BOLD variance explained by DCM, and a strong reduction of the M-EC density and intensity with PP > 95%, especially, for the event-related GLM and DCM designs.

Supplementary Tables

Table 1. The MNI peak coordinates (x, y, z) of the local maxima of *t*-values of the second-level analysis of the Anti-Pro contrast without GSR.

Peak	All-Trials				S-Trials				Blocks			
	<i>x</i>	<i>y</i>	<i>z</i>	<i>t</i>	<i>x</i>	<i>y</i>	<i>z</i>	<i>t</i>	<i>x</i>	<i>y</i>	<i>z</i>	<i>t</i>
LDLPFC	-40	22	28	7.3	-40	22	28	6.9	-40	22	28	7.0
RDLPFC	36	30	28	7.1	36	30	28	6.9	36	26	24	6.2
LPMC	-24	-8	48	16.2	-24	-8	48	16.5	-24	-8	48	15.3

RPMC	24	-6	50	11.8	24	-8	48	12.2	24	-6	50	11.0
LIPS	-34	-46	38	10.8	-34	-46	38	10.7	-34	-46	38	10.7
RIPS	36	-44	40	10.3	36	-44	40	10.6	36	-44	40	9.9
LAI	-32	18	-10	11.8	-32	18	-10	10.6	-32	18	-10	11.4
RAI	30	20	-4	13.1	30	20	-4	12.5	30	20	-4	12.1
AMCC	0	8	48	10.9	-2	6	48	10.5	0	8	48	10.3

The corresponding local maximal t -values are also indicated (in boldface) of all SRC network nodes (first column), considered GLM designs (first row), and the case without GSR. SRC, stimulus-response compatibility; GLM, general linear model; GSR, global signal regression; All-/S-Trials, experimental designs with all trials or only successful trials; Blocks, experimental designs modeled by blocks; L/R, left/right; DLPFC, dorsolateral prefrontal cortex; PMC, premotor cortex; IPS, intraparietal sulcus; AI, anterior insula; AMCC, anterior midcingulate cortex.

Table 2. Sample sizes for different conditions of the data processing without GSR

	All-Trials		S-Trials		Blocks	
	Corrected	Uncorrected	Corrected	Uncorrected	Corrected	Uncorrected
Anti	163/160	215/209	153/151	211/207	173/168	222/213
Anti+Pro	178/176	221/216	170/170	213/208	185/182	218/212

The two subject numbers given in each table cell correspond to the subject samples qualified for BOLD signal extraction for SRC network nodes of individual subjects/explained variance criterion of dynamic causal modeling, see Sec. 2.6 / Sec. 2.7 for details. Used notations: GSR,

global signal regression; All-/S-Trials, experimental designs with all/successful trials; Blocks, experimental designs modeled by blocks; Anti, incompatible contrast; Anti+Pro, incompatible+compatible contrast.

Table 3. Dice's value across different GLM designs with GSR

Dice's D	All-Trials	S-Trials	Blocks
All-Trials	1	0.94	0.94
S-Trials	0.94	1	0.93
Block	0.94	0.93	1

Dice's D is calculated by the following equation: $D=2C/(A+B)$. C denotes overlapped voxels; A and B denote voxels in the condition of A and B. All-Trials, general linear model (GLM) design with all stimuli and responses; S-Trials, GLM design with successfully-responded stimuli and responses; Blocks, GLM design coded by block onset and duration information. GSR, global signal regression.

Table 4. Averaged explained variance (EV) and its standard deviation estimated for all conditions.

	All-Trials		S-Trials		Blocks	
	Corrected	Uncorrected	Corrected	Uncorrected	Corrected	Uncorrected
Anti ¹	23.9±7.1	22.6±7	23.1±6.3	21.6±6.4	23.7±7.6	22.6±7.5
Anti+Pro ¹	25.4±6.9	24.6±7	24.4±6.6	23.6±6.6	23.6±7	22.9±7
Anti ²	24±7.7	23±7.4	23.4±7.1	22±6.9	23.7±7.8	22.8±7.9

Anti+Pro ²	25.1±7.5	24.4±7.6	24.5±7.4	23.8±7.3	23.6±7.7	23.3±7.6
-----------------------	----------	----------	----------	----------	----------	----------

Note: ¹ indicates the conditions with global signal regression (GSR), while ² indicates the conditions without GSR. All-/S-Trials, experimental designs with all/successful trials; Blocks, experimental designs modeled by blocks; Anti, incompatible contrast; Anti+Pro, incompatible+compatible contrast.

Table 5. Numbers of the group-level EC edges of modulatory (matrix B) EC (PP > 95%) within the SRC network without GSR.

	All-Trials		S-Trials		Blocks	
	Corrected	Uncorrected	Corrected	Uncorrected	Corrected	Uncorrected
Anti	34	40	32	43	12	18
Anti+Pro	36	40	37	40	33	35

All modulatory effective connectivity (EC) connections were exceeding 95% of the posterior probability (excluding self-connections) calculated by Parametric Empirical Bayes (PEB) for the considered conditions of the data processing without global signal regression (GSR). All-/S-Trials, experimental designs with all/successful trials; Blocks, experimental designs modeled by blocks; Anti, incompatible contrast; Anti+Pro, incompatible+compatible contrast.

Table 6. Relative differences in parameter certainty between GLM designs estimated from Bayesian Data Comparison (BDC)

GSR	Block > All-Trials	Block > S-Trials	All-Trials > S-Trials
-----	--------------------	------------------	-----------------------

	Anti	Anti+Pro	Anti	Anti+Pro	Anti	Anti+Pro
Corrected	58.1	64.2	62.9	62.4	2.3	-1.1
Uncorrected	66.5	64.0	66.7	63.3	0.5	-0.9

Note: the number in each element indicates a relative difference in parameter certainty estimated from the BDC analysis between conditions of different general linear model (GLM) designs. Used notations are the same as in Table 5. The relative value was extracted between two groups (same size) using Bayesian data comparison (`spm_dcm_bdc.m`), and represents the relative levels of parameter certainty (nats) of the estimated model parameter. A difference between two data sets in the range between 1.1 and 3 nats (natural units) and between 3 and 5 nats can be considered as “positive evidence” and “strong evidence”, respectively. The higher value indicates higher parameter certainty in one condition relative to the other one. For example, Block-based designs showed very strong evidence in parameter certainty compared to event-related designs.

Table 7. Relative differences in parameter certainty between activation contrasts (Anti > Anti+Pro) estimated from Bayesian Data Comparison (BDC)

Activation contrast	AllTrials		STrials		Block	
	Corrected	Uncorrected	Corrected	Uncorrected	Corrected	Uncorrected
Value	9.7	7.9	7.2	7.0	10.4	11.1

Note: the number in each element indicates a relative difference in parameter certainty between activation contrasts (Anti > AntiPro) estimated from the BDC analysis. Used notations are the same as in Table 6.

Table 8. Relative differences in parameter certainty between conditions of GSR (with GSR > without GSR) estimated from Bayesian Data Comparison (BDC)

GSR	All-Trials		S-Trials		Block	
	Anti	Anti+Pro	Anti	Anti+Pro	Anti	Anti+Pro
Corrected	-0.3	-1.9	-0.7	-1.4	0.4	1.5
Uncorrected	0.4	-2.2	-0.3	-2.6	0.1	1.6

Note: the number in each element indicates a relative difference in parameter certainty between conditions of with GSR and without GSR from the BDC analysis. Used notations are the same as in Table 5.

Table 9. Relative differences in parameter certainty (Corrected > Uncorrected)

Significance thresholding	All-Trials		S-Trials		Block	
	Anti	Anti+Pro	Anti	Anti+Pro	Anti	Anti+Pro
Value	1.1	0.4	0.03	0.7	-0.2	-0.2

Note: the number in each element indicates a relative difference in parameter certainty between conditions of corrected and uncorrected from the BDC analysis. Used notations are the same as in Table 5.

Table 10. Averaged absolute intensity of task-evoked modulatory EC (PP > 95%) of all conditions

All-Trials	S-Trials	Blocks
------------	----------	--------

	Corrected	Uncorrected	Corrected	Uncorrected	Corrected	Uncorrected
Anti ¹	0.48	0.46	0.49	0.46	0.34	0.33
Anti+Pro ¹	0.55	0.54	0.56	0.53	0.27	0.26
Anti ²	0.47	0.45	0.49	0.44	0.33	0.30
Anti+Pro ²	0.52	0.5	0.55	0.52	0.27	0.26

Note: ¹ indicates the conditions with GSR, while ² indicates the conditions without GSR. Each element in this table indicates the averaged absolute value of effective connectivity (EC) for each condition. All-Trials, general linear model (GLM) design with all stimuli and responses; S-Trials, GLM design with successfully-responded stimuli and responses; Blocks, GLM design coded by block onset and duration information. Corrected, the condition of corrected significance thresholding; Uncorrected, the condition of uncorrected significance thresholding.

Table 11. MNI peak coordinates (x, y, z) of the local maxima of *t*-values based on the second-level fMRI statistics of the Anti-Pro contrast (from SPM processing)

Peak	All-Trials				Blocks			
	<i>x</i>	<i>y</i>	<i>z</i>	<i>t</i>	<i>x</i>	<i>y</i>	<i>z</i>	<i>t</i>
LDLPFC	-40	28	28	6.6	-40	28	28	6.4

RDLPFC	36	30	26	6.8	38	32	26	6.8
LPMC	-24	-8	48	13.9	-24	-8	48	12.5
RPMC	24	-8	48	10.8	24	-8	48	9.7
LIPS	-32	-46	38	9.6	-32	-46	38	9.8
RIPS	38	-48	42	8.9	38	-48	42	8.4
LAI	-30	18	0	10.8	-30	18	0	9.8
RAI	30	18	0	12.3	30	18	0	11.1
AMCC	-6	4	46	10.7	-4	6	46	9.5

The corresponding local maximal *t*-values are also indicated (in boldface) of all SRC network nodes (first column), considered GLM designs (first row), and the case based on the SPM processing. SRC, stimulus-response compatibility; GLM, general linear model; All-/S-Trials, experimental designs with all trials or only successful trials; Blocks, experimental designs modeled by blocks; L/R, left/right; DLPFC, dorsolateral prefrontal cortex; PMC, premotor cortex; IPS, intraparietal sulcus; AI, anterior insula; AMCC, anterior midcingulate cortex.

Table 12. Summary of subject cohort size qualified for signal extraction and DCM analyses, variance of BOLD signals explained by DCM, and connectivity intensity for the SPM processing

GLM designs	Subjects	Explained variance	Absolute intensity
All-Trials	258/216	19.1±7.4 %	0.33
Blocks	256/173	17.9±8.8 %	0.23

The two subject numbers given in “Subjects” cells correspond to the subject samples qualified for BOLD signal extraction for SRC network nodes of individual subjects/explained variance criterion of DCM,. The two numbers given in “Explained variance” cells correspond to average and standard deviation of explained variance for event-related and block-based GLM cases. The absolute intensity was calculated by average absolute intensity value of evident EC (posterior probability > 95%).

Study 2: Predicting response speed and age from task-evoked effective connectivity

Shufei Zhang^{1,2}, Kyesam Jung^{1,2}, Robert Langner^{1,2}, Esther Florin³, Simon B. Eickhoff^{1,2}, Oleksandr V. Popovych^{1,2}

¹Institute of Neuroscience and Medicine, Brain and Behaviour (INM-7), Research Centre Jülich, Germany

²Institute for Systems Neuroscience, Medical Faculty, Heinrich-Heine University Düsseldorf, Germany

³Institute of Clinical Neuroscience and Medical Psychology, Medical Faculty, Heinrich-Heine University Düsseldorf, Germany

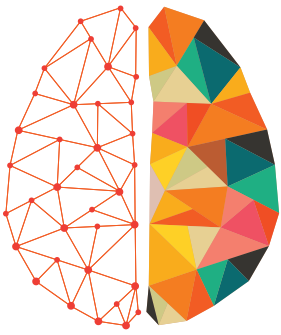
*Corresponding author: o.popovych@fz-juelich.de

Published in Network Neuroscience, 9(2), 591–614.

https://doi.org/10.1162/netn_a_00447

Own contributions

Writing the manuscript, preparing figures, performing data analyses, and contributing to the interpretation of results.



NETWORK NEURO SCIENCE

an open access  journal



Citation: Zhang, S., Jung, K., Langner, R., Florin, E., Eickhoff, S. B., & Popovych, O. V. (2025). Predicting response speed and age from task-evoked effective connectivity. *Network Neuroscience*, 9(2), 591–614. https://doi.org/10.1162/netn_a_00447

DOI:
https://doi.org/10.1162/netn_a_00447

Supporting Information:
https://doi.org/10.1162/netn_a_00447

Received: 11 July 2024
Accepted: 26 January 2025

Competing Interests: The authors have declared that no competing interests exist.

Corresponding Author:
Oleksandr V. Popovych
o.popovych@fz-juelich.de

Handling Editor:
Olaf Sporns

Copyright: © 2025
Massachusetts Institute of Technology
Published under a Creative Commons
Attribution 4.0 International
(CC BY 4.0) license



RESEARCH

Predicting response speed and age from task-evoked effective connectivity

Shufei Zhang^{1,2}, Kyesam Jung^{1,2}, Robert Langner^{1,2}, Esther Florin³,
Simon B. Eickhoff^{1,2}, and Oleksandr V. Popovych^{1,2}

¹Institute of Neuroscience and Medicine, Brain and Behaviour (INM-7), Research Centre Jülich, Jülich, Germany

²Institute for Systems Neuroscience, Medical Faculty, Heinrich-Heine University Düsseldorf, Düsseldorf, Germany

³Institute of Clinical Neuroscience and Medical Psychology, Medical Faculty, Heinrich-Heine University Düsseldorf, Düsseldorf, Germany

Keywords: Task fMRI, Dynamic causal modeling, Analytic flexibility, Machine learning, Brain-based prediction, Stimulus-response compatibility, Functional connectivity

ABSTRACT

Recent neuroimaging studies demonstrated that task-evoked functional connectivity (FC) may better predict individual traits than resting-state FC. However, the prediction properties of task-evoked effective connectivity (EC) remain unexplored. We investigated this by predicting individual reaction time (RT) performance in the stimulus-response compatibility task and age, using intrinsic EC (I-EC; calculated at baseline) and task-modulated EC (M-EC; induced by experimental conditions) with dynamic causal modeling (DCM) across various data processing conditions, including different general linear model (GLM) designs, Bayesian model reduction, and different cross-validation schemes and prediction models. We report evident differences in predicting RT and age between I-EC and M-EC, as well as between event-related and block-based GLM and DCM designs. M-EC outperformed both I-EC and task-evoked FC in RT prediction, while all types of connectivity performed similarly for age. Event-related GLM and DCM designs performed better than block-based designs. Our findings suggest that task-evoked I-EC and M-EC may capture different phenotypic attributes, with performance influenced by data processing and modeling choices, particularly the GLM-DCM design. This evaluation of methods for behavior prediction from brain EC may contribute to a meta-scientific understanding of how data processing and modeling frameworks influence neuroimaging-based predictions, offering insights for improving their robustness and efficacy.

AUTHOR SUMMARY

We investigated how brain task-evoked effective connectivity (EC) can predict individual differences in behavior and age. We examined two types of EC: intrinsic EC (calculated at baseline) and task-modulated EC (induced by experimental conditions) calculated by dynamic causal modeling across various data processing conditions. We found that the task-modulated EC outperformed intrinsic EC in predicting reaction time measured during a stimulus-response task, while both EC types performed similarly in age prediction. Our findings may suggest that different EC types could capture distinct phenotypic traits, with performance influenced by data processing and modeling choices. This evaluation may further promote the application of model-based approaches to behavior prediction from brain connectivity and enhance our understanding of the impact of data processing on the prediction results.

Functional connectivity (FC):
Statistical correlations between brain regions' activity, indicating their functional relationships.

Dynamic causal modeling (DCM):
A computational approach for inferring directed interactions between brain regions from neuroimaging data.

Effective connectivity (EC):
The influence one brain region exerts over another, estimated using causal models like DCM.

Intrinsic effective connectivity (I-EC):
EC reflecting baseline interactions in the absence of task-related modulations.

Task-modulated effective connectivity (M-EC):
EC connections driven by specific task conditions.

INTRODUCTION

Linking individual differences in behavior with individual brain properties is one of the main goals of cognitive neuroscience (Biswal et al., 2010; Huth et al., 2016). Functional magnetic resonance imaging (fMRI) has been instrumental in predicting individual behavior and phenotypes by modeling brain activation and connectivity patterns (Biswal et al., 2010; Fox et al., 2007; van den Heuvel & Pol, 2010). Functional connectivity (FC), the correlation between blood-oxygen-level-dependent (BOLD) signal fluctuations of two brain regions, reveals task-evoked and resting-state coactivation patterns (Biswal et al., 2010; Cole et al., 2014). Although resting-state FC has been widely studied for predicting behaviors and phenotypes (Dosenbach et al., 2010; Heckner et al., 2023; Sripada et al., 2020), accumulating evidence indicates that task-evoked FC may better capture intersubject differences than resting-state FC (Finn & Bandettini, 2021; Finn et al., 2017; Rosenberg et al., 2016), with studies showing improved predictions for reading skills (Jiang et al., 2020), fluid intelligence (Greene et al., 2018), and general cognitive ability (Zhao et al., 2023)—but see Kraljević et al. (2024) for contradictory evidence.

The correlational nature of FC is agnostic to the causal interdependencies between brain regions. These causal aspects of interregional coupling may however be especially informative about individual differences in behavior when studying connectivity patterns during task states. Recent achievements in generative embedding methods have provided powerful frameworks for capturing causal interdependence. Among a few generative embedding methods (Rajapakse & Zhou, 2007; Roebroek et al., 2005; Schlösser et al., 2003), dynamic causal modeling (DCM) (Friston et al., 2003) offers a biologically meaningful approach to estimating brain effective connectivity (EC) from task-evoked fMRI. Within this framework, EC is inferred from DCM in order to estimate the directional influence of a given brain region on another (Friston et al., 2003) and is intended to provide deeper, mechanistic insights by explicitly modeling such causal influences (Friston, 2011). This characteristic may contribute more discriminative features to EC to better identify individual “fingerprints” (Geng et al., 2018). In DCM, intrinsic EC (I-EC) corresponds to the A matrix in the DCM equation (see the *Methods* section), representing baseline connectivity in the absence of task modulation, while task-modulated EC (M-EC) corresponds to the B matrix, capturing changes in connectivity driven by specific experimental conditions (Zeidman, Jafarian, Corbin, et al., 2019). These components thus reflect brain connectivity at baseline and in task-modulated states, respectively.

Building on this, we aimed to explore whether I-EC and M-EC can display such differential roles in prediction. Both of them have been investigated with respect to a range of human cognitive functions such as working memory, finger tapping, response conflict resolution, and reading as well as aging at the level of group-average effects (Boudrias et al., 2012; Cieslik et al., 2011; Jung et al., 2018; Kahan et al., 2019; Loehrer et al., 2016; Morken et al., 2017; Volz et al., 2015). With regard to interindividual differences, recent studies have begun to utilize EC modeling approaches to predict individual behaviors and phenotypes including age differences and task performance either from I-EC or M-EC (Beck et al., 2021; Brodersen et al., 2011; Diersch et al., 2021; Tsvetanov et al., 2016). However, in contrast to extensive comparisons of predictive performance between different types of FC (Greene et al., 2018), prediction performance based on task-evoked EC features and, in particular, the difference between features derived from I-EC versus M-EC components remains unexplored.

We addressed this by using task-evoked EC modeled via DCM for the prediction of (a) individual average reaction time (RT) of incongruent conditions during a spatial stimulus-response compatibility (SRC) task (Fitts & Deininger, 1954; Langner et al., 2015) and (b) age as two

Cross-validation (CV):
A method for evaluating model performance by partitioning data into training and testing subsets.

General linear model (GLM):
A statistical framework for modeling and testing linear relationships in neuroimaging data.

Bayesian model reduction (BMR):
A Bayesian inference technique for optimizing model evidence by simplifying parameters.

Lasso:
A regression technique using L1 regularization for feature selection and prediction accuracy.

Ridge regression:
A regression method employing L2 regularization at the estimation of model parameters.

different (behavioral and demographic) individual characteristics. The spatial SRC task is designed to probe cognitive action control during response conflict processing, associated with an increase of RT in the incongruent condition, relative to the congruent one (Langner et al., 2015), and this incongruity effect was found to be further enhanced in advanced age (Proctor et al., 2005). These characteristics have motivated our endeavor to predict individual age and cognitive action control, as reflected in the incompatibility effects measured by RT. Predicting the distinct characteristics such as age and RT is also important for understanding changes in brain neural dynamics during the SRC task by contrasting the prediction performances for these different behavioral/phenotypic scores.

In this study, we compared the prediction results for individual RT and age using I-EC and M-EC components derived from fMRI data obtained during SRC task performance. Although the I-EC component inferred from task-evoked functional data is not entirely independent of the task-related contexts, it is still considered to reflect brain intrinsic connectivity dynamics by mathematically removing task-relevant variance (Marreiros et al., 2008; Zeidman, Jafarian, Corbin, et al., 2019). This makes it a reasonable candidate for comparison with M-EC components in predictions. Our approach included the following steps: (a) We extracted nodes of the SRC network and estimated I-EC and M-EC for each participant. (b) We calculated the prediction accuracy of I-EC and M-EC for RT and age predictions using 5-fold cross-validation (CV) and conducted sensitivity analyses to examine the impact of various factors. These factors included different general linear model (GLM) and DCM designs (Huettel, 2012; Logothetis, 2008), multiple CV schemes consisting of a 10-fold CV and leave-one-out CV (LOOCV), as well as the Bayesian model reduction (BMR) approach (Friston et al., 2016). (c) We compared the prediction accuracy of the task-evoked EC and FC. Since EC patterns may depend on the sample size (Silchenko et al., 2023), we applied our prediction analyses to a relatively large group of participants ($n > 200$). We in particular show that the type of GLM/DCM design (event-related vs. block-based) and EC modality (intrinsic at baseline vs. task-modulated) have a crucial influence on prediction performance, while the other conditions considered have a rather weak impact. Furthermore, task-evoked EC was found to outperform FC in RT prediction, but not in age prediction.

METHODS

This study investigated the application of task-evoked EC calculated by the DCM approach to the prediction of behavioral data of individual subjects by using a machine-learning approach. We considered the spatial SRC task (Fitts & Deininger, 1954), calculated the task-evoked EC of the respective task-evoked SRC brain network, and used linear regression with the least absolute shrinkage and selection operator (LASSO) regularization (Tibshirani, 1996) to predict RT and age of individual subjects. This was replicated using ridge regression and compared with prediction results based on task-evoked FC features. Furthermore, we considered typical points of analytical flexibility and investigated the impact of data processing, EC calculation, feature extraction, and prediction procedure as explained in detail below.

Experimental Protocol

The present study used fMRI data recorded while participants performed a spatial SRC task (Fitts & Deininger, 1954; Langner et al., 2015). This two-choice reaction task consisted of 24 blocks of trials with response requirements that were either spatially compatible ("Pro") or incompatible ("Anti") with a visual stimulus (Supporting Information Figure S1a). In particular, participants were instructed to respond to lateralized visual stimuli by accurately and

rapidly pressing an ipsilateral (Pro) or contralateral button (Anti), respectively. Before each block, a 2-s instruction was presented to indicate the upcoming condition (Pro or Anti), and each block contained 13 to 16 trials, in which the stimulus was presented for 0.2 s at the beginning of each trial on either the left or right side of the screen with equal probability (50%) for each side. The intervals between trial onsets randomly varied from 2 to 4.5 s according to a uniform distribution, and rest periods between blocks ranging from 15 to 19 s were also randomly jittered according to a uniform distribution. Each task condition (Pro and Anti) was repeated 12 times, with conditions (blocks) and stimuli within each condition being presented in a pseudorandomized order. Trials with responses being too fast or too slow ($RT < 150$ ms or $RT > 1,500$ ms) were excluded, and individual average RT of incongruent (Anti) conditions was extracted as the prediction target.

Participants

Our study included an initial sample of 271 subjects (148 males, 123 females, 18–85 years old, $M_{age} = 52.3 \pm 16.6$ years) recruited from the subject pool of the 1000BRAINS project (Caspers et al., 2014), which was conducted at the Research Centre Jülich. Before entering the study, the written informed consent of each subject was acquired. The study protocol was approved by the ethics committee of the University Duisburg-Essen (reference number: 11-4678) and performed in accordance with the declaration of Helsinki.

MRI Data Acquisition

Details about MRI data included in the 1000BRAINS project can be found elsewhere (Caspers et al., 2014). Structural MRI scans were obtained using an anatomical 3D T1w MPRAGE sequence (Magnetization Prepared Rapid Gradient Echo) with the following parameters: repetition time (TR) = 2.0 s, echo time (TE) = 3.03 ms, flip angle = 9° , 176 sagittal slices, field of view = 256 mm, voxel resolution = $1 \times 1 \times 1$ mm³.

The task fMRI scans were obtained by a gradient-echo echo-planar imaging sequence with the following parameters: TR = 2.03 s, TE = 30 ms, flip angle = 80° , field of view = 200 mm, 33 axial slices (ascending), slice thickness = 3.3 mm, interslice gap = 0.66 mm, voxel resolution = $3.1 \times 3.1 \times 3.3$ mm³, acquisition time = 27 min and 10 s.

Data Processing

In our previous study (Zhang et al., 2024), several data processing and EC calculation conditions were considered with a particular focus on the type of GLM design. The present study aimed to investigate the prediction performance of I-EC and M-EC by considering two different GLM designs (event-related vs. block-based). Briefly, the preprocessing steps (Figure 1) included dummy-volume exclusion, head-motion correction, intensity normalization, co-registration, spatial normalization, smoothing (8-mm Gaussian kernel), covariance regression (24 head-motion parameters, and regressors of white-matter, cerebrospinal-fluid, and global signals), and high-pass temporal filtering (128 s). The individual BOLD signals were modeled through the utilization of two distinct GLM designs: event-related and block-based designs (Supporting Information Figures S1b and S1c). In the event-related design, a step function with a specific onset time of an individual stimulus and a fixed “on” duration of 0.2 s were used for each stimulus. The block-based design incorporated each block’s starting time and full duration as the onset time and duration, respectively. Then, the second-level GLM analyses were used to derive activation maps specifically related to stimulus-response incompatibility (i.e., Anti > Pro condition contrasts; Figures 2a and 2b) for block-based and event-related designs

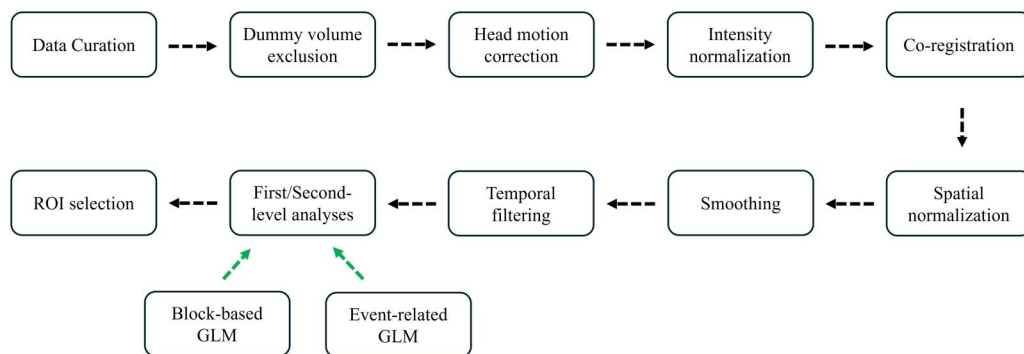


Figure 1. Flow chart for the stimulus-response compatibility task-evoked network node selection. The dashed arrows indicate the processing flow. Abbreviations: ROI, regions of interest; GLM, general linear model.

using FSL (Version 6.0) (<https://fsl.fmrib.ox.ac.uk/fsl/fslwiki>). Afterward, nine regions of interest (ROIs; 10 mm radius) of brain activation were defined based on the observed activation peaks leading to the group-level SRC-related brain network (Figure 2c): anterior midcingulate cortex (AMCC), bilateral intraparietal sulcus (IPS), premotor cortex (PMC), dorsolateral prefrontal cortex (DLPFC), and anterior insula (AI). The selection of ROIs agrees with previous literature on SRC tasks, where both the aging and incompatibility effects on them have been reported (Cieslik et al., 2010; Langner et al., 2015). These ROIs were then overlaid with the first-level

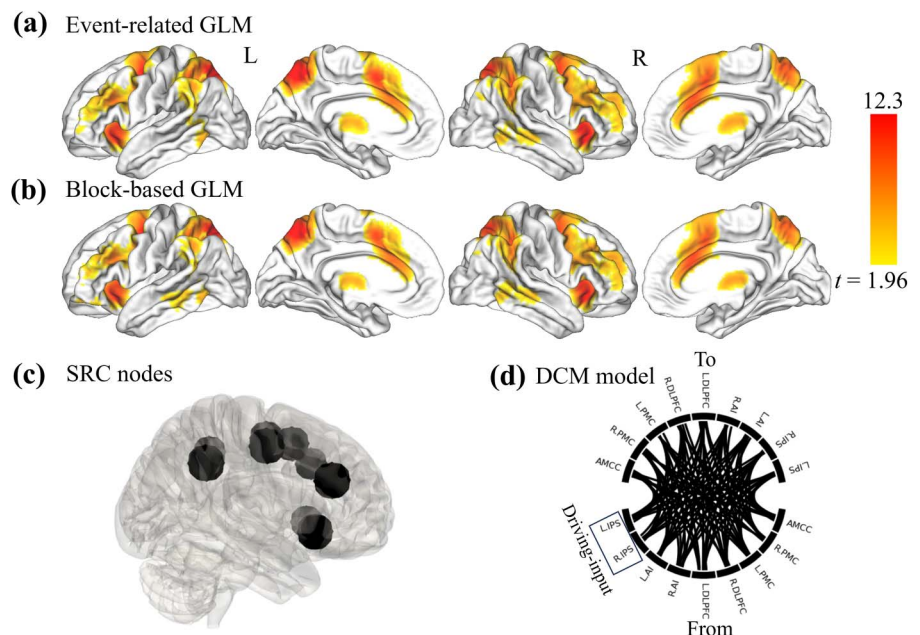


Figure 2. The general DCM workflow. (a, b) Second-level fMRI statistics computed from the incompatible (Anti) > compatible (Pro) activation contrasts. Maps illustrate the t values (scaling given in the color bar) of the t tests reflecting the statistically significant voxels across all subjects with the threshold-free cluster-enhancement (TFCE) and family-wise error (FWE) methods ($p_{TFCE+FWE} < 0.05$). (c) Example of SRC nodes extracted from the maps illustrated in plots (a, b). (d) Schematic illustration of the full-connection DCM model that was implemented in the analysis of effective connectivity (EC). Abbreviations: L/R, left/right; DLPFC, dorsolateral prefrontal cortex; PMC, premotor cortex; IPS, intraparietal sulcus; AI, anterior insula; AMCC, anterior midcingulate cortex. Events, experimental designs with all trials; Block, experimental designs modeled by blocks; TFCE, threshold-free cluster enhancement; FWE, family-wise error.

GLM-derived activation map related to performing the Anti condition of each subject thresholded at $p < 0.05$ and to search for subject-specific activation peaks within the group-level ROIs and dilate these peaks into spheres with a 4-mm radius. Finally, the BOLD time series for all nine individual ROIs (first eigenvariate of all significant voxels within a sphere) were estimated for each subject, which was then modeled by DCM for the full-connection model. For the event-related and block-based GLM and DCM designs, 210 and 213 participants, respectively, were qualified for the extraction of individual BOLD signals of the SRC network, because not all individual ROIs contained significant voxels for some subjects. More details about fMRI data processing as well as extraction of the task-evoked BOLD signals of the SRC network of individual subjects for DCM calculation can be found in Zhang et al. (2024) and in the Supporting Information.

DCM Specification and Analysis

The DCM analysis (Friston et al., 2003) was conducted based on the following model:

$$\frac{dz}{dt} = \left(A + \sum_k B^{(k)} u_k(t) \right) z + Cu(t).$$

Here, z represents the neural states of network ROIs across time points, the matrices A and B stand for parameters of intrinsic and task-modulated connectivity, respectively, and $u_k(t)$ encodes the timing of the experimental condition k . Matrix C represents the influence of all external experimental inputs (stimulation) $u(t)$ on the neural dynamics of the considered ROIs. The observed BOLD response $y(t)$ is modeled by the observation equation:

$$y(t) = h(z(t) + \varepsilon(t))$$

where $h(\cdot)$ represents the hemodynamic response function and $\varepsilon(t)$ indicates the noise. The model was used to infer the coupling parameters of the above matrices such that the simulated BOLD signals best explained the variance of the empirical BOLD signals.

Several DCM parameters are therefore defined as follows: (a) *Driving input* (matrix C) that defines external visual input to the network. Given that IPS nodes were identified as pivotal hubs for sensorimotor integration during visually guided actions (Anderson et al., 2014), we designated the bilateral IPS nodes as the primary driving-input nodes, responsible for receiving external (visual) input in our DCM model (Figure 2d). (b) *I-EC* as given by the connectivity matrix A denotes the unmodulated EC that exists among the network nodes at baseline, that is, in the absence of any experimental task and its modulations. Although I-EC was inferred from our SRC task-related fMRI data, it captures the intrinsic coupling between brain network nodes by mathematically removing task-related variance (Marreiros et al., 2008; Zeidman, Jafarian, Corbin, et al., 2019). (c) *Modulatory EC* (M-EC) as given by the connectivity matrix B that reflects the modulation of EC connections in response to a certain task condition. The interpretation of the connectivity matrices A and B as representing I-EC and M-EC, respectively, depends on how the experimental input u_j is handled. In this study, we considered u_j to vary between 0 and 1, corresponding to the task conditions being off (0) or on (1), instead of mean-centering u_j . When u_j is not mean-centered, as in our case, matrix A reflects the EC parameters of the unmodelled baseline, and matrix B represents the EC parameters modulated by task conditions (Zeidman, Jafarian, Corbin, et al., 2019). Otherwise, if u_j is mean-centered, matrices A and B will represent the averaged EC across all task conditions (on and off) and EC deviations from this overall mean, respectively (Zeidman, Jafarian, Corbin, et al., 2019).

In this study, the timing of the stimulus presentation in the Anti task blocks was selected as the timing of the modulatory input, and the respective contrast was modeled by DCM, which

may represent the connections modulated by individual incompatible responses of the SRC task. In comparison with the Pro condition, the Anti condition is expected to pose higher cognitive demands due to the requirement to resolve spatial incompatibility-induced response conflicts. Consequently, individual performance and estimated EC of the Anti condition can be considered robust indicators reflecting the individual capability to execute and control a complex cognitive action. This way, the DCM design corresponded to that of the GLM used for analyzing the task fMRI data, that is, event-related and block-based designs were simultaneously used for both GLM and DCM. For the event-related design, driving stimuli of all events and modulatory stimuli of the Anti condition were encoded by separate trials, whereas, for the block-based design, driving stimuli of all events and modulatory stimuli of the Anti condition were encoded by blocks. The detailed information can be found in Zhang et al. (2024).

A full-connection model was implemented for estimating I-EC and M-EC (Figure 2d). After individual I-EC and M-EC were inferred, subjects with a low fraction (<10%) of variance explained by DCM were excluded, after which 208 and 205 participants for event-related and block-based designs, respectively, remained for subsequent analyses. Parametric Empirical Bayes (PEB) is a hierarchical modeling approach that can in particular be used to relate brain EC to behaviorally relevant characteristics, allowing for inferences on intersubject differences at the second level (Zeidman, Jafarian, Seghier, et al., 2019). With PEB, one can also estimate brain EC patterns that best explain the average connection across subjects as well as the interindividual EC differences modulated by individual RT or age by utilizing a GLM design matrix. In this context, the design matrix consists of two columns, where the first column contains all ones for the group-mean effects, while the second column includes mean-centered RT or age scores to estimate RT- or age-modulated effects. Such a design matrix enables assessing how individual differences in EC are associated with other individual (e.g., behavioral) characteristics.

As mentioned above, the estimated EC parameters were used as features to predict both individual age and RT averaged over all trials of the incongruent SRC task condition. To keep the number of covariates at a minimum ([https://en.wikibooks.org/wiki/SPM/Parametric_Empirical_Bayes_\(PEB\)](https://en.wikibooks.org/wiki/SPM/Parametric_Empirical_Bayes_(PEB))), we adopted a two-column design matrix of PEB analysis, which only contained all ones and mean-centered RT or age separately. Additionally, a threshold of posterior probability ($PP > 95\%$) was used to extract I-EC and M-EC parameters that were strongly modulated by RT or age.

Machine-Learning Prediction Analysis

The main goal of this study was to compare the prediction accuracy of task-evoked EC of the SRC task network (defined via block-based vs. event-related GLM and DCM designs) with respect to age as well as individual performance level as given by RT. I-EC and M-EC matrices were selected as candidate features, and individual age and RT of the incompatible task condition were chosen as target characteristics to be predicted. An approach to feature selection by masking the features at the group level is widely used in prediction analyses, see, for example, the connectome-based predictive modeling (CPM) approach (Shen et al., 2017). In our study, we considered EC and thus used PEB for the feature selection, since the latter was recommended in the literature for group-level EC analyses (Zeidman, Jafarian, Seghier, et al., 2019). We applied a linear regression model with the LASSO regularization (Tibshirani, 1996) to predict individual differences (RT and age) using the *k*-fold CV scheme. LASSO was chosen for its ability to reduce overfitting, especially in high-dimensional data. By penalizing features with less importance, LASSO ensures that the prediction model focuses on

predictive EC parameters, which improves the model's accuracy and generalizability. In such a way, we randomly split the subject sample into five groups, where four groups were united into a set for model training, whereas the fifth group was kept for model testing and prediction of individual target scores (Figure 3a).

To select EC parameters to be used as features for prediction, a group-level PEB (Zeidman, Jafarian, Seghier, et al., 2019) framework of DCM was employed. During the PEB analysis on the training sets, a PEB design matrix with two columns was used, as mentioned above, to extract the connectivity patterns of strongly evident (with $PP > 95\%$) group-mean EC parameters as well as EC parameters modulated by mean-centered individual age or RT (Figure 3b). These modulated EC parameters at the second-level ($PP > 95\%$) were selected as a mask to extract subject-level EC parameters without any refitting procedures for individuals, which were then used as features to train the prediction model on the training sets and to predict individual RT or age for the testing sets of unseen subjects (Figures 3c and 3d). One prediction round included testing all five subject groups of the 5-fold CV split by selecting them one after another as a testing set (and the respective remainder of the sample as a training set), where all test subjects obtained predicted scores that were compared (correlated) with the empirical ones across subjects (Figure 3e). This procedure was repeated 100 times with different random splits of the sample into five groups, and we obtained a distribution of 100 values of prediction accuracy (i.e., Pearson correlations between empirical and predicted values), which were subsequently averaged to obtain a metric for assessing the prediction performance of the models under the different conditions of data processing and modeling considered here.

To test for the statistical significance of our prediction results, we employed a label-shuffled permutation test (Winkler et al., 2014) within the framework of a 5-fold CV 500 times. For each iteration of the permutation test, the behavioral scores were randomly shuffled among subjects, and then a 5-fold CV procedure was conducted based on the shuffled scores. This way, chance-level prediction distributions (i.e., empirical null distributions) were generated,

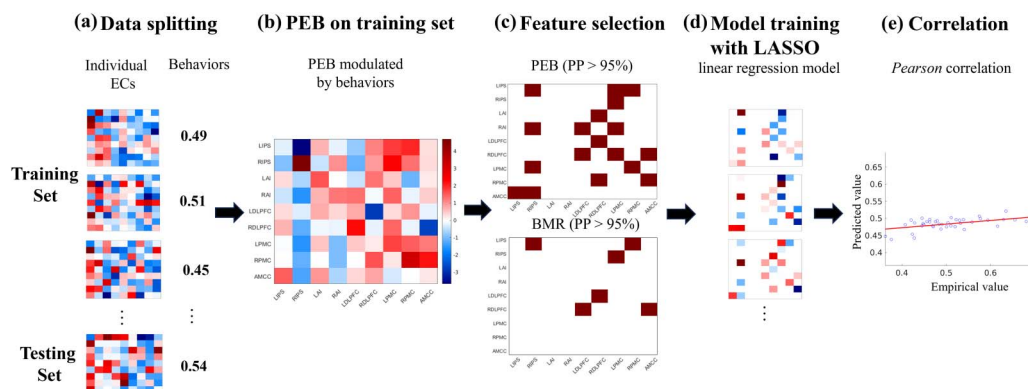


Figure 3. The workflow for prediction of individual behavioral characteristics based on task-evoked EC and PEB results as outlined by Steps (a)–(e). (a) The subjects and their corresponding behavioral characteristics (RT and age) were randomly split into k groups according to the k-fold cross-validation (CV) approach and then united into training and testing sets within CV loops. (b) Individual EC and behavior scores from the training set were analyzed by a PEB analysis to estimate behavior-modulated EC at the group level. (c) EC features are masked based on a high posterior probability ($PP > 95\%$) obtained from PEB or Bayesian model reduction (BMR) analysis. (d) A linear regression model with LASSO regularization was trained on the training set and then applied to predict the behavioral/phenotypic scores of the unseen testing set. (e) Pearson correlation was used to evaluate the similarity between the empirical and predicted values of the testing sets and to indicate the prediction accuracy of the model's performance by averaging the correlation across all testing sets of the CV loop. The procedures (a)–(e) were repeated for several random splits of subjects into k groups to obtain a distribution of the prediction accuracies.

which were subsequently used for comparison with the observed prediction accuracies (correlations) under each data processing condition, using a significance threshold of $p < 0.05$. We also compared the prediction performance between I-EC and M-EC features, and a sample-dependent Cohen's d value was calculated to assess the effect size.

As the number of features used for prediction may influence the discriminative power and model complexity of a machine-learning approach (Cai et al., 2018), we estimated the number of features that were frequently selected for model training and prediction across CV loops. This may also help to evaluate the contribution of every feature to the prediction results. During the prediction procedure, the PEB analysis was performed on each CV iteration for every subject training set, where different patterns of EC edges can be obtained. We followed such variability and calculated the relative frequencies of the features selected for predicting individual RT and age using repeated 5-fold CV. To better visualize feature contribution maps for each case, only EC parameters covarying with RT or age scores and selected by PEB with frequency $\geq 80\%$ across all CV trials were presented. In parallel with extracting prediction contributions of EC features with the frequency of feature selection, we also estimated the average number of EC features selected by PEB across all CV iterations.

GLM and DCM Designs

The types of event-related and block-based GLM designs (Huettel, 2012; Logothetis, 2008) were found to influence DCM parameter estimation (Zhang et al., 2024) and model selection (Daunizeau et al., 2011). Although the event-related design is currently more recommended for modeling brain activity (Petersen & Dubis, 2012), the impact that the type of GLM used in task fMRI data analysis has on the prediction results has not been clarified. Thus, we utilized a LASSO-regularized linear regression model to compare prediction correlations between GLM/DCM designs.

CV Schemes and Predictive Models

Given the reported impact of CV schemes on prediction results in machine-learning studies (Varoquaux et al., 2017), we performed another two analyses in parallel to the repeated 5-fold CV (see the Machine-Learning Prediction Analysis section): repeated 10-fold CV and LOOCV analyses. Furthermore, a ridge-regularized linear regression model (Saunders et al., 1998) was employed as an alternative machine-learning algorithm to validate our prediction results obtained by the LASSO regression model. These parallel analyses were intended to help us evaluate the influence of CV schemes on the prediction results.

BMR

BMR is an approach of DCM that compares evidence from different reduced models with certain combinations of coupling parameters (network edges) switched off (see the DCM Specification and Analysis section) (Friston et al., 2016). This approach can be used to identify the “best” reduced model instead of incorporating a “full” model, where all network edges are allowed to exist and will be optimized by DCM (Zeidman, Jafarian, Seghier, et al., 2019). This BMR approach has largely been applied in data-driven DCM prediction studies (Beck et al., 2021; Diersch et al., 2021), while its impact on prediction outcomes has not been well documented. To assess a possible improvement in individual predictions produced by BMR, an exhaustive search (*spm_dcm_peb_bmc.m*) was included in our prediction workflow (Figure 3c). This automatically evaluated all parameters of the full-connection

model by analyzing PEB files generated from the training set. This algorithm explored different reduced models by selectively removing parameters and retaining those that contribute most significantly to model evidence (Friston et al., 2016). When a reduced model was determined, a threshold of PP > 95% was utilized to mask and extract individual EC features used for prediction.

FC

To investigate prediction accuracies obtained from task-evoked FC, we considered both full task-evoked and task-residual FC (Zhao et al., 2023). The former type of FC was estimated by the pairwise correlation of the preprocessed task-evoked BOLD time series extracted for individual subjects from ROIs of the SRC network, which were the same as those time series specified for EC calculation by DCM. The latter type of FC was estimated by the pairwise correlation between the SRC ROI-based time series of individual subjects after regressing the timing of the experimental event sequence from the BOLD signals (Cole et al., 2014; Cole et al., 2019).

To predict individual performance or age from FC, we adapted the widely used connectome-based CPM approach (Shen et al., 2017). In particular, we applied a sparse feature selection and created two FC masks out of the top 10% of FC edges that were highly positively or negatively correlated with the prediction targets of RT or age (https://github.com/rorytboyle/flexible_cpm). These two masks were then merged into one and used for feature extraction for individual subjects. The selected individual features were then submitted to the LASSO-regularized linear regression model to predict individual age and RT according to the previously described 5-fold CV scheme. Note that, for a better comparison between prediction results for FC and EC, we did not sum up the selected individual FC features as in the default CPM approach (Shen et al., 2017). Rather, we simultaneously used all masked FC edges of individual subjects as separate features.

RESULTS

In this study, we investigated how the task-evoked EC can be used to predict behavioral/phenotypic characteristics (RT performance and age) of individual subjects and how it could be influenced by conditions of fMRI data processing and the respective decisions that the researcher would have to make before and during the prediction analysis. We thus evaluated the influence of (a) using intrinsic (I-EC) or task-modulated (M-EC) EC as given by the DCM-derived connectivity matrices A and B, respectively (see the *Methods* section), (b) using event-related versus block-based GLM and DCM designs, (c) and applying BMR for DCM. Furthermore, we examined the influence of other methodological aspects of the prediction analysis. In particular, we evaluated the influence of different CV schemes and the prediction algorithm used (LASSO regularized linear regression utilized vs. ridge regression). Finally, we compared our EC-based prediction results with those obtained from using task-evoked FC as predictive features. Briefly, we observed that (a) different modalities of EC demonstrated different prediction accuracy for age and RT, where M-EC showed higher prediction accuracy for individual RT, but lower prediction accuracy for individual age than did I-EC; (b) the event-related GLM and DCM designs displayed higher accuracy in predictions than did the block-based designs; (c) employing BMR did not largely improve prediction accuracy; (d) repeated 10-fold CV and LOOCV analyses presented similar prediction patterns to that of repeated 5-fold CV, and the results obtained using LASSO were largely confirmed by using

ridge regression; and (e) task-evoked FC showed higher prediction accuracy for age than did EC, but limited prediction performance for RT.

Task-Evoked EC and Its Relation to Behavior

Task-evoked EC investigated in this study was inferred using DCM within the SRC task-related brain network (Figure 2) for all individual subjects. The individual DCM estimations were then summarized to analyze group-level EC by the PEB technique. To illustrate the EC patterns at the group level for the whole subject sample, we calculated the I-EC and M-EC parameters (network edges) with a high PP of > 95% (Zeidman, Jafarian, Seghier, et al., 2019). The group-mean EC reflecting the connectivity averaged over all subjects and the behavior-related EC reflecting the connectivity covariance with behavioral/phenotypic scores (see the Methods section) are illustrated in Figure 4 for RT- and age-related PEB analyses. For both PEB analyses, the group-mean I-EC featured similar connectivity intensity (0.13 in Figure 4a and 0.12 in Figure 4c) as given by the absolute average of the connectivity parameters with PP > 95%. The group-mean M-EC also showed a similar connectivity intensity for both RT and age (0.33 in Figure 4b for RT and 0.34 in Figure 4d for age), which was higher overall than that of I-EC (compared with Figure 4a and Figure 4c).

Together with the group-mean EC, by the PEB approach, we also calculated the EC parameters that strongly covaried (PP > 95%) with individual RT or age (Figures 4e–4h), where we again observed a higher connectivity intensity of M-EC than I-EC (for RT: 1.9 for M-EC and 0.72 for I-EC; for age: 0.01 for M-EC and 0.004 for I-EC). In summary, M-EC parameters exhibited stronger connectivity intensities associated with both individual RT and age, as compared with I-EC parameters.

Predicting Individual RT and Age by Task-Evoked EC

Based on the observed connectivity patterns of I-EC and M-EC (Figure 4), we evaluated how well the task-evoked EC predicts individual phenotypal and behavioral characteristics. We

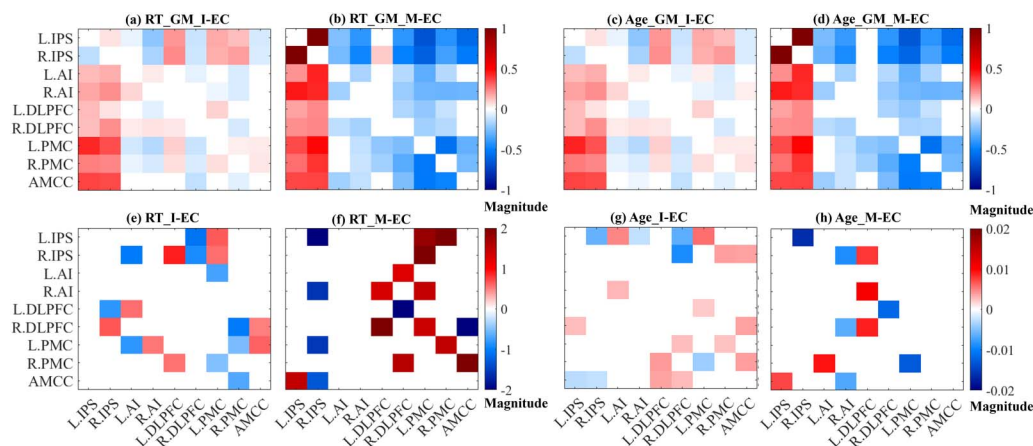


Figure 4. Examples of the group-mean and the behavior-related EC within the SRC task network derived from the event-related design. Panels a–d depict the group-mean EC, I-EC, and M-EC, and panels e–h depict behavior-related EC matrices A and B when either mean-centered RT or mean-centered age was used as the second column in the PEB design matrix (see the Methods section). The SRC task-related network nodes (group-level ROIs) are indicated on the axes (for abbreviations, see Figure 1). The color bars in panels a–d represent the magnitude range of the group-mean EC parameters, while the color bars in panels e–h indicate the magnitude range of behavior-related EC parameters (either for mean-centered RT or mean-centered age). These values depict the strength of the I-EC and M-EC, respectively, within the SRC task-related brain network.

calculated prediction accuracy (correlation between empirical and predicted values) for the prediction of RT and age and plot the respective distributions obtained after 100 repetitions of the 5-fold CV (see the Methods section) in Figure 5 for the considered cases of the event-related and block-based GLM and DCM designs for both I-EC and M-EC (see also Supporting Information Table S1). Our results revealed that, in the case of choosing an event-related GLM and DCM design, much better performance in predicting RT was achieved with M-EC features as compared with I-EC features (mean correlation $r = 0.26$ vs. $r = 0.09$, Cohen's $d = 3.2$; Supporting Information Table S1). On the other hand, I-EC (vs. M-EC) showed higher accuracy in predicting subjects' age (mean $r = 0.28$ vs. $r = 0.22$, Cohen's $d = 1.1$; Supporting Information Table S1). For the block-based GLM and DCM design, both M-EC and I-EC showed rather low prediction performance for age (mean $r = 0.19$ and $r = 0.2$, Cohen's $d = 0.2$) and even less so for RT (mean $r = 0.17$ and $r = 0.1$, Cohen's $d = 1$; see Supporting Information Table S1).

From the eight prediction conditions illustrated in Figure 5, we found that only three cases of the event-related GLM design appeared to be statistically significant (Figure 5, indicated by asterisks), which were evaluated based on the permutation tests (see Supporting Information Table S1 and Supporting Information Figure S2). The features of both I-EC and M-EC were predictive for subjects' age, but only M-EC was predictive for individual RT if derived from the event-related GLM and DCM design. Interestingly, all considered conditions of the block-based design led to insignificant prediction results (Figure 5). These findings suggest that focusing on the event-related design may improve the prediction accuracy related to inter-individual variability and behavioral characteristics when using task-evoked EC. Furthermore, our findings may also suggest focusing on M-EC when task-related behavioral characteristics (RT) are to be predicted, as it strongly outperformed I-EC. While both M-EC and I-EC were

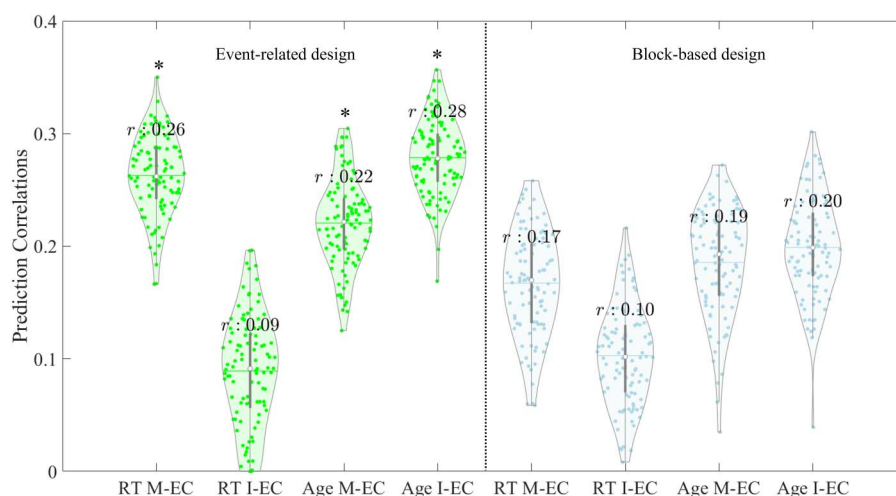


Figure 5. Accuracy distributions of prediction results derived from 100 repetitions of 5-fold CV using LASSO-regularized linear regression for event-related GLM designs (left panel, denoted in green) and block-based designs (right panel, denoted in blue). The correlations between observed and predicted RT and age, based on features from intrinsic effective connectivity (I-EC) and task-modulated effective connectivity (M-EC) matrices, are illustrated as violin plots, with the corresponding labels displayed on the horizontal axis. The mean correlation (r) is calculated by averaging across all repetitions, while each dot represents a single repetition of the prediction correlation derived from one 5-fold CV instance. Asterisks (*) indicate statistical significance in comparisons between the averaged correlations across the 100 repetitions and those from the corresponding 500-times permutation test (see Supporting Information Figure S2).

able to predict age to a moderate degree, the latter showed a somewhat better prediction performance.

We also evaluated how different features (edges of EC) were used in the prediction process. This way, we estimated how frequently one or another feature was selected for the model training and prediction and considered the frequently selected features participating with a frequency $\geq 80\%$ across all CV loops (Figures 6a and 6b). The number of such active features highly contributing to prediction can be compared with an average number of features provided by PEB for model training and prediction at CV instances (Figure 6c).

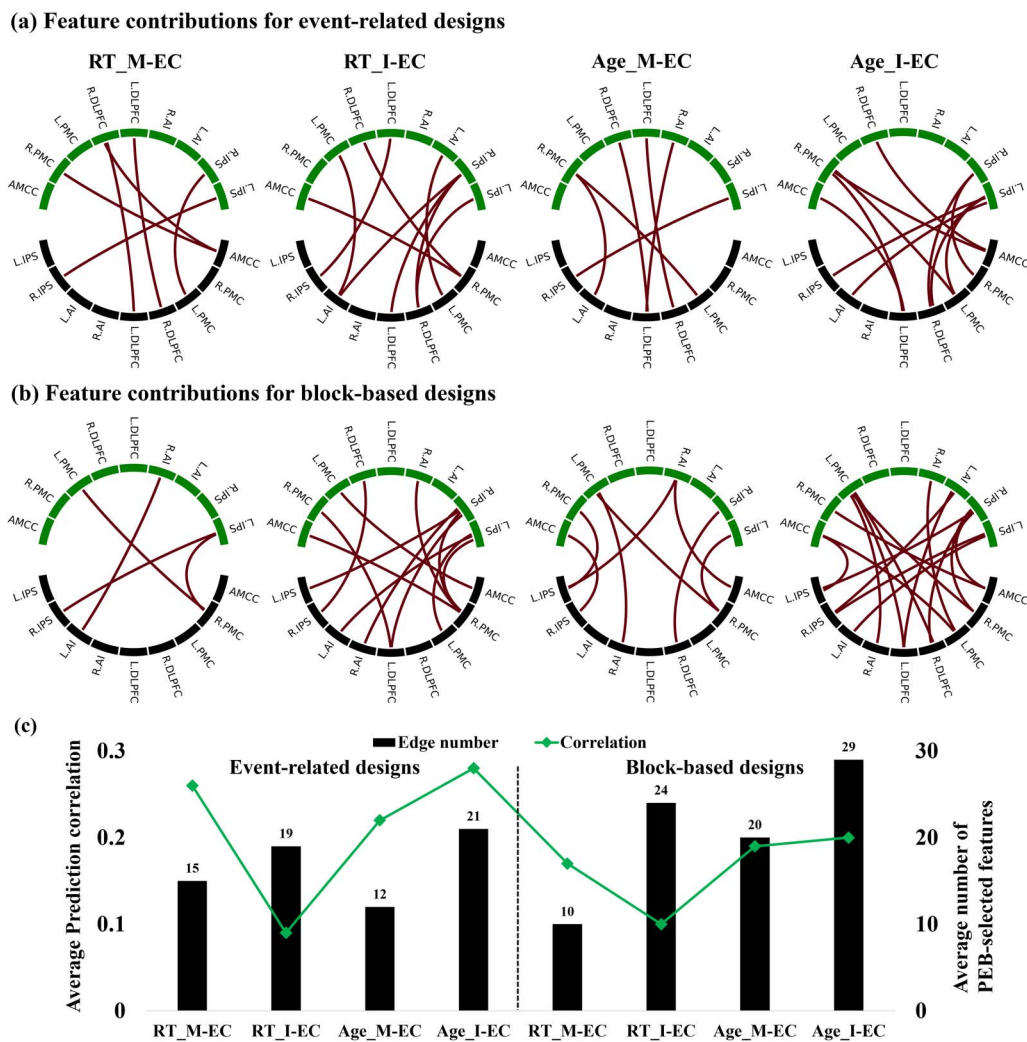


Figure 6. Feature contributions of specific EC edges frequently selected (panels a and b) and the average number of selected features (panel c) across all CV training loops with 100 repetitions for predicting behavioral scores. Panels a and b highlight individual EC edges selected as informative features during predictive modeling with a high frequency ($\geq 80\%$) for event-related and block-based designs, showcasing the specific connections that contribute most significantly to the predictions. In panels a and b, black nodes denote “From” regions, while green nodes indicate “To” regions. The plot titles indicate the prediction target score (RT or age) and EC modality (I-EC or M-EC). In contrast, panel c presents the average number of EC features selected in each prediction loop, regardless of selection frequency, illustrating the overall relationship between prediction correlation (solid green line, left axis) and the average number of EC features (black bars, right axis) across all CV training loops. The numbers above the bars represent the average number of EC features selected by PEB analysis for model training and prediction.

For the event-related GLM and DCM design, we found that the I-EC versus M-EC subnetworks actively contributing to prediction were different for RT prediction including nine and six edges, respectively (Figure 6a). The corresponding average numbers of I-EC and M-EC parameters selected by PEB for RT prediction were 19 and 15, accordingly (Figure 6c). The larger number of the active features (EC parameters) did not, however, consistently positively contribute to prediction accuracy, and more RT-related features of the denser I-EC failed to significantly predict RT measured in the SRC task (Figure 6c). The discussed behavior-related SRC subnetworks also existed for the age prediction and were different from those for RT prediction as well as for both I-EC and M-EC (Figure 6a). Here, in contrast, we observed a slight trend that the larger number of EC parameters selected for the age prediction positively contributed to prediction quality. Notably, the features of M-EC resulted in a somewhat weaker age prediction accuracy than those of I-EC (Figures 6a and 6c).

For the block-based GLM and DCM design, similar observations can be reported, where very different subnetworks of the SRC network actively participated in RT and age prediction by I-EC and M-EC. In particular, only 4 and 12 edges were frequently selected for RT prediction out of 10 and 24 features that on average were suggested by PEB from all M-EC and I-EC connections, respectively (Figures 6b and 6c). Again, a smaller M-EC subnetwork can lead to somewhat better RT prediction than the larger I-EC subnetwork. The EC connectivity patterns frequently employed for prediction are also very different between the two considered GLM and DCM designs of the event-related and block-based types.

In summary, the stability, density, and connectivity pattern of the behavior-related SRC subnetwork frequently selected for model training and prediction could not immediately be assigned to the observed prediction accuracy and might need additional investigation. Nevertheless, by such a 5-fold CV subsampling, we found EC connections of the SRC network that robustly covaried with the considered behavioral scores and can be used for their investigation.

Predicting RT and Age From Task-Evoked FC

We also applied our approach to the prediction of RT and age based on task-evoked FC features calculated by Pearson correlations between task-evoked BOLD time series extracted from the SRC-related network nodes. Despite methodological differences between the EC- and FC-based approaches, we found that the two types of FC (full task-evoked and task-residual; see the Methods section) performed relatively well in the prediction of individual age ($r = 0.29 \sim 0.31$). However, FC succeeded much less in predicting RT for both GLM designs ($r = 0.07 \sim 0.13$), where the task-evoked EC, especially M-EC for the event-related GLM-DCM design, outperformed the task-related FC (see Figure 5 and compare Table 1 and Supporting Information Table S1).

Table 1. Performance of functional connectivity (FC) features in predicting individual reaction time (RT) and age.

GLM design	Event		Block	
	full	res	full	res
RT	0.11 ± 0.04	0.13 ± 0.04	0.07 ± 0.04	0.10 ± 0.05
Age	0.29 ± 0.03	0.30 ± 0.04	0.31 ± 0.04	0.31 ± 0.04

Individual RT and age were separately predicted by individual FC using CPM implemented in a 5-fold CV scheme and repeating the predictive model for each target 100 times to derive an averaged correlation between empirical and predicted values. Considering empty edges in feature selection procedures, we used a sparsity function that selected the top 10% positively and negatively target-correlated edges, respectively, rather than a fixed p value for thresholding, in every training set for modeling.

CV Analysis

We calculated prediction accuracies for different CV schemes for the event-related GLM-DCM design, including a repeated 10-fold CV (Supporting Information Table S2 and Supporting Information Figure S3) and LOOCV (Figure 7a and Supporting Information Table S3). The 10-fold CV revealed a pattern similar to the 5-fold CV, where we still observed that M-EC predicted RT much better than did I-EC (mean $r = 0.28$ vs. $r = 0.14$). On the other hand, I-EC manifested a somewhat better correlation in predicting individual age than did M-EC (mean $r = 0.29$ vs. $r = 0.23$).

For the LOOCV, we also found a similar pattern of prediction results, where M-EC presented a much better correlation than I-EC in predicting individual RT (mean $r = 0.34$ vs. $r = 0.11$) but lower prediction accuracy for age (mean $r = 0.2$ vs. $r = 0.28$).

Despite the prediction correlations were somewhat varying among different CV schemes, we nevertheless observed robust prediction results related to M-EC and I-EC across different CV schemes (see Figure 7a). Indeed, M-EC much outperformed I-EC in predicting RT for all cases considered. EC connectivity may also be used for age prediction, where I-EC demonstrated somewhat better prediction accuracy than did M-EC.

Model Reduction Analysis

We also examined the case when the full DCM model employed above was replaced by a reduced model based on the BMR approach. The prediction performances of I-EC and M-EC for individual RT and age using BMR-extracted features (PP > 95%) are displayed in Figure 7b, Supporting Information Figure S4, and Supporting Information Table S4. The results

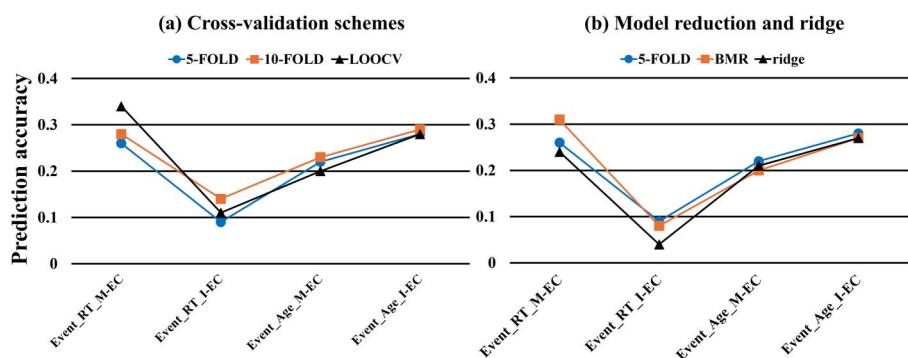


Figure 7. Overview of the mean prediction accuracy of all considered conditions in predicting individual RT and age under the event-related (Event) GLM design with features selected by behavior-related PEB analyses from EC modalities of M-EC and I-EC indicated on the horizontal axis. Plots (a) and (b) indicated the conditions involving cross-validation schemes including 5-fold CV, 10-fold CV, and LOOCV, and applications of the BMR and ridge-regularized regression. Except for LOOCV, the prediction accuracies of all conditions were represented by averaged correlations between empirical and predicted behavioral scores from the repeated k -fold cross-validation analyses.

obtained were similar to our previous observations for the full DCM model. In particular, as before, M-EC showed a much higher prediction accuracy (correlation) for RT than did I-EC ($r = 0.31$ vs. $r = 0.08$), and I-EC showed a stronger prediction correlation for age than did M-EC ($r = 0.27$ vs. $r = 0.2$). These findings indicate that considering the DCM-reduced models via BMR hardly influenced the prediction results and conclusions derived for the full model (see Figure 7b).

Predictive Models

The prediction analysis using ridge-regularized linear regression in a 5-fold CV scheme yielded similar results (Figure 7b and Supporting Information Table S5), which validated our LASSO-regularized prediction model. For the event-related cases, M-EC (vs. I-EC) showed higher prediction accuracy for RT ($r = 0.24$ and $r = 0.04$), but lower accuracy for age ($r = 0.21$ and $r = 0.27$).

DISCUSSION

In this study, we investigated and compared the prediction performance of intrinsic and task-modulatory EC patterns obtained from DCM of task fMRI data. For this, we explored machine-learning-based predictions of individual age and RT performance by LASSO- and ridge-regularized linear regression using two types of task-evoked EC: I-EC as given by matrix A of the DCM model and task-modulatory EC (M-EC, matrix B). We adopted a CV-based PEB analytical strategy to extract I-EC or M-EC parameters as predictive features to avoid data leakage in predicting individual behavioral or phenotypical scores. We compared the prediction results for two different GLM and DCM designs of task fMRI processing and EC estimation, the event-related and block-based designs. We also calculated and compared the prediction results for different CV schemes, when BMR was applied to DCM, as well as when using ridge regression as an alternative machine-learning model and task-evoked FC patterns as feature space.

Our results demonstrated that (a) the event-related GLM-DCM design performed better at predicting individual phenotypes than did the block-based GLM design; (b) using M-EC led to a higher prediction accuracy (correlation) for RT prediction, while I-EC was better for the age prediction in the case of an event-related design; (c) employing BMR did not largely affect prediction accuracy; (d) different CV schemes showed similar prediction patterns, where LOOCV was showing more optimistic results than the 5-fold CV scheme in some cases; (e) the results obtained for the LASSO-based predictive model were largely confirmed by models using ridge regression; (f) task-evoked FC (vs. EC) showed a higher prediction accuracy for age, but a lower accuracy for RT, where the event-related M-EC outperformed FC.

SRC Network

The SRC task is a well-established experimental paradigm to study cognitive action control during conflict processing by employing measures such as RT and error rates in response to task stimuli (Fitts & Deininger, 1954), where shorter RT and higher accuracy is typically observed in a congruent condition, as compared with the incongruent one. In contrast to RT, previous studies also reported an age-related difference in both behavioral performance and connectivity among brain regions (Langner et al., 2015; Proctor et al., 2005). In line with these studies, our findings demonstrated that both age and RT can be predicted by brain EC, albeit the prediction accuracy ranged from weak to moderate (see Figure 5). Moreover, our findings revealed distinct EC patterns that contributed to predicting individual RT and age, as indicated by feature contributions of EC (Figures 6a and 6b). Although we selected nodes

within the SRC network, where the incompatibility effects were present, the connections among these regions exhibited varying degrees of contribution to age and RT prediction. The dissociation of the entire SRC network into different subnetworks actively contributing to age and RT prediction could reveal differently weighted roles of the network nodes (brain regions) and their connectivity for various prediction targets. This could help to evaluate potentially distinct associations to, for example, individual age and RT within the SRC network.

I-EC and M-EC

To our knowledge, the differential roles underlying the prediction performance of I-EC and M-EC extracted from task-evoked fMRI have not been previously investigated. Although I-EC is derived from task fMRI data, it shares similarities with intrinsic connectivity, as I-EC is mathematically freed from task-related variance, allowing it to reflect condition-invariant, spontaneous baseline activity during task-evoked brain states (Marreiros et al., 2008; Zeidman, Jafarian, Corbin, et al., 2019). However, it is important to note that I-EC retains some influences from the task context, making it an imperfect analogy to resting-state data. Despite this shortcoming, I-EC still captures intrinsic connectivity dynamics akin to resting-state connectivity, making it a useful tool for studying intrinsic connectivity even in task-evoked data.

For the event-related GLM design, we found that M-EC exhibited a higher prediction correlation for individual RT than did I-EC. This finding is comparable with the literature on the predictiveness of task-evoked versus resting-state FC, which suggests that task-evoked connectivity may better capture task-specific behavioral differences and variability than does resting-state connectivity and thereby lead to superior prediction results (Gbadeyan et al., 2022; Zhao et al., 2023). This advantage may stem from task manipulations that accentuate brain functional correlation patterns relevant to behavior (Greene et al., 2018; Zhao et al., 2023). Compared with resting-state connectivity, the specificity of a given task, constrained nature, and reduced variability of task-evoked connectivity may allow for better capturing some individual behavioral differences (Buckner et al., 2013; Elton & Gao, 2015; Finn et al., 2017; Geerligs et al., 2015).

We found that I-EC (vs. M-EC) exhibited a slightly higher accuracy in predicting individual age in the event-related GLM design. This is a different pattern of prediction based on I-EC versus M-EC as we observed for RT prediction in spite of some moderate correlation between RT and age. Both types of EC have been identified as decent predictors of individual age (Diersch et al., 2021; Tsvetanov et al., 2016). For instance, Tsvetanov et al. (2016) predicted individual age ($r > 0.3$) using resting-state EC parameters estimated within and between the brain's main networks. Similarly, Diersch et al. (2021) demonstrated that hippocampal excitability of the task-evoked EC was influenced by aging ($r = 0.29$), showing the capability to classify participants into younger and older groups. These findings suggest that both I-EC and M-EC can be influenced by individual age, which justifies their consideration as features for age prediction. The advance of resting-state connectivity for age prediction also aligns with previous studies (Ferreira & Busatto, 2013; Millar et al., 2022; Xiong et al., 2023). For instance, evidence from a multimodal MRI study for brain age prediction (Xiong et al., 2023) has shown a modality-specific prediction difference between the resting-state and task-evoked datasets, where the former outperformed the latter. This difference may relate to the dissociation of BOLD variability between them, where the resting-state BOLD variability may capture different sources of variance and be more sensitive to global age-related (e.g., vascular and white matter) factors than is task-evoked variability (Millar et al., 2020). In line with previous literature, our findings suggest that brain I-EC and M-EC may contribute differently to predicting

individual RT and age. Although we noticed that M-EC and I-EC components in the block-based designs failed to predict individual RT and age ($p > 0.05$), the observed patterns suggest a potential tendency between M-EC and I-EC components in their predictive performance for age and RT.

GLM and DCM Designs

Despite minor differences, the LOOCV and k -fold CV prediction results have shown higher prediction correlations for the event-related design compared with the block-based design (Figure 5). Both I-EC and M-EC estimated from the block-based design resulted in lower and insignificant prediction correlations with individual RT and age, as compared with EC estimated for the event-related design. Previous studies (Bühler et al., 2008; Tie et al., 2009) have compared the impact of GLM designs on task-evoked activations and reported that the block-based design resulted in more widespread brain activations that were not specifically involved in the task compared with the event-related design (Bühler et al., 2008). This difference may be attributed to different hemodynamic response shapes modeled by GLM designs (Mechelli, Henson, et al., 2003; Mechelli, Price, et al., 2003). The event-related design was found to explain the signal variance better, with predicted hemodynamic responses peaking earlier and returning to the baseline later (Mechelli, Henson, et al., 2003). In addition, our previous study (Zhang et al., 2024) reported an overall higher M-EC strength for the event-related design, relative to the block-based design. Taking these results together, the higher prediction correlations with individual performance in the event-related GLM-DCM design may be related to its stronger sensitivity to individual task events. This makes the event-related design a promising modeling approach for better prediction and understanding of behavioral characteristics related to the tasks, for example, RT, as in this study.

CV Schemes and Machine-learning Algorithms

The present study employed a CV-based PEB analytical strategy, which enabled us to estimate behavior-modulated EC efficiently and avoided possible data leakage in prediction. In particular, extracting EC edges with PP > 95% as features from the entire sample, instead of extracting them from every CV loop for the training set, may lead to overoptimistic prediction results (Mwangi et al., 2014). Additionally, despite the instability and bias reported for LOOCV (Varoquaux et al., 2017), our k -fold CV scheme (repeated 100 times) has still displayed a notably consistent prediction pattern also with LOOCV (Figure 7a). In some cases, we, however, observed an enhanced prediction correlation for LOOCV, relative to the 5-fold CV scheme, for example, for M-EC in RT prediction (Supporting Information Tables S1 and S3). Furthermore, the ridge-regularized machine-learning analysis confirmed our results obtained from the LASSO-regularized analysis (Supporting Information Table S5). The relatively consistent prediction patterns obtained across various CV schemes and machine-learning algorithms support the robustness and stability of our findings.

BMR

We explored the possible benefits of employing BMR of DCM for predicting individual RT and age with both types of EC (Figure 7b). However, we observed that the impact of BMR on prediction results was relatively small (Supporting Information Figure S4). BMR refers to the procedure of comparing different reduced models initiated from a prespecified model using Bayesian inversion to find a “winning” model that fits the neural data best (Zeidman, Jafarian, Seghier, et al., 2019). This procedure iteratively switches off the connectivity parameters and compares the PP of these reduced models until the “best” model is captured (Friston et al.,

2016). Several studies have applied BMR to remove connectivity parameters from the full model and to predict individual differences based on the EC of the reduced model (Beck et al., 2021; Diersch et al., 2021). However, the impact of BMR on prediction results has remained unclear without direct comparisons. In our study, we did observe a slightly higher prediction accuracy with BMR in the case of RT prediction using M-EC features (Figure 7b). However, there was still a notably consistent prediction pattern across the cases with BMR and those using the full DCM model. The current findings thus indicate that the impact of BMR on the prediction results is relatively small. More detailed and comprehensive investigations are needed to evaluate the role and significance of BMR in DCM-based prediction analyses.

Joint EC Analysis of I-EC and M-EC

Considering that both I-EC and M-EC components can contribute to changes in neuronal states, we conducted additional prediction analyses with combined features including both I-EC and M-EC components together, and compared the results with those using each component separately (Supporting Information Figure S5). In the event-related design, the combined EC model predicted age with a mean correlation of 0.28 and RT with 0.26. For the block design, age prediction had a correlation of 0.20, while for RT, it was 0.15. Across different CV schemes, the combined analyses showed prediction correlations ranging from 0.28 to 0.33 for RT and from 0.29 to 0.31 for age. When using BMR and ridge-regularized linear regression, the BMR model achieved a prediction correlation of 0.29 for both RT and age, whereas the ridge regression model showed a prediction of 0.24 for RT and 0.28 for age. These results were not significantly different from predictions using I-EC or M-EC alone, indicating that isolating I-EC and M-EC provides comparable prediction accuracy. Additionally, this approach offers more specific insights into which aspect of task-evoked EC is involved in the respective brain-behavior relationships.

FC

We examined task-evoked FC and compared its prediction performance with task-evoked EC. Our findings revealed that task-evoked FC was more predictive of age than was EC, whereas it was less predictive of RT than was task-evoked M-EC (see Table 1 and Supporting Information Table S1). Consistent with previous literature (Greene et al., 2018; Tsvetanov et al., 2016; Zhao et al., 2023), which demonstrated that FC could predict individual task performance and age with a correlation generally greater than 0.2, our results show a comparable prediction of age and RT using task-evoked FC from the SRC network, although RT prediction was lower. Furthermore, although EC was thought to be more discriminative than FC in identifying brain “fingerprints” from a previous resting-state fMRI study (Geng et al., 2018), the moderate improvement in age prediction by task-evoked FC highlights a sophisticated role of task-evoked connectivity measures. This may suggest that FC provides valuable insights in task-evoked contexts, especially for age prediction. Of note, we should also consider methodological variations in the prediction pipeline between EC- and FC-based predictions. These methodological differences in feature selection methods and selected feature numbers might be another source of the observed differences in prediction performance.

Limitations

Some limitations of our approach should be considered and possibly addressed in future research. First of all, as in other task-related studies, also in this study, we extracted group-based ROIs of brain activation based on the entire sample, which may be subject to the risk of data leakage in subsequent prediction analysis. The possible data leakage problem might be

due to the whole-sample second-level fMRI analyses applied to training and test sets together instead of performing them separately for the given training set in each CV loop (Kapoor & Narayanan, 2023; Rosenblatt et al., 2024). The impact of this problem on prediction results, however, is not immediately evident and has to be investigated in a dedicated separate study, which is computationally expensive and would require large computational resources. Here, we nevertheless verified that the second-level fMRI analysis applied to the training sets within CV loops did not lead to notably different ROIs, as compared with the whole-sample case (Supporting Information Figure S6). It is therefore reasonable to assume that the discussed potential data leakage did not have any notable impact on our prediction results and the reported conclusions. Second, while I-EC might approximate resting-state connectivity to a large extent by removing task-related variance, it still retains some influences from the task context, which makes it an imperfect analogy to resting-state connectivity. This partial similarity may affect the comparability of I-EC and resting-state connectivity in capturing spontaneous brain activity. Future research could benefit from estimating I-EC directly from resting-state data and comparing its predictive performance with task-related M-EC to better understand their relative effectiveness and implications for behavioral prediction. Third, we employed a LASSO-regularized linear regression model, which might face problems in case of high collinearity in the data and cannot well account for (non)linear relations between the features of brain EC used for the prediction of behavioral characteristics. Although we confirmed our results using ridge regression, additional investigations are warranted to better clarify this limitation. Finally, while our study provides interesting insights into task-evoked EC within the SRC-related brain network, it is limited by its focus on a specific task paradigm, and a possible generalization of the reported results to other tasks or even to the whole-brain connectome is important. Future research could address these limitations to offer a more comprehensive understanding of brain dynamics and connectivity across different cognitive states and their relations to behavior.

Conclusion

Our study aimed to predict individual RT and age from I-EC and M-EC and investigated the impact of a variety of data processing conditions, including types of DCM-GLM designs, application of BMR as well as diverse CV schemes. Our findings suggest that I-EC and M-EC may capture different phenotypic attributes, in spite of relatively low prediction accuracies observed for both task-evoked EC and FC regarding the prediction of RT or age. Here, M-EC demonstrated higher prediction accuracy for individual RT, whereas I-EC was better predictive of individual age. Furthermore, task-evoked EC outperformed FC in predicting individual RT but presented a slightly lower accuracy for individual age. Notably, prediction performance was significantly affected by the choice of GLM-DCM design, but only slightly influenced by other considered conditions of data processing and analysis, and using the event-related GLM-DCM design may improve prediction accuracy of task-evoked EC for individual RT and age. The presented results can contribute to better applicability of effective brain connectivity to the investigation of interindividual variability in brain-behavior relationships.

ACKNOWLEDGMENTS

The authors gratefully acknowledge computing time on the supercomputer JURECA (Jülich Supercomputing Centre, 2021) at Forschungszentrum Jülich under grant no. "cjinm71." We would like to acknowledge the 1000BRAINS project (Caspers et al., 2014) for providing the dataset. We are also grateful to the "ML hours" initiative from INM-7 and Kevin Wischnewski for informative and useful discussions.

SUPPORTING INFORMATION

Supporting information for this article is available at https://doi.org/10.1162/netn_a_00447.

AUTHOR CONTRIBUTIONS

Oleksandr Popovych: Conceptualization; Funding acquisition; Investigation; Methodology; Project administration; Resources; Software; Supervision; Writing – review & editing. Shufei Zhang: Data curation; Formal analysis; Investigation; Methodology; Resources; Software; Validation; Visualization; Writing – original draft; Writing – review & editing. Kyesam Jung: Formal analysis; Investigation; Methodology; Writing – review & editing. Robert Langner: Formal analysis; Methodology; Project administration; Writing – review & editing. Esther Florin: Conceptualization; Project administration; Supervision; Writing – review & editing. Simon B. Eickhoff: Funding acquisition; Project administration; Supervision; Writing – review & editing.

FUNDING INFORMATION

Oleksandr Popovych, Helmholtz Association and the European Union's Horizon 2020 Research and Innovation Programme, Award ID: 945539, 826421. Oleksandr Popovych, Deutsche Forschungsgemeinschaft (<https://dx.doi.org/10.13039/501100001659>), Award ID: 491111487.

DATA AND CODE AVAILABILITY

The raw data of the 1000BRAINS project used in this study are not immediately available for public sharing because the authors do not have permission to share data. The codes are available at the (<https://github.com/CogPsycho2023/DCMs2>).

REFERENCE

- Anderson, B. A., Laurent, P. A., & Yantis, S. (2014). Value-driven attentional priority signals in human basal ganglia and visual cortex. *Brain Research*, 1587, 88–96. <https://doi.org/10.1016/j.brainres.2014.08.062>, PubMed: 25171805
- Beck, M. M., Spedden, M. E., Dietz, M. J., Karabanov, A. N., Christensen, M. S., & Lundbye-Jensen, J. (2021). Cortical signatures of precision grip force control in children, adolescents, and adults. *eLife*, 10, e61018. <https://doi.org/10.7554/eLife.61018>, PubMed: 34121656
- Biswal, B. B., Mennes, M., Zuo, X.-N., Gohel, S., Kelly, C., Smith, S. M., ... Milham, M. P. (2010). Toward discovery science of human brain function. *Proceedings of the National Academy of Sciences of the United States of America*, 107(10), 4734–4739. <https://doi.org/10.1073/pnas.0911855107>, PubMed: 20176931
- Boudrias, M.-H., Gonçalves, C. S., Penny, W. D., Park, C.-H., Rossiter, H. E., Talelli, P., & Ward, N. S. (2012). Age-related changes in causal interactions between cortical motor regions during hand grip. *NeuroImage*, 59(4), 3398–3405. <https://doi.org/10.1016/j.neuroimage.2011.11.025>, PubMed: 22119651
- Brodersen, K. H., Schofield, T. M., Leff, A. P., Ong, C. S., Lomakina, E. I., Buhmann, J. M., & Stephan, K. E. (2011). Generative embedding for model-based classification of fMRI data. *PLOS Computational Biology*, 7(6), e1002079. <https://doi.org/10.1371/journal.pcbi.1002079>, PubMed: 21731479
- Buckner, R. L., Krienen, F. M., & Yeo, B. T. T. (2013). Opportunities and limitations of intrinsic functional connectivity MRI. *Nature Neuroscience*, 16(7), 832–837. <https://doi.org/10.1038/nn.3423>, PubMed: 23799476
- Bühler, M., Vollstädt-Klein, S., Klemen, J., & Smolka, M. N. (2008). Does erotic stimulus presentation design affect brain activation patterns? Event-related vs. blocked fMRI designs. *Behavioral and Brain Functions*, 4(1), 30. <https://doi.org/10.1186/1744-9081-4-30>, PubMed: 18647397
- Cai, J., Luo, J., Wang, S., & Yang, S. (2018). Feature selection in machine learning: A new perspective. *Neurocomputing*, 300, 70–79. <https://doi.org/10.1016/j.neucom.2017.11.077>
- Caspers, S., Moebus, S., Lux, S., Pundt, N., Schütz, H., Mühleisen, T. W., ... Amunts, K. (2014). Studying variability in human brain aging in a population-based German cohort—Rationale and design of 1000BRAINS. *Frontiers in Aging Neuroscience*, 6, 149. <https://doi.org/10.3389/fnagi.2014.00149>, PubMed: 25071558
- Cieslik, E. C., Zilles, K., Grefkes, C., & Eickhoff, S. B. (2011). Dynamic interactions in the fronto-parietal network during a manual stimulus–response compatibility task. *NeuroImage*,

- 58(3), 860–869. <https://doi.org/10.1016/j.neuroimage.2011.05.089>, PubMed: 21708271
- Cieslik, E. C., Zilles, K., Kurth, F., & Eickhoff, S. B. (2010). Dissociating bottom-up and top-down processes in a manual stimulus–response compatibility task. *Journal of Neurophysiology*, 104(3), 1472–1483. <https://doi.org/10.1152/jn.00261.2010>, PubMed: 20573974
- Cole, M. W., Bassett, D. S., Power, J. D., Braver, T. S., & Petersen, S. E. (2014). Intrinsic and task-evoked network architectures of the human brain. *Neuron*, 83(1), 238–251. <https://doi.org/10.1016/j.neuron.2014.05.014>, PubMed: 24991964
- Cole, M. W., Ito, T., Schultz, D., Mill, R., Chen, R., & Cocuzza, C. (2019). Task activations produce spurious but systematic inflation of task functional connectivity estimates. *NeuroImage*, 189, 1–18. <https://doi.org/10.1016/j.neuroimage.2018.12.054>, PubMed: 30597260
- Daunizeau, J., Preuschoff, K., Friston, K., & Stephan, K. (2011). Optimizing experimental design for comparing models of brain function. *PLOS Computational Biology*, 7(11), e1002280. <https://doi.org/10.1371/journal.pcbi.1002280>, PubMed: 22125485
- Diersch, N., Valdes-Herrera, J. P., Tempelmann, C., & Wolbers, T. (2021). Increased hippocampal excitability and altered learning dynamics mediate cognitive mapping deficits in human aging. *Journal of Neuroscience*, 41(14), 3204–3221. <https://doi.org/10.1523/JNEUROSCI.0528-20.2021>, PubMed: 33648956
- Dosenbach, N. U. F., Nardos, B., Cohen, A. L., Fair, D. A., Power, J. D., Church, J. A., ... Schlaggar, B. L. (2010). Prediction of individual brain maturity using fMRI. *Science*, 329(5997), 1358–1361. <https://doi.org/10.1126/science.1194144>, PubMed: 20829489
- Elton, A., & Gao, W. (2015). Task-related modulation of functional connectivity variability and its behavioral correlations. *Human Brain Mapping*, 36(8), 3260–3272. <https://doi.org/10.1002/hbm.22847>, PubMed: 26015070
- Ferreira, L. K., & Busatto, G. F. (2013). Resting-state functional connectivity in normal brain aging. *Neuroscience & Biobehavioral Reviews*, 37(3), 384–400. <https://doi.org/10.1016/j.neubiorev.2013.01.017>, PubMed: 23333262
- Finn, E. S., & Bandettini, P. A. (2021). Movie-watching outperforms rest for functional connectivity-based prediction of behavior. *NeuroImage*, 235, 117963. <https://doi.org/10.1016/j.neuroimage.2021.117963>, PubMed: 33813007
- Finn, E. S., Scheinost, D., Finn, D. M., Shen, X., Papademetris, X., & Constable, R. T. (2017). Can brain state be manipulated to emphasize individual differences in functional connectivity? *NeuroImage*, 160, 140–151. <https://doi.org/10.1016/j.neuroimage.2017.03.064>, PubMed: 28373122
- Fitts, P. M., & Deininger, R. L. (1954). S-R compatibility: Correspondence among paired elements within stimulus and response codes. *Journal of Experimental Psychology*, 48(6), 483–492. <https://doi.org/10.1037/h0054967>, PubMed: 13221745
- Fox, M. D., Snyder, A. Z., Vincent, J. L., & Raichle, M. E. (2007). Intrinsic fluctuations within cortical systems account for intertrial variability in human behavior. *Neuron*, 56(1), 171–184. <https://doi.org/10.1016/j.neuron.2007.08.023>, PubMed: 17920023
- Friston, K. J. (2011). Functional and effective connectivity: A review. *Brain Connectivity*, 1(1), 13–36. <https://doi.org/10.1089/brain.2011.0008>, PubMed: 22432952
- Friston, K. J., Harrison, L., & Penny, W. (2003). Dynamic causal modelling. *NeuroImage*, 19(4), 1273–1302. [https://doi.org/10.1016/S1053-8119\(03\)00202-7](https://doi.org/10.1016/S1053-8119(03)00202-7), PubMed: 12948688
- Friston, K. J., Litvak, V., Oswal, A., Razi, A., Stephan, K. E., van Wijk, B. C. M., ... Zeidman, P. (2016). Bayesian model reduction and empirical Bayes for group (DCM) studies. *NeuroImage*, 128, 413–431. <https://doi.org/10.1016/j.neuroimage.2015.11.015>, PubMed: 26569570
- Gbadegyan, O., Teng, J., & Prakash, R. S. (2022). Predicting response time variability from task and resting-state functional connectivity in the aging brain. *NeuroImage*, 250, 118890. <https://doi.org/10.1016/j.neuroimage.2022.118890>, PubMed: 35007719
- Geerligs, L., Rubinov, M., Cam-Can., & Henson, R. N. (2015). State and trait components of functional connectivity: Individual differences vary with mental state. *Journal of Neuroscience*, 35(41), 13949–13961. <https://doi.org/10.1523/JNEUROSCI.1324-15.2015>, PubMed: 26468196
- Geng, X., Xu, J., Liu, B., & Shi, Y. (2018). Multivariate classification of major depressive disorder using the effective connectivity and functional connectivity. *Frontiers in Neuroscience*, 12, 38. <https://doi.org/10.3389/fnins.2018.00038>, PubMed: 29515348
- Greene, A. S., Gao, S., Scheinost, D., & Constable, R. T. (2018). Task-induced brain state manipulation improves prediction of individual traits. *Nature Communications*, 9(1), 2807. <https://doi.org/10.1038/s41467-018-04920-3>, PubMed: 30022026
- Heckner, M. K., Cieslik, E. C., Patil, K. R., Gell, M., Eickhoff, S. B., Hoffstädter, F., & Langner, R. (2023). Predicting executive functioning from functional brain connectivity: Network specificity and age effects. *Cerebral Cortex*, 33(11), 6495–6507. <https://doi.org/10.1093/cercor/bhac520>, PubMed: 36635227
- Huetzel, S. A. (2012). Event-related fMRI in cognition. *NeuroImage*, 62(2), 1152–1156. <https://doi.org/10.1016/j.neuroimage.2011.08.113>, PubMed: 21963919
- Huth, A. G., de Heer, W. A., Griffiths, T. L., Theunissen, F. E., & Gallant, J. L. (2016). Natural speech reveals the semantic maps that tile human cerebral cortex. *Nature*, 532(7600), 453–458. <https://doi.org/10.1038/nature17637>, PubMed: 27121839
- Jiang, R., Zuo, N., Ford, J. M., Qi, S., Zhi, D., Zhuo, C., ... Sui, J. (2020). Task-induced brain connectivity promotes the detection of individual differences in brain-behavior relationships. *NeuroImage*, 207, 116370. <https://doi.org/10.1016/j.neuroimage.2019.116370>, PubMed: 31751666
- Jülich Supercomputing Centre (2021). JURECA: Data Centric and Booster Modules implementing the Modular Supercomputing Architecture at Jülich Supercomputing Centre. *Journal of Large-Scale Research Facilities JLSRF*, 7. <https://doi.org/10.17815/jlsrf-7-182>
- Jung, K., Friston, K. J., Pae, C., Choi, H. H., Tak, S., Choi, Y. K., ... Park, H.-J. (2018). Effective connectivity during working memory and resting states: A DCM study. *NeuroImage*, 169, 485–495. <https://doi.org/10.1016/j.neuroimage.2017.12.067>, PubMed: 29284140
- Kahan, J., Mancini, L., Flandin, G., White, M., Papadaki, A., Thornton, J., ... Foltynie, T. (2019). Deep brain stimulation has state-dependent effects on motor connectivity in Parkinson's disease. *Brain*, 142(8), 2417–2431. <https://doi.org/10.1093/brain/awz164>, PubMed: 31219504

- Kapoor, S., & Narayanan, A. (2023). Leakage and the reproducibility crisis in machine-learning-based science. *Patterns*, 4(9), 100804. <https://doi.org/10.1016/j.patter.2023.100804>, PubMed: 37720327
- Kraljević, N., Langner, R., Küppers, V., Raimondo, F., Patil, K. R., Eickhoff, S. B., & Müller, V. I. (2024). Network and state specificity in connectivity-based predictions of individual behavior. *Human Brain Mapping*, 45(8), e26753. <https://doi.org/10.1002/hbm.26753>, PubMed: 38864353
- Langner, R., Cieslik, E. C., Behrwind, S. D., Roski, C., Caspers, S., Amunts, K., & Eickhoff, S. B. (2015). Aging and response conflict solution: Behavioural and functional connectivity changes. *Brain Structure and Function*, 220(3), 1739–1757. <https://doi.org/10.1007/s00429-014-0758-0>, PubMed: 24718622
- Loehrer, P. A., Nettersheim, F. S., Jung, F., Weber, I., Huber, C., Dembek, T. A., ... Timmermann, L. (2016). Ageing changes effective connectivity of motor networks during bimanual finger coordination. *NeuroImage*, 143, 325–342. <https://doi.org/10.1016/j.neuroimage.2016.09.014>, PubMed: 27616642
- Logothetis, N. K. (2008). What we can do and what we cannot do with fMRI. *Nature*, 453(7197), 869–878. <https://doi.org/10.1038/nature06976>, PubMed: 18548064
- Marreiros, A. C., Kiebel, S. J., & Friston, K. J. (2008). Dynamic causal modelling for fMRI: A two-state model. *NeuroImage*, 39(1), 269–278. <https://doi.org/10.1016/j.neuroimage.2007.08.019>, PubMed: 17936017
- Mechelli, A., Henson, R. N. A., Price, C. J., & Friston, K. J. (2003). Comparing event-related and epoch analysis in blocked design fMRI. *NeuroImage*, 18(3), 806–810. [https://doi.org/10.1016/S1053-8119\(02\)00027-7](https://doi.org/10.1016/S1053-8119(02)00027-7), PubMed: 12667857
- Mechelli, A., Price, C. J., Henson, R. N. A., & Friston, K. J. (2003). Estimating efficiency a priori: A comparison of blocked and randomized designs. *NeuroImage*, 18(3), 798–805. [https://doi.org/10.1016/S1053-8119\(02\)00040-X](https://doi.org/10.1016/S1053-8119(02)00040-X), PubMed: 12667856
- Millar, P. R., Luckett, P. H., Gordon, B. A., Benzinger, T. L. S., Schindler, S. E., Fagan, A. M., ... Dominantly Inherited Alzheimer Network. (2022). Predicting brain age from functional connectivity in symptomatic and preclinical Alzheimer disease. *NeuroImage*, 256, 119228. <https://doi.org/10.1016/j.neuroimage.2022.119228>, PubMed: 35452806
- Millar, P. R., Petersen, S. E., Ances, B. M., Gordon, B. A., Benzinger, T. L. S., Morris, J. C., & Balota, D. A. (2020). Evaluating the sensitivity of resting-state BOLD variability to age and cognition after controlling for motion and cardiovascular influences: A network-based approach. *Cereb Cortex*, 30(11), 5686–5701. <https://doi.org/10.1093/cercor/bhaa138>, PubMed: 32515824
- Morken, F., Helland, T., Hugdahl, K., & Specht, K. (2017). Reading in dyslexia across literacy development: A longitudinal study of effective connectivity. *NeuroImage*, 144, 92–100. <https://doi.org/10.1016/j.neuroimage.2016.09.060>, PubMed: 27688204
- Mwangi, B., Tian, T. S., & Soares, J. C. (2014). A review of feature reduction techniques in neuroimaging. *Neuroinformatics*, 12(2), 229–244. <https://doi.org/10.1007/s12021-013-9204-3>, PubMed: 24013948
- Petersen, S. E., & Dubis, J. W. (2012). The mixed block/event-related design. *NeuroImage*, 62(2), 1177–1184. <https://doi.org/10.1016/j.neuroimage.2011.09.084>, PubMed: 22008373
- Proctor, R. W., Vu, K.-P. L., & Pick, D. F. (2005). Aging and response selection in spatial choice tasks. *Human Factors*, 47(2), 250–270. <https://doi.org/10.1518/0018720054679425>, PubMed: 16170937
- Rajapakse, J. C., & Zhou, J. (2007). Learning effective brain connectivity with dynamic Bayesian networks. *NeuroImage*, 37(3), 749–760. <https://doi.org/10.1016/j.neuroimage.2007.06.003>, PubMed: 17644415
- Roebroeck, A., Formisano, E., & Goebel, R. (2005). Mapping directed influence over the brain using Granger causality and fMRI. *NeuroImage*, 25(1), 230–242. <https://doi.org/10.1016/j.neuroimage.2004.11.017>, PubMed: 15734358
- Rosenberg, M. D., Finn, E. S., Scheinost, D., Papademetris, X., Shen, X., Constable, R. T., & Chun, M. M. (2016). A neuromarker of sustained attention from whole-brain functional connectivity. *Nature Neuroscience*, 19(1), 165–171. <https://doi.org/10.1038/nn.4179>, PubMed: 26595653
- Rosenblatt, M., Tejavibulya, L., Jiang, R., Noble, S., & Scheinost, D. (2024). Data leakage inflates prediction performance in connectome-based machine learning models. *Nature Communications*, 15(1), 1829. <https://doi.org/10.1038/s41467-024-46150-w>, PubMed: 38418819
- Saunders, C., Gammerman, A., & Vovk, V. (1998). Ridge regression learning algorithm in dual variables.
- Schlösser, R., Gesierich, T., Kaufmann, B., Vucurevic, G., Hunsche, S., Gawehn, J., & Stoeter, P. (2003). Altered effective connectivity during working memory performance in schizophrenia: A study with fMRI and structural equation modeling. *NeuroImage*, 19(3), 751–763. [https://doi.org/10.1016/S1053-8119\(03\)00106-X](https://doi.org/10.1016/S1053-8119(03)00106-X), PubMed: 12880804
- Shen, X., Finn, E. S., Scheinost, D., Rosenberg, M. D., Chun, M. M., Papademetris, X., & Constable, R. T. (2017). Using connectome-based predictive modeling to predict individual behavior from brain connectivity. *Nature Protocols*, 12(3), 506–518. <https://doi.org/10.1038/nprot.2016.178>, PubMed: 28182017
- Silchenko, A. N., Hoffstaedter, F., & Eickhoff, S. B. (2023). Impact of sample size and regression of tissue-specific signals on effective connectivity within the core default mode network. *Human Brain Mapping*, 44(17), 5858–5870. <https://doi.org/10.1002/hbm.26481>, PubMed: 37713540
- Sripada, C., Rutherford, S., Angstadt, M., Thompson, W. K., Luciana, M., Weigard, A., ... Heitzeg, M. (2020). Prediction of neurocognition in youth from resting state fMRI. *Molecular Psychiatry*, 25(12), 3413–3421. <https://doi.org/10.1038/s41380-019-0481-6>, PubMed: 31427753
- Tibshirani, R. (1996). Regression shrinkage and selection via the lasso. *Journal of the Royal Statistical Society: Series B (Methodological)*, 58(1), 267–288. <https://doi.org/10.1111/j.2517-6161.1996.tb02080.x>
- Tie, Y., Suarez, R. O., Whalen, S., Radmanesh, A., Norton, I. H., & Golby, A. J. (2009). Comparison of blocked and event-related fMRI designs for pre-surgical language mapping. *NeuroImage*, 47, T107–T115. <https://doi.org/10.1016/j.neuroimage.2008.11.020>, PubMed: 19101639
- Tsvetanov, K. A., Henson, R. N. A., Tyler, L. K., Razi, A., Geerligs, L., Ham, T. E., ... Cambridge Centre for Ageing and Neuroscience. (2016). Extrinsic and intrinsic brain network connectivity

- maintains cognition across the lifespan despite accelerated decay of regional brain activation. *Journal of Neuroscience*, 36(11), 3115–3126. <https://doi.org/10.1523/JNEUROSCI.2733-15.2016>, PubMed: 26985024
- van den Heuvel, M. P., & Pol, H. E. H. (2010). Exploring the brain network: A review on resting-state fMRI functional connectivity. *European Neuropsychopharmacology*, 20(8), 519–534. <https://doi.org/10.1016/j.euroneuro.2010.03.008>, PubMed: 20471808
- Varoquaux, G., Raamana, P. R., Engemann, D. A., Hoyos-Ildrobo, A., Schwartz, Y., & Thirion, B. (2017). Assessing and tuning brain decoders: Cross-validation, caveats, and guidelines. *NeuroImage*, 145, 166–179. <https://doi.org/10.1016/j.neuroimage.2016.10.038>, PubMed: 27989847
- Volz, L. J., Eickhoff, S. B., Pool, E.-M., Fink, G. R., & Grefkes, C. (2015). Differential modulation of motor network connectivity during movements of the upper and lower limbs. *NeuroImage*, 119, 44–53. <https://doi.org/10.1016/j.neuroimage.2015.05.101>, PubMed: 26095089
- Winkler, A. M., Ridgway, G. R., Webster, M. A., Smith, S. M., & Nichols, T. E. (2014). Permutation inference for the general linear model. *NeuroImage*, 92(100), 381–397. <https://doi.org/10.1016/j.neuroimage.2014.01.060>, PubMed: 24530839
- Xiong, M., Lin, L., Jin, Y., Kang, W., Wu, S., & Sun, S. (2023). Comparison of machine learning models for brain age prediction using six imaging modalities on middle-aged and older adults. *Sensors*, 23(7), 3622. <https://doi.org/10.3390/s23073622>, PubMed: 37050682
- Zeidman, P., Jafarian, A., Corbin, N., Seghier, M. L., Razi, A., Price, C. J., & Friston, K. J. (2019). A guide to group effective connectivity analysis, part 1: First level analysis with DCM for fMRI. *NeuroImage*, 200, 174–190. <https://doi.org/10.1016/j.neuroimage.2019.06.031>, PubMed: 31226497
- Zeidman, P., Jafarian, A., Seghier, M. L., Litvak, V., Cagnan, H., Price, C. J., & Friston, K. J. (2019). A guide to group effective connectivity analysis, part 2: Second level analysis with PEB. *NeuroImage*, 200, 12–25. <https://doi.org/10.1016/j.neuroimage.2019.06.032>, PubMed: 31226492
- Zhang, S., Jung, K., Langner, R., Florin, E., Eickhoff, S. B., & Popovich, O. V. (2024). Impact of data processing varieties on DCM estimates of effective connectivity from task-fMRI. *Human Brain Mapping*, 45(8), e26751. <https://doi.org/10.1002/hbm.26751>, PubMed: 38864293
- Zhao, W., Makowski, C., Hagler, D. J., Garavan, H. P., Thompson, W. K., Greene, D. J., ... Dale, A. M. (2023). Task fMRI paradigms may capture more behaviorally relevant information than resting-state functional connectivity. *NeuroImage*, 270, 119946. <https://doi.org/10.1016/j.neuroimage.2023.119946>, PubMed: 36801369

Supplementary materials

for the manuscript entitled

Predicting response speed and age from task-evoked effective connectivity

by

Shufei Zhang^{1,2}, Kyesam Jung^{1,2}, Robert Langner^{1,2}, Esther Florin³, Simon B. Eickhoff^{1,2},
Oleksandr V. Popovych^{1,2}

¹Institute of Neuroscience and Medicine, Brain and Behaviour (INM-7), Research Centre
Jülich, Germany

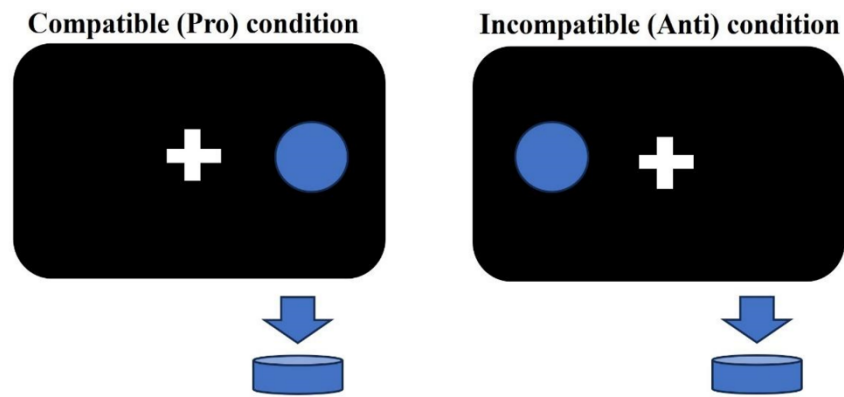
²Institute for Systems Neuroscience, Medical Faculty, Heinrich-Heine University Düsseldorf,
Germany

³Institute of Clinical Neuroscience and Medical Psychology, Medical Faculty, Heinrich-Heine
University Düsseldorf, Germany

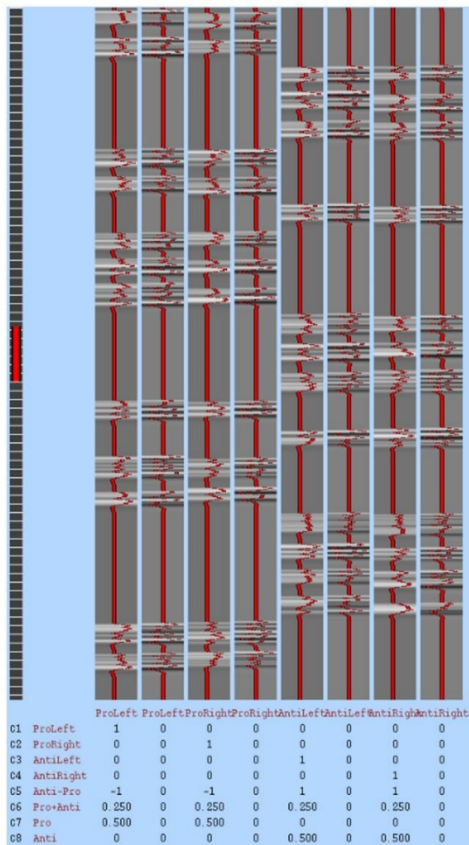
*Corresponding author: o.popovych@fz-juelich.de

Supplementary Figures

(a) Stimulus-response compatibility (SRC) task



(b) Event-related GLM



(c) Block-related GLM

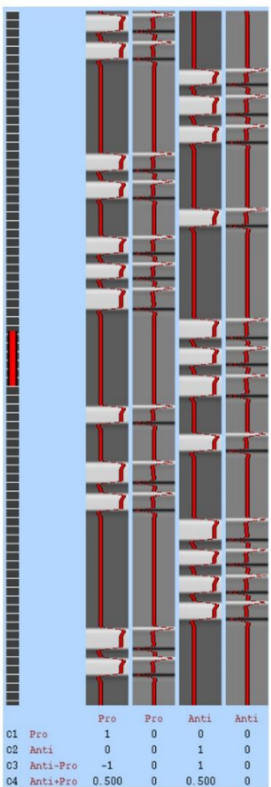


Fig. S1 The overview of the stimulus-response compatibility (SRC) task and general linear model (GLM) designs for event-related and block-based designs. (a) The SRC task includes two conditions: compatible (Pro) and incompatible (Anti) conditions. During the task, participants were instructed to respond to lateralized visual stimuli by accurately and rapidly pressing an ipsilateral (Pro) or contralateral button (Anti), respectively. (b/c) The event-related and block-based GLM designs were implemented in the task-evoked first-level fMRI

analyses, where double-gamma and temporal derivatives were utilized to model individual BOLD signals.

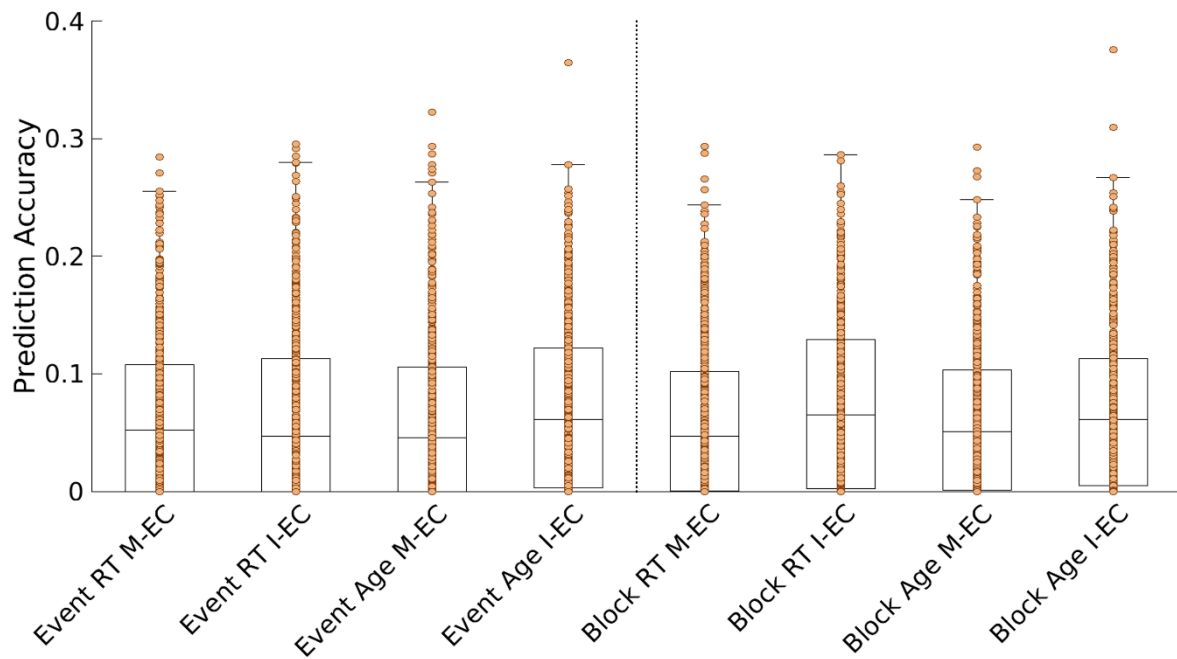


Fig. S2. A summary of label-shuffled permutation tests (500 times) obtained from block/event-related designs and intrinsic/task-modulated effective connectivity (I-EC/M-EC) for reaction time (RT) and age. The orange dot in the figure represents the prediction correlation derived from one fixed 5-fold cross-validation splitting scheme where the behavioral labels were shuffled randomly. Note, that the fixed-5-fold cross-validation splitting scheme was the one showing the highest prediction correlation in the repeating 5-fold analysis.

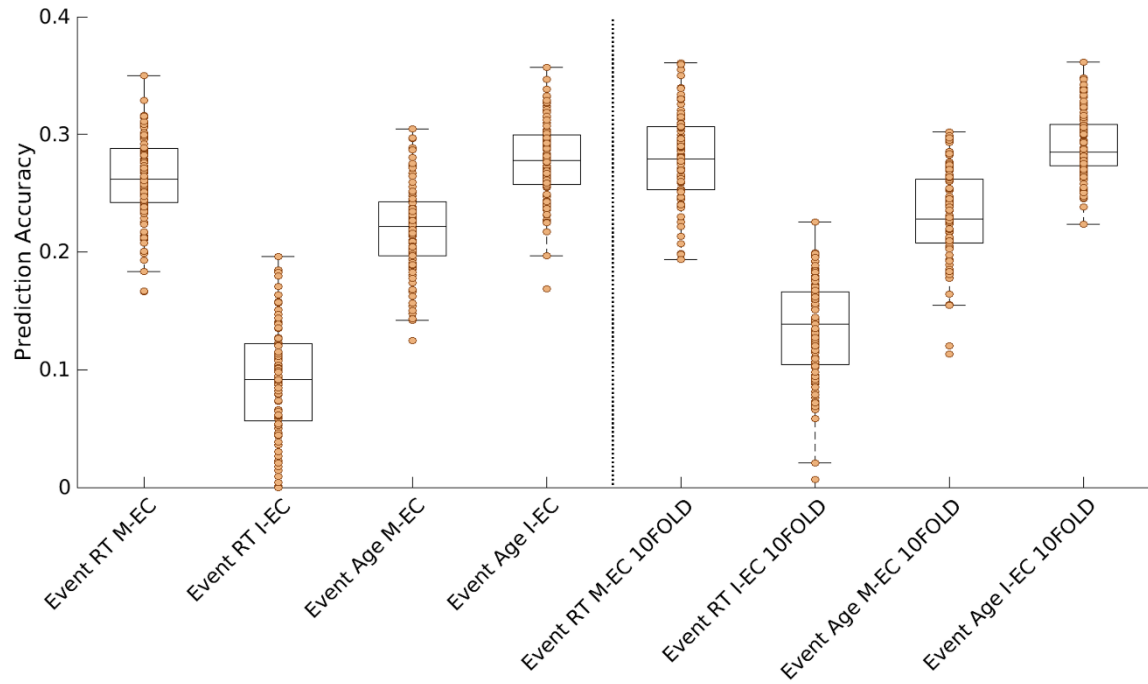


Fig. S3. A summary of prediction results obtained from the event-related design and intrinsic/modulatory effective connectivity (I-EC/M-EC) in predicting individual reaction time (RT) and age using a 5-fold (the left panel) and 10-fold (the right panel) cross-validation approach. The orange dot in the figure represents the prediction correlations derived from one randomly sampled cross-validation instance.

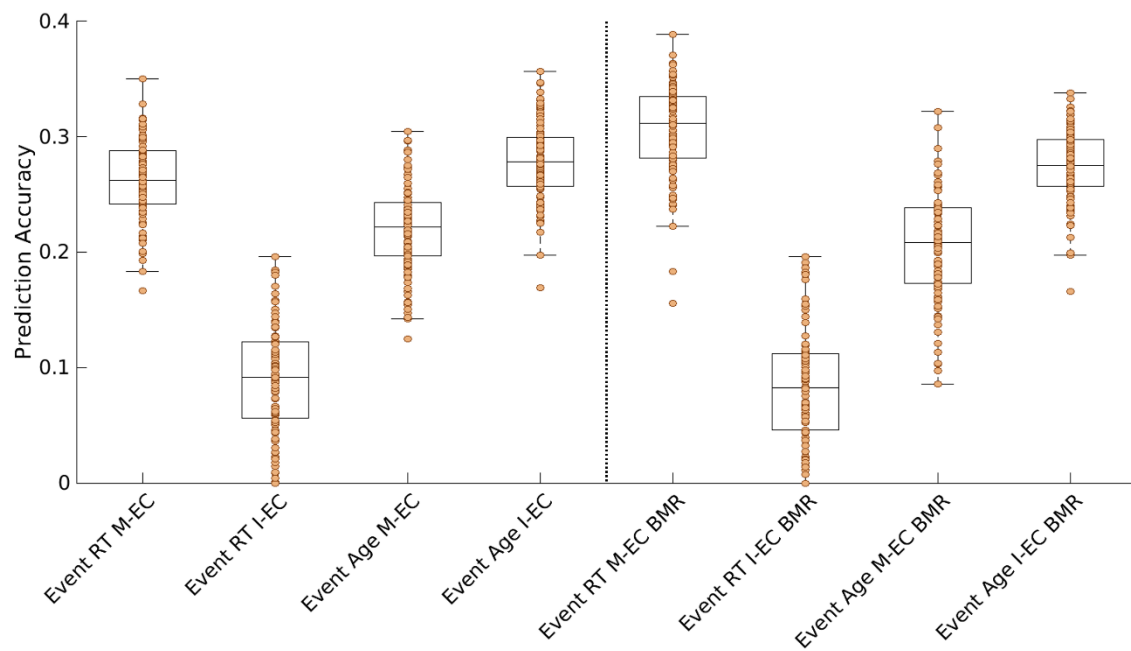


Fig. S4. A summary of prediction results obtained from the event-related design and intrinsic/modulatory effective connectivity (I-EC/M-EC) incorporating prediction cases without (the left panel) and those with Bayesian model reduction (BMR) procedure (the right panel) in predicting individual reaction time (RT) and age using a 5-fold cross-validation approach. The orange dot in the figure represents the prediction correlations derived from one randomly sampled 5-fold cross-validation instance.

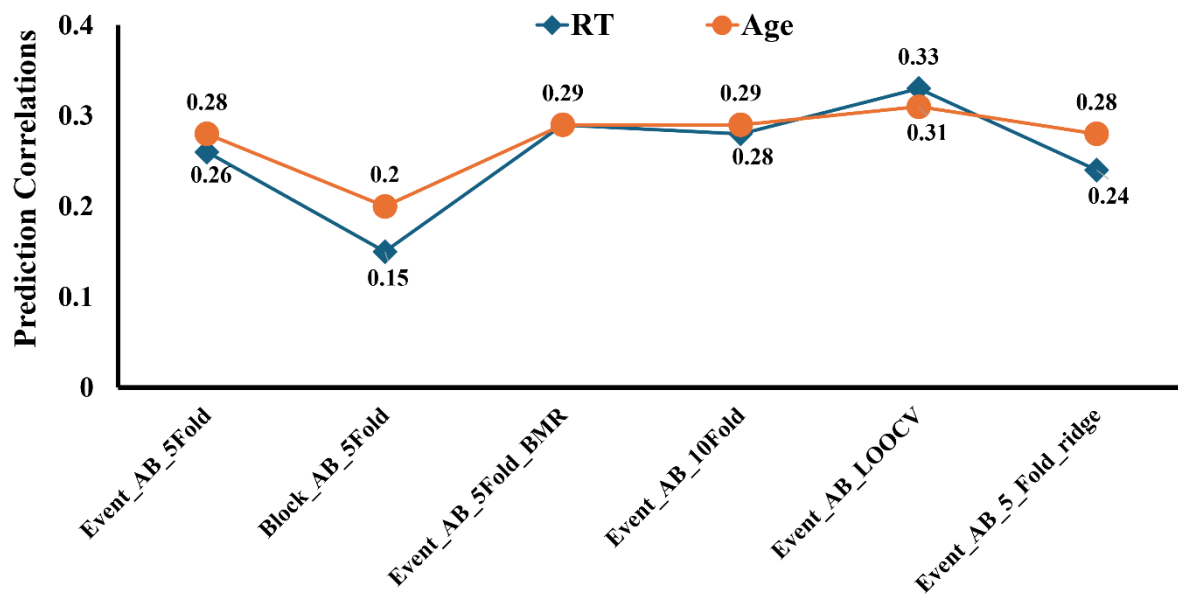


Fig. S5 Overview of the mean prediction accuracy (Pearson's r) across all conditions for predicting individual reaction time (RT) and age in various prediction scenarios. Each model combines intrinsic and task-modulated effective connectivity (EC) parameters, with prediction correlations calculated between empirical and predicted values. The correlations were averaged across 100 iterations of random subject splits for cross-validation (CV) analyses, except for the leave-one-out CV (LOOCV) cases. The horizontal axis represents different prediction conditions involving CV schemes including 5-fold, 10-fold, and LOOCV, applications of Bayesian model reduction (BMR), and ridge-regularized regression. The vertical axis shows the prediction correlations (r).

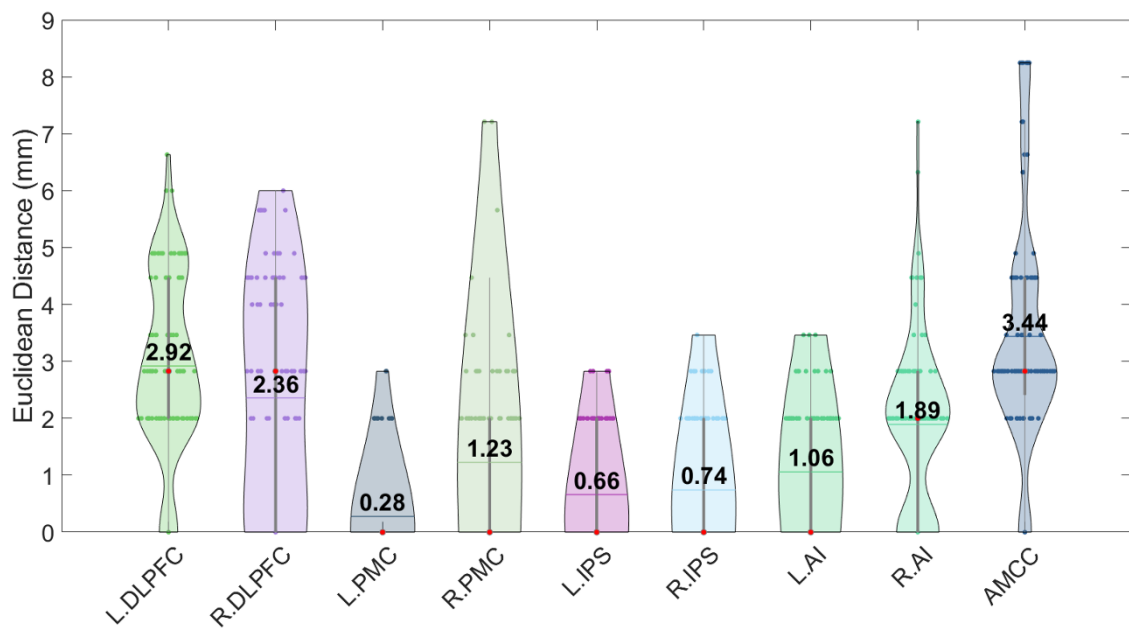


Fig. S6 Variations in Group-Level Peak Coordinates of Regions of Interest (ROIs) During 5-Fold Cross-Validation. The entire sample was split into training and testing sets using a 5-fold cross-validation (CV) approach. For each fold, second-level fMRI analyses were conducted on the training set, and ROIs were identified based on the peak coordinates derived from these analyses. The Euclidean distance between the peak coordinates of ROIs selected from each fold and the ROIs obtained from the full sample was calculated. This process was repeated 20 times, resulting in 100 points per network node. These differences

were visualized as violin plots to illustrate the distribution of variations in ROI coordinates, with the mean value for each violin shown.

Supplementary Tables

Table 1. Prediction performance of the features extracted from intrinsic EC (I-EC) and task-modulated EC (M-EC) for individual reaction time (RT) and age obtained by LASSO regression with 5-fold cross-validation

Predictors	Event		Block	
	M-EC	I-EC	M-EC	I-EC
RT	$r = 0.26 \pm 0.04 *$	$r = 0.09 \pm 0.05$	$r = 0.17 \pm 0.05$	$r = 0.10 \pm 0.04$
Age	$r = 0.22 \pm 0.04 *$	$r = 0.28 \pm 0.03 *$	$r = 0.19 \pm 0.05$	$r = 0.20 \pm 0.04$

The prediction correlations were estimated from a 100-time 5-fold CV, which employed the LASSO-regularized linear regression model. The upper number in the table cells indicates the

averaged correlation r and its standard deviation across repetitions. Asterisks (*) indicate a statistically significant difference ($p < 0.05$) between averaged prediction correlations and label-shuffled permutation tests (500 times), which are displayed in Supplementary Fig. S2.

Table 2. 10-fold prediction performances of M-EC and I-EC in individual RT and age

Predictors	Event	
	M-EC	I-EC
RT	0.28 ± 0.04	0.14 ± 0.04
Age	0.23 ± 0.04	0.29 ± 0.03

The prediction correlations were estimated from a 100-time 10-fold CV, which employed the Lasso-regularized linear regression model. The number in the element shows the averaged correlation between empirical and predicted values, and the second one indicates the standard deviation. M-EC: task-modulated effective connectivity; I-EC: intrinsic effective connectivity; RT: reaction time.

Table 3. LOOCV prediction performances of M-EC and I-EC in individual RT and age

Predictors	Event	
	M-EC	I-EC
RT	0.34	0.11
Age	0.20	0.28

The prediction correlations were estimated from a Leave-one-out cross-validation (LOOCV) scheme, which employed the Lasso-regularized linear regression model. The number in the elements represents the prediction correlation between empirical and predicted values. M-EC: task-modulated effective connectivity; I-EC: intrinsic effective connectivity; RT: reaction time.

Table 4. Prediction performances of M-EC and I-EC in individual RT and age with reduced models

Predictors	Event	
	M-EC	I-EC
RT	0.31 ± 0.04	0.08 ± 0.05
Age	0.20 ± 0.05	0.27 ± 0.03

The prediction correlations were estimated from a 100-time 5-fold CV, which extracted EC connections from reduced models (Bayesian model reduction) and employed the Lasso-regularized linear regression model for prediction. The number in the element shows the averaged correlation between empirical and predicted values, and the second one indicates the standard deviation. M-EC: task-modulated effective connectivity; I-EC: intrinsic effective connectivity; RT: reaction time.

Table 5. The 5-fold prediction performances of M-EC and I-EC in individual RT and age using ridge-regularized linear regression

Predictors	Event	
	M-EC	I-EC
RT	0.24 ± 0.04	0.04 ± 0.05
Age	0.21 ± 0.04	0.27 ± 0.03

The prediction correlations were estimated from a 100-time 5-fold CV, which employed the ridge-regularized linear regression model. The number in the element shows the averaged correlation between empirical and predicted values, and the second one indicates the standard deviation. M-EC: task-modulated effective connectivity; I-EC: intrinsic effective connectivity; RT: reaction time.

Study 3: Network Specificity in Predicting Childhood Trauma Characteristics Using Effective Connectivity

Shufei Zhang^{1,2}, Wei Zheng^{3,4}, Zezhi Li^{3,4}, Huawang Wu^{3,4,*}

¹Institute of Neuroscience and Medicine, Brain and Behaviour (INM-7), Research Centre Jülich, 52425 Jülich, Germany

²Institute for Systems Neuroscience, Medical Faculty, Heinrich-Heine University Düsseldorf, 40225 Düsseldorf, Germany

³The Affiliated Brain Hospital, Guangzhou Medical University, 510370 Guangzhou, Guangdong, China

⁴Key Laboratory of Neurogenetics and Channelopathies of Guangdong Province and The Ministry of Education of China, Guangzhou Medical University, 510180 Guangzhou, Guangdong, China

*Correspondence: huawangwu@gzhmu.edu.cn

Published in Alpha Psychiatry 2025; 26(3): 43988

<https://doi.org/10.31083/AP43988>

Own contributions

Writing the manuscript, preparing figures, performing data analyses, and contributing to the interpretation of results.

Original Article

Network Specificity in Predicting Childhood Trauma Characteristics Using Effective Connectivity

Shufei Zhang^{1,2}, Wei Zheng^{3,4} , Zezhi Li^{3,4}, Huawang Wu^{3,4,*}¹Institute of Neuroscience and Medicine, Brain and Behaviour (INM-7), Research Centre Jülich, 52425 Jülich, Germany²Institute for Systems Neuroscience, Medical Faculty, Heinrich-Heine University Düsseldorf, 40225 Düsseldorf, Germany³The Affiliated Brain Hospital, Guangzhou Medical University, 510370 Guangzhou, Guangdong, China⁴Key Laboratory of Neurogenetics and Channelopathies of Guangdong Province and The Ministry of Education of China, Guangzhou Medical University, 510180 Guangzhou, Guangdong, China*Correspondence: huawangwu@gzhmu.edu.cn (Huawang Wu)

Submitted: 19 September 2024 Revised: 11 November 2024 Accepted: 25 November 2024 Published: 18 June 2025

Abstract

Background: Childhood maltreatment (CM) has become one of the leading psychological stressors, adversely impacting brain development during adolescence and into adulthood. Although previous studies have extensively explored functional connectivity associated with CM, the dynamic interaction of brain effective connectivity (EC) is not well documented. **Methods:** Resting-state functional magnetic resonance imaging data were collected from 215 adults with an assessment using the Childhood Trauma Questionnaire (CTQ). Whole-brain EC was estimated by regression dynamic causal modeling and subsequently down-resampled into seven networks. To predict CTQ total scores, repeated cross-validated ridge-regularized linear regression was employed, with whole-brain and network-specific EC features selected at thresholds of 5% of the strongest positive and negative correlations between EC and scores, as well as 10% and 20% thresholds. Additionally, a least absolute shrinkage and selection operator (LASSO)-regularized linear regression model was utilized as validation analysis. **Results:** Our findings revealed that whole-brain EC showed a marginal association with predicting CTQ total scores, and EC within the default mode network (DMN) significantly predicted these scores. EC features from other networks did not yield significant predictive results. Notably, across varying feature selection thresholds, DMN features consistently demonstrated significant predictive power, comparable to results from LASSO-regularized predictions. **Conclusions:** These findings suggested that brain EC can capture individual differences in CM severity, with the DMN potentially serving as an important predictor related to CM.

Keywords: effective connectivity; childhood maltreatment; regression dynamic causal modeling; default mode network; feature selection

Main points

1. Effective connectivity (EC) can capture individual differences in childhood maltreatment severity.
2. The EC features within the default mode network (DMN) showed the highest prediction correlation over other networks.
3. The DMN may serve as an important predictor associated with childhood maltreatment.

1. Introduction

Childhood maltreatment (CM), which encompasses different forms of maltreatment such as neglect and physical, sexual, and emotional abuse, has become one of the leading psychological stressors, negatively affecting brain development during adolescence and into adulthood [1]. Childhood experiences of adversity are significantly related to the first onset of psychiatric disorders with social-affective disturbances [2]. Individuals with CM may have a higher risk of developing bipolar disorder, depression, substance abuse, and suicidal behaviors [3–5]. Thus, understanding the neural substrate influenced by CM may be es-

sential for creating preventive measures for individuals and offering therapeutic insights for treating psychiatric disorders.

Brain connectivity inferred from resting-state functional magnetic resonance imaging (rs-fMRI) has been widely used to explore the brain-behavior relationship. Functional connectivity (FC), one of the most commonly used connectivity measures, is defined by the pairwise correlation between distant brain regions and is considered a potential biomarker for human brain development and psychological processes [6]. A recent review [7] demonstrated that altered FC in brain regions such as the insula, amygdala, hippocampus, cingulate cortex, and prefrontal cortex is associated with exposure to individual maltreatment. Furthermore, accumulating evidence [8,9] indicates that FC alterations within networks of the default mode network (DMN) and the salience network (SN) contribute to the pathophysiology of mental health disorders and social-affective functioning in individuals with maltreatment exposures. However, these studies [7–9] primarily focused on bidirectional connections and overlooked the dynamic influence that one region has on another [10].



Conversely, effective connectivity (EC), estimated by dynamic causal modeling (DCM), measures directional causal influences among brain regions [11]. This complements FC by a mechanistic explanation of the causal interactions through the modeling of directional causal influences [10] and may offer higher sensitivity than FC in psychopathology [12]. Although EC research related to the CM topic is sparse, a recent study [13] found that CM experiences impaired the medial prefrontal cortex's ability to inhibit the amygdala during emotional processing, suggesting that EC could serve as a potential biomarker for psychiatric disorders. Additionally, unlike FC studies, many EC studies are driven by hypotheses and have typically limited their analyses to fewer than 10 nodes [13,14], exploring the information flow directionality among specific network nodes. Additionally, due to the computational limitations, inferring EC at a whole-brain or large-scale level is challenging [15], leading to a restriction in the analysis of whole-brain and large-scale EC patterns. As emerging evidence suggests that CM is related to altered complex and distributed network architectures [16], examining whole-brain EC allows us to capture dynamic influences across widespread regions. This approach provides a more comprehensive view of how maltreatment experiences may disrupt functional network coupling, enhancing our understanding of CM's neurobiological impact on broad connectivity dynamics.

In this study, we aim to evaluate whole-brain EC in individuals with CM and assess its potential for predicting CM severity. We measured individual CM severity using the Childhood Trauma Questionnaire (CTQ) Short Form [17] and estimated EC for all participants using regression DCM (rDCM) [14], which is a new variant of DCM. We then applied a cross-validated linear regression model to examine the relationship between whole-brain or network-specific EC profiles and CM severity.

2. Methods

2.1 Subjects

We recruited 215 healthy adult participants from Guangzhou Medical University and the surrounding community between July, 2013 and August, 2019. To ensure eligibility, we administered the Structured Clinical Interview for the Diagnostic and Statistical Manual of Mental Disorders–IV Edition (DSM–IV) Non-Patient Edition to all participants, confirming that they had no history of Axis I disorders. Additionally, we excluded anyone with a family history of psychiatric illness among first- to third-degree biological relatives, as well as individuals with a history of seizures, head trauma, significant surgeries or medical conditions, substance abuse or dependence, or contraindications for magnetic resonance imaging (MRI). We excluded nine subjects due to quality control issues of head motion and spatial normalization, leaving 206 subjects eligible for subsequent analysis (Table 1).

All participants were right-handed and provided written informed consent before their involvement in the study. The study protocol received ethical approval from the Institute Research Board of the Affiliated Brain Hospital, Guangzhou Medical University.

2.2 Childhood Maltreatment Assessment

Before MRI scanning sessions, we conducted a thorough assessment of CM severity for all participants using the Chinese version of the CTQ Short Form [17,18]. This self-report scale comprises 28 items, encompassing five distinct dimensions: emotional abuse, physical abuse, sexual abuse, emotional neglect, and physical neglect, and each item is scored from 1 (“never”) to 5 (“very often”). This scale has been widely applied in clinical and non-clinical populations [18], and its Chinese version has shown strong reliability and validity [17]. A detailed assessment of the CTQ scale and subscales for all qualified subjects ($N = 206$) can be seen in Table 1.

2.3 Imaging Protocols

All MRI datasets for all participants were acquired utilizing a 3T Philips Achieva X-series MRI scanner, equipped with an eight-channel phased-array head coil in the Affiliated Brain Hospital, Guangzhou Medical University.

The resting-state fMRI datasets were collected using a gradient-echo echo-planar imaging sequence, with parameters as follows: repetition time (TR) = 2000 ms, echo time (TE) = 30 ms, flip angle = 90° , field of view (FOV) = $220 \text{ mm} \times 220 \text{ mm}$, and acquisition matrix = 64×64 . The scan consisted of 33 transverse interleaved slices, each with a thickness of 4 mm and a gap of 0.6 mm. Throughout the scanning process, participants were instructed to remain at rest with their eyes closed, and none of them reported falling asleep upon being queried immediately after the scan.

A T1-weighted 3D turbo field-echo sequence was employed to acquire the structural datasets, with parameters as follows: TR = 8.2 ms, TE = 3.7 ms, inversion time = 1100 ms, flip angle = 7° , FOV = $256 \text{ mm} \times 256 \text{ mm}$, acquisition matrix = 256×256 , and voxel size = $1 \times 1 \times 1 \text{ mm}^3$. The scan encompassed continuous 188 sagittal slices covering the brain.

2.4 Imaging Preprocessing

The resting-state fMRI images were preprocessed by the Data Processing and Analysis for Brain Imaging (DPABI) pipeline (<http://rfmri.org/dpabi>), as implemented in the Matlab (v 2016a, Mathworks, Natick, MA, USA) platform.

The preprocessing pipeline included the following steps: (1) removal of the first 10 volumes; (2) slice-timing and head-motion correction; (3) co-registration of functional images to structural space; (4) regression of whole-brain, cerebrospinal fluid, and white matter signals, as well as linear trends and Friston-24 head-motion parameters; (5)

non-linear normalization to Montreal Neurological Institute (MNI) space; (6) smoothing with a 5-mm full-width-at-half-maximum; and (7) temporal filtering within a frequency range of 0.01 to 0.1 Hz.

After preprocessing, nine participants were excluded due to quality control issues of the head motion and spatial normalization, and 206 participants were kept for further analyses.

For the estimation of individual EC, we applied the Schaefer atlas [19] (100 parcels, Fig. 1a) to cover the cortex and extracted the first eigenvariate for each region from the preprocessed functional images using *fslmeants*/FSL. This eigenvariate served as the time series data, which was then utilized in the calculation of EC.

2.5 Effective Connectivity Estimation

As a recently developed variant of DCM, *r*DCM was utilized to estimate individual whole-brain EC efficiently [14]. This method transforms conventional linear DCM into the frequency domain, making it a special case of the Bayesian linear regression model [14]. Using this approach, we specified a full-connection model to estimate EC, where a 100-by-100 matrix was built for each subject (Fig. 1b). Additionally, to examine the prediction performance from separate networks, we down-resampled the whole-brain EC matrix into seven networks including the visual network (Vis), somatosensory network (SMN), dorsal attentional network (DAN), ventral attentional network (VAN), limbic network (Lim), fronto-parietal network (FPN), and DMN. This down-sampling grouped parcels based on the Schaefer atlas [19,20], aligning each of the 100 parcels with one of seven networks. We extracted within-network connectivity for each network by selecting matrix entries where nodes shared the same network label. This approach enabled a targeted comparison of whole-brain and network-specific EC predictions.

2.6 Machine Learning

To explore the relationship between whole-brain and network-specific EC and CM severity, we employed a ridge-regularized linear regression model within a 10-fold cross-validation scheme, where EC was specified as features and the total scores summing from all CTQ subscales were used for targets. The cross-validation process involved splitting samples into training and testing sets. In the training set, EC features were correlated with CTQ total scores, and the top 5% of features were extracted based on the highest positive and negative correlations, respectively. A ridge-regularized linear regression model was then trained on the training set, which was subsequently used to predict scores in the testing set, calculating the correlations between predicted and actual scores. An average prediction correlation was calculated across all cross-validation folds.

To improve the stability of prediction performance, we repeated this prediction process 100 times and obtained an average prediction correlation across all iterations for each prediction case. To assess the statistical performance of the prediction model with the feature selection threshold of 5%, we applied a label-shuffled permutation ($n = 500$ times) test, where CTQ total scores were randomly shuffled before each cross-validation loop. The permutation process serves to evaluate the robustness of our model by generating a null distribution of prediction correlations. By comparing the empirical prediction performance against this null distribution, we can determine the statistical significance of our observed results with a threshold of $p = 0.05$. Given that predictions were conducted for the whole brain and each of the seven networks, we additionally applied a Bonferroni-corrected threshold of $p = 0.0063$ ($0.05/8$) for multiple comparisons to the uncorrected p -values obtained from each permutation test. This provides both uncorrected and corrected interpretations, offering a more comprehensive view of our findings.

Considering that feature selection thresholds may impact prediction performance, we repeated our prediction processes with the feature selection conditions of 10% and 20%, which enabled us to confirm the consistency of prediction performance patterns among whole-brain and network-specific predictions. Additionally, to verify our findings, we employed a least absolute shrinkage and selection operator (LASSO)-regularized linear regression model and compared its results with those of the ridge-regularized model at a 5% feature selection threshold.

3. Results

3.1 Demographic Information and CTQ Scores

Table 1 summarizes the demographic characteristics and CTQ scores for the 206 participants included in the study after imaging preprocessing. The sample comprised 91 males and 115 females, with an average age of 25.3 years. Participants had an average of 14 years of education. The mean CTQ total score was 34.7, with subscale averages as follows: emotional abuse, 6.6; physical abuse, 5.8; sexual abuse, 5.3; emotional neglect, 9.6; and physical neglect, 7.3.

3.2 Prediction Results

In this study, we examined the prediction correlation between CTQ total scores and EC features selected from the whole brain and separated networks using a ridge-regularized linear regression model, where a feature selection threshold of 5% was applied. Then, to improve the robustness and consistency of the above predictions, we also employed 10% and 20% feature selection thresholds to examine whole-brain and network-specific EC predictions. Additionally, a LASSO-regularized model was employed to validate the prediction results.

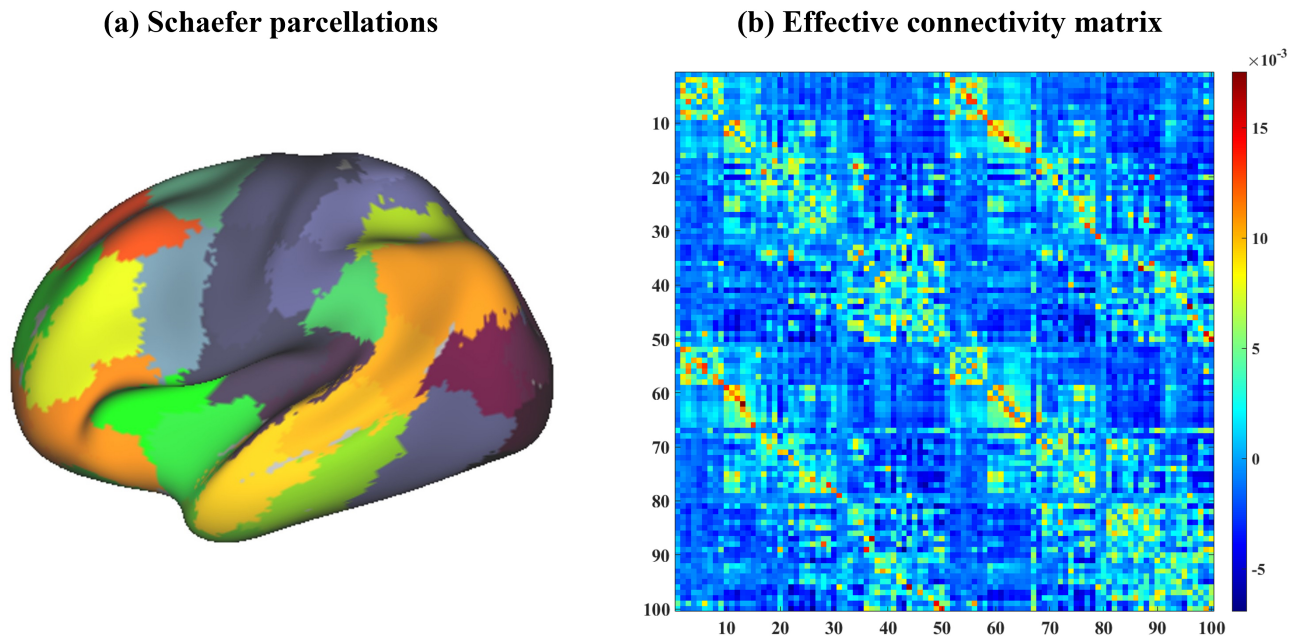


Fig. 1. The Schaefer atlas and effective connectivity (EC) matrix averaged across all participants. (a) shows the utilized Schaefer atlas (100 parcels) used for extracting individual timeseries and the color indicates the different parcellations. (b) illustrates averaged EC across subjects and the color bar indicates the EC magnitude.

Table 1. Demographic information and CTQ scores.

Variable	Subjects (N = 206)
Sex (M/F)	91/115
Age (years)	25.3 ± 6.2 (18~44)
Education (years)	14.0 ± 2.6 (4~22)
Education Level	
0~6 years	1.5%
6~9 years	4.9%
9~12 years	22.3%
>12 years	71.4%
CTQ Total Score	34.7 ± 7.8 (25~61)
Emotional Abuse	6.6 ± 2.1 (5~17)
Physical Abuse	5.8 ± 1.5 (5~13)
Sexual Abuse	5.3 ± 0.8 (5~11)
Emotional Neglect	9.6 ± 4.0 (5~24)
Physical Neglect	7.3 ± 2.5 (5~16)

Note: The percentage of education levels may not sum to 100% due to rounding. Values are presented as means ± standard deviations. Ranges for each variable are indicated in parentheses. Abbreviations: CTQ, Childhood Trauma Questionnaire; M/F, male/female.

When considering a feature selection threshold of 5% (Fig. 2 and Table 2), we found that whole-brain EC features marginally predicted CTQ total scores, with a correlation coefficient of $r = 0.16$. However, when predictions were examined at the network-specific level, only EC features from the DMN successfully predicted CTQ total scores,

yielding a stronger correlation of $r = 0.25$ ($p < 0.05$). In contrast, EC features from other networks, including the Vis, SMN, DAN, VAN, Lim, and FPN, failed to be statistically significant in prediction ($p > 0.05$). Their prediction correlations ranged from 0.1 to 0.15. Notably, EC features from the DMN outperformed those from all other cases in predicting CTQ total scores, exhibiting the highest prediction correlation compared with both the whole-brain and other network-specific predictions. However, when including a multiple-comparison corrected threshold of $p = 0.0063$ (Bonferroni corrected), none of them were statistically significant.

3.3 Feature Selection Thresholds Analysis

To examine the impact of feature selection thresholds on prediction correlations for CTQ total scores, we varied the feature selection thresholds from 5% to 10% and 20% (Table 3). We observed that the significance level of whole-brain EC prediction did not vary across different thresholds, with no significant predictions for CTQ total scores at the 10% or 20% thresholds ($p > 0.05$). In contrast, EC features from the DMN remained statistically significant ($p < 0.05$) even after applying a multiple-comparison correction ($p < 0.0063$) with these thresholds. Importantly, varying the feature selection thresholds did not affect the statistical significance ($p > 0.05$) of EC features in the other networks.

3.4 Validity Analysis

To validate our prediction results obtained from the ridge-regularized linear regression model, we then exam-

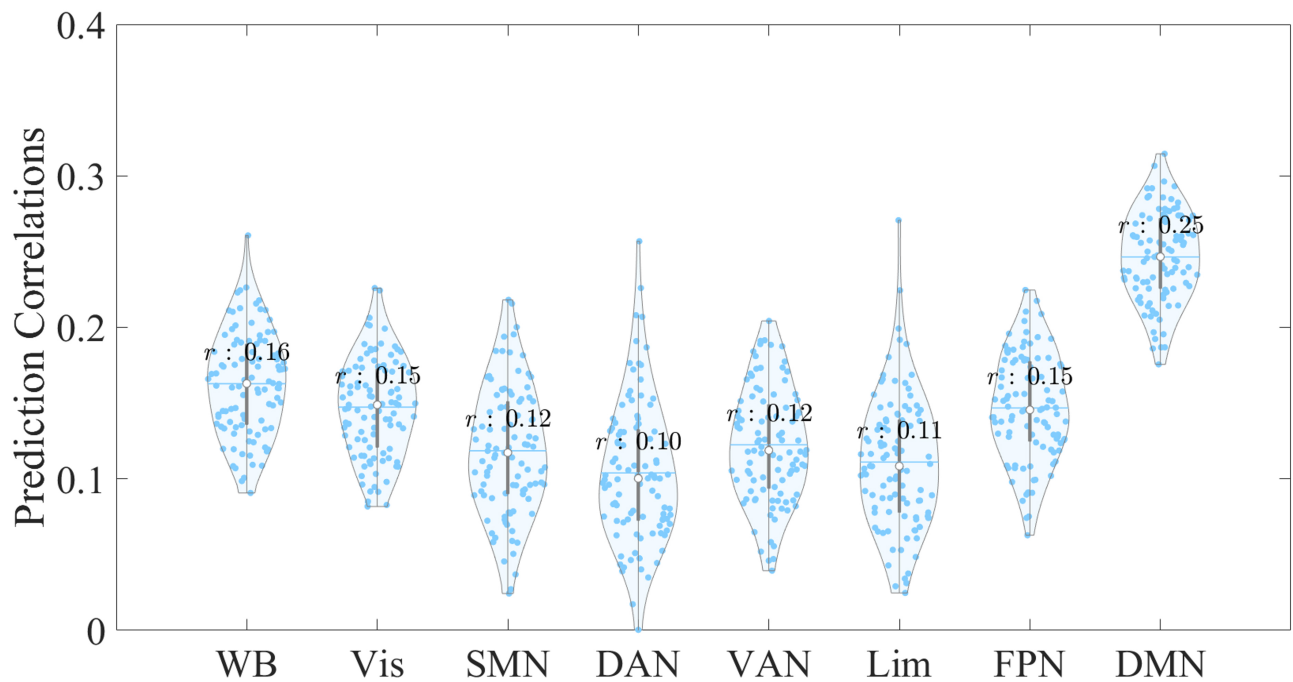


Fig. 2. Violin plot showing the distribution of prediction correlations for whole-brain and network-specific EC features derived from 100 repetitions with a 5% feature selection threshold. The x-axis represents the EC feature sources used to predict the CTQ total scores, while the y-axis indicates the correlation between the empirical and predicted scores. Each dot represents an individual prediction correlation. Abbreviations: WB, whole brain; Vis, visual network; SMN, somatosensory network; DAN, dorsal attentional network; VAN, ventral attentional network; Lim, limbic network; FPN, fronto-parietal network; DMN, default mode network.

Table 2. Correlation coefficients (r) for predicting CTQ total scores using WB and network-specific EC features at a 5% feature selection threshold.

Prediction Correlation	EC feature							
	WB	Vis	SMN	DAN	VAN	Lim	FPN	DMN
r	0.16	0.15	0.12	0.10	0.12	0.11	0.15	0.25
p	0.05	0.33	0.59	0.67	0.58	0.68	0.41	0.02 *

Note: An asterisk (*) indicates statistical significance with a p -value below the threshold for significance ($p < 0.05$) based on permutation testing.

Table 3. Correlation coefficients (r) for predicting CTQ total scores using WB and network-specific EC features at 10% and 20% feature selection thresholds.

Features		WB	Vis	SMN	DAN	VAN	Lim	FPN	DMN
10%	r	0.15	0.16	0.12	0.12	0.11	0.12	0.17	0.24
	p	0.07	0.30	0.56	0.49	0.66	0.67	0.27	0.00 **
20%	r	0.15	0.15	0.12	0.12	0.11	0.12	0.17	0.23
	p	0.08	0.12	0.49	0.56	0.66	0.57	0.21	0.00 **

Note: Double asterisks (**) indicate statistical significance based on the permutation test with a p -value below the Bonferroni-corrected threshold of $p = 0.0063$ for multiple comparisons.

ined the prediction correlations using a LASSO-regularized model (Fig. 3). Our findings were consistent with those of the ridge-regularized model, and EC features within the DMN demonstrated the highest prediction correlation compared with other networks.

4. Discussion

To our knowledge, this study is the first to investigate large-scale network EC for predicting CM severity, employing whole-brain and network-specific EC to predict individual CM severity using a ridge-regularized linear

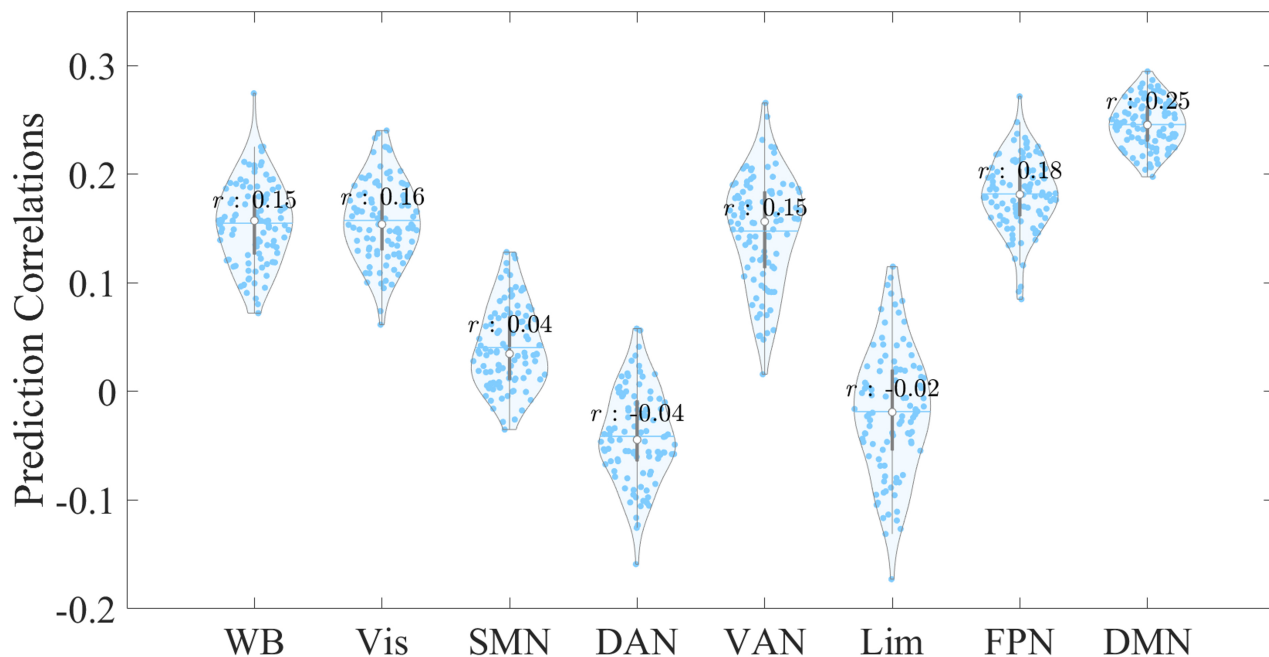


Fig. 3. Violin plot displaying the prediction distributions for whole-brain and network-specific EC features, derived from 100 repetitions at a 5% feature selection threshold using the LASSO-regularized linear regression model. The x-axis represents the EC feature sources used to predict CTQ total scores, while the y-axis shows the correlation between empirical and predicted CTQ total scores. Abbreviations: LASSO, least absolute shrinkage and selection operator.

regression model. Our results suggested that (i) EC features from the DMN show the best prediction performance over other prediction cases and (ii) varying feature selection thresholds may not evidently impact the statistical significance of predictions. Notably, the DMN's predictive validity was further supported by the LASSO-regularized linear regression model. This suggested that the EC features of the DMN may play a crucial role in capturing individual differences in CM severity, which highlighted the potential of DMN connectivity as a more reliable predictor of clinical outcomes compared with connectivity of other large-scale networks.

4.1 Effective Connectivity Prediction

The present study has shown that EC was predictive of individual differences in CM severity. This aligns with previous literature reporting that the EC feature can classify clinical patients from healthy controls well and predict treatment outcomes and behavioral domains [21–23]. This supports the utility of EC as a promising feature in understanding and predicting clinical and behavioral variations.

Our study further demonstrated that EC features within the DMN were superior to those within other networks. The DMN structure primarily includes regions of the medial prefrontal cortex, posterior cingulate cortex, precuneus, and lateral parietal cortex [24]. This network is known to be engaged in internally-focused mental processes such as self-reflection, mind wandering, daydreaming, autobiographical memory retrieval, and future plan-

ning [25–27]. Aberrant activities in the DMN may contribute to multiple dysfunctional psychological processes in self-referential thinking and working memory, and attentional impairments [28,29]. Given that the DMN is crucial in self-referential cognitive functions, it is of great importance in the study of CM [30]. Altered connectivity of the DMN is linked to various psychopathological symptoms in transdiagnostic samples including post-trauma stress disorder (PTSD), major depressive disorder (MDD), and schizophrenia [30–32]. In schizophrenia, the experiences of CM were associated with connectivity variations in the DMN [33]. In MDD, the altered functional coupling within the DMN may contribute to developing depression in individuals with CM [34]. In PTSD, reduced FC within the DMN may lead to self-perception disturbance and link traumatic experiences to the sense of self [35]. Accumulating evidence shows that traumatic exposure adversely impacts DMN connectivity, which in turn leads to psychopathological symptoms associated with maladaptive self-referential processes [30,36]. Additionally, previous reviews have highlighted the DMN as a network of particular interest in non-clinical individuals exposed to CM [7,36,37]. Numerous studies [38–42] have documented altered connectivity within the DMN, as well as between the DMN and other networks, in individuals with CM compared with those without. For instance, Lu *et al.* [38] observed abnormal FC within the DMN and in its connections with the cerebellum and insula in individuals with CM, while Zhao *et al.* [39] reported increased

connectivity within the anterior DMN and reduced connectivity between the posterior DMN and other networks in non-clinical adults with CM. Moreover, DMN connectivity has demonstrated strong predictive contributions for CTQ scores in non-clinical individuals [43], underscoring the DMN's role as a potential biomarker of trauma. Collectively, these findings, together with existing literature on early-life stress [36,44,45], suggested that alterations in DMN connectivity may serve as important neural correlates of early-life adversity. Although research regarding EC and CM is sparse, several studies utilized prior-defined regions of interest to explore EC between the amygdala and medial prefrontal cortex, reporting that traumatic exposures impact the inhibition of the amygdala by the medial prefrontal cortex [13,46]. This may potentially reflect dysfunction in the DMN, contributing to maladaptive emotional responses impacted by traumatic exposures [46]. Consistent with these studies, our findings demonstrated that EC features within the DMN better predicted CM scores than those from other networks, suggesting that the DMN may play a crucial role in influencing CM effects on self-referential and emotional regulation.

4.2 Feature Selection Thresholds and Predictive Models

This study further evaluated the stability of our prediction findings by varying the feature selection thresholds. Although the p -values for the statistical significance of EC prediction were impacted by different feature selection thresholds, the significance of most prediction cases was little influenced. This aligns with previous literature [47,48] suggesting that varying feature selection thresholds (e.g., stricter p values) in selecting correlation-based features may not significantly impact prediction. While those studies primarily used p -values rather than a fixed percentage of connectivity features, our validation analysis across different thresholds demonstrated relatively consistent and robust prediction results, particularly for DMN EC features, where the predictions remained stable across different thresholds. Furthermore, the prediction results obtained from the ridge-regularized model were comparable to those from the LASSO model, showing similar stability of EC features within the DMN.

5. Limitations

Several limitations should be addressed in future studies. First, a key limitation of our study is the relatively low CTQ total and subscale scores reported in Table 1, with a limited number of participants reporting experiences of sexual, physical, or emotional abuse. This distribution suggests that our findings may be more strongly influenced by neglect-related experiences. This outcome may be partly related to the characteristics of our sample, as higher educational levels among participants could potentially impact reporting patterns, with fewer cases of abuse reported relative to neglect. Additionally, the narrow range of sub-

scale scores reduced their predictive power, leading us to focus on the CTQ total score. Future studies including more diverse samples could help examine the distinct impacts of different types of CM. Second, this study assessed the CM severity in healthy participants without measuring psychopathological traits or symptoms such as anxiety or depression. The following studies may incorporate these assessments to better understand their potential influence on CM severity in healthy participants. Third, while our study highlighted the strong predictive correlation of DMN-based EC features in capturing individual differences in CM severity, the choice of performance metrics may influence model comparisons. Future studies should explore more metrics to better understand the relative predictive roles of different networks. Ultimately, the Schaefer atlas may impact network definitions, as it assigns different numbers of parcels to various networks. This variation could influence the predictive power of networks, potentially affecting our findings related to CM severity. Future studies could benefit from exploring alternative atlases or parcellation schemes, which may lead to a more comprehensive assessment of how different networks relate to CM and other forms of childhood adversity.

6. Conclusions

In conclusion, our study suggests that EC can effectively capture individual differences in CM severity, particularly within the DMN, which demonstrated the highest prediction correlations. These findings highlight the DMN's significant potential as a neuroimaging biomarker for the underlying mechanisms of CM.

Availability of Data and Materials

The code and data can be made available upon reasonable request.

Author Contributions

Concept—SZ, HW. Design—SZ, HW. Supervision—HW. Funding—HW. Materials—WZ, ZL, HW. Data Collection and/or Processing—SZ, WZ, ZL, HW. Analysis and/or Interpretation, Literature Search, Writing—SZ. Critical Review—SZ, WZ, ZL, HW. All authors read and approved the final manuscript. All authors have participated sufficiently in the work and agreed to be accountable for all aspects of the work.

Ethics Approval and Consent to Participate

The study protocol received approval from the Institute Research Board of the Affiliated Brain Hospital, Guangzhou Medical University (approval number: 2013 (074), date: 15th, July, 2013). The study was conducted in accordance with the Declaration of Helsinki. The written informed consent was obtained prior before participants who agreed to be involved in the study.

Acknowledgment

Not applicable.

Funding

This work was supported in part by funding from the Natural Science Foundation of Guangdong Province, China (Grant number: 2024A1515011594), Plan on enhancing scientific research in GMU (Grant number: 2024SRP207), and Guangzhou Research-oriented Hospital.

Conflict of Interest

The authors declare no conflict of interest. Wei Zheng is serving as one of Editors in Chief. We declare that Wei Zheng had no involvement in the peer review of this article and has no access to information regarding its peer review. Full responsibility for the editorial process for this article was delegated to Mohammad Ahmadpanah.

References

- [1] Gilbert R, Widom CS, Browne K, Fergusson D, Webb E, Jan-son S. Burden and consequences of child maltreatment in high-income countries. *Lancet*. 2009; 373: 68–81. [https://doi.org/10.1016/S0140-6736\(08\)61706-7](https://doi.org/10.1016/S0140-6736(08)61706-7).
- [2] Green JG, McLaughlin KA, Berglund PA, Gruber MJ, Sampson NA, Zaslavsky AM, *et al.* Childhood adversities and adult psychiatric disorders in the national comorbidity survey replication I: associations with first onset of DSM-IV disorders. *Archives of General Psychiatry*. 2010; 67: 113–123. <https://doi.org/10.1001/archgenpsychiatry.2009.186>.
- [3] Fuller-Thomson E, Baird SL, Dhrodia R, Brennenstuhl S. The association between adverse childhood experiences (ACEs) and suicide attempts in a population-based study. *Child: Care, Health and Development*. 2016; 42: 725–734. <https://doi.org/10.1111/cch.12351>.
- [4] Leza L, Siria S, López-Goñi JJ, Fernández-Montalvo J. Adverse childhood experiences (ACEs) and substance use disorder (SUD): A scoping review. *Drug and Alcohol Dependence*. 2021; 221: 108563. <https://doi.org/10.1016/j.drugalcdep.2021.108563>.
- [5] Merrick MT, Ports KA, Ford DC, Afifi TO, Gershoff ET, Grogan-Kaylor A. Unpacking the impact of adverse childhood experiences on adult mental health. *Child Abuse & Neglect*. 2017; 69: 10–19. <https://doi.org/10.1016/j.chiabu.2017.03.016>.
- [6] Biswal BB, Mennes M, Zuo XN, Gohel S, Kelly C, Smith SM, *et al.* Toward discovery science of human brain function. *Proceedings of the National Academy of Sciences of the United States of America*. 2010; 107: 4734–4739. <https://doi.org/10.1073/pnas.0911855107>.
- [7] Gerin MI, Viding E, Herringa RJ, Russell JD, McCrory EJ. A systematic review of childhood maltreatment and resting state functional connectivity. *Developmental Cognitive Neuroscience*. 2023; 64: 101322. <https://doi.org/10.1016/j.dcn.2023.101322>.
- [8] Goetschius LG, Hein TC, McLanahan SS, Brooks-Gunn J, McLoyd VC, Dotterer HL, *et al.* Association of Childhood Violence Exposure With Adolescent Neural Network Density. *JAMA Network Open*. 2020; 3: e2017850. <https://doi.org/10.1001/jamanetworkopen.2020.17850>.
- [9] Marusak HA, Etkin A, Thomason ME. Disrupted insula-based neural circuit organization and conflict interference in trauma-exposed youth. *NeuroImage. Clinical*. 2015; 8: 516–525. <https://doi.org/10.1016/j.nicl.2015.04.007>.
- [10] Friston KJ. Functional and effective connectivity: a review. *Brain Connectivity*. 2011; 1: 13–36. <https://doi.org/10.1089/brain.2011.0008>.
- [11] Friston KJ, Harrison L, Penny W. Dynamic causal modelling. *NeuroImage*. 2003; 19: 1273–1302. [https://doi.org/10.1016/S1053-8119\(03\)00202-7](https://doi.org/10.1016/S1053-8119(03)00202-7).
- [12] Geng X, Xu J, Liu B, Shi Y. Multivariate classification of major depressive disorder using effective connectivity and functional connectivity. *Frontiers in Neuroscience*. 2018; 12: 38. <https://doi.org/10.3389/fnins.2018.00038>.
- [13] Kessler R, Schmitt S, Sauder T, Stein F, Yüksel D, Grotegder D, *et al.* Long-Term Neuroanatomical Consequences of Childhood Maltreatment: Reduced Amygdala Inhibition by Medial Prefrontal Cortex. *Frontiers in Systems Neuroscience*. 2020; 14: 28. <https://doi.org/10.3389/fnsys.2020.00028>.
- [14] Frässle S, Lomakina EI, Razi A, Friston KJ, Buhmann JM, Stephan KE. Regression DCM for fMRI. *NeuroImage*. 2017; 155: 406–421. <https://doi.org/10.1016/j.neuroimage.2017.02.090>.
- [15] Frässle S, Manjaly ZM, Do CT, Kasper L, Pruessmann KP, Stephan KE. Whole-brain estimates of directed connectivity for human connectomics. *NeuroImage*. 2021; 225: 117491. <https://doi.org/10.1016/j.neuroimage.2020.117491>.
- [16] Teicher MH, Samson JA. Annual Research Review: Enduring neurobiological effects of childhood abuse and neglect. *Journal of Child Psychology and Psychiatry, and Allied Disciplines*. 2016; 57: 241–266. <https://doi.org/10.1111/jcpp.12507>.
- [17] He J, Zhong X, Gao Y, Xiong G, Yao S. Psychometric properties of the Chinese version of the Childhood Trauma Questionnaire-Short Form (CTQ-SF) among undergraduates and depressive patients. *Child Abuse & Neglect*. 2019; 91: 102–108. <https://doi.org/10.1016/j.chiabu.2019.03.009>.
- [18] Bernstein DP, Stein JA, Newcomb MD, Walker E, Pogge D, Ahluwalia T, *et al.* Development and validation of a brief screening version of the Childhood Trauma Questionnaire. *Child Abuse & Neglect*. 2003; 27: 169–190. [https://doi.org/10.1016/S0145-2134\(02\)00541-0](https://doi.org/10.1016/S0145-2134(02)00541-0).
- [19] Schaefer A, Kong R, Gordon EM, Laumann TO, Zuo XN, Holmes AJ, *et al.* Local-Global Parcellation of the Human Cerebral Cortex from Intrinsic Functional Connectivity MRI. *Cerebral Cortex*. 2018; 28: 3095–3114. <https://doi.org/10.1093/cercor/bhx179>.
- [20] Yeo BTT, Krienen FM, Sepulcre J, Sabuncu MR, Lashkari D, Hollinshead M, *et al.* The organization of the human cerebral cortex estimated by intrinsic functional connectivity. *Journal of Neurophysiology*. 2011; 106: 1125–1165. <https://doi.org/10.1152/jn.00338.2011>.
- [21] Bedford P, Hauke DJ, Wang Z, Roth V, Nagy-Huber M, Holze F, *et al.* The effect of lysergic acid diethylamide (LSD) on whole-brain functional and effective connectivity. *Neuropsychopharmacology*. 2023; 48: 1175–1183. <https://doi.org/10.1038/s41386-023-01574-8>.
- [22] Galiouline H, Frässle S, Harrison SJ, Pereira I, Heinzle J, Stephan KE. Predicting future depressive episodes from resting-state fMRI with generative embedding. *NeuroImage*. 2023; 273: 119986. <https://doi.org/10.1016/j.neuroimage.2023.119986>.
- [23] Pallarés V, Insabato A, Sanjuán A, Kühn S, Mantini D, Deco G, *et al.* Extracting orthogonal subject- and condition-specific signatures from fMRI data using whole-brain effective connectivity. *NeuroImage*. 2018; 178: 238–254. <https://doi.org/10.1016/j.neuroimage.2018.04.070>.
- [24] Raichle ME. The brain's default mode network. *Annual Review of Neuroscience*. 2015; 38: 433–447. <https://doi.org/10.1146/annurev-neuro-071013-014030>.
- [25] Raichle ME, MacLeod AM, Snyder AZ, Powers WJ, Gusnard DA, Shulman GL. A default mode of brain function. *Proceed-*

- ings of the National Academy of Sciences of the United States of America. 2001; 98: 676–682. <https://doi.org/10.1073/pnas.98.2.676>.
- [26] Menon V. 20 years of the default mode network: A review and synthesis. *Neuron*. 2023; 111: 2469–2487. <https://doi.org/10.1016/j.neuron.2023.04.023>.
- [27] Buckner RL, Andrews-Hanna JR, Schacter DL. The brain's default network: anatomy, function, and relevance to disease. *Annals of the New York Academy of Sciences*. 2008; 1124: 1–38. <https://doi.org/10.1196/annals.1440.011>.
- [28] Broyd SJ, Demanuele C, Debener S, Helps SK, James CJ, Sonuga-Barke EJS. Default-mode brain dysfunction in mental disorders: a systematic review. *Neuroscience and Biobehavioral Reviews*. 2009; 33: 279–296. <https://doi.org/10.1016/j.neubiorev.2008.09.002>.
- [29] Whitfield-Gabrieli S, Ford JM. Default mode network activity and connectivity in psychopathology. *Annual Review of Clinical Psychology*. 2012; 8: 49–76. <https://doi.org/10.1146/annurev-clinpsy-032511-143049>.
- [30] Valencia N, Seeger FR, Seitz KI, Carius L, Nkrumah RO, Schmitz M, *et al.* Childhood maltreatment and transdiagnostic connectivity of the default-mode network: The importance of duration of exposure. *Journal of Psychiatric Research*. 2024; 177: 239–248. <https://doi.org/10.1016/j.jpsychires.2024.07.022>.
- [31] Doucet GE, Janiri D, Howard R, O'Brien M, Andrews-Hanna JR, Frangou S. Transdiagnostic and disease-specific abnormalities in the default-mode network hubs in psychiatric disorders: A meta-analysis of resting-state functional imaging studies. *European Psychiatry*. 2020; 63: e57. <https://doi.org/10.1192/j.eurpsy.2020.57>.
- [32] Sha Z, Wager TD, Mechelli A, He Y. Common Dysfunction of Large-Scale Neurocognitive Networks Across Psychiatric Disorders. *Biological Psychiatry*. 2019; 85: 379–388. <https://doi.org/10.1016/j.biopsych.2018.11.011>.
- [33] Dauvermann MR, Mothersill D, Rokita KI, King S, Holleran L, Kane R, *et al.* Changes in Default-Mode Network Associated With Childhood Trauma in Schizophrenia. *Schizophrenia Bulletin*. 2021; 47: 1482–1494. <https://doi.org/10.1093/schbul/sba025>.
- [34] Wang X, Liu Q, Fan J, Gao F, Xia J, Liu X, *et al.* Decreased functional coupling within default mode network in major depressive disorder with childhood trauma. *Journal of Psychiatric Research*. 2022; 154: 61–70. <https://doi.org/10.1016/j.jpsychires.2022.07.051>.
- [35] Lanius RA, Terpou BA, McKinnon MC. The sense of self in the aftermath of trauma: lessons from the default mode network in posttraumatic stress disorder. *European Journal of Psychotraumatology*. 2020; 11: 1807703. <https://doi.org/10.1080/20008198.2020.1807703>.
- [36] Holz NE, Berhe O, Sacu S, Schwarz E, Tesarz J, Heim CM, *et al.* Early Social Adversity, Altered Brain Functional Connectivity, and Mental Health. *Biological Psychiatry*. 2023; 93: 430–441. <https://doi.org/10.1016/j.biopsych.2022.10.019>.
- [37] Cosío-Guirado R, Tapia-Medina MG, Kaya C, Peró-Cebollero M, Villuendas-González ER, Guàrdia-Olmos J. A comprehensive systematic review of fMRI studies on brain connectivity in healthy children and adolescents: Current insights and future directions. *Developmental Cognitive Neuroscience*. 2024; 69: 101438. <https://doi.org/10.1016/j.dcn.2024.101438>.
- [38] Lu S, Gao W, Wei Z, Wang D, Hu S, Huang M, *et al.* Intrinsic brain abnormalities in young healthy adults with childhood trauma: A resting-state functional magnetic resonance imaging study of regional homogeneity and functional connectivity. *The Australian and New Zealand Journal of Psychiatry*. 2017; 51: 614–623. <https://doi.org/10.1177/0004867416671415>.
- [39] Zhao H, Dong D, Sun X, Cheng C, Xiong G, Wang X, *et al.* Intrinsic brain network alterations in non-clinical adults with a history of childhood trauma. *European Journal of Psychotraumatology*. 2021; 12: 1975951. <https://doi.org/10.1080/20008198.2021.1975951>.
- [40] Tian T, Li J, Zhang G, Wang J, Liu D, Wan C, *et al.* Default Mode Network Alterations Induced by Childhood Trauma Correlate With Emotional Function and SLC6A4 Expression. *Frontiers in Psychiatry*. 2022; 12: 760411. <https://doi.org/10.3389/fpsy.2021.760411>.
- [41] Ireton R, Hughes A, Klabunde M. A Functional Magnetic Resonance Imaging Meta-Analysis of Childhood Trauma. *Biological Psychiatry. Cognitive Neuroscience and Neuroimaging*. 2024; 9: 561–570. <https://doi.org/10.1016/j.bpsc.2024.01.009>.
- [42] Cisler JM. Childhood Trauma and Functional Connectivity between Amygdala and Medial Prefrontal Cortex: A Dynamic Functional Connectivity and Large-Scale Network Perspective. *Frontiers in Systems Neuroscience*. 2017; 11: 29. <https://doi.org/10.3389/fnsys.2017.00029>.
- [43] Zhang J, Zhao T, Zhang J, Zhang Z, Li H, Cheng B, *et al.* Prediction of childhood maltreatment and subtypes with personalized functional connectome of large-scale brain networks. *Human Brain Mapping*. 2022; 43: 4710–4721. <https://doi.org/10.1002/hbm.25985>.
- [44] Rebello K, Moura LM, Pinaya WHL, Rohde LA, Sato JR. Default Mode Network Maturation and Environmental Adversities During Childhood. *Chronic Stress*. 2018; 2: 2470547018808295. <https://doi.org/10.1177/2470547018808295>.
- [45] Philip NS, Sweet LH, Tyrka AR, Price LH, Bloom RF, Carpenter LL. Decreased default network connectivity is associated with early life stress in medication-free healthy adults. *European Neuropsychopharmacology*. 2013; 23: 24–32. <https://doi.org/10.1016/j.euroneuro.2012.10.008>.
- [46] Chen F, Ke J, Qi R, Xu Q, Zhong Y, Liu T, *et al.* Increased Inhibition of the Amygdala by the mPFC may Reflect a Resilience Factor in Post-traumatic Stress Disorder: A Resting-State fMRI Granger Causality Analysis. *Frontiers in Psychiatry*. 2018; 9: 516. <https://doi.org/10.3389/fpsy.2018.00516>.
- [47] Cai H, Zhu J, Yu Y. Robust prediction of individual personality from brain functional connectome. *Social Cognitive and Affective Neuroscience*. 2020; 15: 359–369. <https://doi.org/10.1093/scan/nsaa044>.
- [48] Zhu J, Li Y, Fang Q, Shen Y, Qian Y, Cai H, *et al.* Dynamic functional connectome predicts individual working memory performance across diagnostic categories. *NeuroImage. Clinical*. 2021; 30: 102593. <https://doi.org/10.1016/j.nicl.2021.102593>.

5. Discussion

The overarching objective of this thesis is to systematically investigate and characterize the EC in task-evoked and resting-state networks and its relationship with aging and behavior. By employing well-established and sophisticated methodological approaches in task-evoked and resting-state EC estimations and machine-learning approaches, this research advances the model-based analysis of brain connectivity by quantifying the impact of data analytical variability and demonstrating its applications across behaviors and clinical domains. Three interconnected studies advance this object by addressing critical gaps and integrating methodological, behavioral, and clinical perspectives. The first study introduces a novel workflow to investigate how data-processing parameters influence task-evoked EC estimates within the SRC network, quantifying their impact on EC strength and certainty, a critical methodological gap in prior research. Based on these methodological insights, the second study contrasts brain intrinsic and task-modulated EC to predict individual age and RT during the SRC task, demonstrating that distinct state-specific connectivity captures different aspects of individual variability. The third study expands the scope to resting-state networks, systematically comparing predictive utilities of resting-state EC features across large-scale networks for childhood trauma. It novelly identifies the DMN as a critical correlate of long-term effects of early-life adversity, highlighting its importance over other networks. Together, these findings not only bridge methodological rigor, behavioral relevance, and clinical insights but also offer new tools and frameworks to link brain connectivity to behaviors across states and populations. The thesis provides a comprehensive perspective on how EC correlates with individual variability in behaviors and clinical outcomes, potentially influencing the direction of future research.

5.1 Data Processing Effects on Task-Evoked EC

Study 1 systematically evaluated how data processing parameters, such as GLM designs, GSR, activation contrasts, and significance thresholding, influence task-evoked EC within the SRC network. Unlike prior studies focusing on isolated parameters (Almgren et al., 2020; Daunizeau et al., 2011), the study introduces a novel workflow to quantify how data processing parameters impact parameter strength and certainty of task-evoked EC estimates across a broader range of parameters. It reveals a unique

trade-off between sensitivity and stability in parameter selection, offering new insights into the methodological variability in EC research.

The results mainly revealed that the GLM designs and activation contrasts impacted the EC strength and parameter certainty, while the GSR and significance thresholding had a minor impact. In detail, event-related GLM designs demonstrate stronger EC connections between the driving input (bilateral IPS nodes) and “internal” nodes within the SRC network compared to block-based designs. It suggests that event-related designs are more sensitive to task-induced modulations, aligning with prior task-evoked fMRI studies (Bühler et al., 2008; Tie et al., 2009), where event-related designs achieved stronger activation and more precise functional localization of putative regions. The difference in sensitivity may relate to variations in the hemodynamic response shapes of GLM designs, where event-related designs better explain the BOLD signal variance, with the modeled hemodynamic responses peaking earlier and returning to baseline more slowly (Mechelli, Henson, et al., 2003; Mechelli, Price, et al., 2003). Conversely, block-based GLM designs exhibit greater certainty in EC parameters. The difference in parameter certainty relates to noise levels (Zeidman, Kazan, et al., 2019), suggesting greater stability in EC estimates modeled by block-based designs.

The selection of activation contrasts strongly influenced EC patterns and parameter certainty. Since task-modulated EC of DCM is context-dependent, the contrast selection reflects the network dynamics related to a specific cognitive process (Kuhnke et al., 2021). Here, this study compared two different contrasts (Anti and Anti+Pro) to assess their impact on EC estimates. The SRC task includes two opposite conditions: Pro (compatible) and Anti (incompatible). The Pro contrast requires participants to respond ipsilaterally, while the Anti demands participants to respond contralaterally, involving a more indirect response selection process that inhibits the automatic response, redirecting attention to the opposite side and initiating a voluntary response (Cieslik et al., 2010). The Anti contrast isolates task-induced modulation in response to incompatible stimuli, while the Anti+Pro contrast combines task-induced modulations in response to both incompatible and compatible events. The former contrast was assumed to be more specific in incompatibility-driven processes (e.g., resolving response conflicts), while the latter aggregates activities across different stimulus types and reflects a general task engagement. The different EC patterns between them may reflect their distinct cognitive

processes and task demands. Additionally, the Anti contrast showed higher data certainty than the Anti+Pro contrast, potentially due to the difference in signal variability. Including the Pro contrast into the Anti+Pro contrast may introduce higher variability by combining low-demand cognitive processes, and thereby lower data certainty in EC estimates.

In summary, data processing parameters, particularly the GLM designs and activation contrasts, strongly influence the parameter strength and certainty of the task-evoked EC estimates. The research underscores the trade-off between sensitivity and stability in parameter selection, highlighting the necessity of evaluating data processing and modeling choices to ensure a robust, reproducible, and biologically meaningful understanding of cognitive processes.

5.2 Behavioral Prediction: Brain State-Specific EC

Having specified how data processing parameters influence task-evoked EC estimates, the thesis explored the behavioral relevance of brain states (intrinsic vs. task-evoked states), specifically investigating how brain intrinsic and task-modulated EC predict individual age and RT. A cross-validated prediction workflow was developed that avoids potential data leakage problems (Rosenblatt et al., 2024). The workflow addresses a critical limitation in prior DCM research (Zeidman, Jafarian, Seghier, et al., 2019), which often extracts features from the entire cohort before cross-validation.

With this workflow, this study revealed that EC from different brain states captures distinct aspects of individual phenotypical and behavioral characteristics. This effect was significantly impacted by GLM design types, aligning with the findings of Study 1. The results demonstrated that task-modulated EC can successfully predict individual RT during the SRC task, whereas the intrinsic EC failed to predict RT. These findings extend the previous literature, which suggests that task-evoked connectivity better captures task-related behavioral variability than resting-state connectivity (Gbadegyan et al., 2022; W. Zhao et al., 2023) by highlighting that this advantage largely depends on GLM designs, a factor not systematically examined in prior work. This improvement may relate to task manipulations that amplify behaviorally relevant functional correlations (Greene et al., 2018). Unlike brain intrinsic connectivity, task-evoked connectivity—with its enhanced specificity, experimental constraints, and lower variability—may more reliably capture individual behavioral differences (Buckner et

al., 2013; Elton & Gao, 2015; Finn et al., 2017; Geerligs et al., 2015).

Additionally, the results revealed that both components of task-evoked EC could successfully predict age, while intrinsic EC showed higher prediction accuracy. These findings align with previous literature, which suggests that both intrinsic and task-modulated EC can predict age (Beck et al., 2021; Diersch et al., 2021; Tsvetanov et al., 2016). The study further identifies divergent EC feature patterns contributing to age prediction between intrinsic and task-modulated EC, indicating that these two states may capture unique aspects of age-related differences in connectivity. Moreover, this finding is consistent with a recent study (Xiong et al., 2023), which reported superior prediction results in resting-state fMRI datasets compared to task-evoked datasets. This improvement may reflect distinct BOLD variability profiles, where the resting-state BOLD variability is more sensitive to age-related factors such as vascular or white matter changes (Millar et al., 2020; Tsvetanov et al., 2016). Notably, the study introduces a novel comparison by examining predictions between intrinsic and task-modulated connectivity in the same dataset, which potentially eliminates confounds from session-specific noise and allows for a rigorous comparison of state-specific effects on prediction.

Interestingly, the study reveals a novel insight in prediction: when considering different GLM designs, both intrinsic and task-modulated EC from block-based designs failed to predict individual age and RT. As discussed in Study 1, the enhanced sensitivity to task modulations may explain the prediction difference between GLM designs, which may be associated with their distinct hemodynamic response shapes (Mechelli, Henson, et al., 2003; Mechelli, Price, et al., 2003). This finding recommends a preference for event-related GLM designs in studies aimed at linking task-evoked connectivity features to behaviors.

In summary, this study advances our understanding of brain state-specific connectivity associated with different types of prediction targets. The results demonstrate that the connectivity modalities of distinct brain states capture distinct aspects of individual variability (e.g., age and RT), and their predictive utilities vary with methodological choices, specifically the GLM designs. This assessment for predicting behaviors from brain EC supports the use of state-specific connectivity frameworks to reliably link brain connectivity to behaviors in future research.

5.3 Default Mode Network as a Trauma Biomarker in Resting-State EC

Building upon the methodological insights from Studies 1 and 2, Study 3 expands the EC research to the resting-state paradigm, focusing on whole-brain and network-specific resting-state EC to predict clinical outcomes, such as CM severity. Unlike the traditional DCM approach used in Studies 1 and 2, which is ideal for task-evoked EC within a network with a limited number of nodes, the computational efficiency of rDCM (Frässle, Manjaly, et al., 2021) makes it particularly suitable for the large-scale resting-state fMRI analysis. Therefore, this study innovatively utilizes rDCM to estimate resting-state EC in large-scale networks and identifies the most robust network biomarker for CM severity across all networks. Despite this methodological difference, both approaches share the core aim of quantifying directed neural influences.

The results revealed that whole-brain EC marginally predicts Childhood Trauma Questionnaire (CTQ) scores, while the EC features of the DMN consistently and robustly predicted CTQ scores, outperforming other networks. These findings are consistent with previous studies (Galiouline et al., 2023; Geng et al., 2018), suggesting that resting-state EC could be a promising measure in predicting individual clinical characteristics.

Furthermore, this study highlights the important role of DMN in shaping CM's effect. The DMN is believed to be involved in internal mental processes, such as mind-wandering, daydreaming, and self-reflection (Menon, 2023; Raichle et al., 2001). Its abnormalities are implicated in aberrant psychological processes such as self-referential thinking and impairments in working memory and attention (Broyd et al., 2009; Whitfield-Gabrieli & Ford, 2012). Due to its crucial role in self-referential mental activities, the DMN's importance was well acknowledged in CM's studies (Valencia et al., 2024). Aberrant DMN connectivity has been linked to multiple psychopathological symptoms in transdiagnostic clinical populations, such as major depressive disorder, post-traumatic stress disorder, and schizophrenia (Doucet et al., 2020; Sha et al., 2019; Valencia et al., 2024). These findings indicate that traumatic experiences impacted DMN's connectivity adversely, which may lead to maladaptive self-referential psychopathological symptoms (Holz et al., 2023; Valencia et al., 2024). Moreover, in line with previous literature on non-clinical participants, abnormal DMN connectivity has been particularly highlighted in individuals with CM exposure (Lu et al., 2016;

Zhao et al., 2021). Moreover, DMN's connectivity features have demonstrated a critical contribution in predicting individual CM severity, emphasizing the DMN as a neuroimaging biomarker for traumatic experiences (Zhang et al., 2022). Collectively, the changes in the DMN connectivity may be an important neural correlate of early-life stress.

The results underscored the pivotal role of the DMN in predicting clinical measures like CM severity, highlighting its potential as a key neuroimaging biomarker for traumatic experiences. This study reinforced the idea that alterations in DMN's connectivity, particularly in individuals with early-life adversity, could serve as a crucial neural correlate of childhood trauma. By comparing predictions across large-scale networks, the thesis offers a comprehensive, whole-brain perspective on EC and its clinical relevance.

5.4 Limitations and Future Directions

While the thesis advances the methodology and prediction applications of EC in linking brain network dynamics to behaviors, a few limitations highlight future implications for refining EC's theoretical and clinical utilities.

The first limitation involves paradigm specificity. The thesis estimated task-evoked EC from an SRC network, which is strongly tied to the incompatibility effect during conflict processing. This specificity may limit the generalizability of both methodological findings and behavioral predictions. Future studies could extend the framework to diverse task paradigms, such as emotion regulation or decision-making processes, to determine whether the methodological choices recommended by the thesis improve EC inference across different task-evoked networks and whether EC demonstrates predictive utilities for other cognitive processes or clinical traits.

Second, sample constraints limit the findings on predicting childhood trauma. The thesis analyzed resting-state EC in a healthy cohort with limited variability in childhood trauma exposure. The relatively low CTQ total scores and narrow ranges may attenuate the association between EC and trauma exposure. Furthermore, the absence of clinically diagnosed trauma-related psychiatric disorders (e.g., depression) limits the generalizability of DMN's EC as a neuroimaging biomarker to clinical populations. Future work may benefit from validating this neuroimaging biomarker in samples with a broader range of childhood trauma severity by

including individuals with significant trauma exposure or trauma-related disorders (e.g., high scores in CTQ total and subscales or depression diagnosis). Additionally, a comparison between sub-clinical and clinical populations helps clarify whether dysfunctional DMN connectivity serves as the neuroimaging biomarker for trauma-related disorders. Integrating resting-state EC with trauma-related symptoms such as depressive rumination or anhedonia may further improve its predictive utility for relapse risks and treatment responses.

Third, methodological limitations arise from the reliance on linear predictive models. The thesis relied on linear models (e.g., Lasso and ridge regression) to predict individual differences in task performance, age, and clinical outcomes, which provided interpretable associations between EC and behaviors. However, these linear predictive algorithms may overlook the complex and non-linear relationships between EC parameters and behaviors or clinical outcomes. Future work may adopt non-linear predictive models (e.g., support vector regression or neural network models) to better capture the complex and non-linear relationship between the brain and behaviors.

Fourth, a lack of explicit psychological interpretation related to the SRC task presents an interpretative challenge. The cognitive processes underlying the SRC task were not explicitly investigated, limiting the interpretation. Future studies may consider exploring cognitive processes such as bottom-up, top-down, conflict detection, and response selection processes and describe how specific processes shape task-evoked EC parameters, which may help bridge the gap between network dynamics and psychology.

Finally, the fifth point concerns cross-state comparisons. The thesis has inferred EC from both task-evoked and resting-state fMRI paradigms, which were obtained from separate cohorts with distinct prediction targets. It precludes a direct evaluation for comparisons of predictive power between two paradigms. Although the thesis has compared the predictive utilities between the brain's intrinsic and task-modulated EC and suggests brain state-specific contributions to behaviors, a within-subject comparison between task-evoked and resting-state EC may further validate the modality-specific predictive utilities between them.

5.5 Conclusion

The thesis aimed to investigate the EC of task-evoked and resting-state networks and their relationship to aging and behavior. It addressed three critical gaps: (1) the impact of methodological variability on EC estimates, (2) the underexplored predictive utility of brain state-specific EC (intrinsic vs. task-modulated) for individual differences in behavior and aging, and (3) the clinical potential of resting-state EC for identifying trauma-related biomarkers.

A key insight is that methodological variability, such as event-related versus block-based GLM designs, strongly influences EC estimates and their interpretation. This finding directly addresses the concern regarding the methodological variability in EC estimations, demonstrating that the present work provides an empirical framework for understanding this variability rather than a simple recommendation. For example, event-related designs enhance sensitivity to task-evoked neural dynamics, whereas block-based designs improve parameter stability. A fundamental trade-off is revealed: sensitivity versus stability. Critically, the trade-off also extends to behavioral predictions: event-related designs better capture individual variability in task-relevant behaviors and aging compared to block-based designs. These findings emphasize that methodological choices should align with research goals rather than seeking a universal "optimal" pipeline.

Building on these methodological insights, a cross-validation machine learning framework demonstrates differential predictive roles of brain state-specific EC. By dissecting the unique contributions of brain intrinsic and task-modulated connectivity, this thesis offers a synthesized perspective on how different brain states contribute to behaviors. Task-modulated EC shows greater relevance to behavioral measures, such as RT, reflecting its sensitivity to context-dependent neural dynamics. In contrast, intrinsic EC better predicts age-related differences, reflecting stable, inherent connectivity patterns that are fundamental to the brain's functional architecture. This divergence indicates that distinct EC components capture unique attributes of behavior and brain organization, underscoring the importance of considering state-specific frameworks when investigating the relationship between brain connectivity and behaviors.

The thesis further extended these insights to the translational potential of EC across large-scale resting-state networks. Despite methodological differences in DCM methods, the consistent theme across all studies is the exploration of EC's utilities in predicting

individual differences, including behaviors or clinical traits. Building on the distinction between task-modulated and intrinsic connectivity, EC at rest may capture stable connectivity patterns of the brain's functional architecture, which are relevant for identifying the long-term effects of early-life adversity. Specifically, DMN's EC emerged as a neural biomarker associated with CM. Due to its central role in self-referential mental activity, altered intrinsic connectivity of the DMN may reflect maladaptive internal states linked to trauma-related psychopathology.

Collectively, this work bridges methodological neuroimaging research with behavioral and clinical applications. While it is recognized that the predictive performance was modest in some instances, the primary contribution of this thesis lies in its systematic establishment of a methodological and conceptual foundation for reliably estimating and interpreting EC. By providing a robust framework for future brain-behavior research, this work advances a cohesive understanding of how EC relates to behavior, aging, and clinical outcomes and enhances both methodological rigor and translational relevance in studies of brain task-evoked and resting-state functional networks.

6. References

- Almgren, H., Van de Steen, F., Razi, A., Friston, K., & Marinazzo, D. (2020). The effect of global signal regression on DCM estimates of noise and effective connectivity from resting state fMRI. *NeuroImage*, 208, 116435.
- Anderson, J. S., Druzgal, T. J., Lopez-Larson, M., Jeong, E.-K., Desai, K., & Yurgelun-Todd, D. (2011). Network anticorrelations, global regression, and phase-shifted soft tissue correction. *Human Brain Mapping*, 32(6), 919-934.
- Beck, M. M., Spedden, M. E., Dietz, M. J., Karabanov, A. N., Christensen, M. S., & Lundbye-Jensen, J. (2021). Cortical signatures of precision grip force control in children, adolescents, and adults. *eLife*, 10, e61018.
- Biswal, B., Yetkin, F. Z., Haughton, V. M., & Hyde, J. S. (1995). Functional connectivity in the motor cortex of resting human brain using echo-planar mri. *Magnetic Resonance in Medicine*, 34(4), 537-541.
- Biswal, B. B., Mennes, M., Zuo, X.-N., Gohel, S., Kelly, C., Smith, S. M., . . . Milham, M. P. (2010). Toward discovery science of human brain function. *Proceedings of the National Academy of Sciences*, 107(10), 4734-4739.
- Botvinik-Nezer, R., Holzmeister, F., Camerer, C. F., Dreber, A., Huber, J., Johannesson, M., . . . Schonberg, T. (2020). Variability in the analysis of a single neuroimaging dataset by many teams. *Nature*, 582(7810), 84-88.
- Boudrias, M.-H., Gonçalves, C. S., Penny, W. D., Park, C.-H., Rossiter, H. E., Talelli, P., & Ward, N. S. (2012). Age-related changes in causal interactions between cortical motor regions during hand grip. *NeuroImage*, 59(4), 3398-3405.
- Broyd, S. J., Demanuele, C., Debener, S., Helps, S. K., James, C. J., & Sonuga-Barke, E. J. S. (2009). Default-mode brain dysfunction in mental disorders: A systematic review. *Neuroscience & Biobehavioral Reviews*, 33(3), 279-296.
- Bruin, W. B., Abe, Y., Alonso, P., Anticevic, A., Backhausen, L. L., Balachander, S., . . . van Wingen, G. A. (2023). The functional connectome in obsessive-compulsive disorder: resting-state mega-analysis and machine learning classification for the ENIGMA-OCD consortium. *Molecular Psychiatry*, 28(10), 4307-4319.
- Büchel, C., & Friston, K. J. (1997). Modulation of connectivity in visual pathways by attention: cortical interactions evaluated with structural equation modelling and fMRI. *Cerebral Cortex*, 7(8), 768-778.

- Buckner, R. L., Krienen, F. M., & Yeo, B. T. T. (2013). Opportunities and limitations of intrinsic functional connectivity MRI. *Nature Neuroscience*, 16(7), 832-837.
- Bühler, M., Vollstädt-Klein, S., Klemen, J., & Smolka, M. N. (2008). Does erotic stimulus presentation design affect brain activation patterns? Event-related vs. blocked fMRI designs. *Behavioral and Brain Functions*, 4(1), 30.
- Buxton, R. B., Uludağ, K., Dubowitz, D. J., & Liu, T. T. (2004). Modeling the hemodynamic response to brain activation. *NeuroImage*, 23, S220-S233.
- Carp, J. (2012). On the Plurality of (Methodological) Worlds: Estimating the Analytic Flexibility of fMRI Experiments. *Frontiers in Neuroscience*, 6, 149.
- Caspers, S., Moebus, S., Lux, S., Pundt, N., Schütz, H., Mühleisen, T. W., . . . Amunts, K. (2014). Studying variability in human brain aging in a population-based German cohort—rationale and design of 1000BRAINS. *Frontiers in Aging Neuroscience*, 6, 149.
- Cieslik, E. C., Zilles, K., Grefkes, C., & Eickhoff, S. B. (2011). Dynamic interactions in the fronto-parietal network during a manual stimulus–response compatibility task. *NeuroImage*, 58(3), 860-869.
- Cieslik, E. C., Zilles, K., Kurth, F., & Eickhoff, S. B. (2010). Dissociating Bottom-Up and Top-Down Processes in a Manual Stimulus–Response Compatibility Task. *Journal of Neurophysiology*, 104(3), 1472-1483.
- Cole, D. M., Smith, S. M., & Beckmann, C. F. (2010). Advances and pitfalls in the analysis and interpretation of resting-state FMRI data. *Frontiers in Systems Neuroscience*, 4, 8.
- Daunizeau, J., Preuschoff, K., Friston, K., & Stephan, K. (2011). Optimizing Experimental Design for Comparing Models of Brain Function. *PLOS Computational Biology*, 7(11), e1002280.
- Diersch, N., Valdes-Herrera, J. P., Tempelmann, C., & Wolbers, T. (2021). Increased Hippocampal Excitability and Altered Learning Dynamics Mediate Cognitive Mapping Deficits in Human Aging. *The Journal of Neuroscience*, 41(14), 3204-3221.
- Dosenbach, N. U. F., Fair, D. A., Cohen, A. L., Schlaggar, B. L., & Petersen, S. E. (2008). A dual-networks architecture of top-down control. *Trends in cognitive sciences*, 12(3), 99-105.

- Doucet, G. E., Janiri, D., Howard, R., O'Brien, M., Andrews-Hanna, J. R., & Frangou, S. (2020). Transdiagnostic and disease-specific abnormalities in the default-mode network hubs in psychiatric disorders: A meta-analysis of resting-state functional imaging studies. *European Psychiatry*, 63(1), e57.
- Eimer, M. (1995). Stimulus-response compatibility and automatic response activation: evidence from psychophysiological studies. *Journal of Experimental Psychology: Human Perception and Performance*, 21(4), 837-854.
- Elton, A., & Gao, W. (2015). Task-related modulation of functional connectivity variability and its behavioral correlations. *Human Brain Mapping*, 36(8), 3260-3272.
- Finn, E. S., Scheinost, D., Finn, D. M., Shen, X., Papademetris, X., & Constable, R. T. (2017). Can brain state be manipulated to emphasize individual differences in functional connectivity? *NeuroImage*, 160, 140-151.
- Fitts, P. M., & Deininger, R. L. (1954). S-R compatibility: correspondence among paired elements within stimulus and response codes. *Journal of Experimental Psychology*, 48(6), 483-492.
- Fox, M. D., Zhang, D., Snyder, A. Z., & Raichle, M. E. (2009). The Global Signal and Observed Anticorrelated Resting State Brain Networks. *Journal of Neurophysiology*, 101(6), 3270-3283.
- Frässle, S., Harrison, S. J., Heinzle, J., Clementz, B. A., Tamminga, C. A., Sweeney, J. A., . . . Stephan, K. E. (2021). Regression dynamic causal modeling for resting-state fMRI. *Human Brain Mapping*, 42(7), 2159-2180.
- Frässle, S., Lomakina, E. I., Kasper, L., Manjaly, Z. M., Leff, A., Pruessmann, K. P., . . . Stephan, K. E. (2018). A generative model of whole-brain effective connectivity. *NeuroImage*, 179, 505-529.
- Frässle, S., Lomakina, E. I., Razi, A., Friston, K. J., Buhmann, J. M., & Stephan, K. E. (2017). Regression DCM for fMRI. *NeuroImage*, 155, 406-421.
- Frässle, S., Manjaly, Z. M., Do, C. T., Kasper, L., Pruessmann, K. P., & Stephan, K. E. (2021). Whole-brain estimates of directed connectivity for human connectomics. *NeuroImage*, 225, 117491.
- Friston, K. J. (2011). Functional and Effective Connectivity: A Review. *Brain Connectivity*, 1(1), 13-36.

- Friston, K. J., Harrison, L., & Penny, W. (2003). Dynamic causal modelling. *NeuroImage*, 19(4), 1273-1302.
- Friston, K. J., Zarahn, E., Josephs, O., Henson, R. N. A., & Dale, A. M. (1999). Stochastic Designs in Event-Related fMRI. *NeuroImage*, 10(5), 607-619.
- Fuller-Thomson, E., Baird, S. L., Dhrodia, R., & Brennenstuhl, S. (2016). The association between adverse childhood experiences (ACEs) and suicide attempts in a population-based study. *Child: Care, Health and Development*, 42(5), 725-734.
- Galioulline, H., Frässle, S., Harrison, S. J., Pereira, I., Heinzle, J., & Stephan, K. E. (2023). Predicting future depressive episodes from resting-state fMRI with generative embedding. *NeuroImage*, 273, 119986.
- Gbadeyan, O., Teng, J., & Prakash, R. S. (2022). Predicting response time variability from task and resting-state functional connectivity in the aging brain. *NeuroImage*, 250, 118890.
- Geerligs, L., Rubinov, M., Cam, C. A. N., & Henson, R. N. (2015). State and Trait Components of Functional Connectivity: Individual Differences Vary with Mental State. *The Journal of Neuroscience*, 35(41), 13949-13961.
- Geng, X., Xu, J., Liu, B., & Shi, Y. (2018). Multivariate Classification of Major Depressive Disorder Using the Effective Connectivity and Functional Connectivity. *Frontiers in Neuroscience*, 12, 38.
- Gerin, M. I., Viding, E., Herringa, R. J., Russell, J. D., & McCrory, E. J. (2023). A systematic review of childhood maltreatment and resting state functional connectivity. *Developmental Cognitive Neuroscience*, 64, 101322.
- Gilbert, R., Widom, C. S., Browne, K., Fergusson, D., Webb, E., & Janson, S. (2009). Burden and consequences of child maltreatment in high-income countries. *The Lancet*, 373(9657), 68-81.
- Goetschius, L. G., Hein, T. C., McLanahan, S. S., Brooks-Gunn, J., McLoyd, V. C., Dotterer, H. L., . . . Beltz, A. M. (2020). Association of Childhood Violence Exposure With Adolescent Neural Network Density. *JAMA Network Open*, 3(9), e2017850.
- Green, J. G., McLaughlin, K. A., Berglund, P. A., Gruber, M. J., Sampson, N. A., Zaslavsky, A. M., & Kessler, R. C. (2010). Childhood Adversities and Adult Psychiatric Disorders in the National Comorbidity Survey Replication I: Associations With First Onset of DSM-IV Disorders. *Archives of General*

Psychiatry, 67(2), 113-123.

- Greene, A. S., Gao, S., Scheinost, D., & Constable, R. T. (2018). Task-induced brain state manipulation improves prediction of individual traits. *Nature Communications*, 9(1), 2807.
- Holz, N. E., Berhe, O., Sacu, S., Schwarz, E., Tesarz, J., Heim, C. M., & Tost, H. (2023). Early Social Adversity, Altered Brain Functional Connectivity, and Mental Health. *Biological Psychiatry*, 93(5), 430-441.
- Huettel, S. A. (2012). Event-related fMRI in cognition. *NeuroImage*, 62(2), 1152-1156.
- Huth, A. G., de Heer, W. A., Griffiths, T. L., Theunissen, F. E., & Gallant, J. L. (2016). Natural speech reveals the semantic maps that tile human cerebral cortex. *Nature*, 532(7600), 453-458.
- Jiang, R., Zuo, N., Ford, J. M., Qi, S., Zhi, D., Zhuo, C., . . . Sui, J. (2020). Task-induced brain connectivity promotes the detection of individual differences in brain-behavior relationships. *NeuroImage*, 207, 116370.
- Jung, K., Friston, K. J., Pae, C., Choi, H. H., Tak, S., Choi, Y. K., . . . Park, H.-J. (2018). Effective connectivity during working memory and resting states: A DCM study. *NeuroImage*, 169, 485-495.
- Kahan, J., & Foltynie, T. (2013). Understanding DCM: Ten simple rules for the clinician. *NeuroImage*, 83, 542-549.
- Kahan, J., Mancini, L., Flandin, G., White, M., Papadaki, A., Thornton, J., . . . Foltynie, T. (2019). Deep brain stimulation has state-dependent effects on motor connectivity in Parkinson's disease. *Brain*, 142(8), 2417-2431.
- Kessler, R., Schmitt, S., Sauder, T., Stein, F., Yüksel, D., Grotegerd, D., . . . Jansen, A. (2020). Long-Term Neuroanatomical Consequences of Childhood Maltreatment: Reduced Amygdala Inhibition by Medial Prefrontal Cortex. *Frontiers in Systems Neuroscience*, 14, 28.
- Korsch, M., Frühholz, S., & Herrmann, M. (2014). Ageing differentially affects neural processing of different conflict types—an fMRI study. *Frontiers in Aging Neuroscience*, 6, 57.
- Kraljević, N., Langner, R., Küppers, V., Raimondo, F., Patil, K. R., Eickhoff, S. B., & Müller, V. I. (2024). Network and state specificity in connectivity-based predictions of individual behavior. *Human Brain Mapping*, 45(8), e26753.

- Kuhnke, P., Kiefer, M., & Hartwigsen, G. (2021). Task-Dependent Functional and Effective Connectivity during Conceptual Processing. *Cerebral Cortex*, 31(7), 3475-3493.
- Langner, R., Cieslik, E. C., Behrwind, S. D., Roski, C., Caspers, S., Amunts, K., & Eickhoff, S. B. (2015). Aging and response conflict solution: behavioural and functional connectivity changes. *Brain Structure and Function*, 220(3), 1739-1757.
- Leonardi, N., Shirer, W. R., Greicius, M. D., & Van De Ville, D. (2014). Disentangling dynamic networks: Separated and joint expressions of functional connectivity patterns in time. *Human Brain Mapping*, 35(12), 5984-5995.
- Lindquist, M. A., Geuter, S., Wager, T. D., & Caffo, B. S. (2019). Modular preprocessing pipelines can reintroduce artifacts into fMRI data. *Human Brain Mapping*, 40(8), 2358-2376.
- Liu, T. T., Frank, L. R., Wong, E. C., & Buxton, R. B. (2001). Detection Power, Estimation Efficiency, and Predictability in Event-Related fMRI. *NeuroImage*, 13(4), 759-773.
- Loehrer, P. A., Nettersheim, F. S., Jung, F., Weber, I., Huber, C., Dembek, T. A., . . . Timmermann, L. (2016). Ageing changes effective connectivity of motor networks during bimanual finger coordination. *NeuroImage*, 143, 325-342.
- Logothetis, N. K. (2008). What we can do and what we cannot do with fMRI. *Nature*, 453(7197), 869-878.
- Lu, S., Gao, W., Wei, Z., Wang, D., Hu, S., Huang, M., . . . Li, L. (2016). Intrinsic brain abnormalities in young healthy adults with childhood trauma: A resting-state functional magnetic resonance imaging study of regional homogeneity and functional connectivity. *Australian & New Zealand Journal of Psychiatry*, 51(6), 614-623.
- Marreiros, A. C., Kiebel, S. J., & Friston, K. J. (2008). Dynamic causal modelling for fMRI: A two-state model. *NeuroImage*, 39(1), 269-278.
- Marusak, H. A., Etkin, A., & Thomason, M. E. (2015). Disrupted insula-based neural circuit organization and conflict interference in trauma-exposed youth. *NeuroImage: Clinical*, 8, 516-525.
- Mechelli, A., Henson, R. N. A., Price, C. J., & Friston, K. J. (2003). Comparing event-related and epoch analysis in blocked design fMRI. *NeuroImage*, 18(3), 806-

- Mechelli, A., Price, C. J., Henson, R. N. A., & Friston, K. J. (2003). Estimating efficiency a priori: a comparison of blocked and randomized designs. *NeuroImage*, 18(3), 798-805.
- Menon, V. (2011). Large-scale brain networks and psychopathology: a unifying triple network model. *Trends in Cognitive Sciences*, 15(10), 483-506.
- Menon, V. (2023). 20 years of the default mode network: A review and synthesis. *Neuron*, 111(16), 2469-2487.
- Menon, V., & Uddin, L. Q. (2010). Saliency, switching, attention and control: a network model of insula function. *Brain Structure and Function*, 214(5), 655-667.
- Merrick, M. T., Ports, K. A., Ford, D. C., Afifi, T. O., Gershoff, E. T., & Grogan-Kaylor, A. (2017). Unpacking the impact of adverse childhood experiences on adult mental health. *Child Abuse & Neglect*, 69, 10-19.
- Millar, P. R., Petersen, S. E., Ances, B. M., Gordon, B. A., Benzinger, T. L. S., Morris, J. C., & Balota, D. A. (2020). Evaluating the Sensitivity of Resting-State BOLD Variability to Age and Cognition after Controlling for Motion and Cardiovascular Influences: A Network-Based Approach. *Cerebral Cortex*, 30(11), 5686-5701.
- Morken, F., Helland, T., Hugdahl, K., & Specht, K. (2017). Reading in dyslexia across literacy development: A longitudinal study of effective connectivity. *NeuroImage*, 144, 92-100.
- Murphy, K., Birn, R. M., Handwerker, D. A., Jones, T. B., & Bandettini, P. A. (2009). The impact of global signal regression on resting state correlations: Are anti-correlated networks introduced? *NeuroImage*, 44(3), 893-905.
- Murphy, K., & Fox, M. D. (2017). Towards a consensus regarding global signal regression for resting state functional connectivity MRI. *NeuroImage*, 154, 169-173.
- O'Connor, E. E., & Zeffiro, T. A. (2019). Why is Clinical fMRI in a Resting State? *Frontiers in Neurology*, 10, 420.
- Power, J. D., Mitra, A., Laumann, T. O., Snyder, A. Z., Schlaggar, B. L., & Petersen, S. E. (2014). Methods to detect, characterize, and remove motion artifact in resting state fMRI. *NeuroImage*, 84, 320-341.

- Power, J. D., Plitt, M., Laumann, T. O., & Martin, A. (2017). Sources and implications of whole-brain fMRI signals in humans. *NeuroImage*, 146, 609-625.
- Proctor, R. W., Vu, K.-P. L., & Pick, D. F. (2005). Aging and Response Selection in Spatial Choice Tasks. *Human Factors*, 47(2), 250-270.
- Raichle, M. E., MacLeod, A. M., Snyder, A. Z., Powers, W. J., Gusnard, D. A., & Shulman, G. L. (2001). A default mode of brain function. *Proceedings of the National Academy of Sciences*, 98(2), 676-682.
- Rajapakse, J. C., & Zhou, J. (2007). Learning effective brain connectivity with dynamic Bayesian networks. *NeuroImage*, 37(3), 749-760.
- Roebroeck, A., Formisano, E., & Goebel, R. (2005). Mapping directed influence over the brain using Granger causality and fMRI. *NeuroImage*, 25(1), 230-242.
- Rosenblatt, M., Tejavibulya, L., Jiang, R., Noble, S., & Scheinost, D. (2024). Data leakage inflates prediction performance in connectome-based machine learning models. *Nature Communications*, 15(1), 1829.
- Schaefer, A., Kong, R., Gordon, E. M., Laumann, T. O., Zuo, X.-N., Holmes, A. J., . . . Yeo, B. T. T. (2018). Local-Global Parcellation of the Human Cerebral Cortex from Intrinsic Functional Connectivity MRI. *Cerebral Cortex*, 28(9), 3095-3114.
- Seghier, M. L., & Friston, K. J. (2013). Network discovery with large DCMs. *NeuroImage*, 68, 181-191.
- Sha, Z., Wager, T. D., Mechelli, A., & He, Y. (2019). Common Dysfunction of Large-Scale Neurocognitive Networks Across Psychiatric Disorders. *Biological Psychiatry*, 85(5), 379-388.
- Shen, X., Finn, E. S., Scheinost, D., Rosenberg, M. D., Chun, M. M., Papademetris, X., & Constable, R. T. (2017). Using connectome-based predictive modeling to predict individual behavior from brain connectivity. *Nature Protocols*, 12(3), 506-518.
- Smith, S. M., Vidaurre, D., Beckmann, C. F., Glasser, M. F., Jenkinson, M., Miller, K. L., . . . Van Essen, D. C. (2013). Functional connectomics from resting-state fMRI. *Trends in Cognitive Sciences*, 17(12), 666-682.
- Teicher, M. H., & Samson, J. A. (2016). Annual Research Review: Enduring neurobiological effects of childhood abuse and neglect. *Journal of Child*

Psychology and Psychiatry, 57(3), 241-266.

- Tie, Y., Suarez, R. O., Whalen, S., Radmanesh, A., Norton, I. H., & Golby, A. J. (2009). Comparison of blocked and event-related fMRI designs for pre-surgical language mapping. *NeuroImage*, 47, T107-T115.
- Tsvetanov, K. A., Henson, R. N., Tyler, L. K., Razi, A., Geerligs, L., Ham, T. E., & Rowe, J. B. (2016). Extrinsic and intrinsic brain network connectivity maintains cognition across the lifespan despite accelerated decay of regional brain activation. *The Journal of Neuroscience*, 36(11), 3115-3126.
- Valencia, N., Seeger, F. R., Seitz, K. I., Carius, L., Nkrumah, R. O., Schmitz, M., . . . Herpertz, S. C. (2024). Childhood maltreatment and transdiagnostic connectivity of the default-mode network: The importance of duration of exposure. *Journal of Psychiatric Research*, 177, 239-248.
- van den Heuvel, M. P., & Hulshoff Pol, H. E. (2010). Exploring the brain network: A review on resting-state fMRI functional connectivity. *European Neuropsychopharmacology*, 20(8), 519-534.
- Varikuti, D. P., Hoffstaedter, F., Genon, S., Schwender, H., Reid, A. T., & Eickhoff, S. B. (2017). Resting-state test-retest reliability of a priori defined canonical networks over different preprocessing steps. *Brain Structure and Function*, 222(3), 1447-1468.
- Volz, L. J., Eickhoff, S. B., Pool, E.-M., Fink, G. R., & Grefkes, C. (2015). Differential modulation of motor network connectivity during movements of the upper and lower limbs. *NeuroImage*, 119, 44-53.
- Whitfield-Gabrieli, S., & Ford, J. M. (2012). Default Mode Network Activity and Connectivity in Psychopathology. *Annual Review of Clinical Psychology*, 8(1), 49-76.
- Xiong, M., Lin, L., Jin, Y., Kang, W., Wu, S., & Sun, S. (2023). Comparison of Machine Learning Models for Brain Age Prediction Using Six Imaging Modalities on Middle-Aged and Older Adults. *Sensors*, 23(7), 3622.
- Yeo, B. T., Krienen, F. M., Sepulcre, J., Sabuncu, M. R., Lashkari, D., Hollinshead, M., . . . Buckner, R. L. (2011). The organization of the human cerebral cortex estimated by intrinsic functional connectivity. *Journal of Neurophysiology*, 106(3), 1125-1165.
- Zeidman, P., Jafarian, A., Corbin, N., Seghier, M. L., Razi, A., Price, C. J., & Friston, K. J. (2019). A guide to group effective connectivity analysis, part 1: First level

- analysis with DCM for fMRI. *NeuroImage*, 200, 174-190.
- Zeidman, P., Jafarian, A., Seghier, M. L., Litvak, V., Cagnan, H., Price, C. J., & Friston, K. J. (2019). A guide to group effective connectivity analysis, part 2: Second level analysis with PEB. *NeuroImage*, 200, 12-25.
- Zeidman, P., Kazan, S. M., Todd, N., Weiskopf, N., Friston, K. J., & Callaghan, M. F. (2019). Optimizing Data for Modeling Neuronal Responses. *Frontiers in Neuroscience*, 12, 986.
- Zhang, J., Zhao, T., Zhang, J., Zhang, Z., Li, H., Cheng, B., . . . Wang, J. (2022). Prediction of childhood maltreatment and subtypes with personalized functional connectome of large-scale brain networks. *Human Brain Mapping*, 43(15), 4710-4721.
- Zhao, H., Dong, D., Sun, X., Cheng, C., Xiong, G., Wang, X., & Yao, S. (2021). Intrinsic brain network alterations in non-clinical adults with a history of childhood trauma. *European Journal of Psychotraumatology*, 12(1), 1975951.
- Zhao, K., Xie, H., Fonzo, G. A., Tong, X., Carlisle, N., Chidharom, M., . . . Zhang, Y. (2023). Individualized fMRI connectivity defines signatures of antidepressant and placebo responses in major depression. *Molecular Psychiatry*, 28(6), 2490-2499.
- Zhao, W., Makowski, C., Hagler, D. J., Garavan, H. P., Thompson, W. K., Greene, D. J., . . . Dale, A. M. (2023). Task fMRI paradigms may capture more behaviorally relevant information than resting-state functional connectivity. *NeuroImage*, 270, 119946.

7. Acknowledgements

This dissertation would not have been completed without the invaluable support and contributions of several individuals. I want to express my sincere gratitude to those who guided and encouraged me throughout this journey.

First and foremost, I extend my deepest appreciation to my supervisor, Oleksandr Popovych, for providing me the opportunity to join his research group as a PhD student. I am profoundly grateful for the resources, mentorship, and constructive feedback he has offered. His scientific rigor, optimism, and dedication to excellence had a profound influence on my academic work. Through this project, I have learned to appreciate research as a source of intellectual fulfillment rather than just a job.

Second, I would like to thank my co-supervisor, Esther Florin, for her expert guidance and valuable insights throughout the development of this thesis. Her professional perspective from another field enriched my work, and her rigorous but supportive mentorship consistently helped me face challenges and refine my direction. Her advice was instrumental in ensuring the successful completion of my project milestones.

Third, I am deeply indebted to Simon Eickhoff and Robert Langner for their invaluable feedback and expertise. Their constructive critiques significantly enhanced the quality of the publications included in this thesis. I have learned immensely from their proficiency in the field, from formulating research questions to scholarly writing.

Additionally, I extend my gratitude to Kevin Wischnewski, Justin Domhof, and Kyesam Jung for their expertise and consultations in the mathematical and neuroimaging domains. Their insightful discussions and collaborative help were indispensable to the success of this work.

Above all, I wish to express my best gratitude to my girlfriend, Honglin Liu, for her unwavering support, patience, and encouragement throughout this journey. Her steadfast belief in me, even in moments of doubt, gave me the strength and resilience to overcome the challenges of doctoral research.

Finally, I would like to acknowledge all colleagues, friends, and family members at the INM-7, Juelich Research Center, who supported me during this endeavor. Their encouragement and patience sustained me through the challenges of doctoral research.

This thesis stands as a testament to the collective effort of those who generously shared their knowledge, time, and enthusiasm. Thank you.